NOVEL SINGLE MOLECULE MAGNETS AND PHOTOSENSITIZERS FOR MOLECULAR PHOTOVOLTAICS BASED ON CUSTOMIZED PHTHALOCYANINES

DOCTORAL THESIS

CAROLINA R. GANIVET

Madrid, 2015

Facultad de Ciencias

Departamento de Química Orgánica

NOVEL SINGLE MOLECULE MAGNETS AND PHOTOSENSITIZERS FOR MOLECULAR PHOTOVOLTAICS BASED ON CUSTOMIZED PHTHALOCYANINES

CAROLINA R. GANIVET

Doctoral Thesis

Supervised by Prof. Tomás Torres Cebada and Dr. Gema de la Torre Ponce

Madrid, 2015

This PhD Thesis has been done at the Department of Organic Chemistry at the Universidad Autónoma de Madrid under the supervisión of Prof. Tomás Torres Cebada and Dr. Gema de la Torre Ponce.

To date, the results reported in this thesis have been published in the following journals and a registered patent:

- *Broadening the absorption of conjugated polymers by "click" functionalization with phthalocyanines.* B. J. Campo, J. Duchateau, C. R. Ganivet, B. Ballesteros, J. Gilot, M. M. Wienk, W. D. Oosterbaan, L. Lutsen, T. J. Cleij, G. de la Torre, R. A. J. Janssen, D. Vanderzande, T. Torres, *Dalton Trans.* **2011**, *40*, 3979-3988.
- *Synthesis and characterization of high molecular weight phthalocyanine-PPV copolymers through post-polimerization functionalization.* J. J. Cid, J. Duchateau, L. Van Severen, C. R. Ganivet, G. de la Torre, P. Vazquez, T. Cleij, L. Lutsen, D. Vanderzande, T. Torres, *J. Porphyrins Phthalocyanines* **2011**, *15*, 659-666.
- *Influence of peripheral substitution on the magnetic behavior of single-ion magnets based on homoh- and heteroleptic Tb^{III} bis(phthalocyaninate).* C. R. Ganivet, B. Ballesteros. G. de la Torre, J. M. Clemente-Juan, E. Coronado, T. Torres, *Chem. Eur. J.* ***2013****, 19,* 1475-1465.
- *Combining novel electron-accepting phthalocyanines and nanorod-like CuO electrodes for p-type dye-sensitized solar cells.* O. Langmar, C. R. Ganivet, A. Lennert, R. D. Costa, G. de la Torre, T. Torres, D. M. Guldi, *Angew. Chem. Int. Ed.* ***2015***. DOI: 10.1002/anie.201501550R1.
- Spanish Patent 2 403 734 (issued 02/26/14), "Heteroleptic Tb^{III} Bis(phthalocyaninate). Synthesis and Application as Single-Molecule Magnets," T. Torres, G. de la Torre, C. R. Ganivet, B. Ballesteros, E. Coronado, J. M. Clemente-Juan.

Other contributions during this thesis have resulted in the following publication:

- *Influence of axial and peripheral ligands on the electronic structure of titanium phthalocyanines.* D. F. Pickup, I. Zegkinoglou, B. Ballesteros, C. R. Ganivet, J. M. Garcia-Lastra, P. L. Cook, P. S. Johnson, C. Rogero, F. de Groot, A. Rubio, G. de la Torre, J. E. Ortega, F. J. Himpsel, *J. Phys. Chem. C* **2013**, *117*, 4410.

Standars abbreviations and acronyms

CB	Conduction band
VB	Valence band
CNT	Carbon nanotube
CS	Charge separation
DBU	1,8-Diazabicyclo[5.4.0]undec-7-ene
o-DCB	*o*-Dichlorobenzene
DCM	Dichloromethane
DDQ	2,3-Dichloro-5,6-dicyano-1,4-benzoquinone
DMAC	*N*,*N*-Dimethylacetamide
DMAE	*N*,*N*-Dimethylaminoethanol
DMF	*N*,*N*-Dimethylformamide
DMSO	Dimethyl sulfoxide
DSS	Dye-sensitized solar cell
EA	Elemental analysis
EI	Electronic impact
EQE	External quantum efficiency
FF	Fill factor
GPC	Gel permeation chromatography
HOMO	Highest occupied molecular orbital
IBX	1-Hydroxy-1,2-benziodoxol-3-(1*H*)-one-1-oxide
IR	Infrared
IPCE	Incident photon-to-current efficiency
ITO	Indiun tin oxide
LUMO	Lowest unoccupied molecular orbital
MALDI	Matrix-assisted laser desorption/ionization

MDMO-PPV	Poly[2-methoxy-5-(3',7'-dimethyloctyloxy)-1,4-phenylenevinylene]
MEH-PPV	Poly[2-methoxy-5-(2-ethylhexyloxy)-1,4-phenylenevinylene]
NBS	*N*-Bromosuccinimide
NHE	Normal hydrogen electrode
NMR	Nuclear magnetic resonance
OPV	Organic photovoltaic
OSC	Organic solar cell
Pc	Phthalocyanine
PCBM	[6,6]-phenyl-C_{61}-butyric acid methyl ester
PCE	Power conversion efficiency
PD	Polidispersity
P3HT	Poly(3-hexylthiophene-2,5-diyl)
ppm	Parts per million
PPV	Poly(*p*-phenylene vinylene)
PS	Polystyrene
PT	Polythiophene
QTM	Quantum tunneling of magnetization
SEC	Size-exclusion chromatography
SEM	Scanning electron miscroscope
SMM	Single molecule magnet
SOMO	Singly occupied molecular orbital
SWNT	Single-wall nanotube
TCB	Trichlorobenzene
THF	Tetrahydrofuran
UV-Vis	Ultraviolet-visible spectrophotometry

Index

Chapter 2. Single-molecule magnets based on terbium(III) bis(phthalocyaninato) complexes

Resumen

La presente tesis doctoral, que lleva por título “Novel single molecule magnets and photosensitizers for molecular photovoltaics based on phthalocyanines” está centrada en el desarrollo y estudio de nuevos materiales funcionales con propiedades electrónicas y magnéticas para su utilización en fotovoltaica molecular y magnetismo, respectivamente. Con respecto al primer cometido, se ha logrado sintetizar copolímeros de poliparafenilenvinileno (PPV) y politiofeno (PT) sustituidos lateralmente con ftalocianinas (Pcs) mediante reacciones de funcionalización de los copolímeros ya formados, como propuesta para solucionar el problema del bajo aprovechamiento energético que supone la nula absorbancia por parte de dichos polímeros en el rango solar de máximo flujo de fotones, zona en la cuál las Pcs presentan una absorción intensa. Para ello se emplearon copolímeros de PPV y PT sintetizados en la U. de Hasselt portadores de un 10% de grupos funcionales reactivos en las cadenas laterales y Pcs asimétricamente funcionalizadas con cadenas alquílicas y un grupo reactivo. Se llevaron a cabo dos tipos de reacciones, una esterificación y otra tipo “click”, resultando ser esta última la más eficaz puesto que es la que mayor número de Pcs incorpora al esqueleto polimérico. Estos materiales poliméricos se caracterizaron estructural y electrónicamente, certificando así el porcentaje de Pcs incorporadas, y se probaron en células de heterounión masiva junto con PCBM ([6,6]-phenyl-C61-butyric acid methyl ester) como material aceptor de electrones. Se estudió la influencia de los distintos grosores de capa activa, generada por técnicas de “spin-coating” de una disolución del material polimérico y PCBM en clorobenceno, así como de las distintas proporciones entre el material dador - el polímero modificado - y el material aceptor en las eficiencias de conversión. Aunque los experimentos de eficiencia cuántica externa (EQE) determinaban que las Pcs contribuyen la generación de fotocorriente en la zona donde presentan su máximo de absorción, las eficiencias de todos los materiales activos resultaron ser inferiores a los materiales sin Pcs incorporadas. Tras realizar experimentos de espectroscopía de ultravioleta-visible en solución y en capa fina, se concluyó que los malos resultados se deben fundamentalmente a la pobre organización que presenta el material polimérico en la capa activa como resultado de la incorporación de los macrociclos. Aunque la organización de este material mejora al cambiar el tipo de disolvente que se utiliza para realizar la deposición de la capa activa, la utilización de PCBM como material aceptor limita el empleo de disolventes alternativos dada su escasa solubilidad en los mismos. Dentro del proyecto también se diseñó la síntesis de Pcs con grupos atractores de electrones en la periferia para convertirlos en unidades aceptoras, de tal forma que tras su incorporación covalente lateral a un copolímero de tipo p, como los derivados de PPV, propiciaría un polímero de “doble-cable”, donde el material dador y aceptor se encuentran unidos covalentemente, lo que excluye la necesidad de

adicionar PCBM para formar la fase activa. Para llevar a cabo esta aproximación, es necesario utilizar copolímeros donde una de cada dos unidades monoméricas incorpore un grupo funcional para su posterior funcionalización con las Pcs. Sin embargo, tras una reacción de tipo “click” entre un copolímero PPV portador de grupos azida y una etinilPc se obtuvo un material altamente insoluble, debido probablemente a la incorporación masiva de Pcs, por lo que se descartó continuar en esta dirección.

La idea de incorporar Pcs como antena de fotones y unidad activa en el copolímero también se desarrolló hacía la síntesis de Pcs como unidades monoméricas, funcionalizadas de tal forma que puedan participar en reacciones de polimerización. El proyecto se encuentra en los primeros estudios de polimerización tras haberse sintetizados una de las Pcs propuestas y ensayado las condiciones óptimas para llevar a cabo la copolimerización de las mismas con otras unidades electroactivas.

Por último, se ha abordado otro proyecto en la área de la fotovoltaica molecular que consiste en la preparación de Pcs con sustituyentes aceptores que puedan ser ancladas a materiales semiconductores de tipo p para obtener células fotosensibilizadas por colorante con una arquitectura “invertida” con respecto a las células Grätzel tradicionales, es decir, donde el material semiconductor inyecta electrones al cromóforo fotoexcitado. Una vez sintetizadas las Pcs aceptoras y caracterizadas convenientemente, se fabricaron las células solares invertidas empleando para ello CuO en forma de nanovarillas, que no había sido utilizado hasta la fecha en la bibliografía. Aunque las eficiencias son discretas, este modelo constituye una prueba de concepto en el campo de las células solares fotosensibilizadas por colorante de tipo p, ya que se ha mostrado la viabilidad de las Pcs como cromóforos en estas células, así como la posibilidad de utilizar diferentes nanoformas de CuO como semiconductor alternativo al comúnmente usado NiO.

La segunda línea investigación de esta tésis está relacionada con el magnetismo a nivel de una sola molécula que presentan los bis(ftalocianinatos) de terbio(III). Con el fin de entender la relación entre la estructura de dichos complejos y la respuesta magnética, se sintetizaron una serie de complejos de Tb(III) tipo “double-decker” en los que se variaba tanto la cantidad como la naturaleza de los sustituyents periféricos, aceptores o dadores, así como el carácter radicálico o aniónico de los complejos. También se estudió la posibilidad de incluir otros macrociclos, como porfirinas o naftalocianinas, y observar la respuesta magnética. Cabe destacar que se ha preparado por primera vez derivados heterolépticos de Tb(III), donde cada uno de los anillos de Pc que forman la estructura de “double-decker” presentan diferente sustitución. Sin embargo no se pudieron obtener complejos con grupos aceptores en los anillos de ftalocianina ni “double-deckers” con porfirinas. El comportamiento como SMMs de los

derivados preparados se estudió para determinar relaciones estructura-actividad de los mismos, que muestran que para conseguir mejores parámetros magnéticos es preferible la presencia de una sola Pc sustituida con grupos dadores, frente al complejo que presenta dichos grupos en ambos anillos. Además, los valores magnéticos fueron mayores para las especies radicálicas frente a las aniónicas. Por último, la incorporación de una naftalocianina en vez de una Pc no afecta demasiado al comportamiento magnético. Cabe destacar que los derivados heterolépticos preparados presentan la mayor barrera de inversión descrita hasta la fecha para SMMs.

Una vez abordado esta parte del estudio de “double-decker” magnéticos, se comenzó la síntesis de especies diméricas con la intención de estudiar las interacciones Tb-Tb en la misma molécula. Estas especies diméricas de complejos de Tb(III) preparadas en este trabajo presentan una estructura innovadora de gran interés para determinar el efecto que las interacciones de spin Tb-Tb pueden tener en las propiedades SMM de los bisftalocianinatos de lantánidos. Los estudios magnéticos sobre estos sistemas se están realizando actualmente.

Introduction to phthalocyanines

Organic molecular materials

In 1959, the promise of nanotechnology was outlined by Nobel Prize Richard Feynman in his famous talk, "There´s plenty of room at the bottom". Since then, the word "nano" has captured considerable attention from almost all scientific disciplines, as it shows the way to the nanometer-scale world where the smallest human-made devices can have a communication with the atoms and molecules of the natural world.[1] In general, nanotechnology and nanoscience refer to the study and manipulation of nanosized materials, which are characterized by their spatial dimensions, ranging from about 0.1 to 500 nm, and they have demonstrated novel applications in numerous fields. Nanomaterials exhibit significantly different chemical and physical properties compared to the bulk materials with the same chemical composition. The unique and unprecedented structural properties of nanomaterials can lead to new generation of devices and technologies; however, the synthesis of nanomaterials with controlled sizes and shapes is a challenging task. For this reason, great efforts have been made by material chemists to pursue useful synthethic methods to access well-defined nanomaterials as well as to explore their practical applications.

Within this context, the incorporation of organic or metallorganic molecules as active components in functional devices has opened the door to a new generation of materials with revolutionary magnetic,[2] optic,[3] and electronic properties.[4] The molecules are synthesized and, in a second stage, organized into supramolecular structures to form the so-called organic molecular materials,[2b,5] which are held together through intermolecular forces, such as hydrogen bonds, van der Waals forces or π-π interactions, among others. Typically in a supramolecular assembly, the individual building blocks retain much of their molecular character, but the overall assembly exhibits new properties and/or is capable of performing a specific function beyond that possible when using the individual components. In other words, the properties will be defined by the

[1] C. N. R. Rao, A. K. Cheetham (Ed. Y. Gogotsi), *Nanomaterials Handbook*, chapter 1, Taylor and Francis Group, **2006**.

[2] a) F. N. Shi, L. Cunha-Silva, R. A. S. Ferreira, L. Mafra, T. Trindade, L. D. Carlos, F. A. A. Paz, J. Rocha, *J. Am. Chem. Soc.* **2008**, *130*, 150; b) D. Grosso, F. Ribot, C. Boissiere, C. Sanchez, *Chem. Soc. Rev.* **2011**, *40*, 829; c) I. Ratera, J. Veciana, *Chem. Soc. Rev.* **2012**, *41*, 303.

[3] P. A. Sullivan, L. R. Dalton, *Acc. Chem. Res.* **2010**, *43*, 10.

[4] a) J. M. Lupton, *Adv. Mater.* **2010**, *22*, 16891; b) D. Beljonne, J. Cornil, L. Muccioli, C. Zannoni, J. L. Bredas, F. Castet, *Chem. Mater.* **2011**, *23*, 591.

[5] a) T. J. Marks, *Science* **1985**, *227*, 881; b) Y. Shirota, *J. Mater. Chem*. **2000**, *10*, 1; c) J. Fan, S. W. Boettcher, C. Tsung, Q. Shi, M. Schierhorn, G. D. Stucky, *Chem. Mater*. **2008**, *20*, 909; d) E. Gomar-Nadal, J. Puigmarti-Luis, D. B. Amabilino, *Chem. Soc. Rev.* **2008**, *37*, 490; e) H. B. Liu, J. L. Xu, Y. J. Li, Y. L. Li, *Acc. Chem. Res.* **2010**, *43*, 1496; f) R. Mas-Balleste, J. Gomez-Herrero, F. Zamora, *Chem. Soc. Rev.* **2010**, *39*, 4220; g) D. Gonzalez-Rodriguez, A. Schenning, *Chem. Mater.* **2011**, *23*, 310.

physicochemical characteristics of their components and their relative ordering beyond the molecule (*Figure 1*).

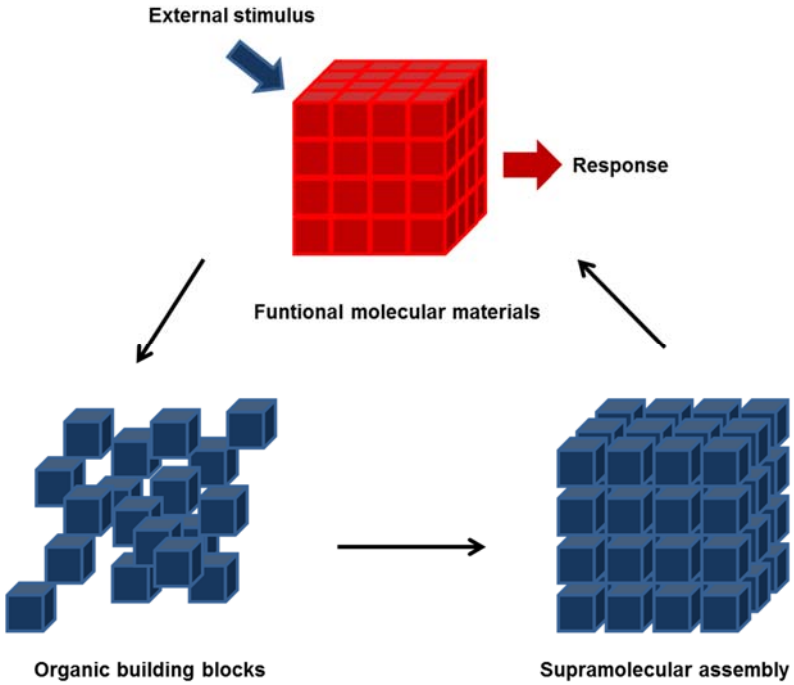

Figure 1.- Functional molecular materials.

These supramolecular systems may exhibit several advantages over inorganic materials. First of all, organic synthetic flexibility offers the possibility to introduce structural modifications on a particular molecule that may considerably change the macroscopic properties of the molecular material. In addition, organic compounds can be designed to be able to organize into different kinds of condensed phases (crystals, liquid crystals,[6] thin films[7]), which facilitates their processing and incorporation into devices. On the other hand, organic molecular materials still present some negative aspects which make their application more difficult,[8] such as chemical, thermal and electromagnetic

[6] a) S. Laschat, A. Baro, N. Steinke, F. Giesselmann, C. Hagele, G. Scalia, R. Judele, E. Kapatsina, S. Sauer, A. Schreivogel, M. Tosoni, *Angew. Chem. Int. Ed.* **2007**, *46*, 4832; b) S. Sergeyev, W. Pisula, Y. H. Geerts, *Chem. Soc. Rev.* **2007**, *36*, 1902; c) B. R. Kaafarani, *Chem. Mater.* **2011**, *23*, 378.

[7] a) M. H. Nurmawati, R. Renu, P. K. Ajikumar, S. Sindhu, F. C. Cheong, C. H. Sow, S. Valiyaveettil, *Adv. Funct. Mater*. **2006**, *16*, 2340; b) R. U. A. Khan, O. Kwon, A. Tapponnier, A. N. Rashid, P. Günter, *Adv. Funct. Mater*. **2006**, *16*, 180; c) *Handbook of Nanoestructured Thin Films and Coatings.* S. Zhang, **2010**, vol 3; d) O. Shekhah, J. Liu, R. A. Fischer, C. Woll, *Chem. Soc. Rev.* **2011**, *40*, 1081.

[8] J. S. Miller, *Adv. Mater*. **1990**, *2*, 98.

instability and low reproducibility of their properties after a given number of operation cycles. Besides, the correlation between macroscopic properties and molecular structure is not often very well understood.

The desired final properties and applications of the material will primarily determine the kind of condensed phase needed, but in most cases they share a common requirement for stable and highly ordered systems. These condensed phases may be obtained in the form of engineered crystals, but research in this field has been mainly focused on the development of liquid crystals, in which molecules are ordered in a quasi-liquid medium that combines the anisotropy of a crystal and the fluidity of an isotropic liquid, and thin films. The production of these films can be achieved by different methods, such as vacuum sublimation or spin-coating (the solvent is evaporated by high-speed spinning of the sample). In order to attain a better control over the thickness and homogeneity of the film, the Langmuir-Blodgett (LB)[9] technique is a very attractive method, requiring amphiphilic molecules so as to get them organized over a water surface and then transferred onto a solid support. Properly functionalized molecular components may also be arranged into porous inorganic structures[10] or over flat surfaces of gold, silver or glass, giving rise to the so-called self-assembled monolayers.[11]

[9] R. T. Andrea, J. Huang, P. Yang, *Acc. Chem. Res.* **2008**, *41*, 166

[10] a) A. Stein, B. J. Melde, R. C. Schroden. *Adv. Mater*. **2000**, *12*, 1403; b) B. L. Chen, S. C. Xiang, G. D. Qian, *Acc. Chem. Res.* **2010**, *43*, 1115.

[11] a) S. A. DiBenedetto, A. Facchetti, M. A. Ratner, T. J. Marks, *Adv. Mater.* **2009**, *21*, 1407; b) *Handbook of Nanophysics. Self-Assembled Monolayers* (Ed. D. K. Sattler) H. Frank, **2011**, vol. 7, pp 1-17.

Properties and applications of organic molecular materials

The non conventional electrical, optic and magnetic properties of organic molecular materials have led to its increasing application in various technologial fields (*Figura 2*).

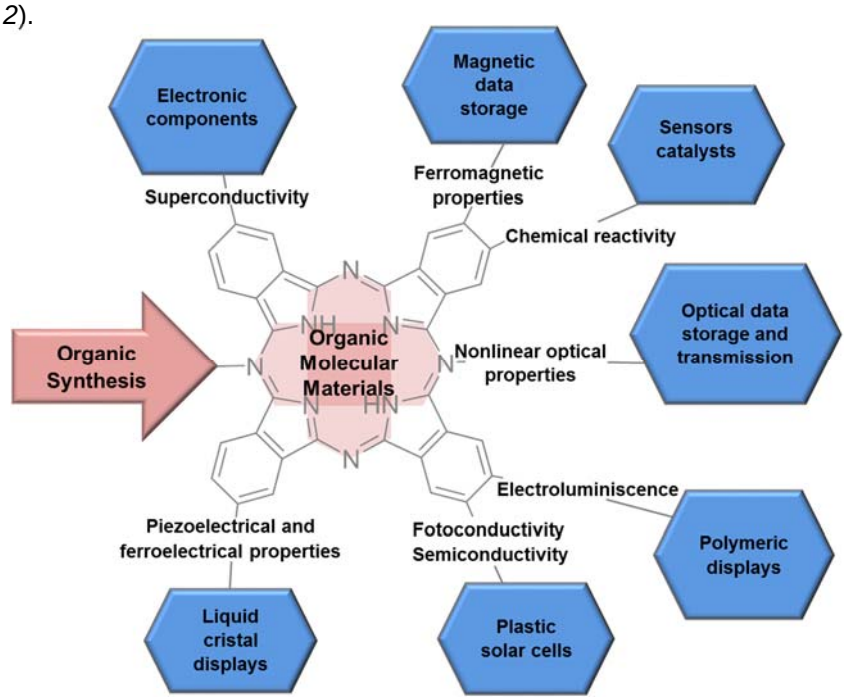

Figure 2.- Some actual and potential applications of organic molecular materials.

Organic molecular systems able to delocalize and transport electron such as π-conjugated polymers[12] or charge-transfer salts[13] may show, if appropriately assembled, conductive, semiconductive or superconductive properties.[14] The chemical or redox characteristics of some organic molecules, together with their semiconducting or optical properties, may be exploited to create highly selective sensors and be applied as catalysts.[15] Ferroelectric liquid crystals[6b] are the basis of an expanding display technology, which is replacing the classic screens based on cathodic rays by high-quality,

[12] a) *Handbook of Conducting Polymers. 3rd Edition* (Ed. T. Skotheim, J. R. Reynolds) CRC Press, **2007**; b) *Design and Synthesis of Conjugated Polymers* (Ed. M. Leclerc, J. F. Morin) Willey-VCH Germany, **2010**; c) A. Facchetti, *Chem. Mater.* **2011**, *23*, 733.
[13] a) C. Rovira, *Chem. Rev.* **2004**, *104*, 5609; b) I. Shinsuke, N. Kensuke, C. Yoshiki, *J. Mater. Chem.* **2007**, *17*, 4122; c) M. Kivala, F. Diedrich, *Acc. Chem. Res.* **2009**, *42*, 235.
[14] a) X. Lu, G. Zhang, W. Wang, X. Li, *Angew. Chem. Int. Ed*. **2007**, *46*, 5772; b) Y. Greenberg, Y. Lumelsky, Y. Silverstein, M. S. Zussman, *J. Mater Sci.* **2008**, *43*, 1664.
[15] K. F. Sun-Joo, R. Guo-Oiang, A. J. Samson, *Chem. Mater*. **2011**, *23*, 682.

less expensive and smaller devices; they are now finding applications in smart windows.[16] For their part, magnetic materials, based on stable radicals (nitroxide radicals), high-spin metal clusters, or their combination, find applications in the field of molecular magnets[17] and data storage.[18] Highly extended π-conjugated systems, formed by cyclocondensation (porphyrins, phthalocyanines) or polymerization (poly(*p*-phenylene vinylenes), polytiophenes) of simple organic molecules, which can absorb and emit light in the visible part of the electromagnetic spectrum, are being intensely studied as active elements for the conversion of light into electricity (solar cells)[19] and viceversa (organic light emitting diodes).[20] Information technology has currently reached the stage where photons are taking the place of electrons as carriers of information, generating faster and more efficient transmission systems. Organic materials with nonlinear optical (NLO) properties,[21] able to manipulate and process optical signals, may constitute very important components in these photonic devices in the handling and processing of optical signals surpassing inorganic materials. This kind of materials are part of photodiodes, organic field-effect transistors (OFETs), polymer grid triodes, organic light-emitting electrochemical cells (OLECs), optocouplers, and lasers.

---

[16] G. M. Debije, *Adv. Func. Mater.* **2010**, *90*, 1498.

[17] a) J. Lehmann, A. Gaita-Arino, E. Coronado, D. Loss, *J. Mater. Chem.* **2009**, *19*, 1672; b) M. Kurmos, *Chem. Soc. Rev.* **2009**, *38*, 1353; c) M. Murrie, *Chem. Soc. Rev.* **2010**, *39*, 1986.

[18] a) E. Coronado, J. R. Galán-Mascarós, C. J. Gómez-García, V. Laukhin, *Nature* **2000**, *408*, 447; b) M. Minguet, D. Luneau, E. Lhotel, V. Villar, C. Paulsen, D. B. Amabilino, J. Veciana*, Angew. Chem. Int. Ed.* **2002**, *41*, 586; d) E. Coronado, P. Day, *Chem. Rev.* **2004**, *104*, 5419; e) Y. Ma, W. Ying, J. Wang, Y. Shang, S. Du, L. Pan, G. Li, L. Yang, H. Gao, Y. Song, *J. Phys. Chem. C* **2009**, *113*, 8548.

[19] a) N. S. Sariciftci, D. Braun, C. Zhang, V. Srdanov, A. J. Heeger, G. Stucky, F. Wudl, *Appl, Phys. Lett.* **1993**, *62*, 585; b) J. J. M. Halls, C. A. Walsh, N. C. Greenham, E. A. Marseglia, R. H. Friend, S. C. Moratti, A. B. Holmes, *Nature* **1995**, *376*, 498; c) S. Guenes, H. Neugebauer, N. S. Sariciftci, *Chem. Rev*. **2007**, *107*, 1324; d) G. Dennler, C. M. Schaber, C. J. Brabec, *Adv Mater.* **2009**, *19*, 1672; e) Y. J. Cheng, S. H. Yang, H. Seng, S. Chain, *Chem. Rev.* **2009**, *19*, 5690; f) C. J. Brabec, S. Gowrisanker, J. M. J. Halls, D. Laird, S. Jia, P. S. Williams, *Adv. Mater.* **2010**, *22*, 3839.

[20] a) J. H. Burroughes, D. D. C. Bradley, A. R. Brown, R. N. Marks, K. Mackay, R. H. Friend, P. L. Burn, A. B. Holmes, *Nature* **1990**, *347*, 539; b) *Organic Light Emitting Devices: Synthesis, Properties and Applications***,** (Eds. K. Mullen, U. Scherf), Wiley-VCH, **2006**; c) J. Li, D. Liu, *J. Mater. Chem.* **2009**, *19*, 7584; d) Y. Tao, C. Yang, J. Qin, *Chem Rev.* **2011**, *40*, 2943. e) L. Xiao, Z. Chen, B. Qu, J. Luo, S. Kong, Q. Gong, J. Kido, *Adv. Mater.* **2011**, *23*, 926.

[21] a) I. Ledoux, J. Zyss, *Chem. Rev*. **1994**, *94*, 77; b) *Nonlinear Optics of Organic Molecules and Polymers* (Ed. H.S. Nalwa, S. Miyata), CRC Press, **1997**; c) G. de la Torre, P. Vázquez, F. Agulló-López, T. Torres, *Chem. Rev*. **2004**, *104*, 3723; d) J. E. Gualteri, M. H. Levi, J. S. Garth, *Chem. Phys. Lett.* **2008**, *133*, 467; e) H. C. Parsh, *Chem. Rev.* **2010**, *110*, 5332.

Phthalocyanines as organic molecular materials

Structure of phthalocyanines

Among the huge variety of organic compounds that can give rise to molecular materials, metallomacrocycles are worth of mention.[22] In this group, phthalocyanines (Pcs)[23] (*Figure 3*) hold a privileged position due to their interesting electronic and physicochemical characteristics, the possibility of organization into different condensed systems, and their multiple applications (dyes, gas sensors, catalysts, optoelectronic devices).

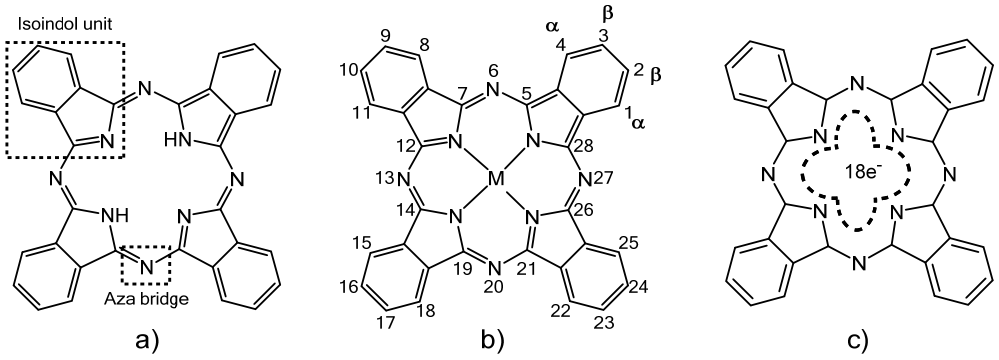

Figure 3.- a) Free-base phthalocyanine; b) metallophthalocyanine; c) main electronic delocalization mode in phthalocyanines.

Pcs are planar aromatic macrocycles constituted by four isoindole units linked together through nitrogen atoms. In *Figure 3* the structures of metal-free and

[22] H. Schultz, H. Lehmann, M. Rein, M. Hanack, *Structure and Bonding 74* (Ed. J. W. Buchler), Springer, Berlin, **1991**, pp. 41-146.

[23] a) *Phthalocyanines. Properties and Applications* (Eds. C. C. Leznoff, A.B.P. Lever), VCH Publishers (LSK) Ltd., Cambridge, **1996**, vols. 1-4; b) *Phthalocyanine Materials. Synthesis, Structure and Function* (Ed. N. B. McKeown), Cambridge University Press, Cambridge, 1998; c) M. Hanack, H. Heckmann, R. Polley in *Methods of Organic Chemistry* (*Houben-Weyl*) (Ed. E. Schaumann), Georg Thieme Verlag, Stuttgart, **1998**, vol. E 9d, p. 717; d) N. Kobayashi, *Curr. Opinion Solid-State Mater. Sci.* **1999**, *4*, 345; e) G. de la Torre, M. Nicolau, T. Torres, *Supramolecular Photosensitive and Electroactive Materials* (Ed. H. S. Nalwa), Academic Press, New York, **2001**, p. 1-111; f) G. de la Torre, C. G. Claessens, T. Torres, *Chem. Comm*. **2007**, 2000; g) M. V. Martínez-Díaz, M. Quintiliani, T. Torres, *Synlett* **2008**, *1*, 1; h) C. G. Claessens, U. Hahn, T. Torres, *Chem. Record*. **2008**, 8, 75; i) Y. Rio, M. S. Rodríguez-Morgade, T. Torres, *Org. Biomol. Chem.* **2008**, *6*, 1877; j) *Structure and Bonding Vol. 135: Fuctional Phthalocyanine Molecular Materials* (Ed. D. M. P. Mingos), Springer, Berlin, **2010**; k) J. Mack, N. Kobayashi, *Chem. Rev.* **2011**, *111*, 281.

metallophthalocyanines, as well as the numbering scheme traditionally used for their nomenclature are shown. The internal and external positions of the fused benzene ring are also commonly known as α- and β-positions, respectively. Their 42 π-electrons are distributed over 32 carbon and 8 nitrogen atoms, but the electronic delocalization mainly takes place on the inner ring, which is constituted by 16 atoms and 18 π-electrons (*Figure 3c*), the outer benzene rings maintaining their electronic structure.[24]

One of the most important attributes of this kind of molecules is their high thermal, chemical and electromagnetic stability, which is a common requirement for most technological applications. They can be heated up to 500 ºC under high vacuum without decomposition, resist the action of non-oxidizing acids and bases, and they are optically stable, tolerating high intensity electromagnetic radiation. Nevertheless, the most remarkable feature that makes these molecules play an exceptional role in the area of material science is their chemical versatility. The hydrogen atoms of the central cavity can be replaced by more than 70 different elements, generating the metallophthalocyanines (MPcs; *Figure 3b*).[23a,b] However, as the coordination number of the macrocycle is four, according to the size and oxidation state of the metal, one or two (in the case of alkalines) can be included into the Pc core. When the metal prefers a higher coordination number, pyramidal, tetrahedral, or octahedral structures result, with one or two axial ligands (*Figure 4a*).[25] Actinide and lanthanide metals give rise to sandwich-type structures with octahedral coordination in which the metal is located between two Pc rings (*Figure 4b*).[26] This structure will be widely explored in *Chapter 2*.

[24] E. Ortí, J. L. Brédas, *J. Chem. Phys.* **1988**, *89*, 1009.

[25] a) M. Hanack, S. Deger, A. Lange, *Coord. Chem. Rev.* **1988**, 115. b) M. Brewis, G. J. Clarkson, V. Goddard, M. Helliwell, A. M. Holder, N. B. McKeown, *Angew. Chem. Int. Ed.* **1998**, *37*, 1092. c) M. Hanack, H. Heckmann, *Eur. J. Inorg. Chem.* **1998**, 367. d) G. Y. Yang, M. Hanack, Y. W. Lee, Y. Chen, M. K. Y. Lee, D. Dini, *Chem. Eur. J.* **2003**, *9*, 2758. e) A. N. Cammidge, G. Berber, I. Chambrier, P. W. Hough, M. J. Cook *Tetrahedron*, **2005**, *61*, 4067. f) K. Kameyana, M. Morisue, A. Satake, Y. Kobuke, *Angew. Chem. Int. Ed*. **2005**, *44*, 4763. g) B. Ballesteros, G. de la Torre, T. Torres, G. L. Hug, G. M. Aminur Rahman, D. M. Guldi, *Tetrahedron* **2006**, *62*, 2097. h) M. S. Rodríguez-Morgade, T. Torres, C. Atienza-Castellanos, D. M. Guldi, *J. Am. Chem. Soc*. **2006**, *128*, 15145.

[26] a) I. S. Kirin, P. N. Moskalev, *Russ. J. Inorg. Chem*. **1971**, *16*, 1687. b) J. Silver, P. J. Lukes, P. K. Hey, J. M. O'Connor, *Polyhedron*, **1989**, *8*, 1631. c) C. Ercolani, A. M. Paoletti, G. Pennesi, G. Rossi, A. Chiesi-Villa, C. Rizzoli, *J. Chem. Soc., Dalton Trans*., **1990**, 1971. d) A. Capobianchi, C. Ercolani, A. M. Paoletti, G. Pennesi, G. Rossi, A. Chiesi-Villa, R. Rizzoli, *Inorg. Chem*. **1993**, *32*, 4605. e) I. Chambrier, D. L. Hughes, J. C. Swarts, B. Isare, M. J. Cook, *Chem. Comm*. **2006**, 3504. f) B. Ballesteros, G. de la Torre, A. Shearer, A. Hausman, M. A. Herranz, D. M. Guldi, T- Torres, *Chem. Eur. J*. **2010**, *16*, 114.

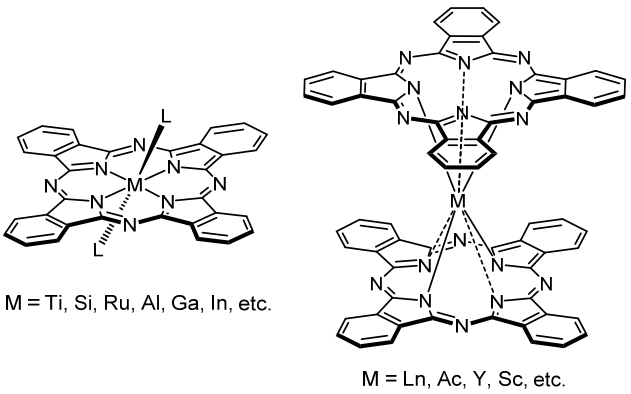

Figure 4.- a) Axial coordination of phthalocyanines; b) bisphthalocyanine.

Unsubstituted Pcs are highly insoluble in solvents other than aromatics with high boiling point like quinoline, chlorobenzene, α-chlorobenzene, nitrobenzene, or strong mineral acids, like sulfuric acid. To increase the solubility of Pcs in common organic solvents or even in aqueous media, a wide variety of substituents can be attached either axially or at the periphery of the macrocycle. Furthermore, this also permits to alter the electronic structure of the system and consequently the properties, and/or the formation of specific and highly ordered condensed phases.

The basic structure of the macrocyle may also be rationally modified, giving rise to Pc analogues (*Figure 5*),[27] via the following strategies: a) atom substitution;[27a] b) extension of the aromatic system;[27c,f] c) formation of dimers or oligomers;[27d] d) variation in the number of isoindole units;[27g] e,f) substitution of one or several isoindole units.[27b,h]

[27] a) N. Kobayashi en Ref. 23a, vol. 2, pp. 97-161; b) S. V. Kudrevich, J. E. van Lier, *Coord. Chem. Rev.* **1996**, *156*, 163; b) M. Nicolau, B. Cabezon, T. Torres, *Coord. Chem. Rev*. **1999**, *231*, 190; c) N. Kobayashi, H. Miwa, V. N. Nemykin, *J. Am. Chem. Soc*. **2002**, *124*, 8007; d) C. G. Claessens, T. Torres, *Angew. Chem. Int. Ed*. **2002**, *41*, 2561; e) G. Y. Yang, M. Hannack, Y. W. Lee, Y. Chen, M. K. Y. Lee, D. Dini, *Chem. Eur. J*. **2003**, *9*, 2758; f) N. Kobayashi, S.-I. Nakajima, H. Ogata, T. Kukuda, *Chem. Eur. J*. **2004**, *10*, 6294; g) T. Torres, *Angew. Chem. Int. Ed*. **2006**, *45*, 2834; h) A- Muranaka, M. Yonehara, M. Uchiyama, *J. Am. Chem. Soc*. **2010**, *132*, 7844**.**

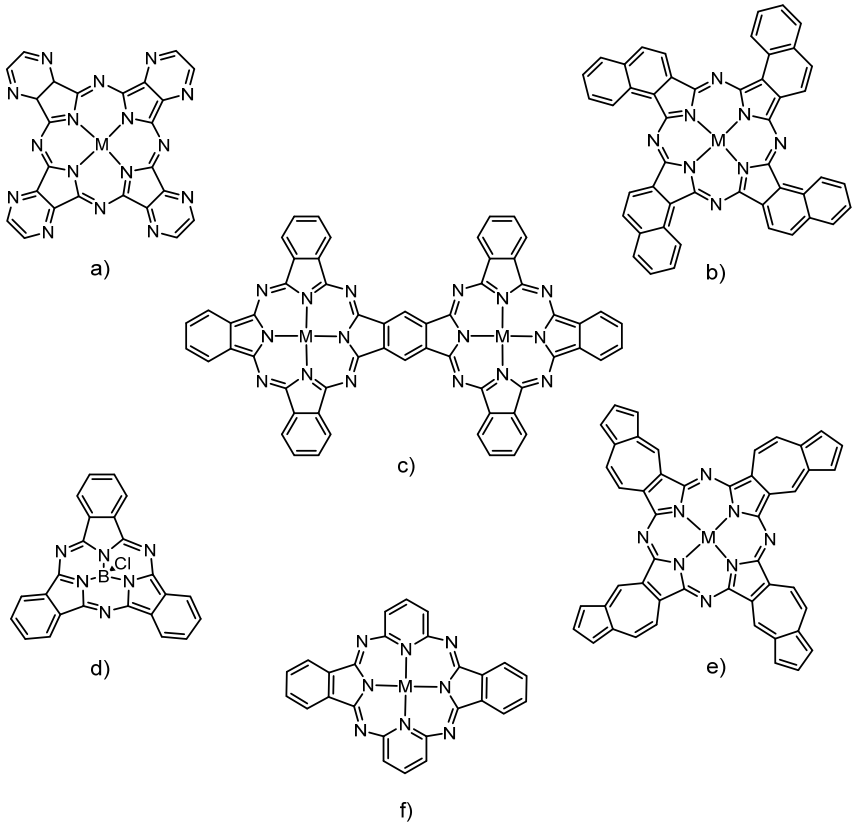

Figure 5.- Phthalocyanine analogues: a) tetrapyrazinoporphyrazine; b) 1,2-naphthalocyanine; c) diphthalocyanine; d) subphthalocyanine; e) azulenecyanine and f) pyridinohemiporphyrazine

Pcs absorb radiation corresponding to visible light and have a high optical stability, reason why Pcs have been traditionally used as dyes and pigments in textile industry and paintings. Moreover, their high extinction coefficient and the photophysical characteristics of their excited states, are continuously finding new applications in distinct fields. During the last years, a lot of effort has been devoted to the synthesis and study of water soluble compounds as photosensitizers in photodynamic therapy for cancer.

The electronic absorption spectrum of these compounds (*Figure 6a*) presents two main bands, the Q-band and the Soret or B-band. The former is usually found in the region of 620-700 nm, and is responsible for the green or blue color of these compounds. This single main band is associated to π-π^* HOMO-LUMO transitions from doubly degenerated orbitals (*Figure 6b*). In the case of metallophthalocyanines, having lower symmetry (D_{4h}), the LUMO is degenerated and only one band is observed. In contrast, the Q-band of metal-free phthalocyanines is split, due to their D_{2h} symmetry. The Soret

band is situated at higher energies in the spectrum and is related to π-π* transitions from lower-energy molecular orbitals.

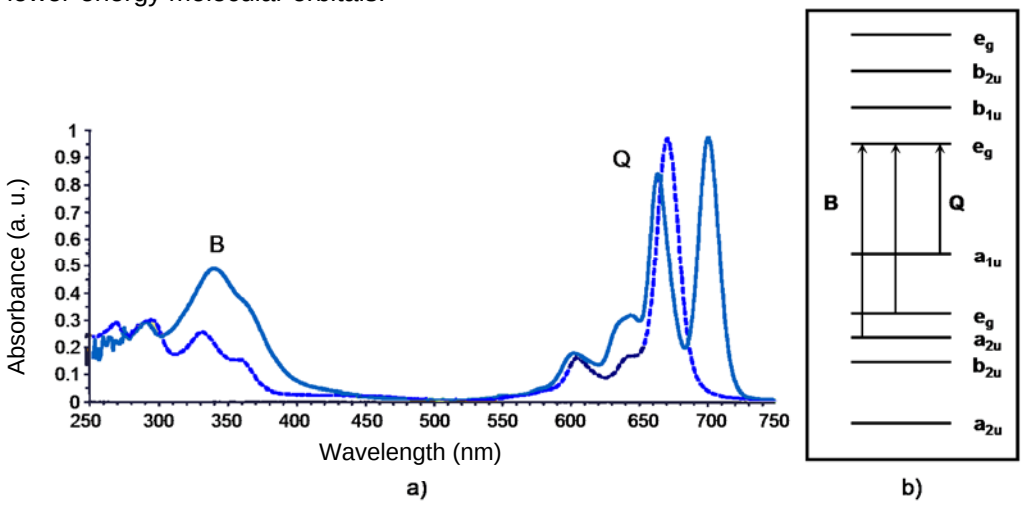

Figure 6.- a) UV-visible spectra of free-base phthalocyanine (solid line) and metallophthalocyanine (dashed line); b) schematic reprentation of the energetic levels and transitions (Q- and B-band) in a metallophthalocyanine.

The chemical versatility of Pcs is associated to the versatility of their electronic and optical properties. The central atom modulates the spectral features depending on their nature or oxidation state. It is also possible to modify the position of the Q-band by extending the aromatic structure of the macrocycle by condensation of benzene rings.[27c,f,h 28] The Q-band of unsymmetrical metallated Pcs, generally leads to a splitting of the band due to a reduction of the symmetry.

Synthesis of phthalocyanines

Symmetrically substituted phthalocyanines

The synthesis of symmetrically substituted Pcs (A_4), that is, bearing identical substituents in each of the four isoindole (A), can be carried out by cyclotetramerization of appropriately substituted precursors, usually phthalonitriles or diiminoisoindolines, or less commonly, by chemical modification over the Pc ring itself. If a metal salt is employed, it acts as a template yielding the corresponding metallophthalocyanine. The most common synthetic methods are depicted in *Scheme 1*.

[28] a) E. Orti, M. C. Piqueras, R. Crespo, J. L. Brédas, *Chem. Mat*. **1990**, *2*, 110. b) E. Orti, R. Crespo, M. C. Piqueras, F. Tomas, *J. Mater. Chem*. **1996**, *6*, 1751.

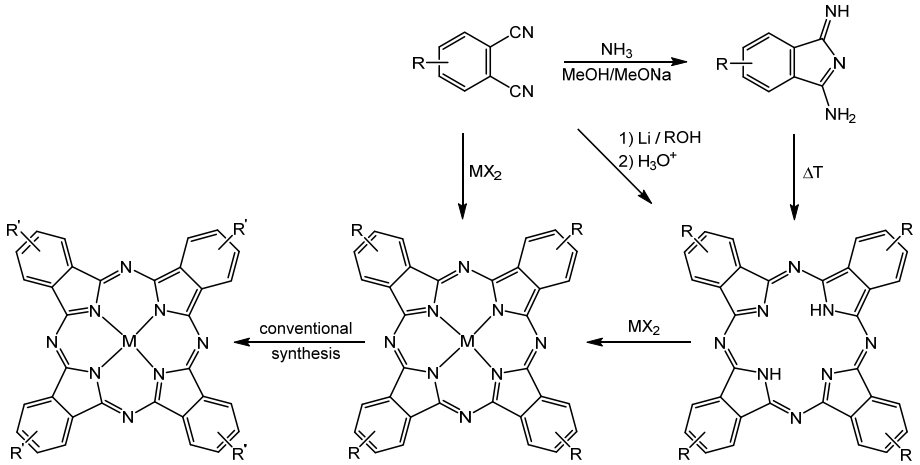

Scheme 1.- Synthesis of tetrasubstituted phthalocyanines.

The most usual method to prepare metallophthalocyanines is the metal-templated reaction of the corresponding phthalonitrile in a solvent with high boiling point (DMAE, DMF, *o*-DCB), where a mixture of phthalonitrile and metal salt is heated. On the other hand, the synthesis of metal-free Pcs is usually carried out employing 1,3-diiminoisoindolines in the same reaction conditions. With phthalonitriles, a basic catalyst as 1,8-diazabicyclo[5.4.0]undec-7-ene (DBU)[29] is employed in the presence of an alcohol, such as *N*,*N*-dimethylaminoethanol or 1-pentanol. Lithium alkoxides are also used with phthalonitriles, giving rise to the lithium Pcs that can be easily converted into the free base by treatment with a mineral acid.[30] Otherwise, free-base Pcs at refluxing temperature of a high-boiling point solvent, in the presence of a metal salt, will be metallated. Moreover, new methods that allow to prepare Pcs with higher efficiencies and rather mild conditions have been described. Treatment of phthalonitriles with metal salts and hexamethyldisilazane in DMF,[31] a double-addition of oximes to phthalonitriles,[32] or the use of microwave radiations.[33]

In the case of using 3- or 4-substituted phthalonitriles as starting materials, the resulting tetrasubstituted Pcs are obtained as mixtures of four structural isomers with C_{4h},

[29] H. Tomoda, S. Saito, S. Ogawa, S. Shiraishi, *Chem. Lett*. **1980**, *9*, 1277.
[30] C. C. Leznoff, M. Hu, K. J. M. Nolan, *Chem. Comm.* **1996**, 1245.
[31] H. Uchida, H. Tanaka, H. Yoshiyama, P. Y. Reddy, S. Nakamura, T. Toru, *Synlett* **2002**, 1649.
[32] M. N. Kopylovich, V. Y. Kukushkin, M. Haukka, K. V. Luzyanin, A. J. L. Pombeiro, *J. Am. Chem. Soc.* **2004**, *126*, 15040.
[33] a) A. Loupy, D. Bogdal, A. Petit, *Tetrahedron*, **2005**, *61*, 179; b) I. Acar, H. Kantekin, Z. Biyikliouglu, *J. Organomet. Chem.* **2009**, *695*, 151; c) A. Was, E. Kaya, C. Elif, H. Kantekin, A. Soeknen, X. Cakir, *J. Organomet. Chem.* **2011**, *696*, 1659.

D_{2h}, C_{2v} and C_{2s} symmetries (*Figure 7*),[34] that sometimes can be separated by chromatographic techniques[35] or obtained separately employing a regioselective synthesis of Pcs.[36]

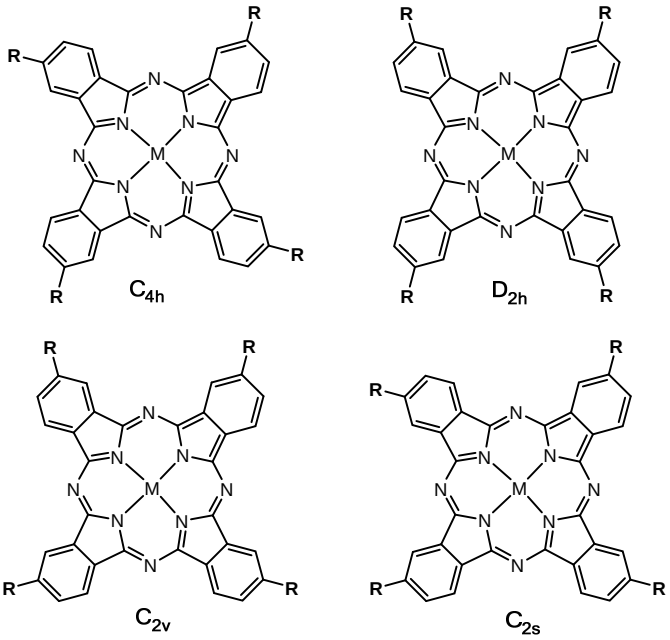

Figure 7.- Structures of the four constitutional isomers of 2(3)-tetrasubstituted metallophthalocyanines.

[34] a) M. Sommerauer, C. Rager, M. Hanack, *J. Am. Chem. Soc.* **1996**, *118*, 1085; b) S. Rodriguez-Morgade, M. Hanack, *Chem. Eur. J.* **1997**, *3*, 7.

[35] a) G. Schmid, M. Sommerauer, M. Hanack, *Angew. Chem. Int. Ed.* **1993**, *32*, 1422; b) S. Rodriguez-Morgade, M. Hanack, *Chem. Eur. J.* **1997**, *3*, 1042; c) W. D. Dabney, F. G. Anila, R. Brian *J. Porphyrins Phthalocyanines* **2004**, *8*, 1300; d) S. Shimizu, H. Zhu, N. Kobayashi, *Chem. Eur. J.* **2010**, *16*, 11151.

[36] a) N. Kobayashi, Y. Kobayashi, T. Osa*, J. Am. Chem. Soc.* **1993**, *115*, 10994; b) D. M. Drew, C. C. Leznoff, *Synlett* **1994**, 623; c) D. M. Drew, C. C. Leznoff, *Can. J. Chem.* **1996**, *74*, 307; d) M. Brewis, G. J. Clarkson, P. Humberstone, S. Makhseed, N. B. McKeown, *Chem. Eur. J.* **1998**, *4*, 1633; e) M. Kimura, Y. Sugihara, T. Muto, K. Hanabusa, H. Shirai, N. Kobayashi, *Chem. Eur. J*. **1999**, *5*, 3495; f) C. C. Leznoff, Z. Li, H. Isago, A. M. D'Ascanio, D. S. Terekhov, *J. Porphyrins Phthalocyanines* **1999**, *3*, 406; g) N. Iida, K. Tanaka, E. Tokunaga, H. Takahashi, N. Shibata, *ChemistryOpen* **2015**, *4*, 102.

Unsymetrically substituted phthalocyanines

The synthesis of Pcs with two different substitution patterns in the isoindole units (A and B) is a more difficult task, and the methodology employed will be chosen depending on the kind of substituents required and on their relative distribution in the final macrocyle (A_3B, A_2B_2 or ABAB).[37] A brief description of the most important methods follows.

a) Solid-phase synthesis[38]

In this method, a phthalonitrile or diiminoisoindoline (B), linked to an insoluble polymer or an inorganic holder, is made to react with an excess of a differently functionalized phthalonitrile or diiminoisoindoline (A). The A_3B phthalocyanine formed is, in a second step, cleaved from the polymer (*Scheme 2*).

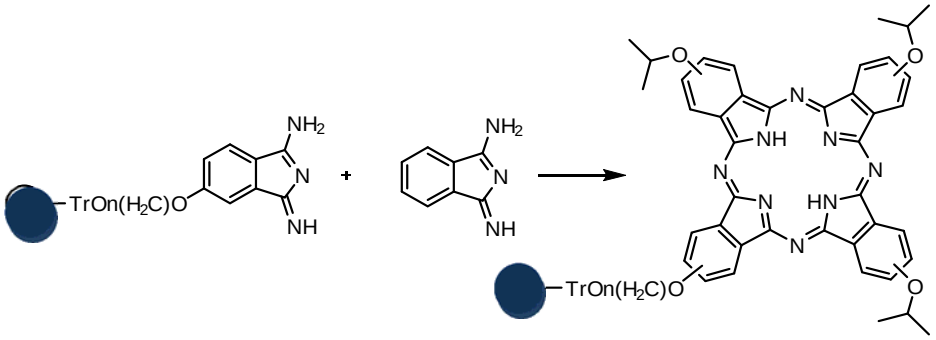

Scheme 2.- Example of solid-phase synthesis of A_3B Pcs

b) Ring expansion reaction[39]

The geometrically constrained subphthalocyanine macrocycle (A_3) may be opened by reaction with a differently substituted diiminoisoindoline (B). Ultimately, the open tetramer formed self-condenses to selectively give an A_3B phthalocyanine, but usually mixtures of non desired by-products are also formed (*Scheme 3*).

---

[37] a) T. Torres, *J. Porphyrins Phthalocyanines* **2000**, *4*, 325; b) G. de la Torre, C. G. Claessens, T. Torres, *Eur. J. Org. Chem*. **2000**, 2821; c) G. de la Torre, T. Torres, *J. Porphyrins Phthalocyanines* **2002**, *6*, 274.

[38] a) C. C. Leznoff, T. W. Hall, *Tetrahedron Lett.* **1982**, *23*, 3023; b) A. Hirth, A. K. Sobbi, D. Wohrle, *J. Porphyrins Phthalocyanines* **1997**, *1*, 275; c) S. S. Erdem, I. V. Nesterova, S. A. Soper, R. P. Hammer, *J. Org. Chem.* **2008**, *73*, 5003; d) M. Mudyina, N. M. Ndingury, A. S. Steven, P. R. Hammer, *J. Porphyrins Phthalocyanines* **2010**, *14*, 891.

[39] a) A. Weitemeyer, H. Kliesch, D. Whorle, *J. Org. Chem.* **1995**, *60*, 4900 ; b) A. Sastre, T. Torres, M. Hanack, *Tetrahedron Lett.* **1995**, *36*, 8501 ; c) A. Sastre, B. del Rey, T. Torres. *J. Org. Chem.* **1996**, *61*, 8591 ; d) A. G. Gurek, O. Bekaroglu, *J. Porphyrins Phthalocyanines* **1997**, *1*, 227.

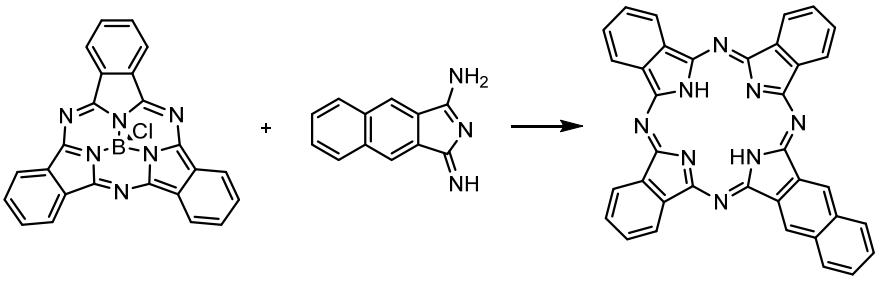

Scheme 3.- Example of ring expansion reaction.

c) Cross-condensation reaction[40,41]

This methodology lies on the reaction between diiminoisoindolines or phthalonitriles (A) and previously dimerized phthalonitriles or diiminoisoindolines (B_2), to yield A_2B_2 phthalocyanines,[40] or precursors that cannot self-condense (B), to obtain ABAB phthalocyanines.[41] Among the latest, the most important derivatives are the 1,1,3-trichloroisoindolenines and phthalonitriles or diiminoisoindolines bearing bulky substituents in the 3- and 6- positions of the benzene ring (*Scheme 4*).

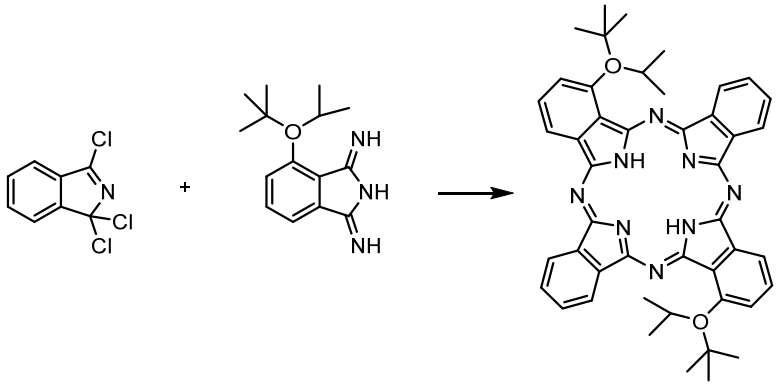

Scheme 4.- Example of cross-condensation reaction.

[40] a) K. J. M. Nolan, M. Hu, C. C. Leznoff, *Synlett* **1997**, 593 ; b) N. Kobayashi, *Chem. Comm.* **1998**, 487 ; c) H. Miwa, N. Kobayashi, *Chem. Lett.* **1999**, 1303; d) N. Kobayashi, H. Miwa, H. Isago, T. Tomura, *Inorg. Chem.* **1999**, *38*, 479.

[41] a) J. G. Young, W. Onyebuagu, *J. Org. Chem.* **1990**, *55*, 2155; b) N. Kobayashi, T. Ashida, T. Osa, *Chem. Lett.* **1992**, 2031; c) S. Dabak, O. Bekaroglu, *New J. Chem.* **1997**, *21*, 267; d) M. Hanack, P. Stihler, *Eur. J. Org. Chem.* **2000**, 303; e) J-. D. Wang, M-. J. Lin, S-. F. Wu, Y. Lin, *J. Organomet. Chem.* **2006**, *691*, 5074.

d) Statistical cyclotetramerization[37]

This is the most utilized methodology, due to its simplicity. It is based on the mixed condensation of two differently functionalized phthalonitriles or diiminoisoindolines (A and B) to produce a mixture of Pcs (*Figure 8*) that, in a second step, are separated by chromatography. Usually, this approach is widely used to prepare A_3B compounds since, when using statistical means, A_2B_2 isomers are quite difficult to separate by chromatographic techniques. Some factors, such as the steric effect of the substituents (employing bulky groups to supress aggregation), the relative reactivity of the different precursors and their relative amount in the reaction (employing a 3:1 molar ratio means that A and B present similar reactivity), have to be taken into account in this case in order to increase the yield of the desired A_3B Pc and facilitate its isolation.

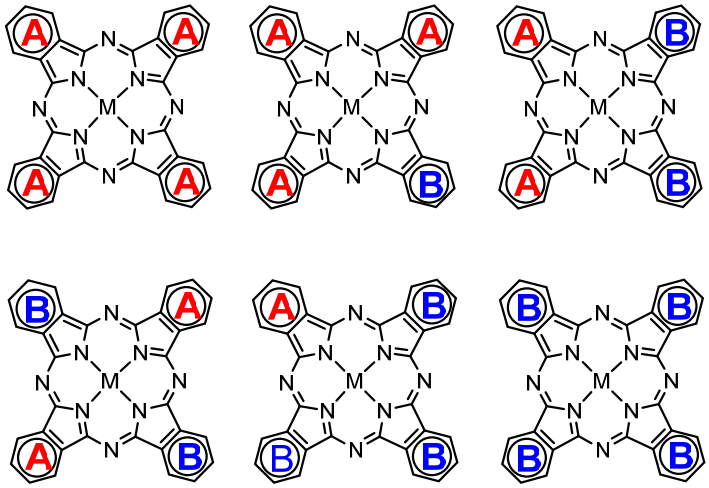

Figure 8.- Mixture of phthalocyanines obtained via statistical cyclotetramerization of two differently functionalized phthalonitriles or diiminoisoindolines, A and B.

Concerning the mechanism of formation of Pcs, several pathways have been proposed. There are, however, some common features to all these mechanistic proposals.[42] In general, the macrocyclization in the presence of sodium of lithium alkoxide usually starts with the formation of the corresponding salt of 1-imido-3-alcoxyindoline (*Scheme 5A*).[43] The next step in the reaction sequence is the nucleophilic attack of this intermediate to the cyano group of another phthalonitrile molecule. A dimer is formed

[42] a) C. R. Rager, G. Schmid, M. Hanack*, Chem. Eur. J.* **1999**, *5*, 280; b) C. C. Leznoff, A. M. Castaño, S. Z. Yildiz, *J. Porphyrins Phthalocyanines* **2000**, *4*, 103.
[43] S. W. Oliver, T. D. Smith, *J. Chem. Soc. Perkin Trans. II* **1987**, 1579.

(*Scheme 5B*), which can now either react with another phthalonitrile unit in the same way to form a trimer (*Scheme 5C*), or undergo self-condensation (*Scheme 5D*).

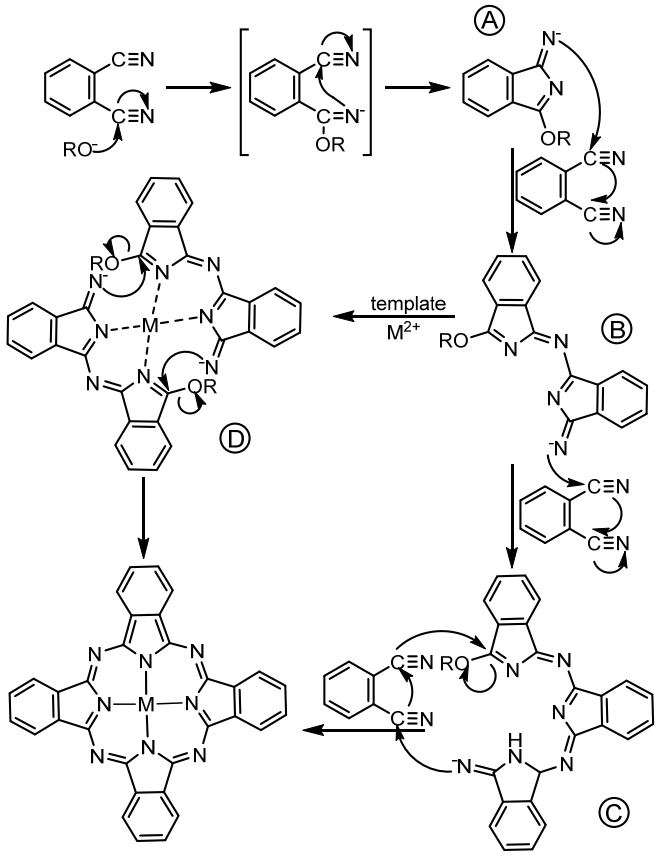

Scheme 5.- Proposed mechanism for the synthesis of metallophthalocyanines by cyclotetramerization of phthalonitriles in the presence of a metal salt.

Another possibility consists on the metal-mediated formation of the Pc ring,[44] that is, a metal cation acts as a template to which the reacting phthalonitriles coordinate during the macrocyclization.

Organization of phthalocyanines

Pc molecules exhibit a natural tendency to aggregate through π-π interactions between the aromatic rings which, together with the suitable choice of the substituents

[44] a) V. W. Day, T. J. Marks, W. A. Wachter, *J. Am. Chem. Soc*. **1975**, *97*, 4519; b) D. Bush, N. Stephenson*, Coord. Chem. Rev*. **1990***, 100,* 119.

and the central element, assist in the formation of multiple and highly ordered condensed phases. In many cases, the type of supramolecular architecture formed can be predicted and it will determine the final properties and applications of the material.[45] So far, the most important organized structures are the following:

a) Crystals[46]

Pcs generally organize into two kinds of polymorphic crystals: the α form and the more thermodynamically stable β crystalline form (*Figure 9*). The main difference between the two of them is the magnitude of the angle between the axis of symmetry of the macrocycle and the stacking axis.

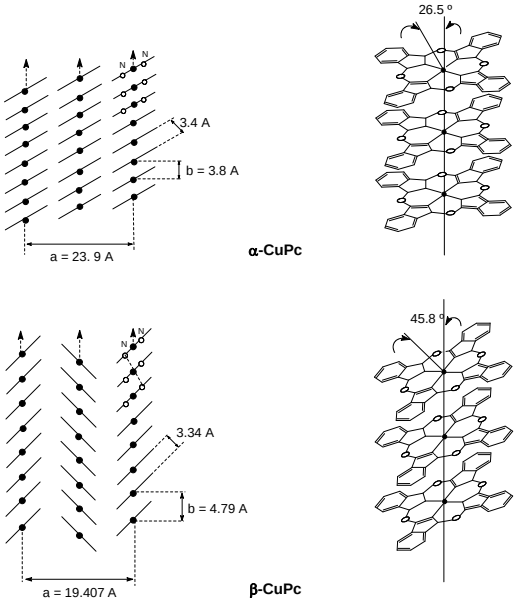

Figure 9.- α and β polymorphic crystalline forms of CuPc.

b) Liquid crystals

In these systems, the Pc is usually substituted by several lipophilic chains that interact creating a fluid medium around the planar aromatic cores, which stack together giving rise to columnar discotic mesophases (*Figure 10*) arranged with different

[45] a) C. F. van Nostrum, R. J. M. Nolte, *Chem. Comm*. **1996**, 2385; b) H. Engelkamp, S. Middelbeek, R. J. M. Nolte, *Science* **1999**, *284*, 785.

[46] a) D. Cho-an, G. Yu, Y. Liu, Y. Guo, X. Sun, J. Zheng, Y. Wen, W. Wu, D. Zhu, Chem. Mater. **2009**, *21*, 4873. b) N. A. Cammidge, H. C. Tseng, I. Chambrier, D. Hughes, J. M. Cook, *Tetrahedron Lett.* **2009**, *50*, 5254. c) T. Honda, T. Kojima, N. Kobayashi, S. Fukuzumi, *Angew. Chem. Int. Ed.* **2011**, *50*, 2725.

bidimensional symmetries (hexagonal, tetragonal). The first mesogenic Pc was synthesized by J. Simon and coworkers in 1982.[47] Since then, a substantial number of liquid crystal Pcs has been described.[48]

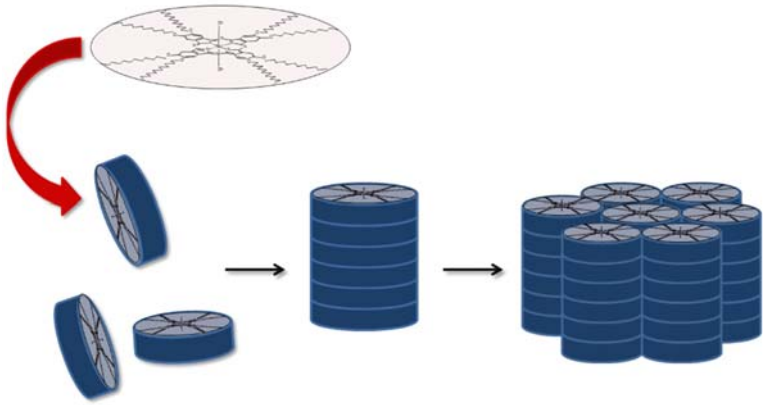

Figure 10.- Example of a liquid-crystalline pthalocyanine.

c) Cofacial polymers

The central atom of the Pc plays a key role in this kind of organization, since the macrocycles can be polymerized through the bridging ligands that connect two central metal atoms, in the so-called "shish-kebab" arquitecture.[49] Likewise, the incorporation of crown ether moieties help to form columnar aggregates in the presence of metal salts (*Figure 11*), due to complexation of the cation together with solvent effects. The aggregated formed with this kind of molecules consist of untilted stacks of eclipsed Pcs.[50]

[47] a) J. Simon, P. Bassoul en Ref. 23b, vol. 2, pp. 223-299.

[48] a) B. del Rey, M.V. Martinez-Diaz, J. Barbera, T. Torres, *J. Porphyrins Phthalocyanines* **2000**, *4*, 569; b) J. C. Swarts, E. H. G. Langner, N. Krokeide-Hove, M. J. Cook, *J. Mater. Chem.* **2001**, *11*, 434; c) J. Hoogboom, P. M. L. Garcia, M. B. J. Otten, J. A. A. W. Elemans, J. Sly, S. V. Lazarenko, T. Rasing, A. E. Rowan, R. J. M. Nolte*, J. Am. Chem. Soc*. **2005**, *127*, 11047; d) A. de la Escosura, M. V. Martinez-Diaz, J. Barbera, T. Torres, *J. Org. Chem.* **2008**, *73*, 1475; e) T. V. Basova, M. Durmus, A. G. Gurek, V. Ahsen, A. Hassan, *J. Phys. Chem. C* **2009**, *21*, 4688; f) M. Ince, M. V. Martinez-Diaz, J. Barbera, T. Torres, *J. Mater. Chem*. **2011**, *21*, 1531.

[49] a) M. Hanack, M. Lang, *Adv. Mat*. **1994**, *6*, 819; b) N. Kobayashi, *Coord. Chem. Rev*. **2002**, *227*, 129; c) P. Samorí, H. Engelkamp, P. A. J. de Witte, A. E. Rowan, R. J. M. Nolte, J. P. Rabe, *Adv. Mater*. **2005**, *17*, 1265; d) P. Chen, X. Ma, M. Liu, *Macromolecules* **2007**, *40*, 4780.

[50] a) C. F. van Nostrum, S. Jv. Picken, R. J. M. Nolte, *Angew. Chem. Int. Ed.* **1994**, *33*, 2173; b) C. F. van Nostrum, S. J. Picken, A.–J. Schouten, R. J. M. Nolte, *J. Am. Chem. Soc*. **1995**, *117*, 9957; c) N. Kobayashi, M. Togashi, T. Osa, K. Ishii, S. Yamauchi, H. Hino, *J. Am. Chem. Soc*. **1996**, *118*, 1073; d) H. Engelkamp, S. Middelbeek, R. J. M. Nolte, *Science* **1999**, *284*, 785; e) J. Sly, P. Kasak, E.

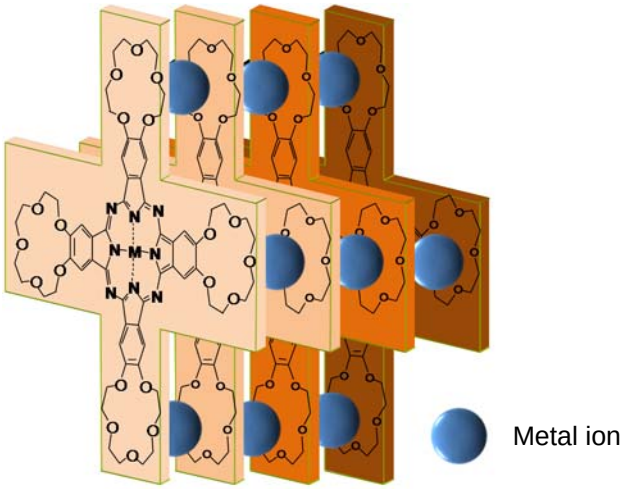

Figure 11.- Schematic representation of the complexes formed by a crown ether substituted Pc and potassium picrate.

d) Thin films

The most direct way to incorporate Pcs in electronic devices is probably by means of thin films, which can be readily prepared by vacuum sublimation,[51] polymeric matrix scattering[52] or spin-coating.[53] Highly ordered Pc films have been prepared by the LB technique and by self-assembly of thiol-substituted macrocycles onto a gold surface.

e) Nanostructures on surfaces

Pcs can self-organize giving rise to nanowires and nanoribbon structures,[54] among others, by organic vapor-phase deposition. The nature of the nanostructure

Gomar-Nadal, C. Rovira, L. Gorriz, P. Thordarson, D. B. Amabilino, A. E. Rowan , R. J. M. Nolte, *Chem. Comm*. **2005**, 1255 ; f) N. Sheng, Y. Zhang, H. Xu, M. Bao, X. Sun, J. Jiang, *Eur. J. Inorg. Chem*. **2007**, 3268.

[51] a) G. E. Collins, V. S. Williams, L.-K. Chau, K. W. Nebesny, C. England, P. A. Lee, T. Lowe, Q. Fernando, N. R. Armstrong, *Synth. Met*. **1993**, *54*, 351; b) M. Yoon, A. Facchetti, C. E. Stern, T. J. Marks, *J. Am. Chem. Soc.* **2006**, *128*, 5792.

[52] T. Minami, K. Sasaki, K. Tsuda, *J. Appl. Phys.* **1983**, *54*, 6764.

[53] a) M. J. Cook, *J. Mater. Chem*. **1996**, *6*, 677; b) M. J. Cook, *Pure Appl. Chem*. **1999**, *71*, 2145; c) S. Xiao, M. Myers, Q. Miao, S. Sanaur, K. Pang, M. L. Steigerwald, C. Nuckolls, *Angew. Chem. Int. Ed.* **2005**, 44, 7390; c) A. Hirao, T. Akiyama, T. Okujima, H. Yamada, H. Uno, Y. Sakai, A. Yoshimasa, S. Aramaki, N. Ono, *Chem. Comm.* **2008**, 4714.

[54] a) W. Y. Tong, A. B. Djurisic, M. H. Xie, A. C. M. Ng, K.Y. Cheung, W. K. Chan, Y. H. Leung, H. W. Lin, S. Gwo, *J. Phys. Chem. B*, **2006**, *110*, 17406 ; b) M. V. Martinez-Diaz, G. Bottari, *J. Porphyrins Phthalocyanines* **2009**, *13*, 471.

depends on the kind of surface and the deposition conditions. In this way, some Pcs have been deposited on graphite,[55] Au(111)[56] and Cu(111).[57]

The utilization of solution-processable techniques for the fabrication of Pc-based nanoscale systems represents a relatively cheap and technological appealing methodology, when compared to vacuum techniques, for the preparation of nanostructured architectures for certain applications. In this context, studies on the nanostructures formed on surfaces by deposition from solutions are of great relevance. For instance, octaalkoxy substituted CuPcs drop-casted on silica surfaces give rise to the formation of highly homogeneous, one-dimensional or two-dimensional aggregates.[58] Also, an example of nanostructures obtained by deposition from solution is depicted in *Figure 12*. A covalently-linked Pc-C_{60} fullerene conjugate is able to self-organize on graphite and graphite-like surfaces forming fibers and films, as revealed by AFM studies.[59,60]

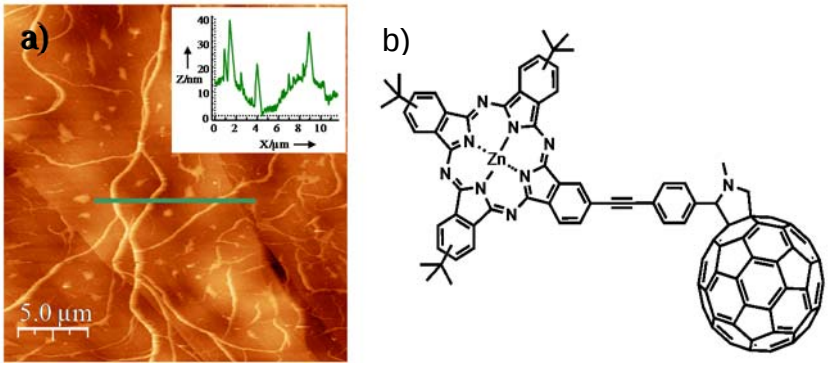

Figure 12.- a) AFM topographic image of the Pc-C_{60} dyad drop-casted on highly oriented pyrolytic graphite (HOPG); the inner picture is the AFM topographic profile (green line); b) molecular structure of the Pc-C_{60} dyad.

[55] a) T. G. Gopakumar, M. Lackinger, M. Hackert, F. Muller, M. Hietschold, *J. Phys. Chem. B* **2004**, *108*, 7839; b) K. Nilson, J. Ahlund, B. Brena, E. Gothelid, J. Schiessling, N. Martensson, C. Puglia, *J. Chem. Phys.* **2007**, *127*, 114702.

[56] a) X. Lu, K. W. Hipps, *J. Phys.Chem. B* **1997**, *101*, 5391; b) Z. H. Zeng, L. Gao, Z. T. Deng, N. Jiang, Q. Liu, D. X. Shi, S. X. Du, H. M. Guo, H. J. Gao, *J. Phys. Chem. C* **2007**, *111*, 9240.

[57] a) Y. Bai, F. Buchner, M. T. Wendhal, I. Kellner, A. Bayer, H. P. Seteinruck, H. Marbach, J. M. Godfried, *J. Phys. Chem. C* **2008**, *112*, 6087; b) Y. Wang, J. Kroger, R. Berndt, W. Hofer, *Angew. Chem. Int. Ed.* **2009**, *48*, 1261.

[58] M. Wang, Y.-L. Yang, K. Deng, C. Wang, *Chem. Phys. Lett.* **2007**, *439*, 76.

[59] G. Bottari, D. Olea, C. Gomez-Navarro, F. Zamora, J. Gomez-Herrero, T. Torres, *Angew. Chem. Int. Ed.* **2008**, *47*, 2026.

[60] G. Bottari, D. Olea, V. Lopez, C. Gomez-Navarro, F. Zamora, J. Gomez-Herrero, T. Torres, *Chem. Comm.* **2010**, *46*, 4692.

Properties and applications of phthalocyanines

Since their first synthesis, early in the 20th century, Pcs have established themselves as blue and green dyestuff par excellence. They are an important industrial commodity, used primarily in inks (especially ballpoint pens), coloring for plastics and metal surfaces, and dyes for jeans and other clothing. More recently, the unique properties of Pcs such as high optical stability, semiconductivity and excellent photophysical properties have widen their possible applications, and therefore, their commercial utility. Potential uses of Pcs include sensing elements in chemical sensors, electrochromic display devices, photodynamic reagents for cancer therapy, information storage systems (optical computers read/write discs), catalysis and electrocatalysis, and liquid crystal color display applications.

a) Optical properties

Organic molecules have found strong relevance as NLO materials. Since Mainman made the first laser in 1960,[61] mainly inorganic materials were studied, however, in the last 30 years organic molecules have found strong relevance in the area of NLO. Molecular candidates for this field must comprise highly polarizable π-systems; for this reason, Pcs and analogues, which present a delocalized π-aromatic cloud, have been widely studied in this area. Research in this field has mainly focused in the study of the second harmonic generation (SHG), in which two incident waves of frequency ω are combined and emitted by the material in a wave of frequency 2ω, and the third harmonic generation (THG), where the emitted wave has a frequency 3ω. In the specific case of second order properties, a noncentrosymmetric structure is also required. Pcs are versatile compounds which can be unsymmetrically substituted with electron-donor and acceptor groups, and therefore, they are very appealing materials in the generation of SHG and THG responses for nonlinear optical technologies.[62] The electronic structure of these macrocyclic compounds appears also adequate for optical limiting (OL), a nonlinear effect consisting on a decrease of the transmittance of the NLO material under high-intensity illumination.[63] This kind of materials can meet different functions, as the

[61] T. H. Maiman, *Nature* **1960**, *187*, 493.

[62] a) G. de la Torre, T. Torres, F. Agullo-Lopez, *Chem. Rev*. **2004**, *104*, 3723; b) M. J. F. Calvete, D. Dini, S. R. Flom, M. Hanack, R. G. S. Pong, J. Shirk, *Eur. J. Org. Chem*. **2005**, 3499; c) M. Drobizhev, M. S. Makarov, A. Rebane, G. De la Torre, T. Torres, *J. Phys. Chem. C* **2008**, *112*, 848; d) M. Quintiliani, J. Perez-Moreno, I. Asselberghs, P. Vazquez, K. Clays, T. Torres, *J. Phys. Chem. C* **2010**, *114*, 6309.

[63] a) S. M. O'Flaherty, S. V. Hold, M. J. Cook, T. Torres, Y. Chen, M. Hanack, W. J. Blau, *Adv. Mater*. **2003**, *15*, 19; b) G. Y. Yang, M. Hanack, Y. W. Lee, D. Dini, J. F. Pan, *Adv. Mater*. **2005**, *17*, 875.

protection of the human eye from intense light sources. SubPc and Pc pigments are essential components in the manufacturing of CDs and DVDs, being most of them patented.[64] Moreover, an optical information recording method based on Pc analogues, with two different wavelengths for read and write, has been patented.[65]

b) Electrical properties

Pcs belong to the group of low-dimensional semiconducting molecular materials,[66] displaying in some cases conductivities in the range of 10^{-4} to 10^{-2} $\Omega^{-1}\cdot cm^{-1}$. Conductivity in metallophthalocyanine systems can be due either to the instrinsic properties of a particular Pc, or to the organization of the molecules at supramolecular level. The bis(phthalocyaninato) lutetium (Pc_2Lu) and lithium phthalocyanine (PcLi) are instrinsic molecular semiconductors, due to their radical nature, and have been applied in some devices such as OFETs.[23j,67,68] The supramolecular organization of Pcs can also be responsible for their conducting properties. The cofacial arrangement of these macrocycles generates new conducting bands through the overlapping of the π-orbitals, thus obtaining a preferential electronic mobility along the stacking axis. This suitable assembly may be achieved by different methods, as the formation of columnar mesophases (see *Figure 10*), "shish-kebab" polymers, aggregates of crown-ether substituted Pcs and alkaline metal salts (see *Figure 11*), or ordered thin films. In many

[64] a) A. Zafirov, S. Rakosvski, J. Bakardjieva-Eneva, L. Prahov, L. Assenova, F. Marrandino (Vivastar Mastering & Materials A.-G., Switzerland), PCT Int. Appl., WO 2002080158 A1, **2002**; b) Y. Usami, T. Kakuta, T. Ishida (Fuji Photo Film Co., Ltd., Japan), Eur. Pat. Appl., EP 1434207 A2, **2004**.

[65] H. Shimizu, D. Morishita (K. K., Taiyo Yuden) Eur. Pat., EP1622138, **2006**.

[66] a) H. Schultz, H. Lehmann, M. Rein, M. Hanack, *Struct. Bonding* **1991**, *74*, 41; b) D. Schlettwein, D. Wohrle, F. Karmann, U. Melville, *Chem. Mater.* **1994**, *6*, 3 ; c) J. Simon, T. Toupance, en *Comprehensive Supramolecular Chemistry*, vol. 10. *Intrinsic molecular semiconductors: electronics and ionoelectronics finalities*, (Ed. D. N. Reinhoudt), Pergamon, Exeter, **1996** ; d) M. Hanack, L. Subramanian, en *Handbook of Organic Conducting Molecules and Polymers*, vol. 1, (Ed. H. S. Nalwa), John Wiley & Sons Ltd, **1997** ; e) M. Hanack, D. Dini, en *ref 18*, vol. 18, pp. 251-280, (Eds. K. M. Kadish, K. M. Smith, R. Guilard), Academic Press, San Diego, CA, **2003** ; f) M. F. Craciun, S. Rogge, M.-J. L. den Boer, S. Margadonna, K. Prassides, Y. Iwasa, A. F. Morpurgo, *Adv. Mater*. **2006**, *18*, 320.

[67] a) G. Guillaud, J. Simon, J. P. Germain, *Coord. Chem. Rev*. **1998**, *178*, 1433; b) *The Phorphyrin Handbook*, M. Bouvet, vol. 19, (Eds. K. M. Kadish, K. M. Smith, R. Guilard), Academic Press, San Diego, CA, **2003**.

[68] a) T. Okuda, S. Shintoh, N. Terada, *J. Appl. Phys*. **2004**, *96*, 3586; b) J. Zhang, J. Wang, H. Wang, D. Yan, *Appl. Phys. Lett*. **2004**, *84*, 142; c) J. Zhang, H. Wang, X. Yan, J. Wang, J. Shi, D. Yan, *Adv. Mater*. **2005**, *17*, 1191; d) M. Ofuji, K. Ishikawa, H. Takezoe, *Appl. Phys. Lett*. **2005**, *86*, 22103; e) T. Yasuda, T. Tsuitsui, *Chem. Phys. Lett*. **2005**, *402*, 395; f) L. Li, Q. Tang, H. Li, W. Hu, X. Yang, Z. Shuai, Y. Liu, D. Zhu, *Pure Appl. Chem*. **2008**, *80*, 2231.

instances, however, the doping of these systems with oxidizing or reducing agents is necessary to increase the conductivity.

The alteration of these semiconducting properties by redox reaction of the Pc with different gases (nitrogen monoxide and dioxide, ammonia) is an interesting phenomenon which has been exploited to design molecular sensors.[69,70]

c) Magnetic properties[23j]

In general, magnetic properties has been less studied because in many cases, metallophthalocyanines with one or more unpaired electrons essentially behave as simple paramagnetic substances. Some complexes, however, can exhibit spontaneous magnetization: d-metal Pcs (Mn(II), Fe(II), Cr(II), Co(II), Ni(II), Cu(II)); π-radical derivatives (LiPc and π-radical bis(Pcs)) and 4f metal Pcs (bis(phthalocyaninato)Tb(III) and Dy(III)). Regarding bis(phthalocyaninate) complexes, their study as single-molecule magnets (SMMs) will be described thoroughly in *Chapter 2*.

Worth mentioning that the application of Pcs in photovoltaic devices, as a result of their optical and electrical properties, is one of the most relevant fields of research for these compounds. It will be developed in depth in *Chapter 1*.

Background in our group

During the last years, our group has been centered in the preparation of Pcs and structural analogues, as well as in the study of their applications as molecular materials.

In the context of phodynamic therapy (PDT), a lot of effort has been devoted to the synthesis and study of water soluble zinc and ruthenium phthalocyanines, decorated with dendrimers as photosensitizers in photodynamic therapy for cancer,[71] in which the active compounds activate molecular oxygen into single oxygen, one of the main reactive species in this therapy. Regarding denditric Pcs, Pc-SWNT supramolecular hybrids

[69] a) J. Souto, M. L. Rodriguez-Mendez, J. A. de Saja, R. Aroca, *Int. J. Electronics* **1994**, *76*, 763; b) V. Parra, A. A. Arrieta, J. A. Fernandez-Escudero, H. Garcia, C. Apetrei, M. L. Rodriguez-Mendez, J. A. de Saja, *Sensors and Actuactors B* **2006**, 54.

[70] a) F. Armand, H. Perez, S. Fouriaux, O. Araspin, J.-P. Pradeau, C. G. Claessens, E. M. Maya, P. Vazquez, T. Torres, *Synth. Met*. **1999**, *102*, 1476; b) Z. Wang, A.-M. Nygrd, M. J. Cook, D. A. Russell, *Langmuir*, **2004**, *20*, 5850.

[71] a) A. R. M. Soares, Joao P. C. Tome, M. G. P. M. S. Neves, A. C. Tome, J. A. S. Cavaleiro, T. Torres, *Carbohydrate Res.* **2009**, 344, 507; b) F. Setaro, M. Brasch, U. Hahn, M. S. T. Koay, J. J. L. M. Cornelissen, A. de la Escosura, T. Torres, *Nano Lett*. **2015**, *15*, 1245.

based on a series of these dendritic, electron-donor Pcs have been reported (*Figure 13*).[72] In these systems, the presence of branched oligoethylene chains as well as the π-extended aromatic nature of Pcs allow for effective non-covalent interaction of the molecules with the carbon nanotube sidewalls.

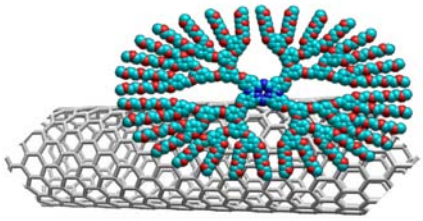

Figure 13.- Schematic representation of the noncovalent assembly of a dendritic Zn(II)Pc onto a carbon nanotube.

In connection with this last example, one of the main goals of the group for many years has been to exploit the formidable photophysical properties of these macrocycles and their analagues to render photoinduced electron transfer processes in donor-acceptor systems. Up to date, a large variety of covalent and supramolecular systems based on Pcs and carbon nanostructures have been described and the photophysical properties of some of them studied both in solution and in solid state, in order to understand the interesting electron and energy transfer properties, and thus, mimic natural photosynthethic systems.[23j,73] Accordingly, several dyads in which a Pc has been coupled to C_{60} fullerene, or endohedral metallofullerenes have been synthesized. For example, the synergistic effect of hydrogen bonding and metal-ligand interactions occurring at two different sites of an amidine-functionalized Zn(II)Pc (*Figure 14*, *A*) has been used to trigger the dissociation of the spontaneously formed Pc dimer (*Figure 14*, *B*) and the concomitant formation of three-component phenothiazine-Pc-C_{60} system.[74]

[72] U. Hahn, F. Setaro, X. Ragas, A. Gray-Weale, S. Nonell, T. Torres, *Phys. Chem. Chem. Phys.* **2011**, *13*, 3385.

[73] a) G. Bottari, G. de la Torre, D. M. Guldi, T. Torres, *Chem. Rev*. **2010**, *110*, 6768; b) G. Bottari, J. A. Suanzes, O. Trukhina, T. Torres, *J. Phys. Chem. Lett*. **2011**, *2*, 905; c) G. de la Torre, G. Bottari, M. Sekita, A. Hausmann, D. M. Guldi, T. Torres, *Chem. Soc. Rev*. **2013**, *42*, 8049; d) G. Bottari, G. de la Torre, T. Torres, Acc. Chem. Res. **2015**, 48, 900, and references there in.

[74] M. Garcia-Iglesias, K. Peuntinger, A. Kahnt, J. Krausmann, P. Vazquez, D. Gonzalez-Rodriguez, D. M. Guldi, T. Torres, *J. Am. Chem. Soc*. **2013**, *135*, 19311.

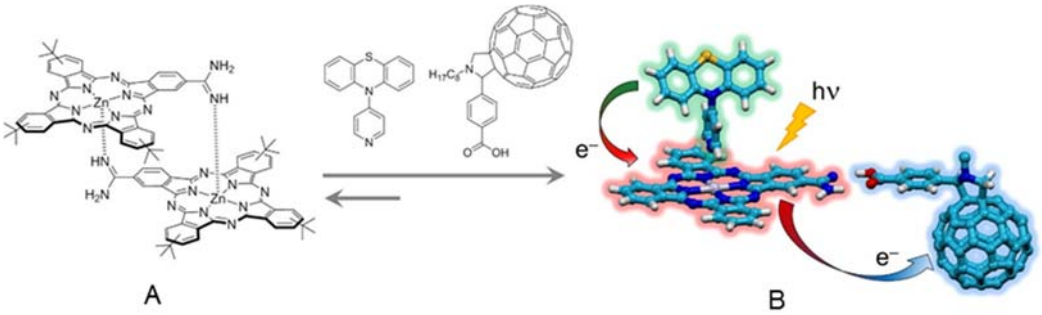

Figure 14.- Self-assembly of photoresponsive, donor-acceptor supramolecular triad B triggered by the disassembly of supramolecular dimer A in the presence of pyridine and benzoic acid derivatives functionalized with a phenothiazine donor and a C_{60} acceptor moiety, respectively.

Other interesting dyads are the one shown in *Figure 15*, prepared by esterification reaction between a C_{60} fullerene derivative and a series of lanthanide(III) bis(Pcs).[26f] Besides the original photophysical studies carried out on these systems, the synthesis of these double-deckers meant the opening of a new research line in the group.

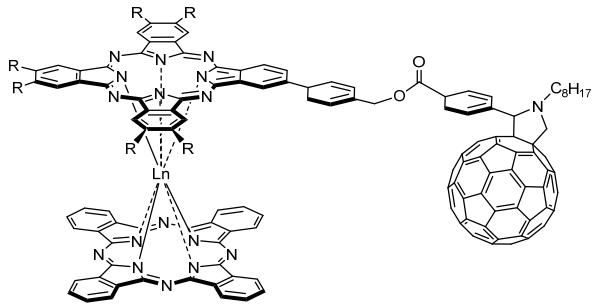

Figure 15.- Structure of double-decker-C_{60} dyad.

Recently, the possibility to use graphene, a rising star in the field of carbon nanostructures owing to its fascinating optical and electrical properties, as a platform to link electroactive Pcs has been explored in the group. Covalent functionalization of the previously exfoliated graphene layers, decorated with carboxylic acid moieties, and hydroxymethyl-containing free-base Pc (*Figure 16*) has been performed.[75] Steady-state and time-resolved spectroscopic techniques were used to assess electronic interactions between the Pc molecules and the graphene layers, demonstrating that electron transfer takes place from the photoexcited Pc to the graphene. More recently, the first reports of

[75] M.-E. Ragoussi, J. Malig, G. Katsukis, B. Butz, E. Spiecker, G. de la Torre, T. Torres, D. M. Guldi, *Angew. Chem. Int. Ed*. **2012**, *51*, 6421.

covalent[76] and supramolecular[77] Pc/ few-layer graphene ensembles showing an inverted graphene-to-Pc photoinduced charge transfer dynamics have been also reported. This behavior is a consequence of the electron-acceptor character of the linked Pcs, which are functionalized with electron-withdrawing alkylsulfonyl groups.

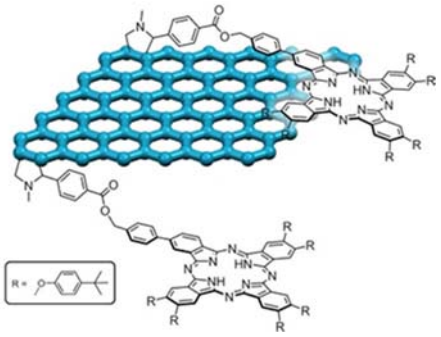

Figure 16.- Schematic representation of the assembly of a Pc and graphene.

Pc-containing conjugated oligomers have been also prepared and utilized to form non-covalent assemblies with graphene or few-layer graphene. In particular, n-type and p-type poly(*p*-phenylene vinylene) (PPV) oligomers containing lateral Zn(II)Pcs (*Figure 17*), were able to assist the exfoliation of graphite in THF to form stable nanohybrids, which featured charge separation evolving from photoexcited Zn(II)Pc to graphene.[78] To explore its potential in solar energy conversion applications, prototype solar cells were prepared, although very low IPCE values (ca. 1%) were achieved.[79]

[76] M.-E. Ragoussi, G. Katsukis, A. Roth, J. Malig, G. de la Torre, D. M. Guldi, T. Torres, *J. Am. Chem. Soc*. **2014**, *136*, 4593.
[77] A. Roth, M.-E. Ragoussi, L. Wibmer, G. Katsukis, G. de la Torre, T. Torres, D. M. Guldi, *Chem. Sci*. **2014**, *5*, 3432.
[78] J. Malig, N. Jux, D. Kiessling, J.-J. Cid, P. Vazquez, T. Torres, D. M. Guldi, *Angew. Chem. Int. Ed*. **2011**, *50*, 3561.
[79] L. Brinkhaus, G. Katsukis, J. Malig, R. D. Costa, M. Garcia-Iglesias, P. Vazquez, T. Torres, D. M. Guldi, *Small* **2013**, *9*, 2348.

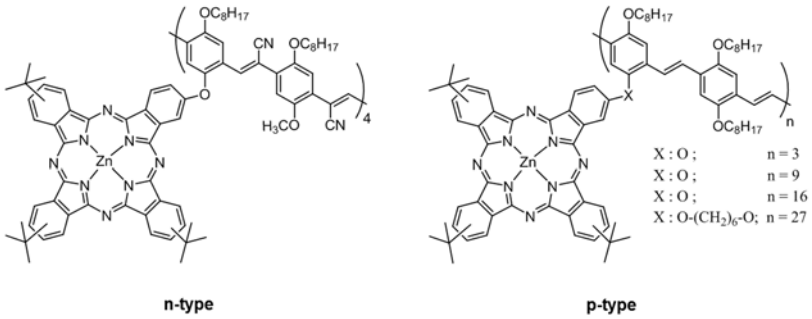

Figure 17.- Structure of oligomers with phthalocyanines as pendant moieties.

These conjugated structures have also led to to supramolecular Pc/single-walled carbon nanotube (SWCNT) ensembles. The ability of conjugated poly(*p*-phenylene vinylene) oligomers bearing pendant Zn(II)Pcs arms to wrap around SWCNTs was recently established (*Figure 18*).[80] Importantly, parameters such as size, n- or p-type character of the oligomer, and distance between the Zn(II)Pc moiety and the conjugated backbone play a decisive role in the stability of the ensembles.

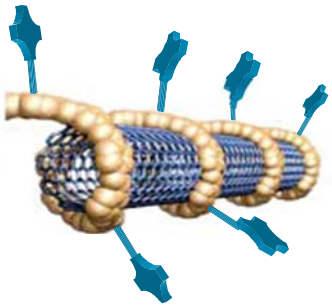

Figure 18.- Schematic representation of the assembly of a SWCNT functionalized with an oligomer bearing Pcs.

The group has also intensively developed research work related to the application of Pcs and analogues as photosensitizers in organic and dye-sensitized solar cells (DSSCs). The most relevant results in the field from us and other will be presented in *Chapter 1*.

[80] a) J. Bartelmess, C.Ehli, J.-J. Cid, M. Garcia-Iglesias, P. Vazquez, T. Torres, D. M. Guldi, *Chem. Sci*. **2011**, *2*, 652; b) J. Bartelmess, C. Ehli, J.-J. Cid, M. Garcia-Iglesias, P. Vazquez, T. Torres, D. M. Guldi, *J. Mater. Chem*. **2011**, *21*, 8014.

General objectives

General objectives

The main goal of this Thesis is the synthesis of new symmetrically and unsymmetrically substituted metallophthalocyanines, which will be explored either as photosensitizers in organic solar cells, in combination with semiconducting PPV- and polythiophene (PT)-polymers, and dye-sensitized solar cells, or as single molecule magnets. More in detail, the objectives of this work are defined as follows:

Chapter 1. New Zn(II)Pcs for molecular photovoltaics.

The first objective is to synthesize customized, unsymmetrically functionalized Pc derivatives with different electronic properties as photo- and electroactive components for molecular photovoltaics, namely for bulk heterojunction (BHJ) and DSSCs. Based on the broad experience gained by our research group, which has been working in this field during the last 10 years, the molecular designs of Pcs for photovoltaic applications is focussed on:

a) Phthalocyanines for polymer-based solar cells

In an effort to make some progress in the plastic solar-cell area, an interesting approach is to obtain a polymeric material with an improved absorption in the visible region (up to 750 nm) by attaching Zn(II)Pc chromophores. The incorporation of the Pcs into polymer architectures can be carried out either by lateral functionalization of a suitable conjugated copolymer (*Figure 19a*), or by using an appropriately functionalized Pc as a monomer for the copolymerization with other electroactive counterparts to form a conjugated skeleton in which the Pc is integrated (*Figure 19b*). In both cases, this would be achieved by the introduction of adequate functional groups in one of the isoindolic units of the Pc that would allow for its covalent incorporation into the polymer.

Finally the Pc-polymer materials prepared would be tested as active components in BHJ solar cells.

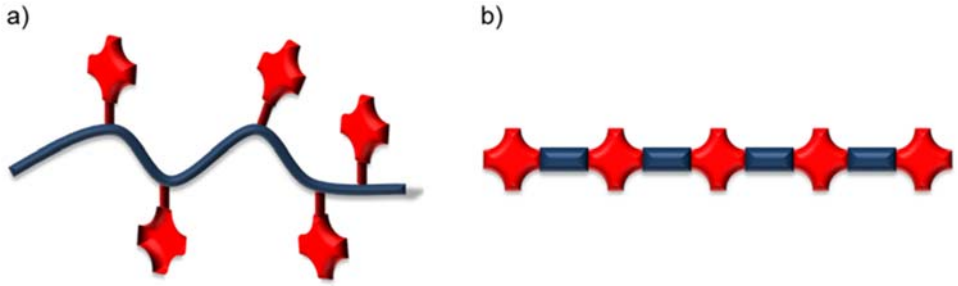

Figure 19.- Representation of a) side-chain and b) main-chain Pc-containing copolymers.

b) Phthalocyanines for p-type dye-sensitized solar cells

Here, the purpose is to synthesize electron-acceptor Zn(II)Pcs having solubilizing and electron-withdrawing (EWG) moieties at three of the isoindoles, aiming at lowering the HOMO/LUMO energy levels of the Pc, and also an adequate anchoring group which would be used to attach the molecules to adequate semiconducting, mesoporous surfaces (*Figure 20*). This rational design is focused on the preparation of cutting-edge, p-type DSSCs, in which the semiconducting metal oxide would inject electrons into the photoexcited Pc as a consequence of its increased electron-acceptor character.

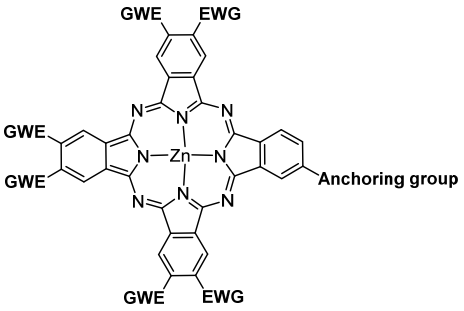

Figure 20.- Molecular structure of a Pc bearing EWG groups at the peripheral positions.

Chapter 2. Single-molecule magnets based on terbium(III) bis(phthalocyaninato) complexes.

The single-molecule magnet behaviour of double-decker Pc lanthanide complexes, structurally similar to those shown in *Figure 4b,* has been reported in the literature, but only on the archetypal, double-decker Tb(III)Pc_2 or Dy(III)Pc_2 with bare macrocyclic rings. An important goal for investigating double-decker, Tb(III)Pc SMMs is to deepen the understanding of the relationship between structure and magnetic behavior. Therefore, the second main objective of this work lies on the preparation of a battery of functionalized double-decker Tb(III)Pc_2 to determine the influence of the peripheral substitution, the role of the oxidation state of the Pc ligands (radical or anionic) and the interactions between Tb(III) ions in covalently linked, dimeric Tb(III)Pc species, on the SMM parameters, that is, barrier energy and blocking temperature.

a) Homoleptic and heteroleptic Tb(III) bis(phthalocyaninato) complexes

Following appropriate synthetic approaches, we will prepare a series of Tb(III) bisphthalocyaninato complexes, holding peripheral substituents of different electronic nature (electron-donor or acceptor) in either one (heteroleptic) or two (homoleptic) of the Pc ligands, and double decker complexes combining also Pc ligands with other related analogues (porphyrin, naphthalocyanine…) (*Figure 21*). Magnetic characterization of

these complexes will allow us to estimate the possible influence of the number and electronic character of the peripheral substituents, as well as the presence or not of a different macrocycle on the SMM behaviour of this type of complexes.

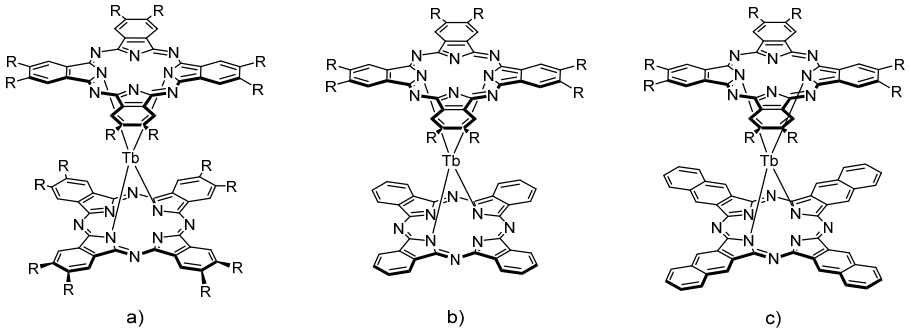

Figure 21.- a) Homoleptic and b) heteroleptic terbium(III) bisphthalocyanine complexes. c) Example of a double-decker complex comprising different macrocyclic ligands.

b) Homoleptic and heteroleptic Tb(III) bis(phthalocyaninato) dimers

To the best of our knowledge, covalently linked Tb(III)Pc_2 dimers have been never reported before. For that reason, we aim to prepare $[Tb(III)Pc_2]_2$ complexes (*Figure 22*), linked together through short and rigid spacers, to study the spin-spin interaction between the two paramagnetic nuclei and, therefore, its repercussion in the SMM parameters with regard to the corresponding monomeric Tb(III)Pc_2 units.

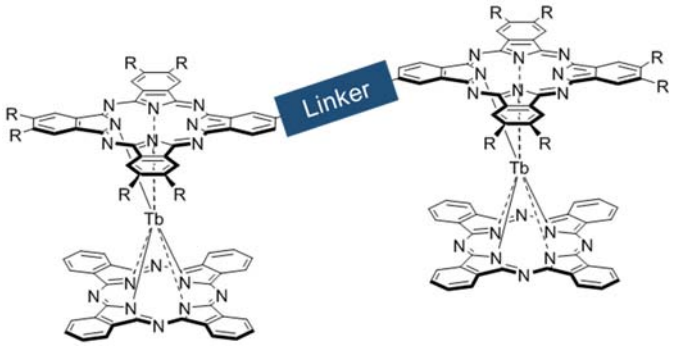

Figure 22.- Schematic representation of a heteroleptic dimer.

Chapter 1. *New Zn(II)Pcs for molecular photovoltaics*

1.1 Introduction

1.1.1 Solar energy

The evolution of mankind before the Industrial Revolution was dependent on the annual cycle of plant photosynthesis for both heat (burning wood) and mechanical energy (human and animal muscle power derived from food and fodder). Steam locomotives, the quintessential machines of the Industrial Revolution, started to use existing energy resources, such as coal, more efficiently. Ever since, industrial development has depended on the availability of cheap and reliable energy sources. On an international scale, the energy required in 2005 was the equivalent of 13 terawatts (TW), which is 13 trillion watts of power. 85% of this energy comes from fossil fuels, which produce large quantities of greenhouse gases. These emissions turn out catastrophic consequences for the Earth as a result of global warming. As energy expenses are growing, it has been estimated that the world's energy consumption will reach 28 TW in 2050.[83] This points out that the society is facing a dilemma: for further economic development, an increase in the energy consumption is necessary. However, this leads to unwanted consequences for the environment due to the emission of pollutants. Therefore, the predicted exhaustion of fossil energy resources and the pressure of environmental constraints are stimulating an intensification of the research on renewable energy sources, which play an essential role in the sustainable development of the environment, economy and society.

Solar, geothermal, ocean, wind, hydropower and biomass are renewable energies that may meet these energy demands. As a matter of fact, solar energy alone possesses the potential of becoming the successor of fossil fuels, which will cover the world's current energetic needs.[84] Sunlight strikes the Earth's surface with enough energy every hour to supply world consumption per annum. This is by far the biggest source of energy available to us, and a great candidate for a transition to a more sustainable production of energy. Furthermore, this energy source is ubiquitous, and it is expected that the deployment of solar energy gives political stability to many areas of the planet because of the more balanced distribution of a primary source of energy.

Solar energy[85] can be transformed into electricity either thermodynamically or electronically. The first method, the solar thermal energy,[86] is usually focused in the

[83] a) R. F. Service, *Science* **2005**, *309*, 548; b) J. Potocnik, *Science* **2007**, *315*, 810.
[84] Q. Schiermeier, J. Tollefson, T. Scully, A. Witze, O. Morton, *Nature* **2008**, *454*, 816.
[85] C. Richter, D. Lincot, C. Gueymard (eds.), *Solar Energy*, Springer, New York, **2013**.
[86] B. Norton, *Harnessing Solar Heat*, Lecture in Energy 18, Springer, Dordrecht, **2014**.

design of optical collectors to generate electricity by heating a fluid to drive a turbine connected to an electrical generator. The second method, instead, converts directly the solar energy into electricity by opto-electronic devices, called solar cells. This efficient production of electricity by means of solar cells is nowadays available and photovoltaics is one of the fastest growing renewable energy technology. In this context, silicon based solar cells[87] are by far the most dominating type of photovoltaic devices with a market share of about 90% (single crystalline, polycrystalline and amorphous forms).[88] Their broad recognition is attributed to their proven and reliable operational capacities, namely, good efficiencies and a lifetime of 20 years. Laboratory cell efficiencies have reached 25% (crystalline),[89] but commercial module efficiencies are still in the range of 15-18%.[90] A combination of an increase in efficiency and a reduction of the production costs of the photovoltaic panels is still necessary to realistically compete with conventional fossil-fuel energy conversion systems. Fifty years of research and innovation have significantly reduced the price of silicon photovoltaics, but, despite this effort, its complex production hampers a much wider application of it. Another drawback is that silicon panels are very heavy and rigid in shape. In this regard, both organic photovoltaics and hybrid devices with active inorganic and organic materials have attracted significant attention as a lower cost alternative to their purely inorganic relatives.[91] Organic materials fulfill many requirements for solar cells, such as strong optical absorption, easy manufacturing in thin films, chemical tailoring to tune their properties, and low-cost synthesis,[92] as shown in the next sections. However, long-term stability is still an issue.

---

[87] M. A. Green, *Philos. Trans. R. Soc. A* **2013**, *371*, 20110413.

[88] IRENA (International Renewable Energy Agency), *Renewable Energy Technologies: Cost Analysis Series. Solar Photovoltaics*, **2012**. Available at: http://www.irena.org/DocumentDownloads/Publications/RE_Technologies_Cost_Analysis-SOLAR_PV.pdf (Accessed Jan. 2015).

[89] M. A. Green, K. Emery, Y. Hishikawa, W. Warta, E. D. Dunlop, *Prog. Photovolt: Res. Appl.* **2015**, *23*, 1.

[90] T. Saga, *NPG Asia Mater*. **2010**, *2*, 96.

[91] N. S. Lewis, *Science* **2007**, *315*, 798.

[92] a) A. W. Hains, Z. Liang, M. A. Woodhouse, B. A. Gregg, *Chem. Rev.* **2010**, *110*, 6689; b) J. Roncali, *Acc. Chem. Res*. **2009**, *42*, 1719; c) P. M. Beaujuge, J. M. J. Frechet, *J. Am. Chem. Soc*. **2011**, *133*, 20009; d) Z. X. Wang, F. J. Zhang, J. Wang, X. W. Xu, J. Wang, Y. Liu, Z. Xu, *Chin. Sci. Bull*. **2012**, *57*, 4143; e) M. Pfannmoller, W. Kowalsky, R. R. Schroder, *Energy Environ. Sci*. **2013**, *6*, 2871; f) J. Yu, Y. Zheng, J. Huang, *Polymers* **2014**, *6*, 2473; g) F. C. Krebs, N. Espinosa, M. Hosel, R. R. Sondergaard, *Adv. Mater*. **2014**, *26*, 29; h) T. R. Andersen, H. F. Dam, M. Hosel, M. Helgesen, J. E. Carle, T. T. Larse-Olsen, S. A. Gevorgyan, J. W. Andreasen, J. Adams, N. Li, F. Machui, G. D. Spyropoulos, T. Ameri, N. Lemaitre, M. Legros, A. Scheel, D. Gaiser, K. Kreul, S. Berny, O. R. Lozman, S. Nordman, M. Valimaki, M. Vilkman, R. R. Sondergaard, M. Jorgensen, C. J. Brabec, F. C. Krebs, *Energy Environ. Sci.* **2014**, *7*, 2925.

1.1.2 Classification of solar cells

First reports on photovoltaic concepts date back to the end of the XIX century with two major contributions; one from Becquerel in 1839, describing photocurrent,[93] and the first real reports on photoconductivity made by Smith and Adams in 1873 and 1876, respectively, working on selenium.[94,95] It was not until the beginning of the XX century that photoconductivity in an organic compound, namely, anthracene, was observed.[96,97] The commercial potential of these photoconductive materials has encouraged the research in this subject, and the variety of devices has broadened to encompass all fields of development. Solar cells can be broadly classified depending upon the type of active material used, manufacturing technique, type of junction formed or even the generation. A classification based on the type of material (inorganic, organic or hybrid when both are present) is shown below (the record conversion efficiencies for the different technologies reported in this section are updated until January 2015).

- **Inorganic solar cells**. The technology used to make most of the solar cells fabricated so far, borrows heavily from the microelectronics industry, where silicon prevails as semiconductor. The first silicon solar cell was developed by the Bell Telephone Lab in 1954, showing an efficiency of 6%.[98] Much research has followed because silicon is safe and the second most abundant element on Earth. The crystalline solar cells, either mono- or polycrystalline, are known as 1st generation solar cells. Their maximum efficiencies, 25.0% and 20.4% (*Figure 23,* SunPower, Solibro), respectively, are close to the Shockley–Queisser theoretical limit, *i.e.* 33%.[99] Crystalline silicon solar cells dominate the photovoltaic market, despite the fact that an important drawback of this kind of photovoltaic cells is to get pure silicon. The production costs of such modules are very high, which motivated engineers and scientists to search for 2nd generation solar cells by addressing factors such as easy and low-cost production, as well as high performances.

2nd generation, thin film inorganic solar cells[100] appeared in the early 60s (although they did not raise too much expectations until the 90s), as a consequence of

[93] a) A. E. Becquerel, *Compt. Rend. Acad. Sci*. **1839**, *9*, 145; b) A. E. Becquerel, *Compt. Rend. Acad. Sci*. **1839**, *9*, 561.
[94] W. Smith, *Nature* **1873**, *7*, 303.
[95] W. G. Adams, R. E. Day, *Proc. R. Soc. London* **1876**, *25*, 113.
[96] A. Pochettino, *Acad. Lincei. Rend*. **1906**, *15*, 355.
[97] M. Volmer, *Ann. Physik* **1913**, *40*, 775.
[98] D. M. Chapin, C. S. Fuller, G. L. Pearson, *J. Appl. Phys*. **1954**, *25*, 676.
[99] W. Shockley, H. J. Queisser, *J. Appl. Phys*. **1961**, *32*, 510.
[100] L. M. Peter, *Phil. Trans. R. Soc. A* **2011**, *369*, 1840.

the development of cost-efficient, thin film technologies. Nowadays they have proved to be a strong alternative to classical silicon photovoltaics. Modules based primarily on chemical vapour deposited amorphous silicon (maximum efficiency of 13.4%, *Figure 23*, LG Electronics), as well as polycrystalline InSe, CdTe (maximum efficiency of 21.5%, *Figure 23*, First Solar), $CuInGaSe_2$ (known as CIGS) (maximum efficiency of 21.7%, *Figure 23*, ZSW) have yielded outstanding performances. When compared to 1st generation solar cells, they are, in general, less efficient, but also less expensive. Thin film solar cells are designed in such a way that they use less material, resulting in lower-cost, manufacturing processes. Some drawbacks, like resource scarcity and toxicity of the active materials, triggered research on 3rd generation solar cells during the last two decades.

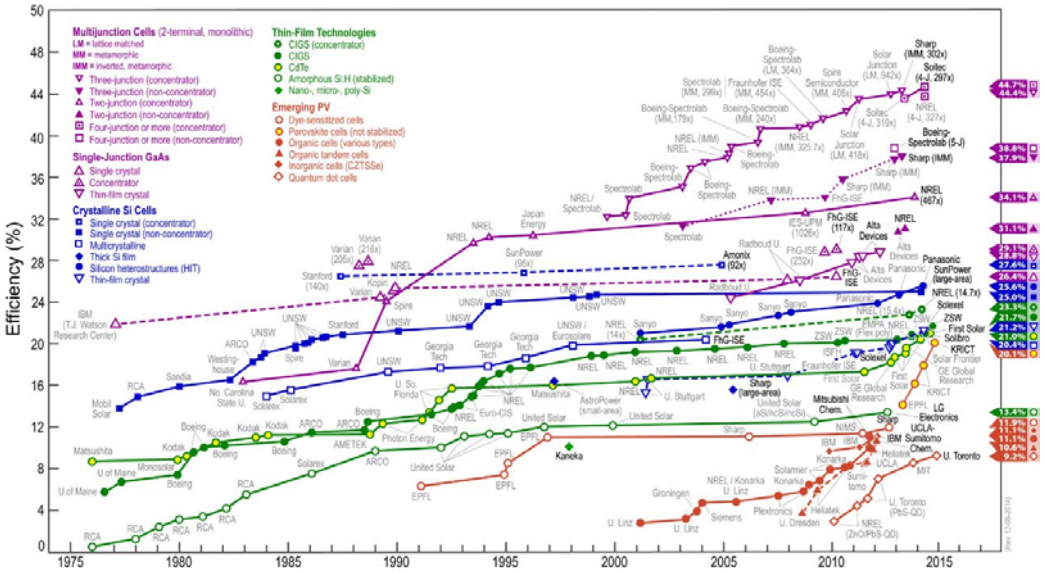

Figure 23.- Historical trends in cell efficiency for different photovoltaic technologies (this plot is courtesy of the National Renewable Energy Laboratory, Golden, CO, USA).

In the latter generation, highly efficient solar cells are based on environmentally friendly materials that allow inexpensive solvent-based fabrication techniques. Leading examples are low-cost, thin-film solar cells based on novel concepts like hot carrier solar cells, multiple exciton generation, tandem or multijunction solar cells.[101] By means of

[101] M. A. Green, *Third Generation Photovoltaics*, Springer-Verlag, Berlin, **2003**.

these cells, the Shockley-Queisser limit as defined for 1st generation solar cells is expected to be bypassed.[102]

- **Organic solar cells**. All-organic photovoltaics, as well as hybrid solar cells, are considered also as a type of 3rd generation devices, and have the merits of low cost, stability, simple fabrication and flexibility.[103]

In the late 50s and 60s, it was discovered that many common dyes, such as methylene blue, many important biological molecules like carotenes and chlorophylls, and other porphyrins and related synthetic analogues such as phthalocyanines, had semiconducting properties. These dyes, where among the first organic materials to exhibit the photovoltaic effect. As early as 1958, Kearns *et al*. reported the photovoltaic effect of a cell based on a single layer (Schottky or monolayer solar cell) of magnesium phthalocyanine, which had a photovoltage of 200 mV.[104] From then on, organic materials have gained broader interest and several new concepts associated to the configuration of the device have been presented. A milestone came in 1986 when Tang used a two-component, donor:acceptor active layer (planar bilayer heterojunction, PHJ, or p-n solar cell, *Figure 24a*).[105] This structural modification benefits from the facile formation of the charge carriers (electrons and holes) by electron transfer from the photoexcited donor to the acceptor component. Also, the separated charge transport layers ensure connectivity with the correct electrode and give the separated charge carriers only a small chance to recombine with their counterparts. The drawback is that only excitons (*i.e.* electron-hole pairs formed by light excitation) formed very close tho the interface between donor and acceptor layers are able to dissociate. To overcome this structural problem, the concept of bulk-heterojunction (BHJ, *Figure 24b*) was introduced by Yu *et al*,[106] in which a blend of a donor and an acceptor with a bicontinual phase separation is formed.[92b,107,108] The advantage of this type of cell is the large interface area, if molecular mixing occurs on a scale that allows for a good contact between materials, and that enables most of the excitons to reach the p-n interface. Ultimately, another type of architectures called tandem solar cells (*Figure 24c*), have gained a lot of attention. They consist in a

[102] C. A. Nelson, N. R. Monahan, X. –Y. Zhu, *Energy Environ. Sci*. **2013**, *6*, 3508.
[103] a) F. G. Brunetti, R. Kumar, F. Wudl, *J. Mater. Chem*. **2010**, *20*, 2934; b) J. L. Delgado, P.-A. Bouit, S. Filippone, M. A. Herranz, N. Martin, *Chem. Comm*. **2010**, *46*, 4853; c) K. A. Mazzio, C. K. Luscombe, *Chem. Soc. Rev*. **2015**, *44*, 78; d) J. Yan, B. R. Saunders, *RSC Adv*. **2014**, *4*, 43286.
[104] D. Kearns, M. Calvin, *Chem. Phys*. **1958**, *29*, 950.
[105] a) C. W. Tang, *Appl. Phys. Lett*. **1986**, *48*, 183; b) C. W. Tang, *US* Patent, 4, 164, 431, **1979**.
[106] G. Yu, J. Gao, J. C. Hummelen, F. Wudl, A. J. Heeger, *Science* **1995**, *270*, 1789.
[107] M. Hiramoto, H. Fujiwara, M. Yokoyama, *Appl. Phys. Lett*. **1991**, *58*, 1062.
[108] J. J. M. Halls, C. A. Walsh, N. C. Greenham, E. A. Marseglia, R. H. Friend, S. C. Moratti, A. B. Holmes, *Nature* **1995**, *376*, 498.

combination of two or more single junction cells (one on top of the other) that absorb in different wavelength ranges. Their advantage is that a combination of absorbing molecules can allow for a large spectral coverage with efficient absorption, which would be difficult to obtain with a single heterojunction.[109,110]

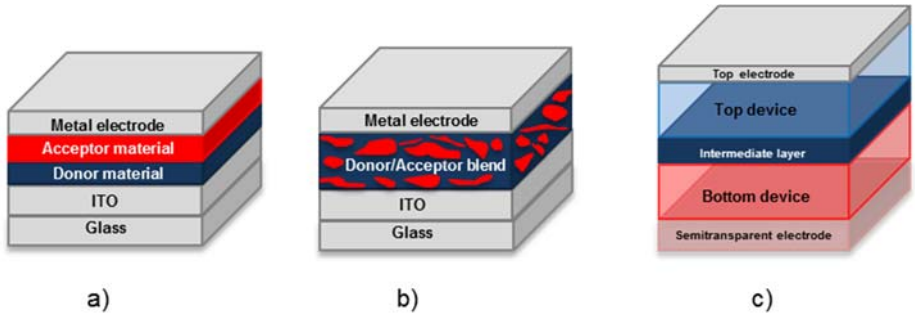

Figure 24.- Schematic representation of a) planar bilayer, b) bulk heterojunction and c) tandem solar cell.

From a different point of view, another classification of the organic solar cells based on the active material can be established: polymer-based photovoltaic cells, also known as plastic solar cells,[111] which are constituted by conjugated polymers; and small molecule-based photovoltaic devices, in which discrete chromophores form the active layer.[92b,112]

[109] a) A. Hadipour, B. de Boer, P. W. M. Blom, *Adv. Funct. Mater*. **2008**, *18*, 169; b) T. Ameri, G. Dennler, C. Lungenschmied, C. J. Brabec, *Energy Environ. Sci*. **2009**, *2*, 347; c) T. Ameri, N. Li, C. J. Brabec, *Energy Environ. Sci*. **2013**, *6*, 2390; d) M. Riede, C. Uhrich, J. Widmer, R. Timmreck, D. Wynands, G. Schwartz, W.-M. Gnehr, D. Hildebrandt, A. Weiss, J. Hwang, S. Sundarraj, P. Erk, M. Pfeiffer, K. Leo, *Adv. Funct. Mater*. **2011**, *21*, 3019.

[110] a) J. Y. Kim, K. Lee, N. E. Coates, D. Moses, T.-Q. Nguyen, M. Dante, A. J. Heeger, *Science* **2007**, *317*, 222; b) S. Sista, Z. Hong, L.-M. Chen, Y. Yang, *Energy Environ. Sci*. **2011**, *4*, 1606; c) J. You, L. Dou, Z. Hong, G. Li, Y. Yang, *Prog. Polym. Sci*. **2013**, *38*, 1909; d) O. Adebanjo, B. Vaagensmith, Q. Qiao, *J. Mater. Chem. A* **2014**, *2*, 10331.

[111] a) C. J. Brabec, N. S. Saricifti, J. C. Hummelen, *Adv. Funct. Mat*. **2001**, *11*, 15; b) J. Peet, M. L. Senatore, A. J. Heeger, G. C. Bazan, *Adv. Mater*. **2009**, *21*, 1521; c) C. J. Brabec, S. Gowrisanker, J. J. M. Halls, D. Laird, S. Jia, S. P. Williams, *Adv. Mater*. **2010**, *22*, 3839; d) D. Gendron, M. Leclerc, *Energy Environ. Sci*. **2011**, *4*, 1225; e) J. Peet, A. J. Heeger, G. C. Bazan, *Acc. Chem. Res*. **2009**, *42*, 1700.

[112] a) J. Roncali, P. Frere, P. Blanchard, R. de Bettignies, M. Turbiez, S. Roquet, P. Leriche, Y. Nicolas, *Thin Solid Films* **2006**, *511-512*, 567; b) B. Walker, C. Kim, T.-Q. Nguyen, *Chem. Mater*. **2011**, *23*, 470; c) A. Mishra, P. Bauerle, *Angew. Chem. Int. Ed*. **2012**, *51*, 2020; d) M. Wang, F. Wudl, *J. Mater. Chem*. **2012**, *22*, 24297; e) Y. Lin, Y. Li, X. Zhan, *Chem. Soc. Rev.* **2012**, *41*, 4245; f) W. Hu (ed.), Y. Lin, X. Zhan, *Organic Optoelectronics,* Wiley-VCH Verlag GmbH & Co. KGaA,

Regarding efficiencies, while polymeric tandem solar cells have reached a conversion efficiency of 10.6% (*Figure 23,* UCLA-Sumitomo Chem.),[113] it is worth noting that the record in multi-junction architectures is held by Heliatek,[114] that recently reported a tandem oligomer-based device with a certified power conversion efficiency of 12%. The best conversion efficiency for a single junction device has been achieved by Mitsubishi Chemical, reaching a 11.7% value.[115]

- **Hybrid solar cells**. Apart from the fully organic solar cells, combinations of organic-inorganic materials have been of great relevance in recent years. In this sense, the development of dye-sensitized solar cells (DSSCs) in the 90s opened up new horizons in the area of photovoltaics, and entered dynamically the race for cost-efficient devices functioning at the molecular and nanoscale levels.[116] The seminal paper by O'Regan and Grätzel in 1991[117] introduced a pioneering architecture, an n-type DSSC, in which an organic light-absorbing dye is anchored to a mesoporous inorganic n-type semiconductor film (this semiconductor operates as photoanode) and filled in with a redox-active electrolyte. This type of DSSCs has shown a tremendous potential and nowadays is a real alternative to the standard silicon photovoltaics,[118] with the obtained efficiencies growing from 7% in the seminal report,[117] using ruthenium complexes as the dye, to the current 13.0% employing porphyrins as sensitizers and eliminating the need for rare and costly, ruthenium-based sensitizers as a requirement for high efficiencies.[119] Alternatively, p-type DSSCs (an active photocathode) have been also explored but they have not exhibit yet energy conversion values as high as conventional DSSCs. This has been ascribed to drawbacks associated with the electrolytes and the p-type

Weinheim, Germany, **2013**, Chapter 18. *Organic Solar Cells Based on Small Molecules*; g) Y. Chen, X. Wan, G. Long, *Acc. Chem. Res*. **2013**, *46*, 2645; h) A. F. Eftaiha, J.-P. Sun, I. G. Hill, G. C. Welch, *J. Mater. Chem. A* **2014**, *2*, 1201; i) J. Roncali, P. Leriche, P. Blanchard, *Adv. Mater*. **2014**, *26*, 3821.

[113] J. You, L. Dou, K. Yoshimura, T. Kato, K. Ohya, T. Moriaty, K. Emery, C.-C. Chen, J. Gao, G. Li, Y. Yang, *Nat. Commun*. **2013**, *4*, 1446.

[114] Heliatek GmbH, *Heliatek consolidates its technology leadership by establishing a new world record for organic solar technology with a cell efficiency of 12%*, **2013**. Available at: http://www.heliatek.com/newscenter/latest_news/neuer-weltrekord-fur-organische-solarzellen-heliatek-behauptet-sich-mit-12-zelleffizienz-als-technologiefuhrer/?lang=en (Accessed Jan. 2015).

[115] Mitsubishi Chemical Corporation, *Achieved power conversion efficiency of 11.7%, the highest in the world!*, Available at: http://www.m-kagaku.co.jp/english/r_td/strategy/technology/topics/opv/index.html (Accessed Jan. 2015).

[116] a) A. Hagfeldt, G. Boschloo, L. Sun, L. Kloo, H. Pettersson, *Chem. Rev*. **2010**, *110*, 6595; b) M. K. Nazeeruddin, E. Baranoff, M. Gratzel, *Solar Energy* **2011**, *85*, 1172.

[117] B. O'Regan, M. Gratzel, *Nature* **1991**, *353*, 737.

[118] H. S. Jung, J.-K. Lee, *J. Phys. Chem. Lett*. **2013**, *4*, 1682.

[119] S. Mathew, A. Yella, P. Gao, R. Humphry-Baker, B. F. E. Curchod, N. Ashari-Astani, I. Tavernelli, U. Rothlisberger, M. K. Nazeeruddin, M. Gratzel, *Nat. Chem*. **2014**, *6*, 242.

semiconductors,[120] and to date, there is just one example of comparable efficiency, *i.e.* 2.51%.[121] Other important point is the growing tendency nowadays to develop all-solid-state devices versus the liquid-based DSSCs, which represents a step forward into the future commercialization.[122]

Beyond the architecture, there are some materials that need a special mention, like quantum dots[123] and perovskites.[124] The latter is a new family of solar cells that have a very good chance of contributing to large scale solar energy production based on their high efficiency and compatibility with scalable processes. Perovskites have the general formula of ABX_3 (*Figure 25*) where A and B are monovalent and divalent ions, respectively. X is either O, C, N or a halogen.

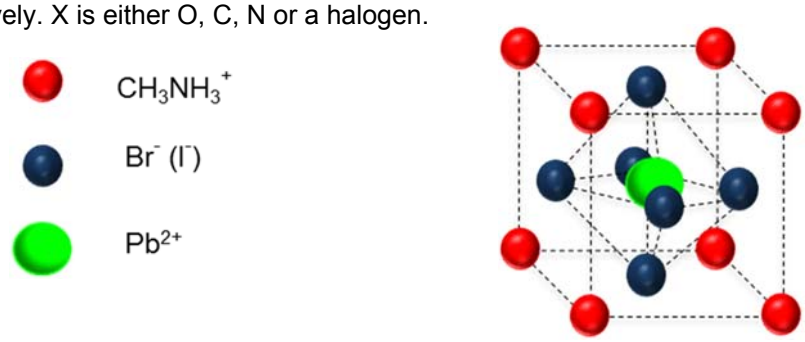

Figure 25.- Structure for $CH_3NH_3PbBr_3$, a common perovskite currently used for solar cell applications.

The field of perovskite-sensitized solar cells has grown exponentially since the first peer-reviewed journal publication of a perovskite-sensitized solar cell came in 2009,

[120] F. Odobel, Y. Pellegrin, E. A. Gibson, A. Hagfeldt, A. L. Smeigh, L. Hammarstrom, *Coord. Chem. Rev*. **2012**, *256*, 2414.
[121] I. R. Perera, T. Daeneke, S. Makuta, Z. Yu, Y. Tachibana, A. Mishra, P. Bauerle, C. A. Ohlin, U. Bach, L. Spiccia, *Angew. Chem. Int. Ed*. **2015**, *54*, 3758.
[122] a) P. Docampo, S. Guldin, T. Leijtens, N. K. Noel, U. Steiner, H. J. Snaith, *Adv. Mater*. **2014**, *26*, 4013; b) A. Fakharuddin, R. Jose, T. M. Brown, F. Fabregat-Santiago, J. Bisquert, *Energy Environ. Sci*. **2014**, *7*, 3952.
[123] a) M. A. Halim, *Nanomaterials* **2013**, *3*, 22; b) M. R. Kim, D. Ma, *J. Phys. Chem. Lett*. **2015**, *6*, 85.
[124] a) H. J. Snaith, *J. Phys. Chem. Lett*. **2013**, *4*, 3623; b) M. A. Loi, J. C. Hummelen, *Nat. Mater*. **2013**, *12*, 1087; c) S. Kazim, M. K. Nazeeruddin, M. Gratzel, S. Ahmad, *Angew. Chem. Int. Ed*. **2014**, *53*, 2812; d) M. He, D. Zheng, M. Wang, C. Lin, Z. Lin, *J. Mater. Chem. A* **2014**, *2*, 5994; e) P. Gao, M. Gratzel, M. K. Nazeeruddin, *Energy Environ. Sci*. **2014**, *7*, 2448; f) M. A. Green, A. Ho-Baillie, H. J. Snaith, *Nature Photon*. **2014**, *8*, 506; g) H.-S. Kim, S. H. Im, N.-G. Park, *J. Phys. Chem. C* **2014**, *118*, 5615; h) G. Giorgi, K. Yamashita, *J. Mater. Chem. A* **2015**, DOI: 10.1039/c4ta05046k; i) W.-J. Yin, J.-H. Yang, J. Kang, Y. Yan, S.-H. Wei, *J. Mater. Chem. A* **2015**, DOI: 10.1039/c4ta05033a.

where a 3.5% efficient sensitized solar cell employing $CH_3NH_3PbI_3$ as absorber and the iodide/triiodide redox couple was reported.[125] Tremendous progress in the area via morphology optimization (thickness and homogeneity),[126] and broadening the absorption and photostability,[127] has, indeed, resulted in unique efficiencies currently reaching 20.1% (*Figure 23*, KRICT). Only the the toxicity of lead and the moisture-sensitivity of perovskites can prevent this type of devices from a bright future.[128]

1.1.3 Characteristic parameters of solar cells

The properties of photovoltaic devices can be characterized by plotting the measured current output J of the cell versus the voltage output V of the cell (J-V graph). In the dark, this J-V curve passes through the origin, since at that moment no current is flowing through the device and no potential is present. By exposing the photovoltaic device to light, the J-V curve shifts downwards, as can be seen in *Figure 26*. The most important characteristic parameters of photovoltaic devices can be found on this J-V curve.

Open-circuit voltage (V_{OC}): It is the maximum possible voltage across a photovoltaic device. This is the voltage across the cell, in sunlinght, when no current is flowing through the device.

Short-circuit current (I_{SC}): It is the current that flows through an illuminated solar cell when there is no external resistance *i.e.* when the electrodes are simply connected or short-circuited. I_{SC} is the maximum current that a photovoltaic device is able to produce. Under un external load, the current will always be less than I_{SC}. The short-circuit current depends on a number of factors, such as the area of the solar cell. To remove the dependence of the solar cell area, it is more common to list the short-circuit current density (J_{SC} in mA/cm^2), rather than the short circuit current (I_{SC} in mA).

Maximum power point (M_{pp}): It is the point (V_m, J_m) on the I-V curve at which the maximum power is produced. Power is the product of current I and voltage V. This is represented in *Figure 26* as the area of the rectangle formed between a point on the I-V

[125] A. Kojima, K. Teshima, Y. Shirai, T. Miyasaka, *J. Am. Chem. Soc*. **2009**, *131*, 6050.
[126] J. Burschka, N. Pellet, S.-J. Moon, R. Humphry-Baker, P. Gao, M. K. Nazeeruddin, M. Gratzel, *Nature* **2013**, *499*, 316.
[127] G. E. Eperon, S. D. Stranks, C. Menelaou, M. B. Johnston, L. M. Herz, H. J. Snaith, *Energy Environ. Sci*. **2014**, *7*, 982.
[128] N. K. Noel, S. D. Stranks, A. Abate, C. Wehrenfennig, S. Guarnera, A.-A. Haghighirad, A. Sadhanala, G. E. Eperon, S. K. Pathak, M. B. Johnston, A. Petrozza, L. M. Herz, H. J. Snaith, *Energy Environ. Sci*. **2014**, *7*, 3061.

curve and the axes I and V. The maximum power point is that point on the I-V curve at which the area of the resulting rectangle, I x V, is largest.

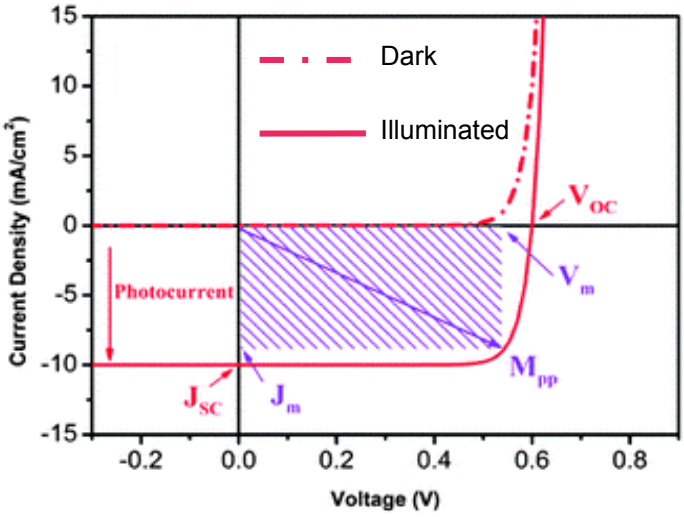

Figure 26.- Typical I-V curve for any type of solar cell in the dark and under illumination (the most important photovoltaic parameters are indicated).

Fill Factor (FF): It is the ratio of its actual maximum power output to its theoretical power output, if current and voltage would be at their maxima, I_{SC} and V_{OC}, respectively. This is a very important property used to measure photovoltaic device performance. It is a measure of the 'squareness' of the I-V curve. FF can be written down as follows (*Eq. 1*).

$$FF = \frac{Jm \times Vm}{Jsc \times Voc} \qquad \textit{Eq. 1}$$

Power Conversion Efficiency (PCE or η): It is the ratio of power output, Pout, to power input, Pin. PCE measures the amount of power produced by a photovoltaic device relative to the power available in the incident solar radiation. Pin is the sum over all wavelengths, which usually has a value of 100 mW/cm^2 when solar simulators are used. This is the most general way to define the efficiency of a photovoltaic device. PCE can be written down as follows (*Eq. 2*).

$$\mathrm{PCE}\ (\eta) = \frac{\mathrm{Pout}}{\mathrm{Pin}} \times 100\% = \frac{\mathrm{Jm}\times\mathrm{Vm}}{\mathrm{Pin}} \times 100\% = \frac{\mathrm{Jsc}\times\mathrm{Voc}\times\mathrm{FF}}{\mathrm{Pin}} \times 100\% \qquad \textit{Eq. 2}$$

PCE is one of the most important parameters to characterize solar cell performances. In order to compare results from various devices, regardless of the design and active material, photovoltaic cells are all subject to the same standard test conditions. The cells are typically illuminated at a constant density of roughly 100 mW/cm^2, which is defined as the standard '1 Sun' value, with a spectrum consistent to an air-mass global value of 1.5 (AM 1.5G), at a temperature of 25 ºC. Air mass describes the spectrum of radiation and can be defined a the amount of atmosphere though which sunlight has to travel to reach the Earth's surface. This is abbreviated as AM x, in which x is the inverse of the cosine of the zenith angle of the sun. The above mentioned AM1.5G conditions correspond to the spectrum and irradiance of sunlight incident with a zenith angle of 48.2º (*Figure 27*).

External Quantum Efficiency (EQE): Also known as Incident Photon to Current Efficiency (IPCE), is another important parameter for solar cell characterization. It is calculated by the number of electrons extracted in an external circuit divided by the number of incident photons at a certain wavelength under short-circuit condition. EQE can be written down as follows (*Eq. 3*)

$$\mathrm{EQE}\ (\lambda) = \frac{\text{number of electrons}}{\text{number of incident photons}} = \frac{\mathrm{Jsc}\ (\lambda)/e}{\mathrm{Pin}\ (\lambda)/(hc/\lambda)} = \frac{\mathrm{Jsc}\ (\lambda)hc}{\mathrm{Pin}\ (\lambda)e\lambda} \qquad \textit{Eq. 3}$$

where λ is the wavelength, *e* is the elementary charge, *h* is the Planck constant, and *c* is the speed of light in vacuum.

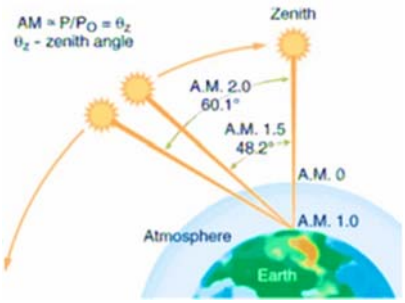

Figure 27.- The air-mass value AM 0 equates to insolation at sea level with the Sun at its zenith. AM 1.0 represents sunlight with the Sun at zenith above the Earth's atmosphere. AM 1.5 is the same, but with the Sun at an oblique angle of 48.2º, which simulates a longer optical path through the Earth's atmosphere; AM 2.0 extends that oblique angle to 60.1º.

1.2 Organic Solar Cells (OSCs)

In general terms, the photovoltaic process for organic photovoltaic (OPV)[129] cells starts when light is absorbed by the organic active layer, and an electron from the HOMO is promoted to the LUMO by formation of an exciton (electron-hole pair). After exciton dissociation, the electron migrates to the cathode, and the hole moves to the anode. A fundamental difference in the working principle of solar cells based on organic materials with regard to conventional inorganic photovoltaic cells, is that, in the latter, the absorption of photons with energies greater than the bandgap of the semiconductor results in the direct generation of free charge carriers (electron and holes) that are able to diffuse under an externally applied electric field to their respective electrodes. On the other hand, organic materials characteristically have a much lower dielectric constant than their inorganic counterparts, and this results in the generation of tighly coulombically bound electron-hole pairs upon photoabsorption, with a binding energy of about 0.5 eV, rather than free charge carriers.[130] In addition, organic semiconductors do not exhibit band-like transport behaviour, the charge carriers moving along by a hopping mechanism between localized states.[131,132] The chargecarrier mobilities in organic semiconductors are, therefore, inherently low, with typical values less than 10^{-2} cm^2/Vs. These differences between inorganic and organic materials drive the structural design of organic solar cells.[133]

Almost all current organic photovoltaic solar cells have a planar layered structure, in which the organic active layer(s) is (are) sandwiched between two different electrodes (*Figure 28*). One of them has to be transparent, for transmission of the incoming sunlight. A transparent conductive oxide, such as indium tin oxide (ITO), is often used as anode. The other electrode, cathode, is usually a metal such as aluminium.

---

[129] T. M. Clarke, J. R. Durrant, *Chem. Rev*. **2010**, *110*, 6736.

[130] a) R. N. Marks, J. J. M. Halls, D. D. C. Bradley, R. H. Friend, A. B. Holmes, *J. Phys. Condens. Matter* **1994**, *6*, 1379; b) P. B. Miranda, D. Moses, A. J. Heeger, *Phys. Rev. B* **2001**, *64*, 081201.

[131] Since organic semiconductors do not have a three dimensional periodical lattice structure, charge transport in polymers cannot be described by standard semiconductor model. Instead, localized states are formed and charge carriers proceed from one such a state to another (hopping), thereby absorbing or emitting phonons to overcome the energy difference between those states. Conwell and Mott proposed the concept of hopping conduction in 1956 to describe impurity in inorganic semiconductors.

[132] For a full treatment of the theory of charge transport in conjugated organic materials, the reader is referred to this review: V. Coropceanu, J. Cornil, D. A. S. Filho, Y. Oliver, R. Silbey, J.-L. Bredas, *Chem. Rev*. **2007**, *107*, 926.

[133] B. A. Gregg, M. C. Hanna, *J. Appl. Phys*. **2003**, *93*, 3605.

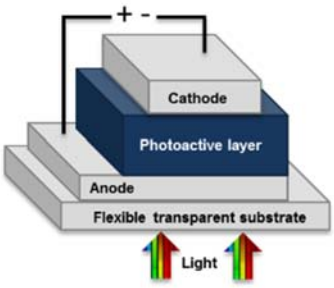

Figure 28.- General built-up of photovoltaic cell.

1.2.1 Architectures and device operating principles

First organic photovoltaic devices were designed as a single organic layer sandwiched between two metal electrodes of different work functions,[134,135] which generate an electric field that drives electrons and holes to, respectively, anode and cathode. Reported power conversion efficiencies did not surpass 0.5%, owing to the fact that excitons (localized and tightly bound electron-hole pairs) formed upon light illumination do not dissociate readily in most organic semiconductors, as is the case for inorganic derivatives, and the electrical field developed by the asymmetric work functions of the electrodes in an OPV does not provide the necessary driving force for charge separation.[103c] Instead, the exciton diffuses within the organic layer or it recombines. Since exciton diffusion lengths for most organic solar cells are below 5-10 nm,[136] only those excitons generated in a small region within less than this length from the contacts contribute to the photocurrent. Hence, the main weakness of single layer architectures was the extensive charge recombination. As a consequence, much single layer devices have small efficiencies and are only used to study specific device properties.[137]

[134] B. R. Weinberger, M. Akhtar, S. C. Gau, *Synth. Met*. **1982**, *4*, 187.
[135] S. Glenis, G. Tourillon, F. Garnier, *Thin Solid Films* **1986**, *139*, 221.
[136] a) J. J. M. Halls, K. Pichler, R. H. Friend, S. C. Moratti, A. B. Holmes, *Appl. Phys. Lett*. **1996**, *68*, 3120; b) D. E. Markov, E. Amsterdam, P. W. M. Blom, A. B. Sieval, J. C. Hummelen, *J. Phys. Chem. A* **2005**, *109*, 5266; c) D. E. Markov, C. Tanase, P. W. M. Blom, J. Wildeman, *Phys. Rev. B* **2005**, *72*, 045217; d) Y. Wang, H. Benten, S. Ohara, D. Kawamura, H. Ohkita, S. Ito, *ACS Appl. Mater. Interfaces* **2014**, *6, 14108.*
[137] a) T. A. Abdalla, W. Mammo, B. Workalemahu, *Synth. Met*. **2004**, *144*, 213; b) F. T. Reis, D. Mencaraglia, S. O. Saad, I. Seguy, M. Oukachmih, P. Jolinat, P. Destruel, *J. Non-Cryst. Solids* **2004**, *338*, 599; c) G. D. Sharma, S. K. Sharma, M. S. Roy, *Thin Solid Films* **2004**, *468*, 208.

1.2.1.1 Planar heterojunction devices

As outlined above, in 1986 a significant boost in the OPV performance roadmap came when Tang used a two-component donor:acceptor active layer, consisting of a copper phthalocyanine (donor) and a perylene derivative (acceptor), in a planar heterojunction device. A record, for that time, efficiency of 1.0% was reported.[105] The general principle behind heterojunction devices is to use two organic materials with different electron affinities and ionization potentials. In this manner, exciton (electron and hole) dissociation at the heterojuntion (interface) of the two components will be favoured, since the electron will be accepted by the organic material with the largest electron affinity and the hole by the organic material with the lowest ionization potential.

The schematic structure of a heterojunction photovoltaic device is outlined in *Figure 29*. In classical architectures, holes are transported to the anode and electrons are transported to the cathode (*Figure 29a*). The anode must be transparent because through it the light can enter to the solar cell. In this case, the anode, typically consists of a substrate that is coated with a high work function transparent conducting electrode, and modified with an interfacial hole selective/electron blocking layer between the electrode and the active layer. The most common materials in the OPV field used for these electrodes are indium tin oxide (ITO) on glass substrates modified with a 40 nm thick poly(3,4-ethylenedioxythiophene):poly(styrenesulfonate) (PEDOT:PSS) interfacial layer. These materials are favourable due to their large optical transparency and good charge transport properties. The PEDOT:PSS hole transporting layer smoothens out the ITO surface, seals the active layer from oxygen and prevents the diffusion of ITO into the active layer, which can lead to unwanted traps. However, there exist several issues with the ITO/PEDOT:PSS combination, including the brittleness of both glass and ITO, which does not allow for roll to roll processing, the rarity and price of indium, and the acidity of PEDOT:PSS which induces the degradation of devices. The active layers, containing the donor and acceptor components are deposited on the top of the PEDOT:PSS layer. There are four roles that need to be filled by the active layer in a heterojunction solar cell: light absorption, exciton generation, exciton dissociation, and charge separation (the acceptor material takes the electrons and the donor material, the holes). The conducting materials must be semiconductors so that the cell can maintain an output voltage and not just produce photoconductivity. If the charge carriers are generated far from the electrodes, the materials will also need to be efficient charge conductors (long carrier lifetimes) so that the charges are not lost before collection (*vide infra*).

A low work function metal, typically aluminium, is used as the cathode on the top of the active layer. Most of the time, a very thin layer of lithium fluoride (5-10 Å) is placed in between the active layer and the cathode, which serves as protecting layer between

the aluminium and the organic components of the device. To a lesser extent, devices with an inverted structure (*Figure 29b*), that is with an ITO bottom cathode and a high work function metal anode, have also been studied.[138]

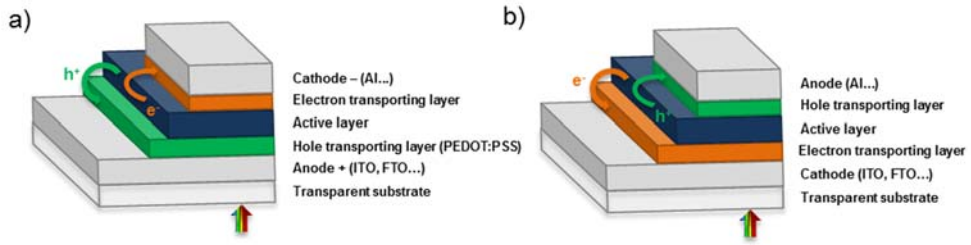

Figure 29.- Schematic configuration of an organic photovoltaic system: a) classical (transparent anode, collecting holes); b) inverted (transparent cathode, collecting electrons).

In a typical heterojunction photovoltaic device four processes occur during the conversion of solar energy into electrical energy *(Figure 30*). When light is absorbed by the donor component, an electron is promoted from the HOMO to the LUMO forming an exciton (step 1; photoinduced exciton generation). This formed exciton moves towards a donor/acceptor interface *via* a chemical potential gradient (step 2; exciton diffusion to the interface) where the electron can transfer to the LUMO of the acceptor material, forming a charge transfer complex, which will be favourable to occur when the energy difference between the LUMO of the donor and the acceptor is greater than the binding energy of the exciton. This energy difference is typically on the order of a couple hundred meV, depending on the materials employed, and any absorbed energy in excess of this exciton binding energy will be lost in these systems. Electron and hole are now on different materials, but remain strongly bound by coulomb interactions. The charge transfer state can become a charge separated state, or free charge carriers, (step 3; exciton dissociation) if the distance between the electron and hole becomes greater than the coulomb capture radius. Any dissociated charges can be then transported through p-type or n-type domains to the electrodes, with holes being collected at the anode and electrons being collected at the cathode (step 4; charge collection), where they can be used to do work in an external circuit.

[138] T. Ameri, G. Dennler, C. Waldauf, H. Azimi, A. Seemann, K. Forberich, J. Hauch, M. Scharber, K. Hingerl, C. J. Brabec, *Adv. Mater*. **2010**, *20*, 1592.

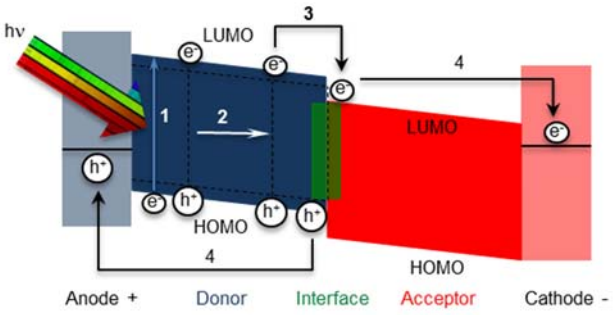

Figure 30.- Schematic of the operating principles of OPV, highlighting the desired transport of charge pairs generated at interface (green) through the donor (red) and acceptor (blue) materials.

Not all the light that is falling onto the photovoltaic device is converted into photocurrent. There can be a large number of alternative processes, which usually limit the efficiency of a device.[139] For example, not all the incoming photons are absorbed by the active layer. This is a result of the limited bandgap and thickness of the active layer. In addition, excitons which are created too far from the donor/acceptor interface (the exciton diffusion length is limited to 5-10 nm),[136] are not able to dissociate into free charge pairs within the lifetime of the exciton and therefore, by-processes (*i.e.* fluorescence, non-radiative) occur, which make the exciton decay back to its ground state. Other loss mechanisms are the recombination of the geminate electron hole pair across the donor/acceptor interface (referred to as geminate recombination) and recombination of free charges during transportation to the electrodes All these energy losses have a direct bearing on the solar cell efficiency, and obviously characteristic parameters such as J_{SC}, V_{OC} and FF are also impacted by them. For instance, the EQE, which describes the overall efficiency of the four main processes of the photovoltaic process in OPVs, can also be described as follows (Eq. 4).

$$\mathrm{EQE}\,(\lambda) = \eta\mathrm{abs}\,(\lambda) \times \eta\mathrm{diff}\,(\lambda) \times \eta\mathrm{ct}\,(\lambda) \times \eta\mathrm{coll}\,(\lambda) \qquad \textit{Eq. 5}$$

where η_{abs} is the photoabsorption efficiency, η_{diff} is the exciton diffusion efficiency to the donor/acceptor interface, η_{CT} is the charge transfer efficiency, η_{coll} is the charge collection

[139] a) D. Veldman, S. C. J. Meskers, R. A. J. Janssen, *Adv. Funct. Mater*. **2009**, *19*, 1939; b) C. W. Schlenker, M. E. Thompson, *Chem. Comm*. **2011**, *47*, 3702; c) U. Hormann, J. Kraus, M. Gruber, C. Schuhmair, T. Linderl, S. Grob, S. Kapfinger, K. Klein, M. Stutzman, H. J. Krenner, W. Brutting, *Phys. Rev. B* **2013**, *88*, 235307; d) W. Li, K. H. Hendriks, A. Furlan, M. M. Wienk, R. A. J. Janssen, *J. Am. Chem. Soc*. **2015**, DOI: 10.1021/ja5131897.

efficiency, and λ is the wavelength of interest. EQE values close to 1 for a specified wavelength indicate efficient current generation for light absorbed at that wavelength, with limited recombination losses. Increasing recombination or reflection losses result in lower EQE values. The J_{SC} is dependent on efficient light-harvesting, carrier generation and mobility, while the V_{OC} is proportional to the energy difference between the HOMO of the donor and the LUMO of the acceptor.[140] In this respect, molecular orbital levels, absorption coefficients, morphology of the layers and molecular diffusion length are the main factors that control the final result. Research in the field has flourished in the last decade and the rational design of new optimized materials has led to PCEs above 10%.[141]

1.2.1.2 Bulk heterojunction devices

The seminal work by Tang about PHJ,[105] paved the way for the development of other donor/acceptor type architectures, including the *solution processed* BHJ type architecture with increased donor/acceptor interfacial areas (*Figure 31*). These BHJ devices present a unique blended film of a donor and an acceptor as active layer, this feature overcoming the diffusion problem. The great advantage in comparison to PHJ is that, upon controlling the morphology of the active layer into an interpenetrating, bicontinuous network of the donor and the acceptor, one can achieve, first, high interfacial area within the BHJ active layer for efficient exciton dissociation and, second, efficient collection of charges. The BHJ architecture relies on finding a balance between charge generation and transport, and can be limited by charge carrier lifetimes. All these factors are significantly affected by the morphology of the layer at the nanoscale, which is probably the major challenge in BHJ devices.

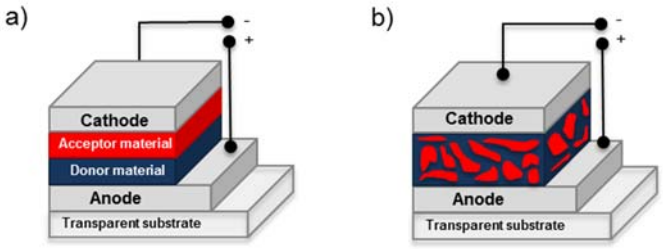

Figure 31.- Comparative, schematic representations of a) a planar and b) bulk heterojunction devices.

[140] a) C. J. Brabec, A. Cravino, D. Meissner, N. S. Sariciftci, T. Fromherz, M. T. Rispens, L. Sanchez, J. C. Hummelen, *Adv. Funct. Mater*. **2011**, *11*, 374; b) B. Qi, J. Wang, *J. Mater. Chem.* **2012**, *22*, 24315.

[141] a) M. C. Scharber, D. Muhlbacher, M. Koppe, P. Denk, C. Waldauf, A. J. Heeger, C. J. Brabec, *Adv. Mater*. **2006**, *18*, 789; b) T. Umeyama, H. Imahori, *J. Mater. Chem. A* **2014**, *2*, 11545.

This concept has been mainly applied to devices containing semiconducting polymers as hole-transport materials in combination with C_{60} fullerene, which holds unique features for its application in OPVs, for instance, small reorganization energy associated with charge transfer reactions. In 1995, Yu *et al*. made the first BHJ photovoltaic cell,[106] in which the active layer consisted of poly[2-methoxy-5-(2'-ethylhexyloxy)-1,4-phenylenevinylene] (MEH-PPV)[142] derivative as donor, and C_{60} as acceptor, showing a PCE of 2.9%. One limitation of this approach is the relative low solubility of fullerenes in normal solvents. This problem was solved by Wudl *et al*.[143] by synthesizing a number of C_{60}-derivatives with increased solubility (like the well-known [6,6]-phenyl-C_{61}-butyric acid methyl ester, commonly called PCBM), which allows to increase the amount of fullerene used for the production of the PV cells. Besides PPV derivatives, many other types of conjugated polymers, such as polythiophenes, have been used in fullerene BHJ devices in the search of higher efficiencies. Also in 1995, the first reports of polymer/polymer bulk heterojunction devices came independently from two research groups,[108,144] both working with the same PPV-derivatives: poly(2,5,2',5'-tetrahexyloxy-7,8'-dicyanodi-*p*-phenylenevinylene) (CN-PPV), as acceptor, and MEH-PPV as donor. From then on, a large number of studies have been done to find suitable polymer donor/polymer acceptor (all-polymer) bulk heterojunction devices,[145] which present PCEs reaching 3.0-4.8%.[146] More research needs to be done in the search for good acceptor polymers.[147] Hence, the combination of conjugated polymers and

[142] F. Wudl, G. Srdanov, **1993**, US patent 5,189,136.
[143] J. C. Hummelen, B. W. Knight, F. LePeq, F. Wudl, J. Yao, C. L. Wilkins, *J. Org. Chem*. **1995**, *60*, 532.
[144] G. Yu, A. J. Heeger, *J. Appl. Phys*. **1995**, *78*, 4510.
[145] A. Facchetti, *Mater. Today* **2013**, *16*, 123.
[146] a) E. Zhou, J. Cong, Q. Wei, K. Tajima, C. Yang, K. Hashimoto, *Angew. Chem Int. Ed*. **2011**, *50*, 2799; b) N. Zhou, H. Lin, S. J. Lou, X. Yu, P. Guo, E. F. Manley, S. Loser, P. Hartnett, H. Huang, M. R. Wasielewski, L. X. Chen, R. P. H. Chang, A. Facchetti, T. J. Marks, *Adv. Energy Mater*. **2014**, *4*, 1300785; c) Y. Zhou, T. Kurosawa, W. Ma, Y. Guo, L. Fang, K. Vandewal, Y. Diao, C. Wang, Q. Yan, J. Reinspach, J. Mei, A. L. Appleton, G. I. Koleilat, Y. Gao, S. C. B. Mannsfeld, A. Salleo, H. Ade, D. Zhao, Z. Bao, *Adv. Mater*. **2014**, *26*, 3767; d) Y.-J. Hwang, T. Earmme, S. Subramaniyan, S. A. Jenekhe, *Chem. Comm*. **2014**, *50*, 10801; e) T. Earmme, Y.-J. Hwang, N. M. Murari, S. Subramaniyan, S. A. Jenekhe, *J. Am. Chem. Soc*. **2013**, *135*, 14960; f) D. Mori, H. Benten, I. Okada, H. Ohkita, S. Ito, *Adv. Energy Mater*. **2014**, *4*, 1301006; g) T. Earmme, Y.-J. Hwang, S. Subramaniyan, S. A. Jenekhe, *Adv. Mater*. **2014**, *26*, 6080.
[147] a) J. J. M. Halls, J. Cornil, D. A. dos Santos, R. Silbey, D.-H. Hwang, A. B. Holmes, J. L. Bredas, R. H. Friend, *J. Phys. Rev. B* **1999**, *60*, 5721; b) H. J. Snaith, A. C. Arias, A. C. Morteani, C. Silva, R. H. Friend, *Nano Lett*. **2002**, *2*, 1353; c) F. Zhang, M. Jonforsen, D. M. Johansson, M. R. Anderson, O. Inganas, *Synth. Met*. **2003**, *138*, 555; d) A. J. Breeze, Z. Schlesinger, S. A. Carter, H. Tillmann, H.-H. Horhold, *Sol. Energ. Mat. Sol. Cells* **2004**, *83*, 263; e) M.-F. Falzon, M. M. Wienk, R. A. J. Janssen, *J. Phys. Chem. C* **2011**, *115*, 3178; f) Y. Kim, E. Lim, *Polymers* **2014**, *6*, 382.

fullerenes remains the most common approach towards the active layer in BHJ devices. As a result, control of the morphology in polymer:fullerene BHJ devices is of considerable importance;[148-149] in the case of small molecule-based solar cells, morphology of the active layer is also critical, although less problematic.[92b]

Although the preparation of solution-processed polymer:fullerene BHJ solar cells is very simple, the proper control of the processing parameters is complex, and involves detailed studies of the influence of many factors, *e.g*. the choice of solvent,[150] the speed of evaporation, the solubility, the miscibility of donor and acceptor materials, the concentration of the solution, the weight ratio of the active components, the molecular weight of the conjugated polymer,[151] the casting method (drop-casting or spin-coating), *etc*. The optimum set of parameters may obviously change with different material combinations.

For instance, the influence of the casting solvent and casting method on the morphology was extensively investigated in poly[2-methoxy-5-(3',7'-dimethyloctyloxy)-1,4-phenylenevinylene] (MDMO-PPV) and PCBM layers. These investigations include the fine tuning of the optimal ratio of the donor and acceptor materials in devices. The PCE of BHJ solar cells based on 1:4 weight ratio of MDMO-PPV:PCBM could be improved from approximately 1 % to 2.5 % (AM 1.5) by simply changing the solvent from which the active layer was cast.[152-154] Atomic force microscopy (AFM) investigations showed that rather large, *i.e*. 100 – 200 nm clusters were formed in the toluene cast films, meanwhile a smooth surface morphology was observed for the chlorobenzene cast films. Transmission electron microscopy (TEM) and AFM studies[155] assigned the large clusters to a PCBM-rich phase. The large-scale phase separation in toluene yielded smaller photocurrents, since it impedes the dissociation of all generated excitons, and therefore,

---

[148] a) H. Hoppe, M. Niggemann, C. Winder, J. Kraut, R. Hiesgen, A. Hinsch, D. Meissner, N. S. Sariciftci, *Adv. Funct. Mater*. **2004**, *14*, 1005; b) H. Hoppe, N. S. Sariciftci, *J. Mater. Chem*. **2006**, *16*, 45; c) C. Kastner, D. A. M. Egbe, H. Hoppe; *J. Mater. Chem. A* **2015**, *3*, 395.

[149] K. R. Graham, C. Cabanetos, J. P. Jahnke, M. N. Idso, A. E. Labban, G. O. N. Ndjawa, T. Heumueller, K. Vandewal, A. Salleo, B. F. Chmelka, A. Amassian, P. M. Beaujuge, M. D. McGehee, *J. Am. Chem. Soc*. **2014**, *136*, 9608.

[150] J. Liu, Y. Shi, Y. Yang, *Adv. Funct. Mater*. **2001**, *11*, 420.

[151] C. Nicolet, D. Deribew, C. Renaud, G. Fleury, C. Brochon, E. Cloutet, L. Vignau, G. Wantz, H. Cramail, M. Geoghegan, G. Hadziioannou, *J. Phys. Chem. B* **2011**, *115*, 12717.

[152] S. E. Shaheen, C. J. Brabec, N. S. Sariciftci, F. Padinger, T. Fromherz, J. C. Hummelen, *Appl. Phys. Lett*. **2001**, *78*, 841.

[153] J. M. Kroon, M. M. Wienk, W. J. H. Verhees, J. C. Hummelen, *Thin Solid Films* **2002**, *403*, 223.

[154] T. Aernouts, W. Geens, J. Poortmans, P. Heremans, S. Borghs, R. Mertens, *Thin Solid Films* **2002**, *403*, 297.

[155] T. Martens, J. D'Haen, T. Munters, Z. Beelen, L. Goris, J. Manca, M. D'Olieslaeger, D. Vanderzande, L. De Schepper, R. Andriessen, *Synth. Met*. **2003**, *138*, 243.

lowers the overall PCE. The high PCBM ratio (MDMO-PPV:PCBM, 1:4) is needed for an efficient electron transport, which demonstrates that a minimun grain size of PCBM is necessary to guarantee enough pathways for the electrons. Another interesting finding was related to the casting method; further investigations have focused on the difference in the resulting morphology after drop-casting or spin-coating of the films.[155] Smaller PCBM domains are observed in spin-coated films than in drop-cast films due to the faster evaporation rate during spin-coating which tends to freeze the blend, resulting in smaller and more dispersed PCBM domains, while the slower evaporation in drop-casting allows the PCBM to coalesce into larger domains.

Several techniques and a variety of materials have been used to sort out these morphological problems, like changing the fullerene derivative for other acceptor molecule or polymer as aforementioned. An alternative approach includes active layers made of "double cable" polymers (*Figure 32*). This concept was introduced to have a control on the morphology at the molecular level by preparing intrinsically bipolar materials,[156] in which the donor and acceptor photoactive units are covalently linked within the same molecule in order to prevent phase separation. Electrons created by photoinduced electron transfer are transported by hopping between the pendant acceptor moieties (n-cable), leaving the remaining holes on the polymer, which are transported along the conjugated chain (p-cable). In comparison to the bulk-heterojunction, the effective donor/acceptor interfacial area is maximized within the double-cable design, and phase separation is prevented. Ideally, the realization of double-cable polymers brings the p/n-heterojunction to the molecular level. In addition, the interaction between the donor conjugated backbone and the acceptor moieties may be tuned by varying the chemical structure (nature and length) of their connecting fragments. In particular, by introducing an insulating spacer between the n-type and p-type "cable", the ground state interaction between the electron donor and acceptor moieties can be prevented, but its length must be appropriate to facilitate photoinduced electron transfer.

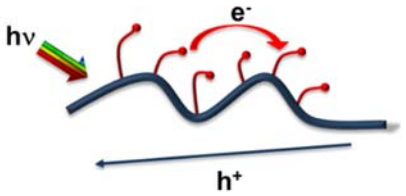

Figure 32.- Ideal representation of "double-cable" polymers. The charge carriers generated by photoinduced charge transfer can be transported within one molecule, therefore viewed as a "molecular heterojunction".

[156] A. Cravino, N. S. Sariciftci, *Nat. Mater*. **2003**, *2*, 360.

In 2001 Ramos *et al*. reported for the first time the use of a double cable polymer in an organic solar cell, comprising a PPV derivative with pendant fullerenes.[157] and most of the "double–cable" polymers reported so far contain covalently linked fullerene moieties.[158] Unfortunately, it is difficult to achieve significant load of fullerenes due to reduced solubility of the "double-cable" polymer. The use of different acceptor molecules is still much less widespread, although examples can be found emloying anthraquinone moieties[159] or perylene diimide (PDI) as pendant groups.[160] As an example of "double-cable" polymer containing another acceptor unit rather than fullerenes a carbazole-bithiophene backbone functionalized with PDI units as electron acceptors is depicted in *Figure 33*. In general the PCE of organic solar devices employing "double-cable" materials, is rather low. This indicates the presence of loss mechanisms due to the recombination of electrons and holes and poor charge transport. Apparently, too intimate mixing results in the occurrence of too small mean free paths.

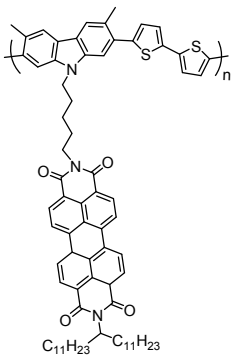

Figure 33.- Chemical structure of a carbazole based "double cable" polymer with pendant PDIs groups.

1.2.2 Advanced organic materials for solar cells

Many material combinations have been tried that fit the necessary requirements for their use in solar cell devices, namely, intense absorption of light, semiconducting character, good charge mobility and complementary electron donor/acceptor character.

---

[157] A. M. Ramos, M. T. Rispens, J. K. J. van Duren, J. C. Hummelen, R. A. J. Janssen, *J. Am. Chem. Soc*. **2001**, *123*, 6714.

[158] a) J. Roncali, *Chem. Soc. Rev*. **2005**, *34*, 483; b) F. Giacalone, N. Martin, *Chem. Rev*. **2006**, *106*, 5136; c) A. Cravino, N. S. Sariciftci, *J. Mater. Chem.* **2002**, *12*, 1931; d) M. Li, P. Xu, J. Yang, S. Yang, *J. Mater. Chem*. **2010**, *20*, 3953; e) B. Gholamkhass, T. J. Peckham, S. Holdcroft, *Polym. Chem*. **2010**, *1*, 708; f) N. Berton, I. Fabre-Francke, D. Bourrat, F. Chandezon, S. Sadki, *J. Phys. Chem. B* **2009**, *113*, 14087.

[159] a) M. Catellani, S. Luzzati, N.-O. Lupsac, R. Mendichi, R. Consonni, A. Famulari, S. V. Meille, F. Giacalone, J. L. Segura, N. Martin, *J. Mater. Chem*. **2004**, *14*, 67; b) D. K. Mohamad, S. S. Chauhan, H. Yi, A. J. Cadby, D. G. Lidzey, A. Iraqi, *Sol. Energy Mater. Sol. Cells* **2011**, *95*, 1723.

[160] D. K. Mohamad, A. Fischereder, H. Yi, A. J. Cadby, D. G. Lidzey, A. Iraqi, *J. Mater. Chem*. **2011**, *21*, 851.

Generally, these materials fall into two main categories depending on their size: polymers and small molecules. Polymer solar cells, as mentioned above, are processed from solution in organic solvents to form BHJ devices, whereas small molecule solar cells are processed mainly using thermal evaporation deposition in a high vacuum environment to build PHJ cells with a more precise control of the thickness and morphology of the active layers. Using the solution process to fabricate small molecule solar cells has recently been gaining momentum, although the film quality and crystallization is expected to be an issue.

In the following section, the most efficient materials in both small molecule and polymer solar cells will be described.

1.2.2.1 Small molecules-based solar cells

For some years, small molecule solar cells were built in PHJ arquitectures by high vacuum evaporation techniques of chromophores such as Pcs, PDIs, C_{60} fullerenes, among others, but solution-processed BHJ devices were only reserved for polymers. In spite of the plentiful advantages of polymers employed as the light harvester and electron donor in OPVs, limitations related to the reproducibility of their synthesis, purification, and inherent electronic properties sparked the search for alternatives, the most promising solution liying in soluble small conjugated molecules. Research in the field was initiated in 2006,[112a] and since then the use of many classes of chromophores, such as oligothiophenes, triphenylamines, borondipyrromethene (BODIPY), diketopyrrolopyrroles, and other π-conjugated molecules in OPVs has been described.[92c,112c,i,161] Solution processing (spin-coating, inkjet printing, dip-coating, spraying technique) has, been employed, giving rise to a vast number of successful configurations.[112b]

Oligothiophenes are among the most-studied organic semiconductors, owing to their intriguing charge transport characteristics and tunable optoelectronic properties.[162] Initial studies in vacuum-deposited OPVs with 3D oligothiophenes, showed low efficiencies, attributed to the poor absorption characteristics of the material.[92b,112i] A number of other oligothiophene analogues and configurations have been prepared and tested.[112c] However, a significant boost in performance was observed with oligothiophene DR3TBDTT, having a benzo[1,2-b:4,5-b′]dithiophene (BDT) unit as the central building block (*Figure 34*). This oligothiophene presents improved conjugation and, therefore improved light-harvesting and J_{SC}, and long alkyl chains to enhance solubility and hence processability. Solar cells fabricated with the architecture

[161] M. V. Martinez-Diaz, G. de la Torre, T. Torres, *Chem. Comm*. **2010**, *46*, 7090.
[162] A. Mishra, C.-Q. Ma, P. Bauerle, *Chem. Rev*. **2009**, *109*, 1141.

ITO/PEDOT:PSS/DR3TBDTT:$PC_{70}BM$/LiF/Al gave 8.12% (V_{OC}: 0.93 V and J_{SC}: 13.17 mA/cm^2), which is the highest, to date, reported efficiencyiy for solution-processed small-molecule single-junction OPVs.[163]

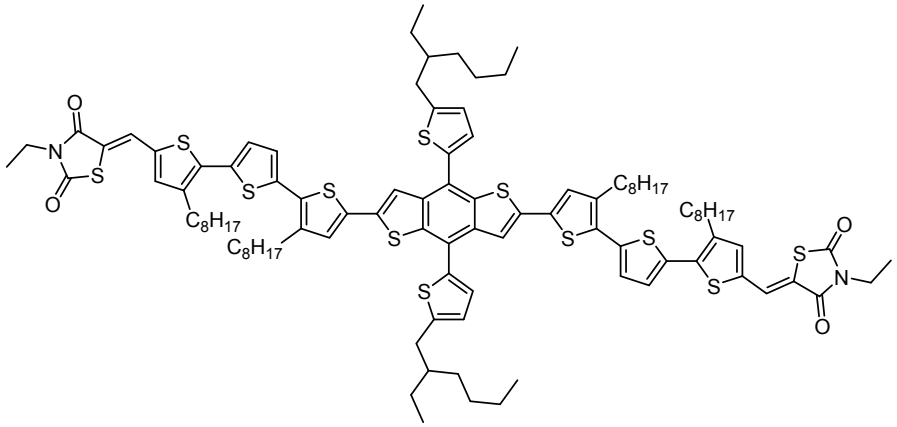

Figure 34.- Chemical structure of a successful oligothiophene-based dyes: DR3TBDTT.

Among other organic dyes, intriguing results have been observed with oligoacenes, particularly pentacene[164] and rubrene (*Figure 35 a and b*),[165] reaching efficiencies around 3%, and also with squaraine dyes. Squaraines present several interesting features, such as high extinction coefficients, photochemical stability and possibility to design other small molecular structures. The squaraine represented in *Figure 35c* showed the highest reported PCE (3.10%) in vacuum-evaporated squaraine systems.[166] Later, this dye was used in a solution-processed device, with $PC_{70}BM$ as the acceptor counterpart, and the efficiency rose to 5.20%.[167] Recently, a donor–acceptor–acceptor (D–A–A) structure, based on an electron-donating ditolylaminothienyl moiety, connected to an electron-withdrawing dicyanovinylene via a pyrimidine group (DTDCTP, *Figure 35d*), was recently prepared and studied in vacuum-processed devices, bringing about remarkable results.[168] In particular, optimized DTDCTP:C_{70} PHJ architectures gave

[163] J. Zhou, Y. Zuo, X. Wan, G. Long, Q. Zhang, W. Ni, Y. Liu, Z. Li, G. He, C. Li, B. Kan, M. Li, Y. Chen, *J. Am. Chem. Soc*. **2013**, *135*, 8484.
[164] S. Yoo, B. Domercq, B. Kippelen, *Appl. Phys. Lett*. **2004**, *85*, 5427.
[165] A. K. Pandey, J.-M. Nunzi, *Adv. Mater*. **2007**, *19*, 3613.
[166] S. Wang, E. I. Mayo, M. D. Perez, L. Griffe, G. Wei, P. I. Djurovich, S. R. Forrest, M. E. Thompson, *Appl. Phys. Lett*. **2009**, *94*, 233304.
[167] G. Wei, S. Wang, K. Sun, M. E. Thompson, S. R. Forrest, *Adv. Energy Mater*. **2011**, *1*, 184.
[168] S.-W. Chiu, L.-Y. Lin, H.-W. Lin, Y.-H. Chen, Z.-Y. Huang, Y.-T. Lin, F. Lin, Y.-H. Liu, K.-T. Wong, *Chem. Comm*. **2012**, *48*, 1857.

a PCE of 6.4% with a V_{OC} of 0.95 V, J_{SC} of 12.1 mA/cm^2 and FF of 0.56. The impressive V_{OC} was attributed to the low-lying HOMO level (-5.46 eV) of the donor material.

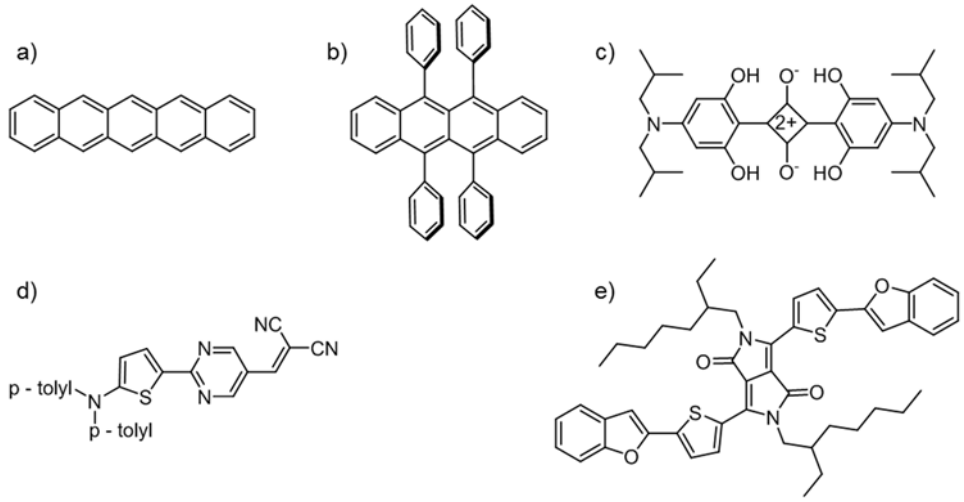

Figure 35.- Chemical structure of some successful small molecules used in OPVs: a) pentacene, b) rubrene, c) squaraine, d) DTDCTP and e) a diketopyrrolopyrrole derivative.

Noteworthy are also the results that have been obtained with diketopyrrolopyrroles (DPP)[169] in solution-processed systems. DPP are attractive building blocks in terms of synthetic versatility. Modification of the main structure with benzofuran substituents led to the derivative represented in *Figure 35e*, which exhibited increased intermolecular chromophore interaction through high conjugation as well as stabilized HOMO levels.[170] In detail, a deep HOMO of -5.2 eV was observed and when blended with $PC_{70}BM$, it gave a V_{OC} higher than 0.9 V, a J_{SC} of 10 mA/cm^2 and an overall efficiency of 4.4%.

From a different angle, notwithstanding the great success of porphyrins in dye-sensitized solar cells, as this will be discussed further in another section, this class of compounds has not been as triumphant in OPVs due to their reduced absorption in the red region of the visible spectrum and the lower charge-carrier mobility and exciton–

[169] a) M. Grzybowski, D. T. Gryko, *Adv. Optical Mater*. **2015**, *3*, 280; b) B. P. Karsten, J. C. Bijleveld, R. A. J. Janssen, *Macromol. Rapid Commun*. **2010**, *31*, 1554; c) D. Chandran, K.-S. Lee, *Macromol. Res*. **2013**, *21*, 272.

[170] B. Walker, A. B. Tamayo, X.-D. Dang, P. Zalar, J.-H. Seo, A. Garcia, M. Tantiwiwat, T.-Q. Nguyen, *Adv. Funct. Mater*. **2009**, *19*, 3063.

diffusion length of the evaporated films.[161] In terms of Pcs, their important role in organic solar cells is explained below.

Phthalocyanines in small molecules-based solar cells

Pcs are preferred photosensitizers for utilizing them as active component in solar cells.[161,171] Apart from their unique electronic properties, and chemical structure they show an extended photoresponse at 600-800 nm, where the photons flux is maximum. This means that only extremely thin films are necessary to absorb a substantial fraction of the solar photons. Owing to the reduced solubility of unsubstituted phthalocyanines, these dyes have been usually incorporated in heterojunction devices by vacuum-sublimation techniques. On the other hand, chemically modified Pcs, holding peripheral and/or axial substituents can be processed from solution. Additionally, suitable functionalization allows for the tuning of the electronic properties.

After the first reports on planar solar cells based on Pcs and perylene derivatives previously commented,[105] device performance was significantly increased by combination of planar and bulk heterojunction architectures or stacking of different cells in the tandem concept. An interesting development came by combining a vacuum-deposited Cu(II)Pc/C_{60} thin film in a ITO/PEDOT:PSS/Cu(II)Pc/C_{60}/bathocuproine/Al format, obtaining 4.2% PCE under 4.4 suns.[172] An impressive enhancement was observed when the same active materials were used in a hybrid heterojunction geometry, attaining 5% PCE.[173] As well, a tandem configuration consisting of two hybrid heterojunctions stacked in series (*Figure 36*), employing CuPc/CuPc:C_{60}(1:1)/C_{60} as active layers, brought about a further increase in PCE to 5.7%.[174]

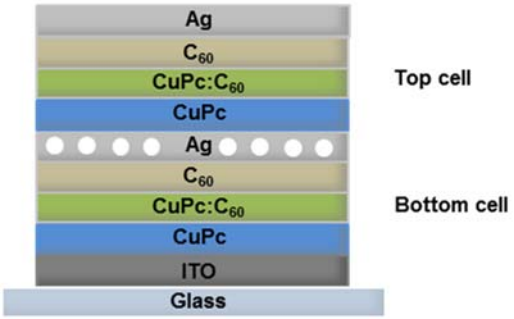

Figure 36.- Schematic structure of the tandem organic solar cell realized by Forrest *et al.*

[171] a) M. V. Martínez-Diaz, T. Torres, in *Handbook of Porphyrin Science* (Eds.: K. Kadish, K. M. Smith, R. Guilard), World Scientific Press, Singapur, **2010**, Vol. *10*, Chapter 45; b) M. G. Walter, A. B. Rudine, C. C. Wamser, *J. Porphyrins Phthalocyanines* **2010**, *14*, 759; d) H. Imahori, T. Umeyama, K. Kurotobi, Y. Takano*, Chem. Comm*. **2012**, *48*, 4032.
[172] J. Xue, S. Uchida, B. P. Rand, S. R. Forrest, *Appl. Phys. Lett*. **2004**, *84*, 3013.
[173] J. Xue, B. P. Stand, S. Uchida, S. R. Forrest, *Adv. Mater*. **2005**, *17*, 66.
[174] J. Xue, S. Uchida, B. P. Rand, S. R. Forrest*, Appl. Phys. Lett*. **2004**, *85*, 5757.

The Pc derivatives mostly used for vacuum-deposited small-molecule solar cells are Cu and Zn complexes that have similar absorption properties. The power conversion efficiency of a solar cell shows the importance of obtaining simultaneously a high J_{sc} and V_{oc}. Therefore, researchers have concentrated their efforts on improving the limited open-circuit voltage. This clearly shows that there is still room for improvement of efficiency by modification of Pc structures.

Along the same lines, one of the most suprising molecules in the area of OPVs is subphthalocyanines (SubPcs).[175] These compounds are non-planar, lower homologues of Pcs comprising a 14-π electron aromatic macrocycle consisting of three diiminoisoindole units *N*-fused around a central boron atom. SubPcs, in contrast with their related congeners, the planar Pcs, possess a peculiar conical structure, which provides them with relatively high solubility and low tendency to aggregate. The strong light absorption properties in the visible region (500-700 nm) together with the tunability of their π-conjugated system render them an excellent material for the production of small molecule OPVs. This Pc analogue can be used both as the molecular donor and acceptor of the device. In this regard, SubPc-Cl:C_{70} architectures have achieved 5.4% efficiencies in vacuum-deposited systems (*Figure 37*).[176] Alternatively, fullerene-free cells consisting of the same SubPc as the donor and a perchlorated SubPc-Cl (*Figure 37*) as the acceptor have accomplished PCEs of 2.7%.[177] The good performance in this case was attributed to the increased V_{OC} compared to a similar SubPc–C_{60} combination. Interestingly, when the same perchlorated SubPc acceptor was paired with a subnaphthalocyanine (SubNc-Cl; *Figure 37*) as the donor counterpart in a SubNc-Cl:SubPc-Cl configuration, an outstanding 6.4% was reported.[178] The result was rationalized on the basis of complementary absorption of the two subphthalocyanine analogues, the reduced recombination at the interface and the improved energetic alignment. These are the so-called ‘‘all SubPc based-devices’’. Lastly, when SubPc-Cl and SubNc-Cl were used both as acceptors in a three-layer vacuum-processed architecture with α-sexithiophene (*Figure 37*) as the donor, a record (in fullerene-free systems) 8.4% efficiency was accomplished.[179]

---

[175] C. G. Claessens, D. Gonzalez-Rodriguez, M. S. Rodriguez-Morgade, A. Medina, T. Torres, *Chem. Rev*. **2014**, *114*, 2192.

[176] R. Pandey, Y. Zou, R. J. Holmes, *Appl. Phys. Lett*. **2012**, *101*, 033308.

[177] P. Sullivan, A. Duraud, I. Hancox, N. Beaumont, G. Mirri, J. H. R. Tucker, R. A. Hatton, M. Shipman, T. S. Jones, *Adv. Energy Mater*. **2011**, *1*, 352.

[178] B. Verreet, K. Cnops, D. Cheyns, P. Heremans, A. Stesmans, G. Zango, C. G. Claessens, T. Torres, B. P. Rand, *Adv. Energy Mater*. **2014**, *4*, 1301413.

[179] K. Cnops, B. P. Rand, D. Cheyns, B. Verreet, M. A. Empl, P. Heremans, *Nat. Commun*. **2014**, *5*, 3406.

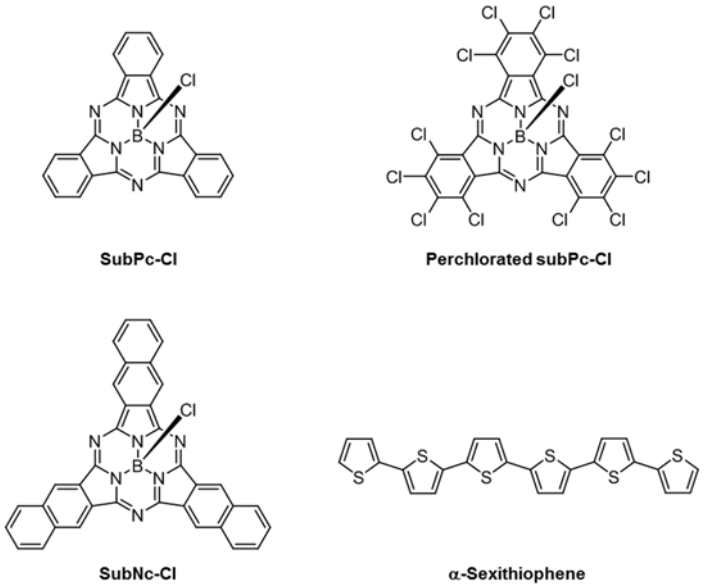

Figure 37.- Structures of donor and acceptor subphthalocyanine analogues and a oligothiophene known as α-sexithiophene.

1.2.2.2 Polymer-based solar cells

Plastic solar cells are attractive owing to a number of advantageous features including their efficient solution processing with low manufacturing energy requirements. As mentioned above, plastic solar cells comprise a semiconducting electron-donor polymer, performing also as light-absorbing material, and a fullerene derivative as the electron acceptor.[111c,e,180] Fullerenes promote ultrafast charge separation and long exciton diffusion length, and are also characterized by their small reorganization energy, high electron affinity, beneficial molecular shape and easy accessibility, which renders them ideal electron acceptors in OPVs.[181] Numerous derivatives have been prepared for solar cell applications,[103b,182] but the highly soluble PCBM (*Figure 38*)[143] is still a benchmark n-type structure for OPVs.[108b] On the other hand, the inherent limitation of the most commonly used C_{60} fullerenes, namely their weak absorption in the visible region, has triggered the preparation of other fullerenes, like C_{70} derivatives (*Figure 38*) , which

[180] a) B. C. Thompson, J. M. J. Frechet, *Angew. Chem. Int. Ed*. **2008**, *47*, 58; b) P. Khlyabich, B. Burkhart, A. E. Rudenko, B. C. Thompson, *Polymer* **2013**, *54*, 5267; c) X. Yang (ed.), W. Ma, *Semiconducting Polymer Composites*, Wiley-VCH Verlag GmbH & Co. KGaA, Weinheim, Germany, **2013**, Chapter 12. *Fullerene/Conjugated Polymer Composite for the State-of-the-Art Polymer Solar Cells*.

[181] L. A. A. Petterson, L. S. Roman, O. Inganas, *J. Appl. Phys*. **1999**, *86*, 487.

[182] Y. He, Y. Li, *Phys. Chem. Chem. Phys*. **2011**, *3*, 1970.

exhibit significantly stronger absorption over a wider range of the visible spectrum than C_{60} derivatives.[183] To overcome the scarce bandgap tunability of fuller-based acceptors, some research has also been devoted to the use of non-fullerene n-type organic molecules with strong absorption in the visible range and easy-to-modify structures and electronic leves, such as perylenediimides, diketopyrrolopyrroles,[169,184] benzothiadiazoles (BT),[185] and dicyanovinylenes,[186] among others, as alternative acceptors for OPVs.[112h,187,188] Performances, though, remain consistently poor (less than 3%), with the exception of perylenediimides (*Figure 38*)[189] that have shown intriguing behaviour and efficiencies up to 6.1%.[190] Alternatively, small molecule donor/polymer

[183] a) S. Pfuetzner, J. Meiss, A. Petrich, M. Riede, K. Leo, *Appl. Phys. Lett*. **2009**, *94*, 223307; b) M. M. Wienk, J. M. Kroon, W. J. H. Verhees, J. Knol, J. C. Hummelen, P. A. van Hal, R. A. J. Janssen, Angew. Chem. Int. Ed. 2003, 42, 3371.

[184] a) Y. Lin, P. Cheng, Y. Li, X. Zhan, *Chem. Comm*. **2012**, *48*, 4773; b) Y. Lin, Y. Li, X. Zhan, *Adv. Energy Mater*. **2013**, *3*, 724; c) H. Patil. W. X. Zu, A. Gupta, V. Chellappan, A. Bilic, P. Sonar, A. Rananaware, S. V. Bhosale, S. V. Bhosale, *Phys. Chem. Chem. Phys*. **2014**, *16*, 23837.

[185] a) P. E. Schwenn, K. Gui, A. M. Nardes, K. B. Krueger, K. H. Lee, K. Mutkins, H. Rubinstein-Dunlop, P. E. Shaw, N. Kopidakis, P. L. Burn, P. Meredith, *Adv. Energy Mater*. **2011**, *1*, 73; b) J. T. Bloking, X. Han, A. T. Higgs, J. P. Kastrop, L. Pandey, J. E. Norton, C. Risko, C. E. Chen, J.-L. Bredas, M. D. McGehee, A. Sellinger, *Chem. Mater*. **2011**, *23*, 5484; c) J. T. Bloking, T. Giovenzana, A. T. Higgs, A. J. Ponec, E. T. Hoke, K. Vandewal, S. Ko, Z. Bao, A. Sellinger, M. D. McGehee, *Adv. Energy Mater*. **2014**, *4*, 1301426.

[186] a) T. Zhou, T. Jia, B. Kang, F. Li, M. Fahlman, Y. Wang, *Adv. Energy Mater*. **2011**, *1*, 431, b) Y. Fang, A. K. Pandey, A. M. Nardes, N. Kopidakis, P. L. Burn, P. Meredith, *Adv. Energy Mater*. **2013**, *3*, 54.

[187] a) P. Sonar, J. P. F. Lim, K. L. Chan, *Energy Environ. Sci*. **2011**, *4*, 1558; b) C. L. Chochos, N. Tagmatarchis, V. G. Gregoriou, *RSC Adv*. **2013**, *3*, 7160; c) Y. Lin, X. Zhan, *Mater. Horiz*. **2014**, *1*, 470.

[188] a) Y. Zhou, L. Ding, K. Shi, Y.-Z. Dai, N. Ai, J. Wang, J. Pei, *Adv. Mater*. **2012**, *24*, 957; b) T. V. Pho, F. M. Toma, B. J. Tremolet de Villers, S. Wang, N. D. Treat, N. Eisenmenger, G. M. Su, R. C. Coffin, J. D. Douglas, J. M. J. Frechet, G. C. Bazan, F. Wudl, M. L. Chabinyc, *Adv. Energy Mater*. **2014**, *4*, 1301007; c) S. Holliday, R. S. Ashraf, C. B. Nielsen, M. Kirkus, J. A. Rohr, C.-H. Tan, E. Collado-Fregoso, A.-C. Knall, J. R. Durrant, J. Nelson, I. McCulloch, *J. Am. Chem. Soc*. **2015**, *137*, 898; d) H. Li, T. Earmme, S. Subramaniyan, S. A. Jenekhe, *Adv. Energy Mater*. **2015**, DOI: 10.1002/aenm.201402041.

[189] a) E. Kozma, M. Catellani, *Dyes Pigments* **2013**, *98*, 160; b) Q. Yan, Y. Zhou, Y.-Q. Zheng, J. Pei, D. Zhao, *Chem. Sci*. **2013**, *4*, 4389.

[190] a) G. Ren, E. Ahmed, S. A. Jenekhe, *Adv. Energy Mater*. **2011**, *1*, 946; b) S. Rajaram, R. Shivanna, S. K. Kandappa, K. S. Narayan, *J. Phys. Chem. Lett*. **2012**, *3*, 2405; c) X. Zhang, Z. Lu, L. Ye, C. Zhan, J. Hou, S. Zhang, B. Jiang, Y. Zhao, J. Huang, S. Zhang, Y. Liu, Q. Shi, Y. Liu, J. Yao, *Adv. Mater*. **2013**, *25*, 5791; d) Y. Zang, C.-Z. Li, C.-C. Chueh, S. T. Williams, W. Jiang, Z.-H. Wang, J.-S. Yu, A. K.-Y. Jen, *Adv. Mater*. **2014**, *26*, 5708; e) Y. Zhong, M. T. Trinh, R. Chen, W. Wang, P. P. Khlyabich, B. Kumar, Q. Xu, C.-Y. Nam, M. Y. Sfeir, C. Black, M. L. Steigerwald, Y.-L. Loo, S. Xiao, F. Ng, X.-Y. Zhu, C. Nuckolls, *J. Am. Chem. Soc.* **2014**, *136*, 15215; f) W. Jiang, L. Ye, X. Li, C. Xiao, F. Tan, W. Zhao, J. Hou, Z. Wang, *Chem. Comm*. **2014**, *50*, 1024; g) R. Singh, E. Aluicio-Sarduy, Z.

acceptor OPVs have been less studied; despite this, very recently an efficiency of 2.1% was achieved for an acceptor naphthalenedicarboximide copolymer.[191]

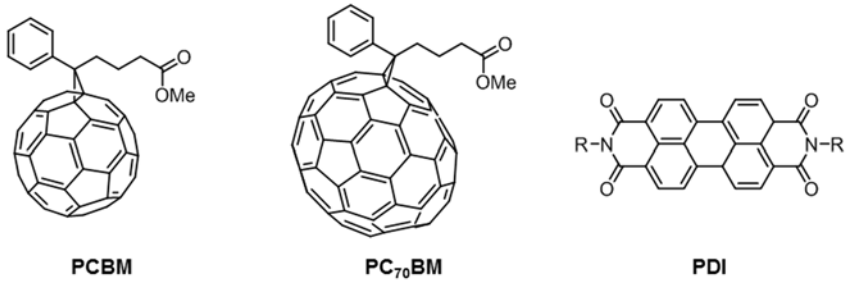

Figure 38.- Chemical structure of typical acceptors used in plastic solar cells.

Conjugated polymers usually play the role of electron donors in plastic solar cells. Since Shirakawa, MacDiarmid, and Heeger demonstrated in 1977 that the conductivity of conjugated polymers can be increased by doping,[192] which earned them the Nobel Prize in Chemistry in 2000, these unique materials have been used successfully for a wide range of optical and electronic applications, *e.g.* light emitting diodes,[193] optical lasers,[194] and solar cells. *Figure 39* shows the major classes of traditional conjugated polymers. With the exceptions of polyacetylene and polyaniline, these materials consist of sequentially linked aromatic units.

Kan, T. Ye, R. C. I. MacKenzie, P. E. Keivanidis, *J. Mater. Chem. A* **2014**, *2*, 14348; h) Z. Lu, B. Jiang, X. Zhang, A. Tang, L. Chen, C. Zhan, J. Yao, *Chem. Mater*. **2014**, *26*, 2907; i) P. E. Hartnett, A. Timalsina, H. S. S. R. Matte, N, Zhou, X. Guo, W. Zhao, A. Facchetti, R. P. H. Chang, M. C. H. Hersam, M. R. Wasielewski, T. J. Marks, *J. Am. Chem. Soc*. **2014**, *136*, 16345; j) H. Li, T. Earmme, G. Ren, A. Saeki, S. Yoshikawa, N. M. Murari, S. Subramaniyan, M. J. Crane, S. Seki, S. A. Jenekhe, *J. Am. Chem. Soc*. **2014**, *136*, 14589; k) Y. Lin, Y. Wang, J. Wang, J. Hou, Y. Li, D. Zhu, X. Zhan, *Adv. Mater*. **2014**, *26*, 5137; l) X. Zhang, J. Yao, C. Zhan, *Chem. Comm*. **2015**, *51*, 1058; m) X. Zhang, C. Zhan, J. Yao, *Chem. Mater*. **2015**, *27*, 166; n) Y. Liu, C. Mu, K. Jiang, J. Zhao, Y. Li, L. Zhang, Z. Li, J. Y. L. Lai, H. Hu, T. Ma, R. Hu, D. Yu, X. Huang, B. Z. Tang, H. Yan, *Adv. Mater*. **2015**, *27*, 1015.

[191] Z. Li, J. D. A. Lin, H. Phan, A. Sharenko, C. M. Proctor, P. Zalar, Z. Chen, A. Facchetti, T.-Q. Nguyen, *Adv. Funct. Mater*. **2014**, *24*, 6989.

[192] C. K. Chiang, C. R. Fincher, Y. W. Park, A. J. Heeger, H. Shirakawa, E. J. Louis, S. C. Gau, A. G. MacDiarmid, *Phys. Rev. Lett*. **1977**, *39*, 1098.

[193] a) J. H. Burroughes, D. D. C. Bradley, A. R. Brown, R. N. Marks, K. Mackay, R. H. Friend, P. L. Burns, A. B. Holmes, *Nature* **1990**, *347*, 539; b) R. H. Friend, R. W. Gymer, A. B. Holmes, J. H. Burroughes, R. N. Marks, C. Taliani, D. D. C. Bradley, D. A. Dos Santos, J. L. Bredas, M. Logdlund, W. R. Salaneck, *Nature* **1999**, *397*, 121; c) A. Kraft, A. C. Grimsdale, A. B. Holmes, *Angew. Chem. Int. Ed*. **1998**, *37*, 402.

[194] M. D. McGehee, A. J. Heeger, *Adv. Mater*. **2000**, *12*, 1655.

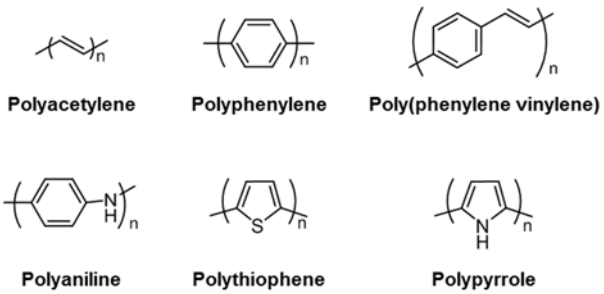

Figure 39.- Chemical structure of some important conjugated polymers.

The solubility of the polymer is an important issue in BHJ solar cells. Due to their tendency to aggregate and a low entropy of dissolution, unsubstituted conjugated polymers like those shown in *Figure 39* are insoluble. To render them soluble, an obvious necessity for enabling solution processing, they have to be functionalized along the backbone with flexible alkyl chains. Branched chains particularly those containing racemic chiral centers, are the best at inducing solubility, but often produce amorphous materials. Straight chain alkyl groups, when judiciously placed along the backbone, can afford solubility and crystallinity. In poly[3-hexylthiophene-2,5-diyl] (P3HT), for instance, the alkyl chains are extended in the solid state, and van der Waals interactions between alkyl groups on adjacent chains help induce crystallinity.

The electrical properties of conjugated polymers are determined by their electronic structure. Overlap of adjacent atomic p_z-orbitals results in a band structure that nearly approximates a typical inorganic semiconductor, with a filled valence band consisting of π-bonding molecular orbitals and an empty conduction band consisting of π^*-antibonding molecular orbitals (*Figure 40*). The energy spacing between the HOMO and the LUMO is the bandgap (E_g).[195]

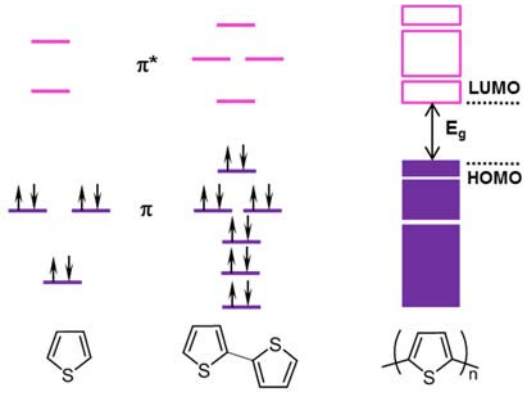

Figure 40.- Qualitative diagram of the π molecular orbitals of thiophene, bithiophene, and polythiophene. As the chain length is extended, bands are formed and the electronic structure starts to resemble that of an inorganic semiconductor.

[195] J. L. Reddinger, J. R. Reynolds, *Advances in Polymer Science*, Springer-Verlag, Berlin,**1999**, Vol. *145*, Chapter *Molecular Engineering of π-Conjugated Polymers*.

Despite possessing an electronic band structure that resembles inorganic semiconductors, conjugated polymers do not typically exhibit band-like charge transport. This is primarily due to structural disorder in the solid state, as well as their tendency to form polaronic structures. When a charge is introduced into a conjugated polymer by oxidation or reduction, a region of the chain structurally distorts, producing a low-energy state, known as a polaron state, within the bandgap. The charge is not typically delocalized over the whole chain, but instead spreads over a characteristic length, typically 8-10 aromatic units for a polymer such as polythiophene. The polaron moves in the solid by hopping to adjacent chains through π-stacking interactions. Because this process involves deformation of the lattice, it has an activation energy. Thus charge transport in conjugated polymers is almost always thermally activated, and charge mobility increases with increasing temperature. Charge mobilities in conjugated polymers can vary widely from 10^{-6} - 1 cm^2/Vs because they can be influenced by several factors. Structural disorder in solid films produces trap states that slow the movement of polarons. Therefore, achieving a high degree of crystallinity in a conjugated polymer film is very important for achieving high mobility. Additionally, as charge hopping is mediated by π-stacking, a short π-stacking distance between chains (less than 4 Å) is necessary for high mobility. Finally, charge transport in conjugated polymers is often highly anisotropic (due again to the dependence on π-stacking), and mobilities can vary by several orders of magnitude depending on which direction they are measured.Regarding bandgap, their control is critical for the design of polymers for solar applications, as E_g determines light absorption, and it can be varied by modification of, for instance,[196] side groups, steric hindrance and π conjugated length.[197] The ideal bandgap for a light absorbing material in polymer-fullerene-based solar cell is around 1.5-1.7 eV, lower than the typical 2.0 eV of the polymers in *Figure 39*.[141a] As commented in the BHJ device section, the polymers of choice for the preparation of the earliest plastic OPVs, were MEH-PPV, MDMO-PPV (*Figure 41)*, and other PPV-based materials,[111c,e,180] which showed efficiencies under 3%.[183b] The large bandgap of these polymers (over 1.9 eV) did not allow for effective harvesting of photons, which limited significantly further optimization of the device performance.

[196] a) J. Cornil, D. A. dos Santos, D. Beijonne, J. L. Bredas, *J. Phys. Chem*. **1995**, *99*, 5604; b) W. B. Davis, M. R. Wasielewski, M. A. Ratner, *Int. J. Quantum Chem*. **1999**, *72*, 463; c) F. Bartha, I. A. Howard, P. Geerlings, C. Van Alsenoy, D. Vanderzande, T. J. Cleij, F. Bogar, *Int. J. Quantum Chem*. **2006**, *106*, 1912.

[197] R. Hoffmann, C. Janiak, C. Kollmar, *Macromolecules* **1991**, *24*, 3725.

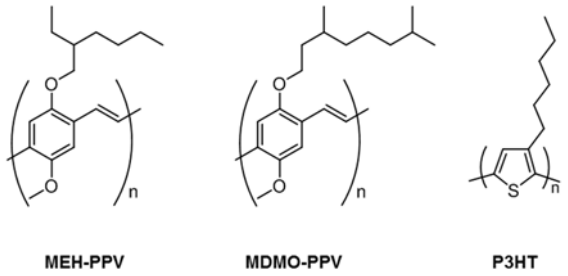

Figure 41.- Chemical structure of some successful polymers used in the earliest plastic solar cells.

Polythiophenes, and especially P3HT (*Figure 41*), subsequently came under the spotlight and performances boosted to 5%,[198] due to a better HOMO–LUMO alignment and carrier mobilities that resulted in enhanced short-circuit current densities. Although limited absorption of P3HT (~1.9 eV bandgap) and small V_{OC} of the P3HT:PCBM combination (0.6 V) have narrowed their commercialization,[199] they have remained a standard platform for fundamental research in organic photovoltaics.[200] These limitations shifted interest towards the so-called low bandgap polymers, and fortunately, many synthetic strategies have been explored towards the preparation of these materials.[201] The most common approach is the donor-acceptor strategy, which is based on the alternation of electron donor and electron acceptor units in the same polymer.[202] The high energy level of the HOMO of the donor component and the low energy level for the LUMO of the acceptor results in a lower bandgap due to intra-chain charge transfer (*Figure 42*). Polymers with bandgaps as low as 0.3 eV have been obtained in this manner.[203] A disadvantage is that donor-acceptor polymers typically have extinction coefficients up to an order of magnitude lower than their homopolymer counterparts. This is a result of poor spatial overlap between the HOMO and LUMO orbitals due to their localization on different aromatic units.

[198] a) W. Ma, C. Yang, X. Gong, K. Lee, A. J. Heeger, *Adv. Funct. Mater*. **2005**, *15*, 1617; b) J. Y. Kim, S. H. Kim, H.-H. Lee, K. Lee, W. Ma, X. Gong, A. J. Heeger, *Adv. Mater*. **2006**, *18*, 572.
[199] a) G. Dennler, M. C. Scharber, C. J. Brabec, *Adv. Mater*. **2009**, *21*, 1323; b) Y. Ling, L. Yu, *Polym. Rev*. **2010**, *50*, 454; c) G. Li, R. Zhu, Y. Yang, *Nat. Photonics* **2012**, *6*, 153.
[200] M. T. Dang, L. Hirsch, G. Wantz, *Adv. Mater*. **2011**, *23*, 3597.
[201] J. Roncali, *Chem. Rev*. **1997**, *97*, 173.
[202] A copolymer employing electron acceptor and donor units, is used as the donor material in the active layer of a solar cell; therefore, an acceptor material, like PCBM, is also required.
[203] H. A. M. van Mullekon, J. A. J. M. Vekemans, E. E. Havinga, E. W. Meijer, *Mater. Sci. Eng*. **2001**, *32*, 1.

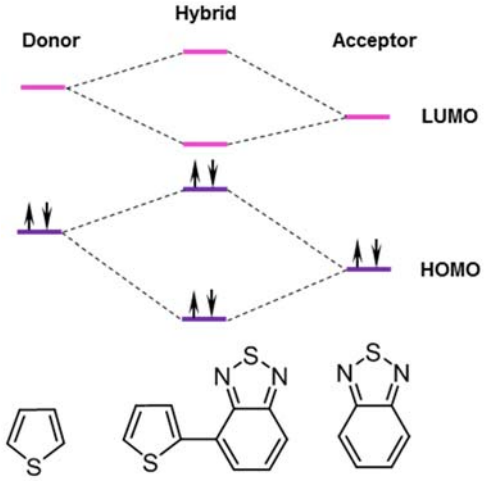

Figure 42.- Qualitative diagram of HOMO-LUMO interactions between an aromatic donor unit (thiophene) and an aromatic acceptor (benzothiadiazole) as the two are joined. The resulting dimer has a considerably narrowed HOMO-LUMO gap. This is meant to illustrate the principle behind the design of narrow bandgap polymers by alternating donor and acceptor units in the mains chains.

Efforts are mainly focused on synthetic manoeuvres to tailor their energy levels, not only for effective light-harvesting, but also for better matching of the HOMO–LUMO levels with those of the acceptor, yielding high V_{OC} while extending the bandgaps to 800-900 nm. Hundreds of conjugated low bandgap donor–acceptor polymers, based on benzo[1,2-b:4,5-b′]dithiophene (BDT),[204] fluorene, carbazole, diketopyrrolopyrrole (DPP),[169,205,206] and cyclopentadithiophene among others[141b,199,207] have been synthesized in recent years, and among those, thieno[3,4-b]thiophene-based structures

[204] a) Y. Liang, L. Yu, *Acc. Chem. Res.* **2010**, *43*, 1227; b) X. Xu, Y. Wu, J. Fang, Z. Li, Z. Wang, Y. Li, Q. Peng, *Chem. Eur. J*. **2014**, *20*, 13259.
[205] B. Tieke, A. R. Rabindranath, K. Zhang, Y. Zhu, *Beilstein J. Org. Chem*. **2010**, *6*, 830.
[206] a) M. M. Wienk, M. Turbiez, J. Gilot, R. A. J. Janssen, *Adv. Mater*. **2008**, *20*, 2556; b) P. Sonar, S. P. Singh, E. L. Williams, Y. Li, M. S. Soh, A. Dodabalapur, *J. Mater. Chem*. **2012**, *22*, 4425; c) J. Yuan, X. Huang, F. Zhang, J. Lu, Z. Zhai, C. Di, Z. Jiang, W. Ma, *J. Mater. Chem*. **2012**, *22*, 22734; d) X. Hu, L. Zuo, W. Fu, T. T. Larsen-Olsen, M. Helgesen, E. Bundgaard, O. Hagemann, M. Shi, F. C. Krebs, H. Chen, *J. Mater. Chem*. **2012**, *22*, 15710; e) Y. Li, P. Sonar, S. P. Singh, Z. E. Ooi, E. S. H. Lek, M. Q. Y. Loh, *Phys. Chem. Chem. Phys*. **2012**, *14*, 7162; f) K. H. Hendriks, W. Li, M. M. Wienk, R. A. J. Janssen, *Adv. Energy Mater*. **2013**, *3*, 674; g) Y. Li, P. Sonar, L. Murphy, W. Hong, *Energy Environ. Sci*. **2013**, *6*, 1684; h) O. Kwon, J. Jo, B. Walker, G. C. Bazan, J. H. Seo, *J. Mater. Chem. A* **2013**, *1*, 7118; i) J. Z. Low, W. T. Neo, Q. Ye, W. J. Ong, I. H. K. Wong, T. T. Lin, J. Xu, *J. Polym. Sci. A Polym. Chem*. **2015**, DOI: 10.1002/pola.27564.
[207] a) E. Bundgaard, F. C. Krebs, *Sol. Energy Mater. Sol. Cells* **2007**, *91*, 954; b) P.-L. T. Boudreault, A. Najari, M. Leclerc, *Chem. Mater*. **2011**, *23*, 456.

have exhibited the most promising behavior, presenting optimally low bandgaps and efficiencies reaching 7–9%.[141b] The most successful derivative is polythieno[3,4-b]-thiophene-co-benzodithiophene (PTB7; *Figure 43*), which stands out as the most widely used and best performing polymer in BHJ OPVs,[208] due to its optimal bandgap and morphology. Lately, overall efficiencies of PTB7-containing devices reached 9.2%, with a V_{OC} of 0.75 V and an exceptional J_{SC} of 17.46 mA/cm^2.[209] Notably, in two hot-off-the-press reports, the 10% threshold was just surpassed with devices based on a PTB7 derivative (PTB7-Th) by applying advanced light manipulation and manufacturing techniques to control photon harvesting and electron mobility.[208c,d] Attention should also be drawn to DPP-containing polymers such PDPP3T*alt*TPT (*Figure 43*), which alternates DPP units as the electron deficient unit with electron rich terthiophene and thiophene-phenylene-thiophene segments and presents remarkable results.[210] BHJ solar cells frabicated from layers comprising this material as electron donor with $PC_{70}BM$ as electron acceptor, show PCEs up to 8.0%. Another successful low-band gap polymer is the prototype polycarbazole poly[N-9'-heptadecanyl-2,7-carbazole-alt-5,5-(4',7'-di-2-thienyl-2',1',3'-benzothiadiazole)] (PCDTBT; Figure 43), which has attained high performances, in the order of 7.5%, with a VOC of 0.90 V.[211] Its exceptional behavior is attributed to its relatively deep HOMO energy (5.5 eV), which results in the observed high V_{OC}.[212]

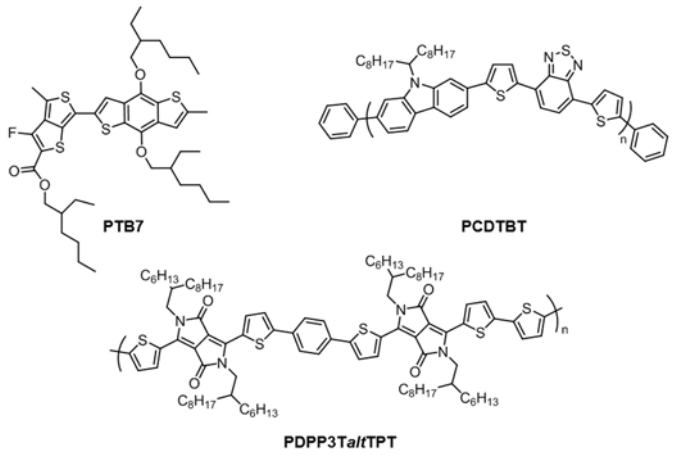

Figure 43.- Chemical structure of some successful polymers used in low bandgap solar cells.

[208] a) L. Lu, L. Yu, *Adv. Mater*. **2014**, *26*, 4413; b) Z. He, C. Zhong, X. Huang, W. Y. Wong, H. Wu, L. Chen, S. Su, Y. Cao, *Adv. Mater*. **2011**, *23*, 4636; c) J.-D. Chen, C. Cui, Y.-Q. Li, L. Zhou, Q.-D. Ou, C. Li, Y. Li, J.-X. Tang, *Adv. Mater*. **2015**, *27*, 1035; d) S.-H. Liao, H.-J. Jhuo, P.-N. Yeh, Y.-S. Cheng, Y.-L. Li, Y.-H. Lee, S. Sharma, S.-A. Chen, *Sci. Rep*. **2014**, *4*, 6813.

[209] Z. He, C. Zhong, S. Su, M. Xu, H. Wu, Y. Cao, *Nat. Photonics* **2012**, *6*, 591.

[210] K. H. Hendriks, G. H. L. Heintges, V. S. Gevaerts, M. M. Wienk, R. A. J. Janssen, *Angew. Chem. Int. Ed*. **2013**, *52*, 8341.

[211] S. Beaupre, M. Leclerc, *J. Mater. Chem. A* **2013**, *1*, 11097.

[212] S. H. Park, A. Roy, S. Beaupre, S. Cho, N. Coates, J. S. Moon, D. Moses, M. Leclerc, K. Lee, A. J. Heeger, *Nat. Photonics* **2009**, *3*, 297.

Improving the photon harvesting: Phthalocyanine-containing polymers

As mentioned above, a largely explored route to broaden the absorption window of solution processed plastic solar cell is to use low bandgap polymers. Another plausible route is adding a chromophore with strong absorption in the visible to a polymer:fullerene BHJ layer in order to enhance the spectral coverage. This can be visualized in *Figure 44*, where the absorption spectra of common conjugated polymers, a dye, and PCBM are depicted together with the solar AM1.5 irradiance photon flux.

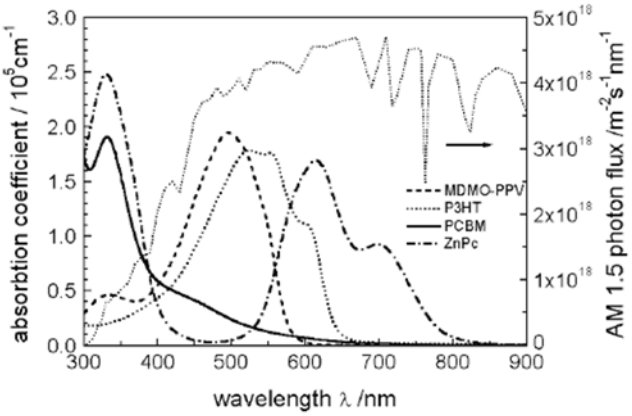

Figure 44.- Absorption spectra of P3HT, PCBM, and a ZnPc, together with the AM1.5 solar photon flux spectrum.

Recently, photoconversion properties extended more than 150 nm toward longer wavelengths have been demonstrated on a P3HT/PCBM blend mixed with a peripherally substituted octabutoxy H_2Pc, as compared to a device without such Pc-sensitization.[213] Maximum internal quantum efficiencies of *ca*. 40% were observed in the main absorption region of the Pc (*i.e.* around 700 nm) for a 10:10:1 ratio of P3HT, PCBM and H_2Pc, respectively. A similar work employing ring-expanded Pcs fused with fluorene, which resulted in a narrower band gap of the dye, also shows improved results.[214] In 2009, a work by Ohkita and co-workers reported a PCE of 2.7% of annealed, spin-coated BHJ devices containing a 10:10:1 ratio of P3HT, PCBM and bis(tri-*n*-hexylsilyloxide) Si(IV)Pc (*Figure 45*), a 20% larger value than the corresponding control device without Pc-sensitization (*i.e.* 2.2%).[215] By constrast, a device based on the P3HT/PCBM/ZnPc blend

[213] E. M. J. Johansson, A. Yartsev, H. Rensmo, V. Sundstrom, *J. Phys. Chem. C* **2009**, *113*, 3014.
[214] S. Yamamoto, M. Kimura, *ACS Appl. Mater. Interfaces* **2013**, *5*, 4367.
[215] S. Honda, T. Nogami, H. Ohkita, H. Benten, S. Ito, *ACS Appl. Mater. Interfaces* **2009**, *1*, 804.

has a lower PCE (1.1%). The key issue of this ternary solar cell[216] is that the Si(IV)Pc derivative holds axially-linked, branched hydrocarbon chains, which avoid the formation of Pc aggregates and, therefore, permit the allocation of the Si(IV)Pc molecules at the donor (P3HT)/acceptor (PCBM) interface. EQE measurements indicate that the Si(IV)Pc molecules can contribute to the photocurrent generation by either direct photoexcitation or as energy funnels for P3HT excitons at the P3HT/PCBM interface.[217] Subsequent studies have shown that the unique performance of bis(tri-*n*-hexylsilyloxide) Si(IV)Pc is not solely due to its frontier orbital energies and bulky substituents,[218] but also might be due to its extraordinary tendency to cristallize in the interface.[219]

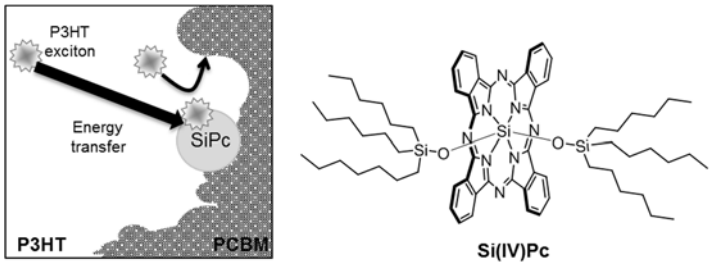

Figure 45.- Schematic representation of SiIV)Pc sensitized P3HT/PCBM solar cell.

Later, the same group developed quaternary OPVs using two near-infrared sensitizers, bis(trihexylsilyloxide) Si(IV)Nc and the Si(IV)Pc employed before, as additives to P3HT/PCBM blends, the cells showing enhanced PCEs up to 4.3%.[220] Few more studies were then carried out using Si(IV)Nc, together with PCBM and P3HT in ternary blends[221] or in combination with an acceptor polymer.[222] Several authors have

[216] To further explain the ternary solar cell concept: a) Y.-C. Chen, C.-Y. Hsu, R. Y.-Y. Lin, K.-C. Ho, J. T. Lin, *ChemSusChem*, **2013**, *6*, 20; b) F. Goubard, G. Wantz, *Polym. Int*. **2014**, *63*, 1362.
[217] S. Honda, S. Yokoya, H. Ohkita, H. Benten, S. Ito, *J. Phys. Chem. C* **2011**, *115*, 11306.
[218] H. Xu, T. Wada, H. Okhita, H. Benten, S. Ito, *Electrochim. Acta* **2013**, *100*, 214.
[219] B. H. Lessard, J. D. Dang, T. M. Grant, D. Gao, D. S. Seferos, T. P. Bender, *ACS Appl. Mater. Interfaces* **2014**, *6*, 15040.
[220] S. Honda, H. Ohkita, H. Benten, S. Ito, *Chem. Comm*. **2010**, *46*, 6596.
[221] B. Lim, J. T. Bloking, A. Ponec, M. D. McGehee, A. Sellinger, *ACS Appl. Mater. Interfaces* **2014**, *6*, 6905.
[222] H. Xu, H. Ohkita, T. Hirata, H. Benten, S. Ito, *Polymer* **2014**, *55*, 2856.

also reported good results using porphyrin dyes blended directly with P3HT[223] or MEH-PPV.[224]

An alternative approach to the blends is to incorporate a chromophore into the polymeric chain, in order to obtain higher photocurrents and increased PCEs in BHJ devices of these materials with PCBM. There are different ways in which a chromophore can be part of a polymer, but in general, the covalent linkages can be used to control the ordering and arrangement of the dye units. The dye-containing polymers can be classified by the way in which the chromophore is incorporated within the macromolecular structure as either network, main-chain or side-chain polymers, and also, the incorporation of the dye molecule as polymer end-groups. The side-chain polymers (*Figure 46a*) are an effective solution for the incorporation of photosensitizers such as phthalocyanines and/or porphyrins, which are dyes that have produced good results in all types of solar photovoltaic cells.[161] In addition, the covalent binding of the these macrocycles to the polymer may avoid the aggregation phenomena and enforce the photosensitizer to interact with both the main chain of the semiconducting polymer and the acceptor PCBM, thus allowing energy transfer from the polymer to the dye molecules and subsequent electron tranfer from the photoexcited dye to PCBM. In addition to the lateral functionalization, the incorporation of highly light-absorbing chromophores in the main chain of a copolymer structure is also an attractive approach to prepare active materials for organic solar cells.

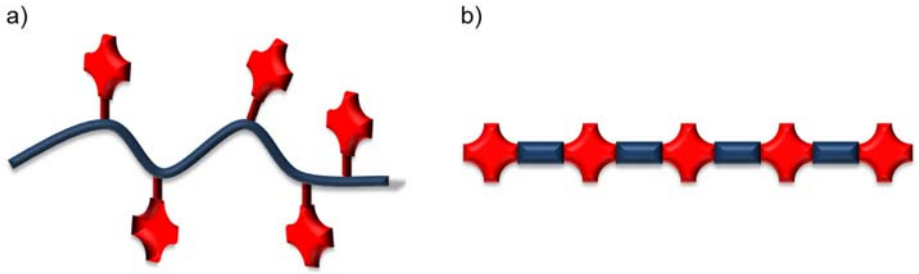

Figure 46.- Representation of a) side-chain chromophore-containing polymer and b) main-chain chromophore polymer.

[223] a) K. Takahashi, M. Asano, K. Imoto, T. Yamaguchi, T. Komura, *J. Phys. Chem. B* **2003**, *107*, 1646; b) J.-J. Yun, H.-S. Jung, S.-H. Kim, E.-M. Han, V. Vaithianathan, S. A. Jenekhe, *Appl. Phys. Lett*. **2005**, *87*, 123102; c) K. B. Burke, W. J. Belcher, L. Thomsen, B. Watts, C. R. McNeill, H. Ade, P. C. Dastoor, *Macromolecules* **2009**, *42,* 3098.

[224] a) P. C. Dastoor, C. R. McNeill, H. Frohne, C. J. Foster, B. Dean, C. J. Fell, W. J. Belcher, W. M. Campbell, D. L. Officer, I. M. Blake, P. Thordarson, M. J. Crossley, N. S. Hush, J. R. Reimers, *J. Phys. Chem. C* **2007**, *111*, 15415; b) N. A. Cooling, X. Zhou, T. A. Sales, S. E. Sauer, S. J. Lind, K. C. Gordon, T. W. Jones, K. B. Burke, P. C. Dastoor, W. J. Belcher, *Sol. Energy Mater. Sol. Cells* **2012**, *98*, 308.

Tetraphenylporphyrins have been incorporated into polymeric structures and tested in BHJ solar cells. An example is an organic solar cell device which organized fullerenes and porphyrins for efficient electron transfer through a polypeptide structure (*Figure 47a*), resulting in a PCE of 1.6%.[225] More recently a co-polymerization approach was described, to produce a panchromatic polymer absorber.[226] Specifically, introduction of a porphyrin–pyrene pendant, endowed with 2,6-bis(dodecyloxy)phenyl substituents to prevent aggregation, in a polythiophene chain exhibited powerful absorption features and reached an impressive PCE of 8.0% in conjuction with $PC_{70}BM$ (*Figure 47b*).

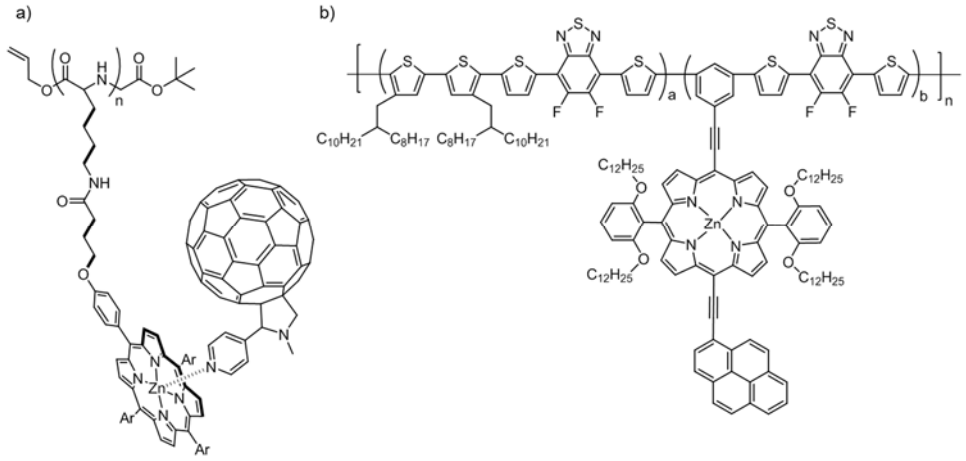

Figure 47.- Structure of some successful polymers with lateral porphyrins used in OPV devices.

On the other hand, many more reports exemplify efforts to increase the light-harvesting properties of the p-type donor phase in a bulk heterojunction solar cell by incorporating strongly light-absorbing chromophores into the backbone of the conjugated polymer phase. The first example of the synthesis and polymer solar cell applications of conjugated polymers with porphyrins as a unit of the main chain was reported by Bo *et al*. in 2008,[227] employing conjugated alternating porphyrin-dithienothiophene copolymers (both units are electron-rich) as active materials (*Figure 48a*). The bad performances

[225] T. Hasobe, K. Saito, P. V. Kamat, V. Troiani, H. Qiu, N. Solladie, K. S. Kim, J. K. Park, D. Kim, F. D'Souza, S. Fukuzumi, *J. Mater. Chem*. **2007**, *17*, 4160.
[226] Y.-H. Chao, J.-F Jheng, J.-S. Wu, K.-Y. Wu, H.-H. Peng, M.-C. Tsai, C.-L. Wang, Y.-N. Hsiao, C.-L. Wang, C.-Y. Lin, C.-S. Hsu, *Adv. Mater*. **2014**, *26*, 5205.
[227] X. Huang, C. Zhu, S. Zhang, W. Li, Y. Guo, X. Zhan, Y. Liu, Z. Bo, *Macromolecules* **2008**, *41*, 6895.

obtained (efficiencies were lower than 0.4%) promoted the incorporation of electron-acceptor units, *i.e.* benzothiadiazole, to have novel low bandgap conjugated copolymers. Namely, an active material based on conjugated polymers containing porphyrins, thiophenes and BTs, together with PCBM, showed a PCE of 0.91% (*Figure 48b*).[228] Although the PCE was improved by the incorporation of D–A structures, it is far from bringing out the full potential of porphyrins in polymer solar cells. The large drop of absorption between the Soret and Q bands as well as less efficient conjugation length in the main chain owing to the large dihedral angles between the porphyrin and adjacent aryl group is responsible for the limitation in the photovoltaic properties. Lowered mobilities are associated with the large dihedral angle between porphyrin monomers that limit both the crystallinity of the obtained films and the extent of π-conjugation overlap within the polymer chains.[227,228,229]

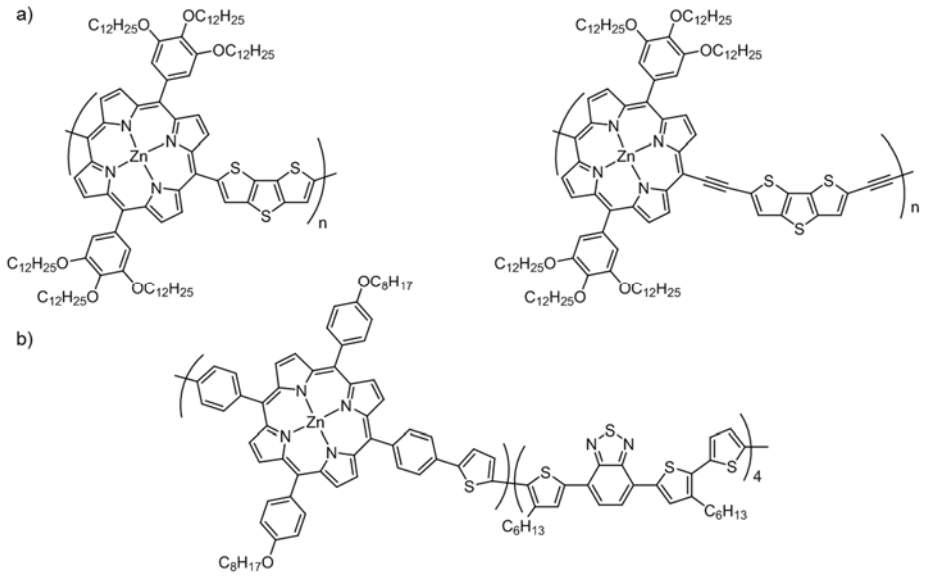

Figure 48.- Structures of porphyrin-based conjugated polymers.

[228] W. Zhou, P. Shen, B. Zhao, P. Jiang, L. Deng, S. Tan, *J. Polym. Sci. A Polym. Chem*. **2011**, *49*, 2685.

[229] a) T. Umeyama, T. Takamatsu, N. Tezuka, Y. Matano, Y. Araki, T. Wada, O. Yoshikawa, T. Sagawa, S. Yoshikawa, H. Imahori, *J. Phys. Chem. C* **2009**, *113*, 10798; b) N. Xiang, Y. Lu, W. Zhou, H. Huang, X. Guo, Z. Tan, B. Zhao, P. Shen, S. Tan, *Eur. Polym. J*. **2010**, *46*, 1084; c) J. Y. Lee, H. J. Song, S. M. Lee, J. H. Lee, D. K. Moon, *Eur. Polym. J*. **2011**, *47*, 1686; d) H. Zhan, S. Lamare, A. Ng, T. Kenny, H. Guernon, W.-K. Chan, A. B. Djurisic, P. D. Harvey, *Macromolecules* **2011**, *44*, 5155.

To avoid the large porphyrin–aryl dihedral angles in porphyrin polymers with meso-linkage, Wang and co-workers recently proposed an edge-fused model (*Figure 49*) to incorporate the porphyrin in the polymer. Thus, copolymers comprising a quinoxalino[2,3-*b*]porphyrin moiety as a new acceptor unit, oligothiophene π-bridges with different lengths, and electron-rich units, such as carbazole,[230] fluorene[231], BDT[231] or DPP[232] have been prepared. These polymers displayed a broad absorption over the entire spectrum of visible light and a large π extension through the polymer because of lower dihedral angles. The polymer solar cell fabricated from the blend of the porphyrin-DPP-containing polymer and $PC_{70}BM$ (*Figure 49*), showed a PCE value as high as promising as 5.07%, which is 3 times higher than that of the solar cell fabricated from the D-A copolymer lacking the porphyrin units.[232]

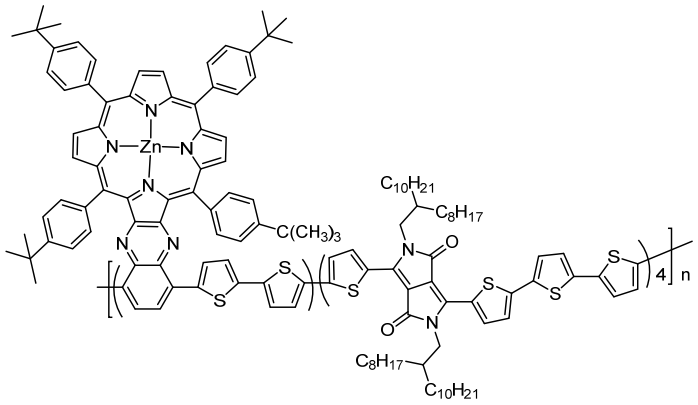

Figure 49.- Structure of quinoxalino[2,3-*b*]porphyrin-DPP-based conjugated copolymer.

Obviously, phthalocyanines are a good alternative to porphyrins, since they can increase the absorption in the red/near infrared region of the solar spectrum owing to their high extinction coefficients; however, the studies about Pc-containing polymers to be employed in BHJ solar cells are only a few and the tendency is the incorporation of Pc macrocycles as pendant groups. Torres *et al*. have studied n- and p-type conjugated PPV oligomers, bearing pendant Zn(II)Pcs linked through an oxygen atom and different

[230] a) S. Shi, X. Wang, Y. Sun, S. Chen, X. Li, Y. Li, H. Wang, *J. Mater. Chem*. **2012**, *22*, 11006; b) S. Shi, P. Jang, S. Chen, Y. Sun, X. Wang, K. Wang, S. Shen, X. Li, Y. Li, H. Wang, *Macromolecules* **2012**, *45*, 7806.

[231] P. Jiang, S. Shi, S. Chen, X. Wang, H. Wang, Y. Li, X. Li, *J. Polym. Sci. A Polym. Chem*. **2013**, *51*, 2243.

[232] L. Wang, S. Shi, D. Ma, S. Chen, C. Gao, M. Wang, K. Shi, Y. Li, X. Li, H. Wang, *Macromolecules* **2015**, *48*, 287.

linkers, with potential applications in organic solar cells (*Figure 50*).[233] Later, the p-type oligomers have been employed together with SWCNTs, where the Zn(II)Pc wraps around the nanotube,[82] and graphene.[80,81]

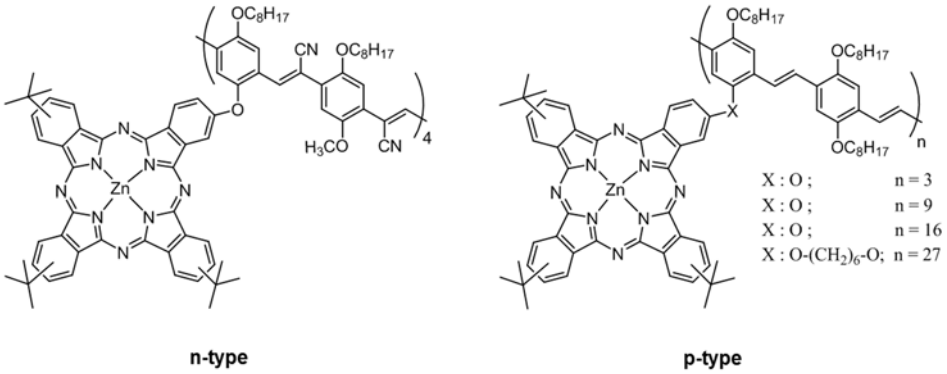

Figure 50.- Structure of oligomers with phthalocyanines as pendant moieties.

The same research group has also prepared donor-acceptor materials based on a polynorbornene framework to which both Pcs and C_{60} electroactive pendant units are randomly attached (*Figure 51a*).[234] After solar devices were constructed, the good match between the IPCE and the absorption spectra of thin films of the copolymer confirmed the ability of the material to create charge carriers from absorbed photons with wavelengths up to 800 nm. Finally, also the "double-cable" concept was explored. Polythiophenes bearing electron-acceptor Ni(II)Pc chromophores were studied as donor-acceptor materials, where the electron-poor Pcs units were appropiately substituted with electron-withdrawing alkylsulfonyl groups (*Figure 51b*).[235] The photophysical characterization showed good charge photogeneration arising from the photoinduced

[80] J. Malig, N. Jux, D. Kiessling, J.-J. Cid, P. Vazquez, T. Torres, D. M. Guldi, *Angew. Chem. Int. Ed*. **2011**, *50*, 3561.
[81] L. Brinkhaus, G. Katsukis, J. Malig, R. D. Costa, M. Garcia-Iglesias, P. Vazquez, T. Torres, D. M. Guldi, *Small* **2013**, *9*, 2348.
[82] a) J. Bartelmess, C.Ehli, J.-J. Cid, M. Garcia-Iglesias, P. Vazquez, T. Torres, D. M. Guldi, *Chem. Sci*. **2011**, *2*, 652; b) J. Bartelmess, C. Ehli, J.-J. Cid, M. Garcia-Iglesias, P. Vazquez, T. Torres, D. M. Guldi, *J. Mater. Chem*. **2011**, *21*, 8014.
[233] J.-J. Cid, C. Ehli, C. Atienza-Castellanos, A. Gouloumis, E.-M. Maya, P. Vazquez, T. Torres, D. M. Guldi, *Dalton Trans*. **2009**, *20*, 3955.
[234] A. de la Escosura, M. V. Martinez-Diaz, T. Torres, R. H. Grubbs, D. M. Guldi, H. Neugebauer, C. Winder, M. Drees, N. Serdar Sariciftci, *Chem. Asian J*. **2006**, *1*, 148.
[235] M. V. Martinez-Diaz, S. Esperanza, A. de la Escosura, M. Catellani, S. Yunus, S. Luzzati, T. Torres, *Tetrahedron Lett*. **2003**, *44*, 8475.

electron transfer from the polythiophene backbone to the Pc moieties. Thereby, Pcs satisfied two functions in the final material: harvesting light in the lower energy region of the spectrum and generating charge carriers.

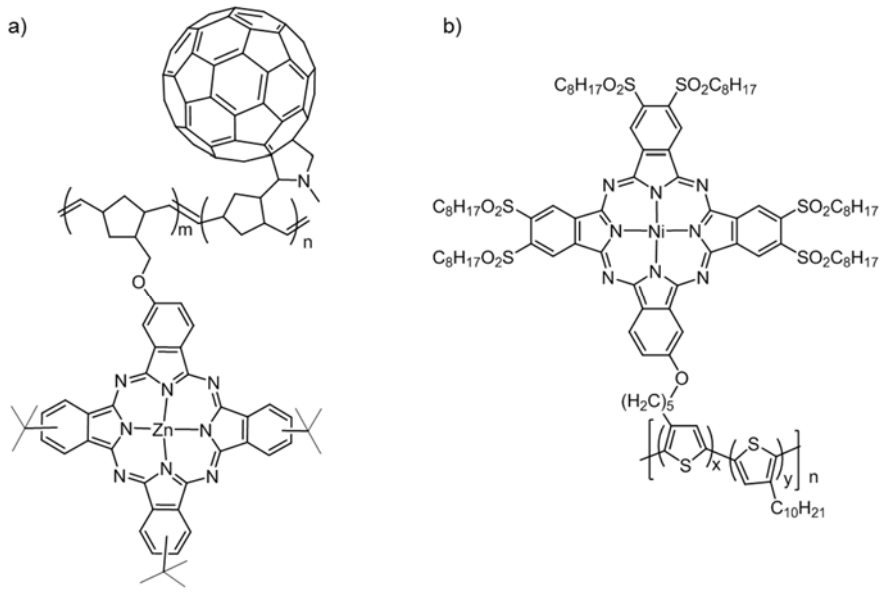

Figure 51.- Structure of a) polynorbornenes bearing Pcs and C_{60} moieties as pendant groups; b) polythiophenes bearing electron-acceptor Pcs.

1.2.3 Objectives

The main goal of the present section of chapter 2 is to synthesize Pc derivatives with different electronic properties as photo- and electroactive components to be implemented into conjugated polymer chains, with the final aim of building BHJ solar cells with the prepared materials. The molecular design of Pcs and Pc-containing polymers has been done taking into account the literature precedents, and also the broad experience gained by our research group, which has been working in this field during the last 10 years.

Lateral functionalization of conjugated polymers with phthalocyanines

In an effort to make some progress in the plastic solar-cell area, an interesting approach is to obtain a polymeric material with an improved absorption in the visible region (up to 750 nm) by attaching Pcs through a post-polymerization process. Linked Pcs can also have a prominent role in the charge separation process taking place in the cell. To achieve this goal, lateral derivatization of conjugated, MDMO-PPV- and P3HT-type copolymers holding adequate functional groups will be carried out by covalent reactions with unsymmetrically substituted Pcs, which will hold solubilizing groups to facilitate purification and solubilization of the final material, and also an adequate functional group to perform the planned reactions (*Figure 52*). In order to test the role of the type of bridge between the Pc and the polymer, two differents reactions will be used: esterification and “click” MDMO-PPV and P3HT reaction. Zinc is selected as the central metal owing to the chemical and photochemical stability of the Zn(II)Pc complexes.

On the other hand, preparation of electron-acceptor Pcs for lateral functionalization of conjugated polymers in a double-cable architecture is also an objective of this thesis. As mentioned in the previous section, the double-cable approach has been envisioned as a way to suppress the phase separation phenomena that occurs in typical polymer/fullerene BHJ devices. Although Pcs have been commonly used as electron-donors in photovoltaic devices, the introduction of electron-withdrawing peripheral substituents can make these macrocycles suitable to replace the C_{60} units in double-cable polymers.

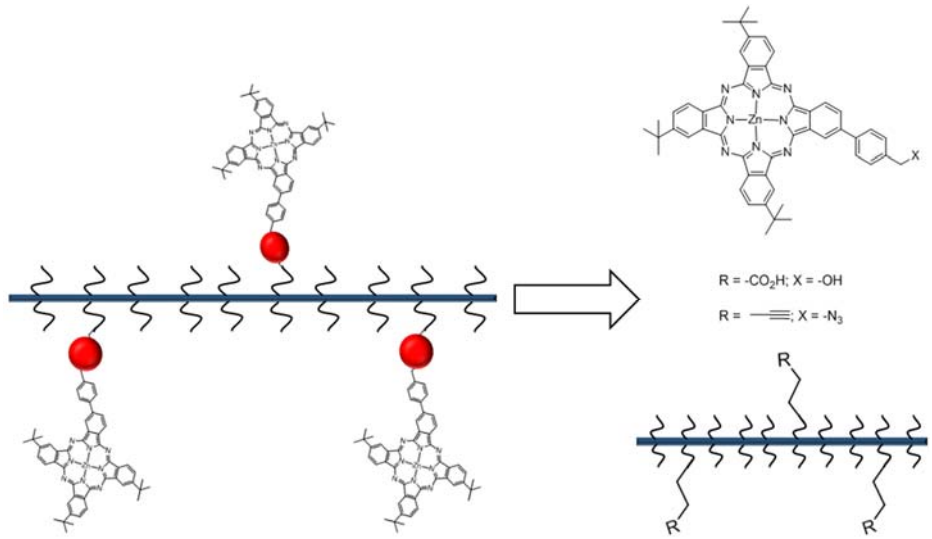

Figure 52.- Retrosynthetic analysis of polymers with lateral functionalization.

A new donor-acceptor PPV-based material, where the acceptor components are electron-poor Zn(II)Pc units appropriately substituted with alkylsulfonyl groups (*Figure 53*), will be synthesized. Substitution of Pc macrocycle with electron withdrawing groups[236,237] usually depressed the HOMO and LUMO levels and renders attractive n-type semiconductors for application in the field of organic electronic materials. In this regard, several Pc derivatives with strong electron withdrawing substituents such as, F,[238,239] Cl,[238] CN,[238] CO_2R,[240] NO_2 and SO_2R[241] groups, at peripheral or non-peripheral positions, have been reported for the purpose of fabricating n-type organic semiconductors. Among them, the alkylsulfonyl group plays an important role, not only

[236] E. A. Lukyanets, V. N. Nemykin, *J. Porphyrins Phthalocyanines* **2010**, *14*, 1.
[237] R. Guo, L. Zhang, Y. Zhang, Y. Bian, J. Jiang, *J. Porphyrins Phthalocyanines* **2011**, *15*, 964.
[238] a) Q. Tang, H. Li, Y. Liu, W. Hu, *J. Am. Chem. Soc*. **2006**, *128*, 14634; b) M.-M. Ling, Z. Bao, *Org. Electron*. **2006**, *7*, 568; c) Y. Oh, S. Pyo, M. H. Yi, S.-K. Kwon, *Org. Electron*. **2006**, *7*, 77; d) M. L. Tang, J. H. Oh, A. D. Reichardt, Z. Bao, *J. Am. Chem. Soc*. **2009**, *131*, 3733; e) H. Jiang, J. Ye, P. Hu, F. Wei, K. Du, N. Wang, T. Ba, S. Feng, C. Kloc, *Sci. Rep* **2014**, *4*, 7573.
[239] Z. Bao, A. J. Lovinger, J. Brown, *J. Am. Chem. Soc*. **1998**, *120*, 207.
[240] a) S. Sergeyev, E. Pouzet, O. Debever, J. Levin, J. Gierschner, J. Cornil, R. G. Aspe, Y. H. Geerts, *J. Mater. Chem*. **2007**, *17*, 1777; b) B. Tylleman, R. Gomez-Aspe, G. Gbabode, Y. H. Geerts, S. Sergeyev, *Tetrahedron* **2008**, *64*, 4155; c) P. Ma, J. Kan, Y. Zhang, C. Hang, Y. Bian, Y. Chen, N. Kobayshi, J. Jiang, *J. Mater. Chem*. **2011**, *21*, 18552.
[241] a) B. Tylleman, G. Gbabode, C. Amato, C. Buess-Herman, V. Lemaur, J. Cornil, R. G. Aspe, Y. H. Geertes, S. Sergeyev, *Chem. Mater*. **2009**, *21*, 2789; b) Y. Zhang, P. Ma, P. Zhu, X. Zhang, Y. Gao, D. Qi, Y. Bian, N. Kobayashi, J. Jiang, *J. Mater. Chem*. **2011**, *21*, 6515.

promoting a considerable stabilization of the HOMO and the LUMO level of Pc, but also increasing the solubility due to the flexible alkyl chains. Several alkylsulfonyl-containing unsymmetrical Pc derivatives have been synthesized by our group and studied as non-linear optical chromophores.[49d,242] Therefore, the strong electron accepting 2-ethylhexylsulfonyl group was chosen in our research project to increase the solubility in the final material. Also, the incorporation of a reactive functional group (*i.e.* a terminal alkynyl) will be necessary to perform the reaction with an adequate PPV copolymer (*i.e.* holding pending azides).

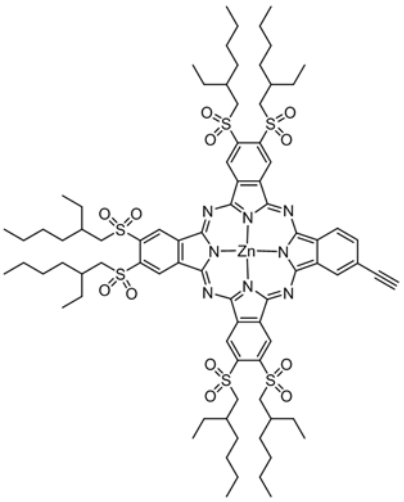

Figure 53.- Molecular structure of phthalocyanine bearing sulfonyl groups and a triple bond at the peripheral positions.

Phthalocyanines as monomers for copolymerization

Another interesting approach is to incorporate Pcs into the main chain of conjugated, polymeric structures. In view of previous results with porphyrins, the most promising structures could be those in wich the Pc is linked to the main chain through one of the fused benzene ends of the macrocycle. To this end, *tert-butylated* Zn(II)Pcs substituted in two α-positions of the same isoindole with good leaving groups, such as trifluoromethanesulfonate, will be synthesized for further coupling with appropriate monomers (*Figure 54*). Another objective is to move the reactive position towards the exterior of the the Pc macrocycle aiming at facilitating the polymerization process. Then, copolymerization with will be performed in collaboration with Prof. McCulloch at Imperial College.

[49] d) A. de la Escosura, M. V. Martinez-Diaz, J. Barbera, T. Torres, *J. Org. Chem.* **2008**, *73*, 1475.
[242] a) E. M. Maya, P. Vazquez, T. Torres, *Chem. Eur. J*. **1999**, *5*, 2004; b) E. M. Maya, C. Garcia, E. M. Garcia-Frutos, P. Vazquez, T. Torres, *J. Org. Chem*. **2000**, *65*, 2733; c) A. de la Escosura, M. V. Martinez-Diaz, P. Thordarson, A. E. Rowan, R. J. M. Nolte, T. Torres, *J. Am. Chem. Soc*. **2003**, *125*, 12300; d) A. de la Escosura, M. V. Martinez-Diaz, D. M. Guldi, T. Torres, *J. Am. Chem. Soc*. **2006**, *128*, 4112.

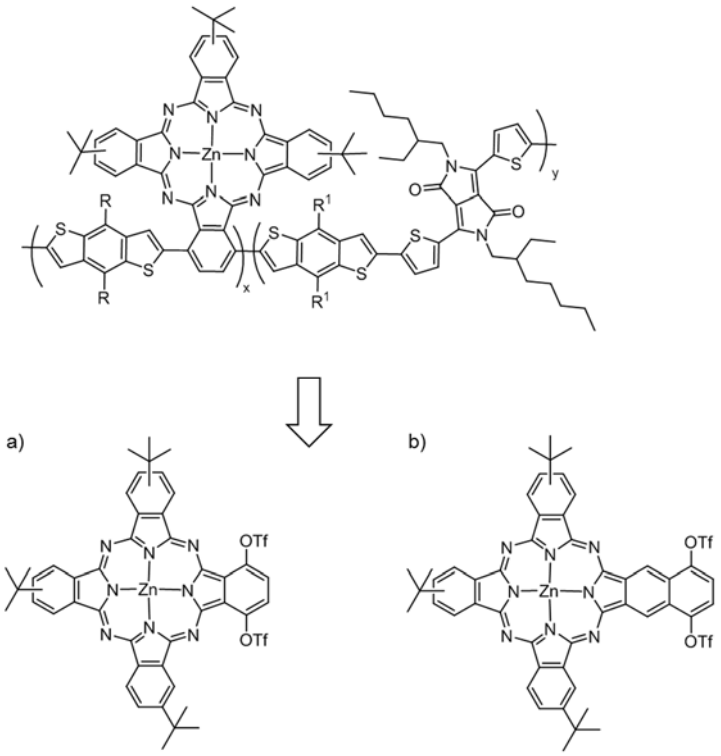

Figure 54.- Structure of phthalocyanines with 2 α-positions occupied by good leaving groups. As shown the retrosynthesis, 2 different phthalocyanines are proposed.

Photovoltaic studies of Pc-containing polymers in bulk heterojunction devices

Finally, all of the new polymeric derivatives will be tested in BHJ devices in collaboration with Prof. R. Janssen at Eindhoven University. Typical photovoltaic parameters such as EQE, J_{SC}, V_{OC}, FF and PCE will be achieved

1.2.4 Results and discussion

1.2.4.1 Synthesis of phthalocyanines

Phthalocyanines for lateral functionalization of conjugated polymers

The synthesis of the targeted unsymmetrically β-substituted Zn(II)Pcs for the functionalization of copolymers requires the preparation of appropriately functionalized precursors, namely substituted phthalonitriles. First, the synthesis of 4-iodophthalonitrile (**2**) was carried out according to literature procedures,[243] as shown in *Scheme 6*.

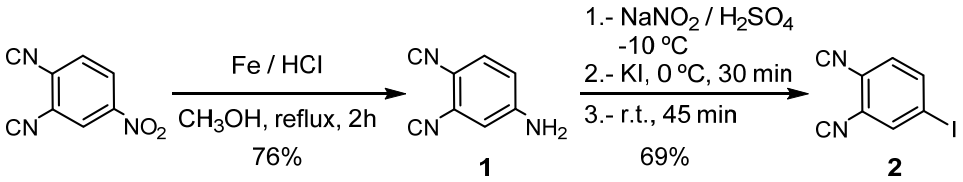

Scheme 6.- Synthesis of 4-iodophthalonitrile **(2)**.

The chemoselective reduction of 4-nitrophthalonitrile with iron in a mixture of concentrated hydrochloric acid and methanol, gave 4-aminophthalonitrile (**1**),[243a] which was transformed to 4-iodophthalonitrile (**2**) in 69% yield via diazotization and subsequent nucleophilic aromatic substitution reactions in the presence of potassium iodide.[243b]

4-(4'-Hydroxymethyl)phenylphthalonitrile (**3**) was synthesized in 80% yield by palladium-catalyzed Suzuki-Miyaura cross-coupling reaction,[244] employing phthalonitrile **2** and commercially available 4-(hydroxymethy)phenylboronic acid in excess of K_2CO_3, $Pd(PPh_3)_4$ as catalyst and THF/H_2O as solvent mixture (*Scheme* 7).

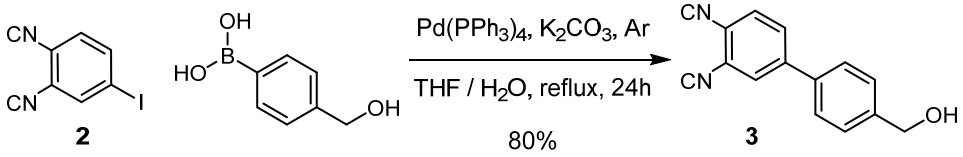

Scheme 7.- Synthesis of 4-(4'- hydroxymethyl)phenylphthalonitrile **(3)**.

The above mentioned phthalonitriles contain functional groups that will allow the covalent linkage of the target Pcs to the polymer backbone. However, only one functional group in one isoindole is needed for such a bonding. For that, unsymmetrically

[243] a) J. Griffiths, B. Roozpeikar, *J. Chem. Soc., Perkin Trans. 1* **1976**, 42; b) S. M. Marcuccio, P. I. Svirskaya, S. Greenberg, A. B. P. Lever, C. C. Leznoff, K. B. Tomer, *Can. J. Chem*. **1985**, *63*, 3057.
[244] B. Ballesteros, S. Campidelli, G. de la Torre, C. Ehli, D. M. Guldi, M. Prato, T. Torres, *Chem. Comm*. **2007**, 2950.

functionalized A_3B Pcs have to be prepared holding solubilizing moieties at the other three of the isoindoles. As previously stated in the introduction section, the synthesis of unsymmetrically substituted Pcs is usually based on the statistical route. This common method consists in the mixed condensation of two differently functionalized precursors, either phthalonitriles or diiminoisoindolines (A and B). However, this methodology generates a statistical mixture of all the possible differently substituted macrocycles (A_4, A_3B, AABB, ABAB, AB_3 and B_4). On this regard, some factors such as the steric volume of the substituents, and the relative reactivity and ratios of the two precursors have to be taken into account in order to reduce the formation of other Pcs and, therefore, to attain optimal conversions into the desired Pcs and facilitate their isolation. This approach has been successfully employed in the synthesis of the target Pcs. In our case, branched alkyl substituents groups were selected to functionalize the Pcs, affording both solubility and non-aggregating features that facilitate the isolation of the target Pcs.

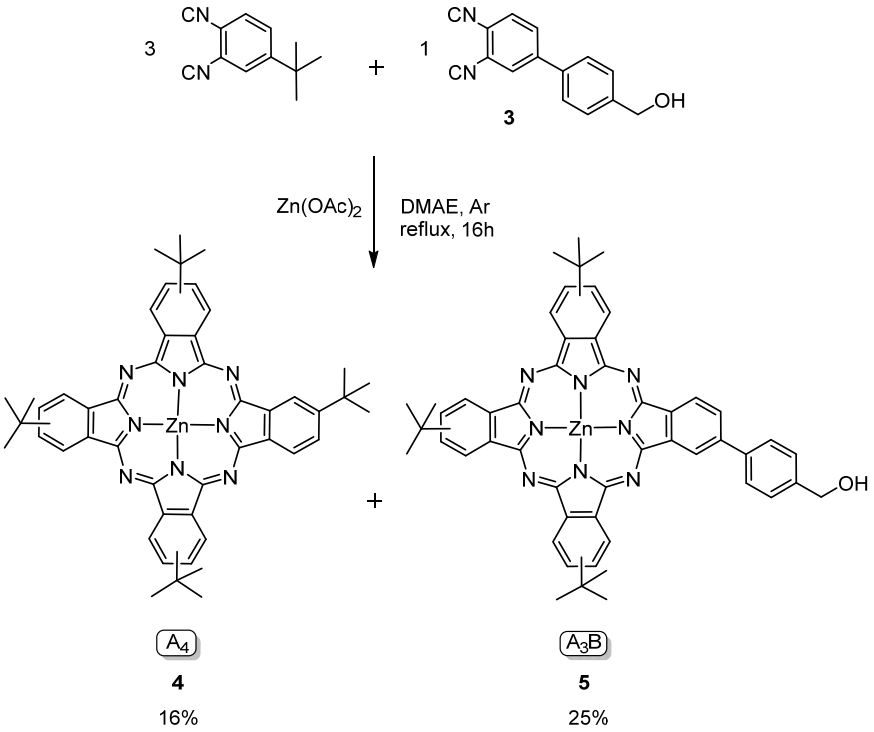

Scheme 8.- Synthesis of Pc **5**.

First, the statistical ciclotetramerization reaction of commercially available 4-(*tert*-butyl)phthalonitrile and compound **3** in a 3:1 ratio (*Scheme 8*), was carried out in the

presence of $Zn(OAc)_2$ and DMAE as solvent. The mixture of Pcs was purified by silica gel column chromatography using hexane/dioxane (2:1) as the eluent, leading to the isolation of the symmetrical Pc **4** (16%; identified by TLC for comparison with commercial sources), followed by the desired product **5** (25%). Coloured products with lower R_f, probably containing other unsymmetrically substituted Pcs were not eluted from the column. The unsymmetrically functionalized Zn(II)Pc **5** contains one hydroxymethylphenyl moiety for further linkage to the polymer, and three *tert*-butyl groups at the other isoindole positions for providing solubility to the final material. Pc **4** and **5** were obtained as mixtures of inseparable structural isomers (4 and 8 possible regioisomers, respectively).

Bearing in mind that we aim to connect the Pc to the backbone by means of effective click chemistry reactios, we proceeded to transform the alcohol function into an azide moiety. Bromination of Zn(II)Pc **5** employing mild, Appel reaction conditions (using CBr_4 as a halide source and triphenylphosphine as the phosphorus reagent) gave Pc **6** in high yield (*Scheme 9*). Subsequently, the transformation of this compound into the azide derivative **7** by a nucleophilic substitution with an excess sodium azide was also performed in excellent yield (90%).

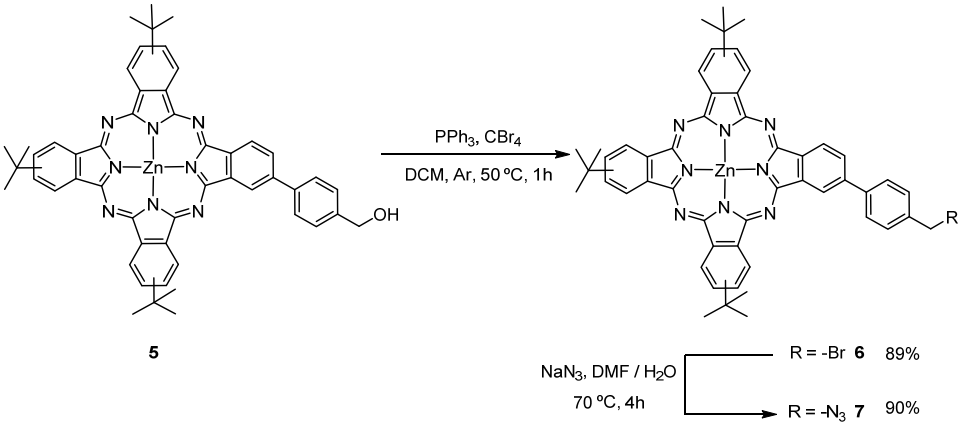

Scheme 9.- Synthesis of Pcs **6** and **7**.

All compounds were completely soluble in organic solvents and fully characterized by ^{1}H-NMR, FT-IR and UV-Vis spectroscopy, and MALDI-MS. ^{1}H-NMR spectra of these compounds confirms the successful transformation of the hydroxyl moiety into the bromo and azide functionalities through the chemical shift of the adjacent methylene signal. Also, FT-IR technique reveals the presence of an azide group. Pc **7** shows the typical N_3 stretching band at 2166 cm^{-1} (*Figure 55*).

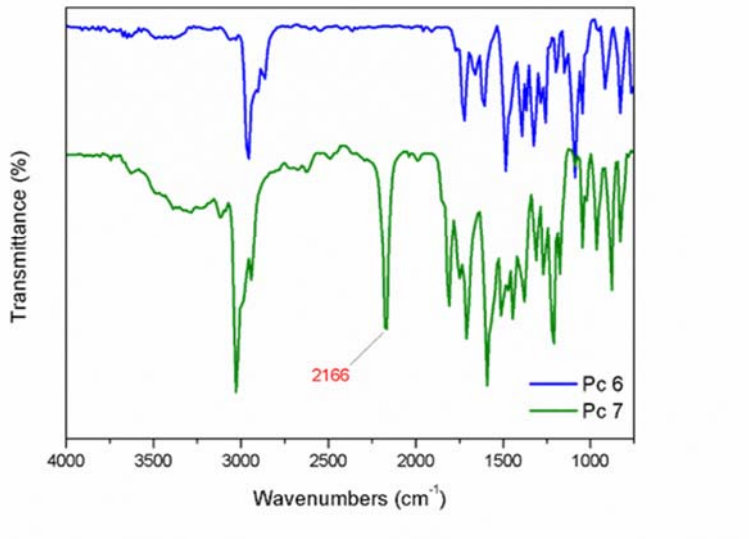

Figure 55.- Comparison of FT-IR spectra of Zn(II)Pc **6** (blue line) and Zn(II)Pc **7** (green line). The green spectrum shows the characteristic azide band.

The absorption spectra of Pcs **5**, **6** and **7** show similar intense Q bands at 675 nm and B bands at 350 nm, which implies that these small changes at the periphery of the macrocycle do not affect to the π-π* transitions.

The next step was the preparation of an electron-acceptor Pc holdingalkylsulfonyl groups at the periphery for the "double-cable" architecture. The synthesis started with the preparation of 4,5-dichlorophthalonitrile (**11**)[245] in four steps (*Scheme 10*). The quantitative dehydration of 4,5-dichlorophthalic acid yielded the cyclic anhydride **8**, which was reacted with formamide, followed by the treatment with ammonium hydroxide to give phthalamide **10**. The latter compound was dehydrated with thionyl chloride to afford 4,5-dichlorophthalonitrile (**11**) in 87% yield. Then, the dicyano compound **12**, bearing 2-ethylhexylthioether moieties, was obtained in *ca*. 80% yield by reaction of **11** with 2-ethylhexane-1-thiol. Straightforward oxidation of **12** led to 4,5-bis(2-ethylhexylsulfonyl)phthalonitrile (**13**) in high yield (95%).

[245] D. Wohrle, M. Eskes, K. Shigehara, A. Yamada, *Synthesis* **1993**, *2*, 194.

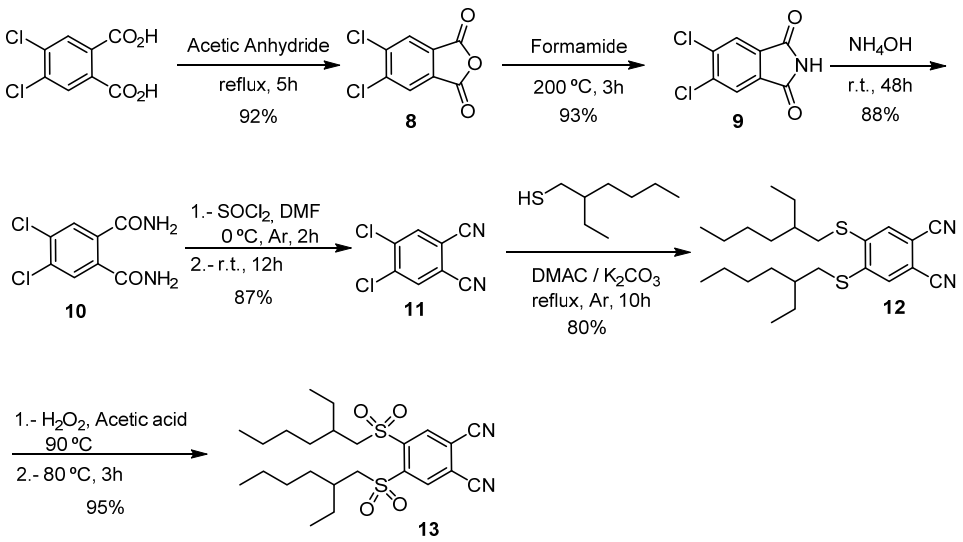

Scheme 10.- Synthesis of phthalonitrile **13**.

The synthesis of alkylsulfonyl-containing Ni(II), Pd(II) and Zn(II) Pc derivatives by cyclic tetramerization of the corresponding phthalonitriles or diiminoisoindoles precursors had been previously reported by our group. Although typical solvents for the condensation reaction are high-boiling alcohols, (*i.e.* penthanol), a refluxing mixture of DMF and *o*-DCB was used in this case in order to avoid nucleophilic displacement of the sulfonyl groups by an alcohol solvent.[242] Therefore, this procedure has been employed in the synthesis of the unsymmetrically substituted Zn(II)Pc **15** (*Scheme 11*, *route A)*, bearing three branched alkylsulfonyl groups (which play the role of electron-acceptor moieties and facilitate chromatographic isolation) and one iodine moiety that will be further converted into the targeted terminal alkyne. Thus, the condensation reaction of a 1:3 molar ratio of phthalonitriles **2** and **13** was carried out in the presence of $Zn(OAc)_2$. The statistical mixture of Pcs was purified by column chromatography, leading to the isolation of the symmetrically substituted Pc **14** as the major component, followed by a small amount of the desired compound iodoPc **15**. In order to improve the yield in **15**, other molar ratios were tested, and the best results obtained with a 2:3 molar ratio of phthalonitriles **2** and **13**. This reaction allowed to isolate Pcs **14** and **15** in 20% and 25% yields, respectively. However, the chromatographic purification was specially arduous in this case due to the very similar polarities of the two Pcs.

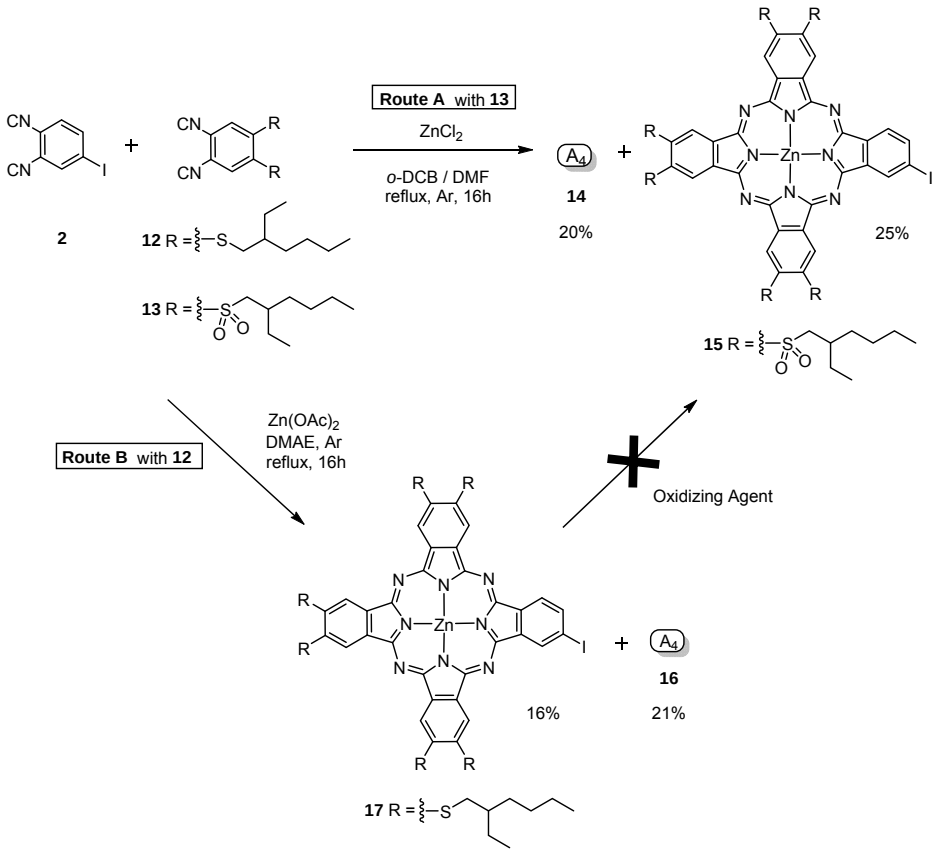

Scheme 11.- Two possible routes for the synthesis of Zn(II)Pc **15**.

Trying to sort out the isolation difficulties, we planned an alternative route to synthesize iodoPc **15** *(Scheme 11, route B)*, which relies on a six-fold oxidation of the corresponding hexakis(alkylthio)phthalocyanine **17** following a reported procedure for related thioalkyls Pcs.[241a] The synthesis of Zn(II)Pc **17** was performed by statistical condensation of phthalonitriles **2** and **12** in a 1:3 ratio, respectively, in refluxing DMAE. Symmetrical Pc **16** and the target Pc **17** were isolated in 21% and 16% yields, respectively. However, the oxidation step was not successful in any of the tested conditions (H_2O_2 and MCPBA).

The next step was the introduction of a terminal acetylene over iodoPc **15** (*Scheme 12*) by a Sonogashira coupling between **15** and trimethylsilylacetylene using $PdCl_2(PPh_3)_2$ and CuI as catalytic mixture. The trimethylsilyl-protected derivative, obtained in the reaction, was subjected to the deblocking reaction without further purification. Thus, the treatment of the crude with TBAF gave the alkynyl-containing Pc **18** in an overall 21% yield.

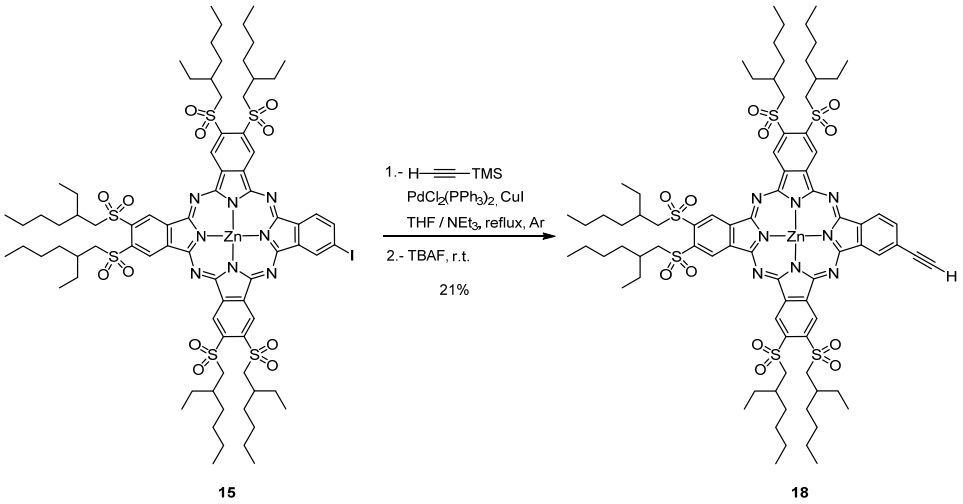

Scheme 12.- Synthesis of functionalized alkynyl-containing Zn(II)Pc **18**.

The absorption spectra of iodo derivative Pcs **15** and **17** in comparison to that of the alkynyl-containing Pc **18** are depicted in *Figure 56*. The electronic spectrum of Pc **15** is characterized by a split Q band (701 and 672 nm), as a result of the reduction of symmetry due to the presence of the alkylsulfonyl groups and the effect of these electron-acceptor acceptor groups on the electronic levels of the aromatic core. For the analogous alkylthioether derivative Pc **17,** a unique Q band at 697 nm is observed. Pc **18** shows, however, a main Q band at 697 nm and a shoulder at 675 nm.

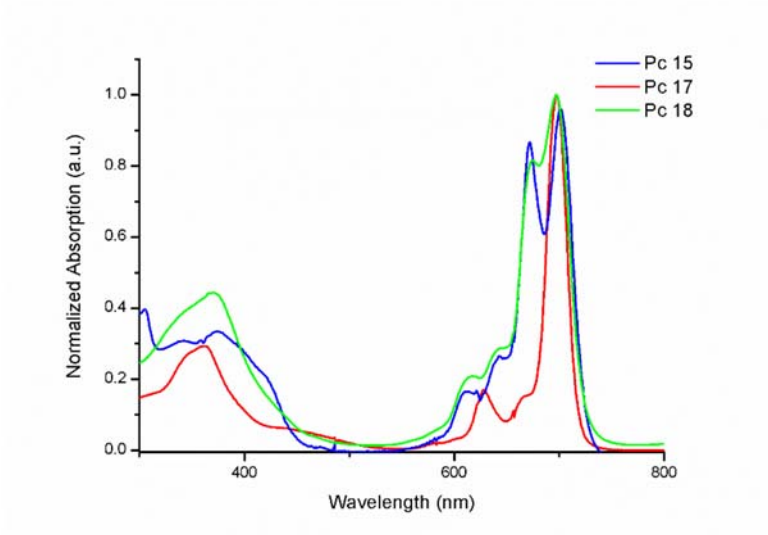

Figure 56.- Comparison of absorption spectra of Zn(II)Pc **15** (blue line), Zn(II)Pc **17** (red line) and Zn(II)Pc **18** (green line).

Synthesis of phthalocyanines as monomers for copolymerization

The synthesis of A_3B Zn(II)Pc substituted in the α-positions of one isoindolic unit with leaving groups for further coupling reactions with organometallic species was attempted in different ways (*Schemes 13 and 14*).

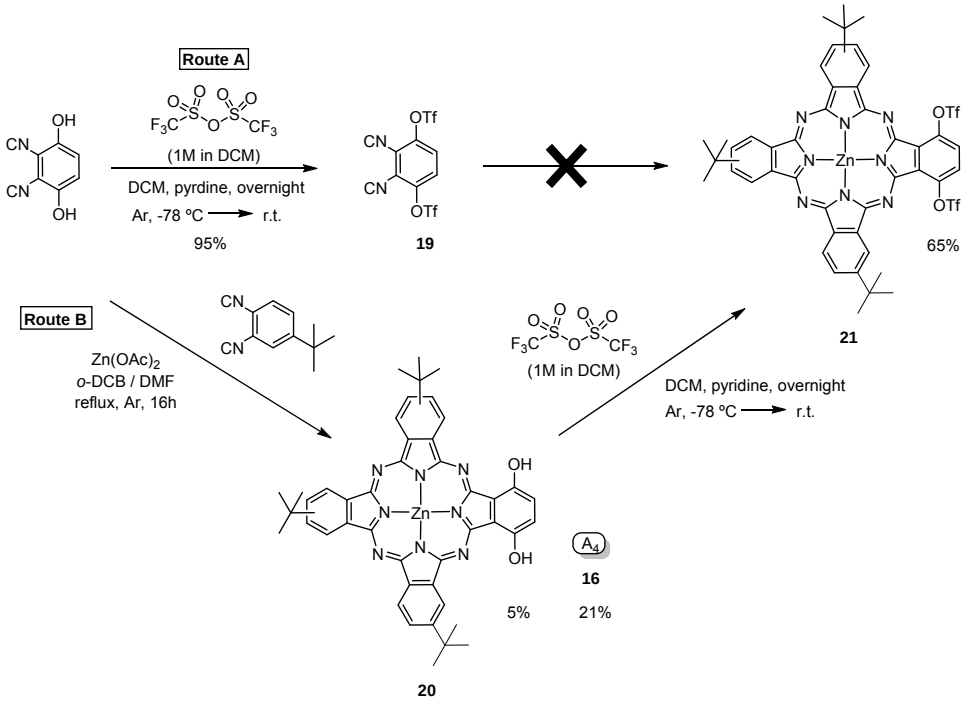

Scheme 13.- Two possible routes for the synthesis of Zn(II)Pc **21**.

Starting from commercially available 2,3-dicyanohydroquinone, the preparation of 3,6-bis(trifluoromethanesulfonyloxy)phthalonitrile **19** was performed following a previously reported method in 95% yield. Subsequently, cyclotetramerization reaction of **19** and 4-(*tert*-butyl)phthalonitrile in the presence of $Zn(OAc)_2$ was performed in a refluxing mixture of *o*-DCB and DMF (again, it was necessary to avoid nucleophilic solvents) (*Scheme 13*, *route A*). In these conditions, only the symmetrically substituted *tert*-butyl Zn(II)Pc **4** was obtained.Apparently, phthalonitrile **19** suffers degradation when heating over 100 ºC; therefore, a post-functionalization route is a good alternative since, higher temperatures are required to prepare Pcs. The synthesis of α-dihydroxy Zn(II)Pc **20** relies on refluxing a 3:1 mixture of commercially available 4-(*tert*-butyl)phthalonitrile and 2,3-dicyanohydroquinone in the presence of $Zn(OAc)_2$ in a mixture of *o*-DCB and DMF (*Scheme 13*, *route B*). The chromatographic separation of the resulting mixture of Pcs was notably facilitated by the presence of the hydroxyl moieties. Symmetrical *tert*-

butyl Zn(II)Pc **4** was the first one eluted, followed by Pc **20**, that was isolated in a frustrating 5% yield. No improvements were achieved neither by changing the solvent to 1-penthanol, DMAE or *o*-DCB, nor by modifying the molar ratios. Decomposition of the starting dicyanohydroquinone seemed to be the reason of the low yield. Eventually, triflation of **20** afforded Zn(II)Pc **21** in overall 3% yield.

Aiming at increasing the overall yield, a new synthetic strategy employing more robust phthalonitriles, was developed as depicted in *Scheme 14*.

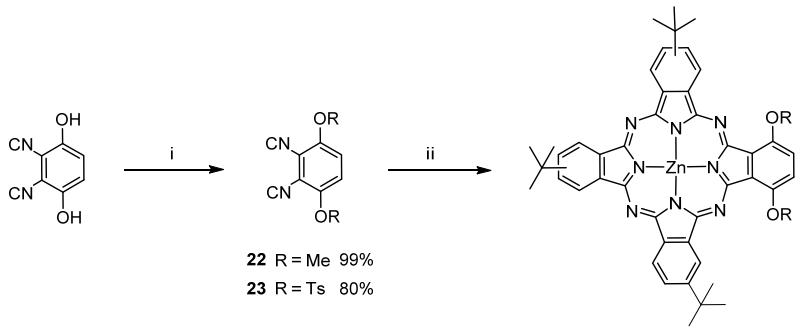

Scheme 14.- Reagents and conditions: <u>*Methyl route*</u> (i) dimethyl sulfate, K_2CO_3, 2-butanone, heat; (ii) 4-*tert*-butylphthalonitrile, $Zn(OAc)_2$, DMAE, DBU. <u>*Tosyl route*</u> (i) *p*-toluenesulfonyl chloride, K_2CO_3, acetone, heat; (ii) 4-*tert*-butylphthalonitrile, $Zn(OAc)_2$, *o*-DCB / DMF.

Phthalonitriles **22** and **23** were synthesized according to procedures previously described. The reaction for the synthesis of phthalocyanine **24**, carried out in the presence of $Zn(OAc)_2$ in DMAE, led just to the tetra(*tert*-butyl)Zn(II)Pc **4**. The change of solvent, *e.g.* 1-penthanol or a mixture of *o*-DCB and DMF, did not afford better results. On the other hand, tosylatePc **25** could be isolated in a 8% yield. Partial cleavage of the tosylate group was detected and, in fact, a Pc holding one deprotected hydroxyl group and one tosylate in the same isoindole was also isolated in 3% yield. Worth of mention is that Zn(II)Pc **20** was not detected. The deprotection step was performed over a mixture of the bis- and monotosylate derivatives in a basic media, giving Zn(II)Pc **20** in a low yield for the last two steps, and in an overall 3% yield, so that we set aside this approach.

All the compounds were characterized by mass spectrometry, ^{1}H-NMR, UV-Vis and FT-IR spectroscopy..

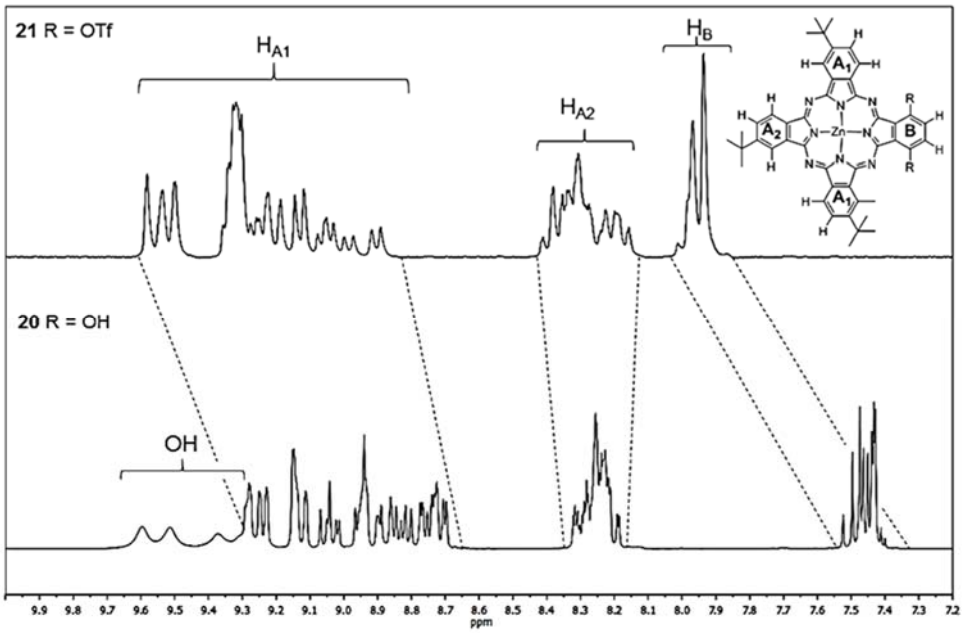

Figure 57.- Comparison of partial ^{1}H-NMR spectra (300 MHz) in THF-d_8 of Zn(II)Pcs **20** (bottom) and **21** (top).

The ^{1}H-NMR spectra of Zn(II)Pcs **20** and **21** in THF-d_8 (*Figure 57*) show several multiplets in the aromatic region, between 9.5-7.4 ppm, corresponding to the Pc protons. The presence of well-defined signals indicate that the compounds are not aggregated in solution at this concentration (*ca* 10^{-3} M) . On the other hand, the high multiplicity of the signals is consistent with the presence of a mixture of regioisomers. Worth of mention is that the signals of the protons at isoindole B in compound **21** exhibited downfield shifts, which can be interpreted in terms of the electron-withdrawing nature of the triflate group. The presence of this group was also noticed to a lesser extent on protons of isoindole A_1. Worth of mention is that the ^{19}F-NMR spectrum of triflate Pc derivative **21** consists of a single peak. In this case, the six F nuclei are not sensitive to the different chemical environment imposed by the presence of regioisomers.

The absorption spectra of Zn(II)Pcs **21** and its precursor **20** in THF is shown in *Figure 58*. Both spectra exhibit sharp Q bands, but whereas for **20** a single band is observed at 706 nm, **21** exhibits a blue-shifted split band with maxima at 688 and 654 nm.

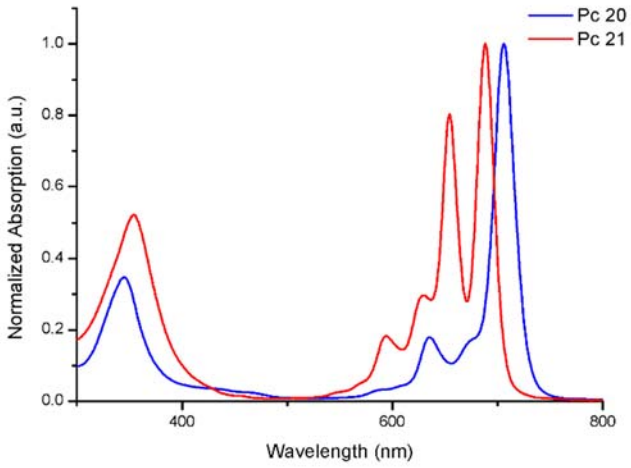

Figure 58.- Comparison of albsorption spectra of Zn(II)Pcs **20** (solid line) and **21**(dashed line) in THF.

Another objective regarding the preparation of Pc-containing copolymers is to move the reactive position at the Pc towards the exterior of the macrocycle and thus to increase its reactivity in metal-catalyzed coupling reactions. For that purpose a naphthalene dicarbonitrile precursor containing triflate groups at the 5,8 positions has to be prepared. The most simple approach seemed to be using 2,3-dibromonaphthalene (**A**) as building block *(Scheme 15*). An indirect route to obtain the quinone derivative **C** was contemplated using 6,7-dibromo-1-naphthol (**B**).[246] However, the synthesis of this naphthol requires three steps: treatment of **A** with a nitric-sulphuric acid mixture for mononitration of naphthalene, reduction of the nitro compound to the corresponding amine with hydrazine hydrate, and finally diazotization followed by hydrolysis. An additional step for the oxidation to quinone **C** implies an overall four-step route, too many a priori. On the other hand, the straightforward oxidation of **A** to quinone **C**, was discarded in view of the literature precedents. Finally, routes A and B, based on a Diels-Alder reaction, were tackled.

[246] A. Ashnagar, J. M. Bruce, P. Lloyd-Williams, *J. Chem. Soc., Perkin Trans. 1* **1998**, 559 and references therein.

Scheme 15. Alternatives approaches to obtain the target naphthalene.

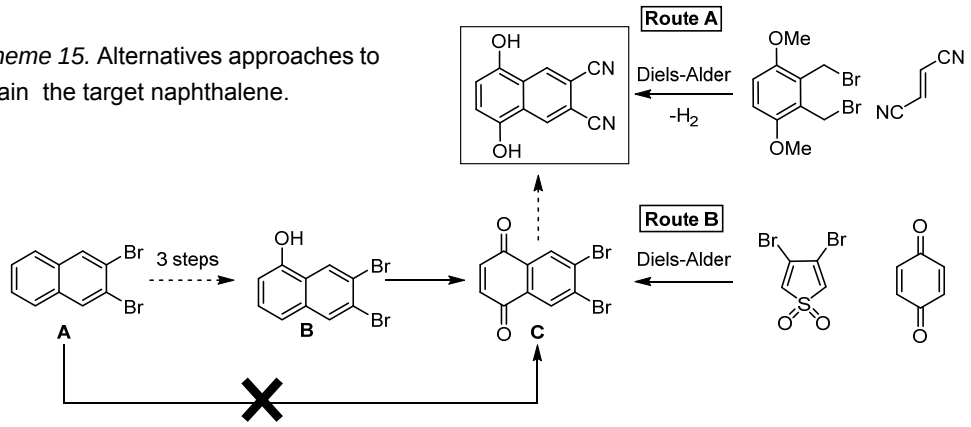

The first methodology, as it is depicted in route A (*Scheme 16*), includes the preparation of the α,α'-dibrominated compound **27**, by -methylation of 2,3-dimethylhydroquinone followed by double benzylic bromination with NBS. Compound **27** was subjected to reaction with Rieke nickel to generate the *o*-xylilene derivative, which shall react with fumaronitrile to give the Diels Alder aduct **28**. However, treatment of α,α'-dibromo-3,6-dimethoxy-*o*-xylene (**27**) with nickel powder prepared in DME, did not lead to *in situ* generation of the diene.

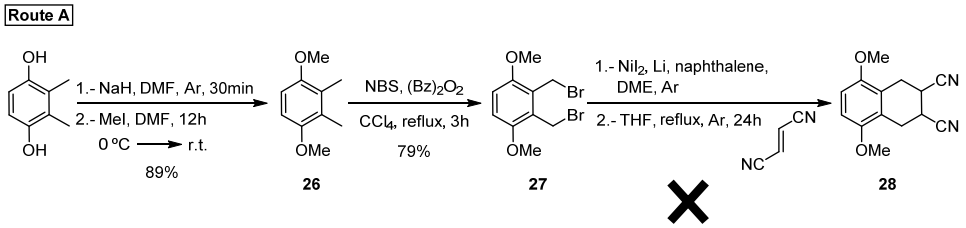

Scheme 16.- Attempts to prepare 5,8-dimethoxy-1,2,3,4-tetrahydronaphthalene-2,3-dicarbonitrile (**28**).

Route B (*Scheme 17*) also follows the Diels-Alder cycloaddition, but between benzoquinone as dienophile and 3,4-dibromothiophene 1,1-dioxide (**29**) as diene, according to a literature procedure.[247] A large excess (10 equivalents) of benzoquinone was used to suppress the formation of two unwanted compounds: the symmetrical anthraquinone derivative and the product from the homodimerization of sulfone **29**. Naphthoquinone **30** was subsequently reduced and methylated to avoid addition of the cyanide ions to the quinonic carbonyl group (C=O) during the formation of the

[247] D. Bailey, V. E. Williams, *Tetrahedron Lett*. **2004**, *45*, 2511.

naphthalonitrile. Thus, compound **31** was prepared by treatment of **30** with sodium dithionite as reducing agent, followed by O-methylation with NaH and MeI.

Finally, some cyaniation attempts were made using the classical Rosenmund-von Braun's conditions (CuCN, DMF, 150 ºC). Apart from the safety issues due to the use of a huge excess of cyanide, the reaction conditions tried never led to reasonable conversions into **32**. One of the major problems of the Rosenmund von Braun reaction is that in a polar solvent such as DMF, the transition metal ions like Cu^+ can provoke the templated tetramerization of the (na)phthalonitriles formed in the course of the reaction to produce copper (na)phthalocyanine. This is a strong limitation to obtain good conversions into the naphthalonitrile, since the reaction has to be stopped when it just starts to turn green in order to avoid the formation of copper (na)phthalocyanine. According to this, the final reaction mixture always contained the unreacted dibromo **31**, the bromocyano monosubstitution product and traces of copper naphthalocyanine, and as a general observation, the naphthalonitrile yield did not reach 25% for any tested conditions (reduction of the number of equivalents of CuCN and of the reaction time). The reaction temperature was always constant, 150 ˚C, because below this temperature the cyanation did not take place.

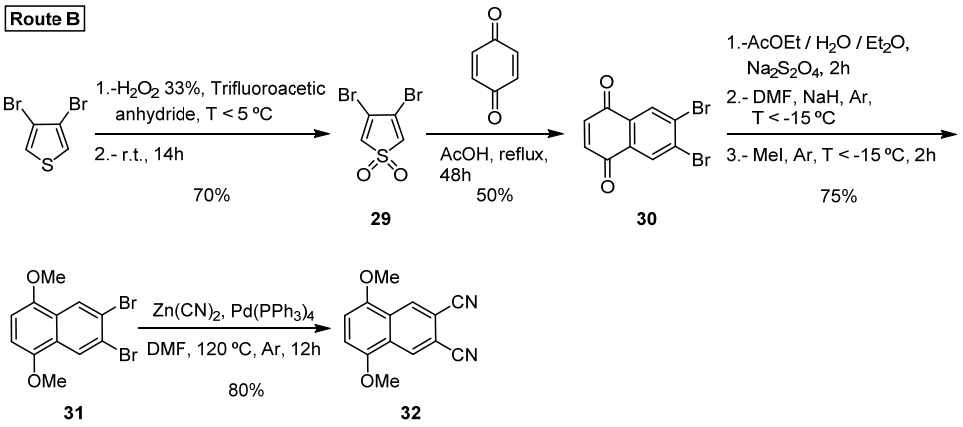

Scheme 17.- Synthesis of compound **32**.

To solve this problem, the tandem zinc-palladium catalyzed cyanation reported by Barret *et al*. was found to be a good alternative. The reaction was tried on the dimethoxy derivative **31**, adapting the literature conditions: 0.3 equivalents of $Pd(PPh_3)_4$,

and 1.2 equivalents of $Zn(CN)_2$, all in DMF at 120 ºC for 6 hours.[248] These conditions afforded product **32** in a very high 80% yield, which made it the method of choice.

At this point, we decided to try the formation of the A_3B Pc derivative by statistical condensation of **32** and 4-*tert*-butyl phthalonitrile (*Scheme 18*, route C). The former idea was to prepare compound **33** which could be further demethylated to give dihydroxy compound **34**.

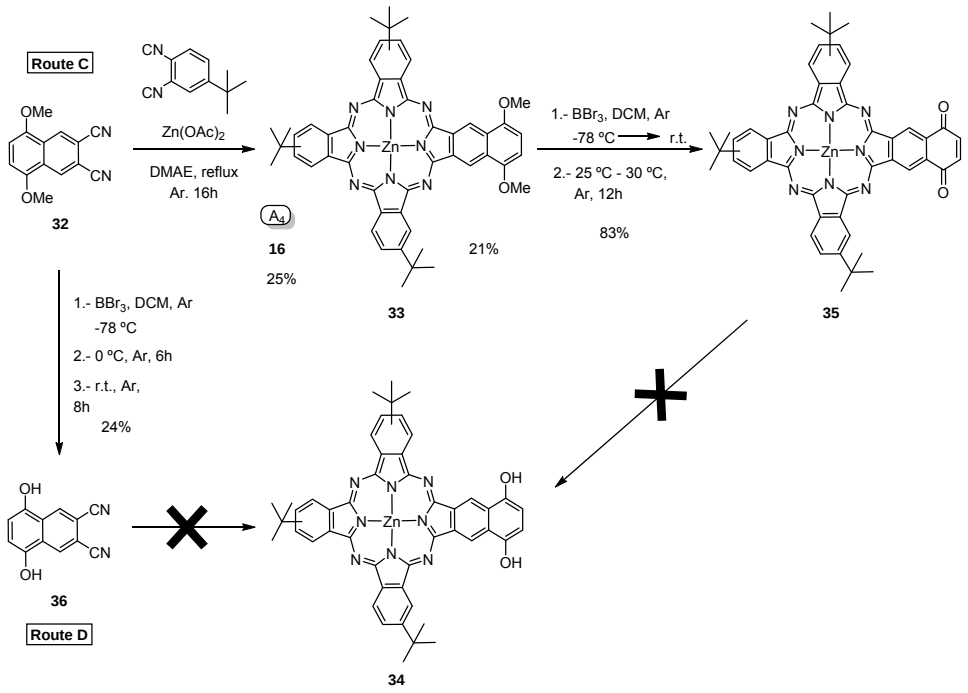

Scheme 18.- Two possible routes for the synthesis of hydroquinone-containing Zn(II)Pc.

Therefore, naphthalonitrile **32** was treated with $Zn(OAc)_2$ and commercially available 4-*tert*-butylphthalonitrile in refluxing DMAE (*Scheme 18*, route C*)*. The chromatographic separation of the mixture of Pcs formed was easy, and Pc **33** was isolated in 21% yield. The demethylation of the dimethoxyPc **33** was carried out by treatment with BBr_3 during 12h. FT-IR and MS analysis of the compound obtained in these conditions led us to conclude that quinone-containing Zn(II)Pc **35** had been formed, instead of the expected hydroquinone-containing Zn(II)Pc **34**.

[248] a) M. Alterman, A. Hallberg, *J. Org. Chem*. **2000**, *65*, 7984; b) F. Jin, P. N. Confalone, *Tetrahedron Lett*. **2000**, *41*, 3271.

At this stage, the use of a mild reducing agent to convert **35** into the desired final product **34** was considered, in particular the use of sodium dithionite. However, compound **35** was reluctant to react in any of the tested conditions, and almost all the starting material was always recovered. This bottleneck led us to consider route D, that is deprotection of naphthalonitrile **32** to obtain compound **36** which could condensate with 4-*tert*-butylphthalonitrile to form the target Pc **34**. Thus, deprotection of **32** was accomplished using BBr_3 as a reported in the literature, affording 5,8-dihydroxynaphthalonitrile (**36**) in low yield. This naphthalonitrile seemed to degradate under the reaction conditions and, in fact, when it was subjected to the classical conditions for the synthesis of Pcs together with 4-*tert*-butylphthalonitrile, a brown tar was obtained with no traces of Pc **34**.

In light of these bad results, the research for new alternatives was desestimated. On the other hand, it has not escaped our notice that quinone-derivative Zn(II)Pc **35** could have interesting redox properties, but this is beyond the scope of this thesis.

1.2.4.2 Synthesis of Pc-containing conjugated copolymers

PPV- and PT-type copolymers with phthalocyanines as light – harvesting units

The synthesis of MDMO-PPV copolymers containing pendant Pc units was performed in collaboration with Dr. Laurence Lutsen and Prof. Dr. Dirk Vanderzande at Hasselt University in the framework of a EU-RTN project. They prepared copolymer **37** from adequate substituted sulfinyl precursors and subsequent hydrolysis of the ester group using a basic media, with almost quantitative conversion, as shown in *Scheme 19*.[249] As a result, the copolymer presents one terminal carboxylic acid every ten *p*-phenylene vinylene repeating units. Analytical size-exclusion chromatography (SEC) measurements[250] of this copolymer were performed *versus* polystyrene standards using

[249] a) J. Duchateau, L. Lutsen, W. Guedens, T. J. Cleij, D. Vanderzande, *Polym. Chem*. **2010**, *1*, 1313; b) L. Lutsen, P. Adriaensens, H. Becker, A. J. Van Breemen, D. Vanderzande, J. Gelan, *Macromolecules* **1999**, *32*, 6517.

[250] Size-exclusion chromatography (SEC) is a chromatographic method in which molecules in solution are separated by their size, and it is usually applied to large molecules such as polymers. SEC is widely used polymer characterization method because of its ability to provide good molar mass distribution (M_W) results for polymers. This technique involves forcing a polymer solution through a matrix of cross-linked polymer particles at a pressure of up to several hundred bar. The limited accessibility of stationary phase pore volume for the polymer molecules results in shorter elution times for high-molecular-mass species. The use of low dispersity standards allows the user to correlate retention time with molecular mass.

THF as the eluent. The observed molecular weight polymer[251] is $M_w = 2.7 \cdot 10^5$ g/mol (PDI x= 3.2),[252] which confirms that a high molecular weight polymer was obtained.

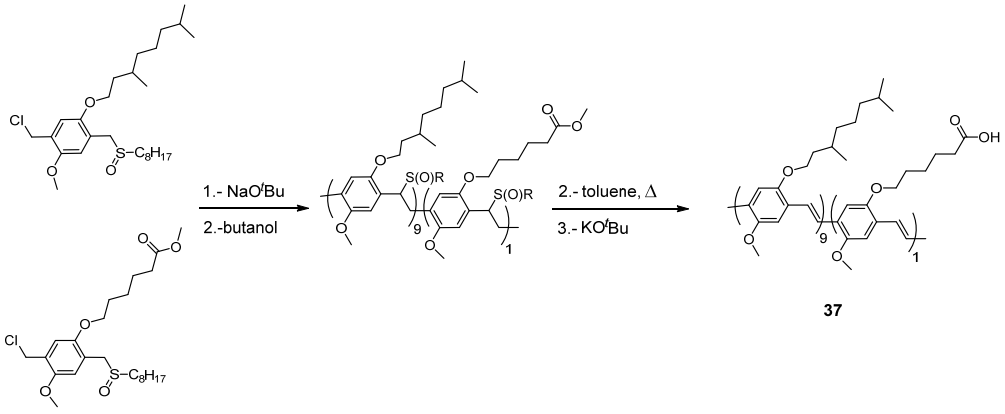

Scheme 19.- Synthesis of carboxy copolymer **37**.

With this polymer in our hands, the following step towards the preparation of Pc-containing copolymers was the esterification reaction,[249] between carboxy-MDMO-PPV **37** and hydroxymethyl Zn(II)Pc **5**. The reaction was carried out in dry DCM under nitrogen atmosphere and protected from light, using DCC and DMAP as condensation agents (*Scheme 20*). The Pc-functionalized copolymer **38** was filtered off and washed extensively with acetone to remove the excess of unreacted Zn(II)Pc **5**.

[251] Weight average molecular weight (M_W) takes into account the molecular weight of a chain in determining contributions to the molecular weight average. The more massive the chain, the more the chain contributes to M_W. Another interesting parameter is the number average molecular weight (M_n), which represents the statistical average molecular weight of all the polymer chains in the sample. M_n is more sensitive to molecules of low molecular mass, while M_W is more sensitive to molecules of high molecular mass.

[252] The polydispersity index (PDI) is used as a mesure of the broadness of a molecular weight distribution of a polymer and is calculated as M_W divided by M_n. It indicates the distribution of individual molecular masses in a batch of polymers. The PDI has a value equal to or greater than 1, but as the polymer chains approach uniform chain length, the PDI approaches unity. The best controlled synthetic polymers (narrow polymers used for calibrations) have a PDI of 1.02 to 1.10. Step polymerization reactions typically yield values of PDI of around 2.0, whereas chain reaction yield values between 1.5 and 20.

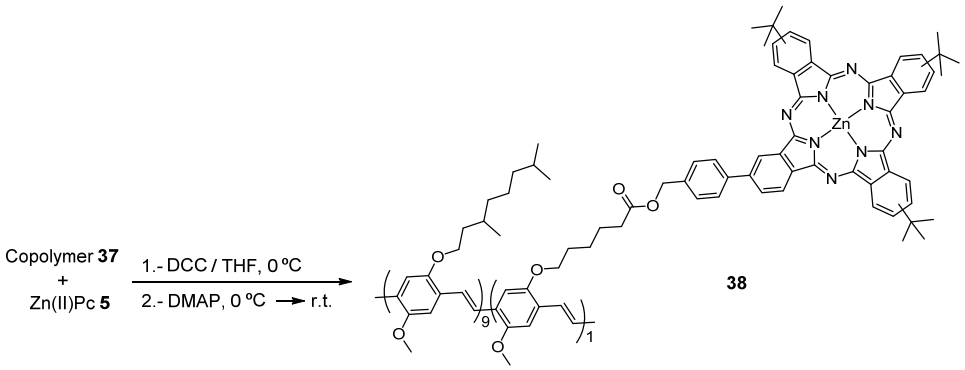

Scheme 20.- Synthesis of functionalized Pc-PPV copolymer **38**.

The final material, Pc-PPV **38**, showed to be quite soluble in THF, which allowed us to fully characterize it by ^{1}H-NMR, FT-IR and UV-Vis spectroscopy.. Successful conversion of the conjugated copolymer in Pc-PPV **38** is evidenced by ^{1}H-NMR spectroscopy (*Figure 59*). All the characteristics peaks for the attached Zn(II)Pc units – namely aromatic protons resonating in the 9.8-8.0 range and the $\underline{CH_2}$OCO- methylene at 5.28 ppm – are present in the spectrum of copolymer Pc-PPV **38**. The integration of the signals is consistent with a high degree of conversion of the carboxylic acid to the corresponding ester group.

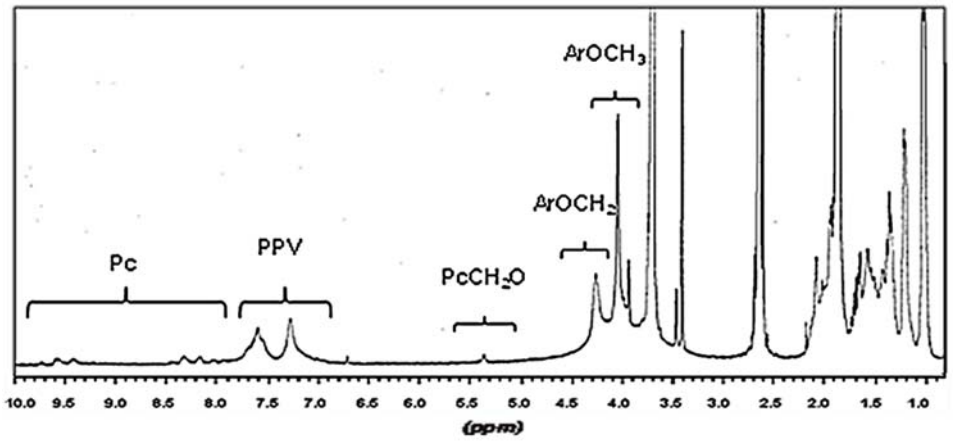

Figure 59.- ^{1}H-NMR spectrum of Pc-PPV **38** in THF-d_8.

The lateral functionalization of carboxyl-PPV copolymer **37** with Pc **5** is also confirmed by FT-IR, where the carbonyl vibration at 1709 cm^{-1} of the carboxylic acid shifts to a higher frequency, 1733 cm^{-1}, due to the formation of the ester bond. Analytical SEC

of Pc-PPV **38** was performed using polystyrene standards in THF. The observed M_w value in THF solutions is $3.1 \cdot 10^5$ g/mol, which is comparable to the platform copolymer, with a M_w value of $2.7 \cdot 10^5$ g/mol. However, it should be noted that there is a moderate increase in the polidispersity upon functionalization. Whereas carboxy-PPV copolymer **37** presents a polydispersity value of 3.2, for Pc-PPV **38** the polydispersity is 4.4, reflecting a broadening of the molecular weight distribution.

The quality of the conjugated polymeric system and the successful attachment of Pc **5** to the precursor carboxyl-containing copolymer, are further confirmed *via* UV-Vis measurements in THF. As can be seen in *Figure 60*, the λ_{max} of the π-π^* transitions of the post-functionalized copolymer Pc-PPV **38** is positioned at 510 nm, namely the same spectral region than the transition observed for the starting copolymer (λ_{max} = 507 nm). In addition to the peak positions, also the shapes of the UV-Vis absorption of the conjugated backbone are identical. Also the Q-band of the attached Zn(II)Pcs is clearly visible in the spectrum at λ = 676 nm. The height of this peak is directly related to the amount of Zn(II)Pcs molecules present in the material. Considering the typical absorption coefficient of both the copolymer **37** (ε = 28.000 M^{-1} in THF), and the Q-band of Zn(II)Pc **5** (ε = 200.000 M^{-1} in THF), the functionalization of the PPV skeleton with Zn(II)Pcs was estimated to be around 7%.

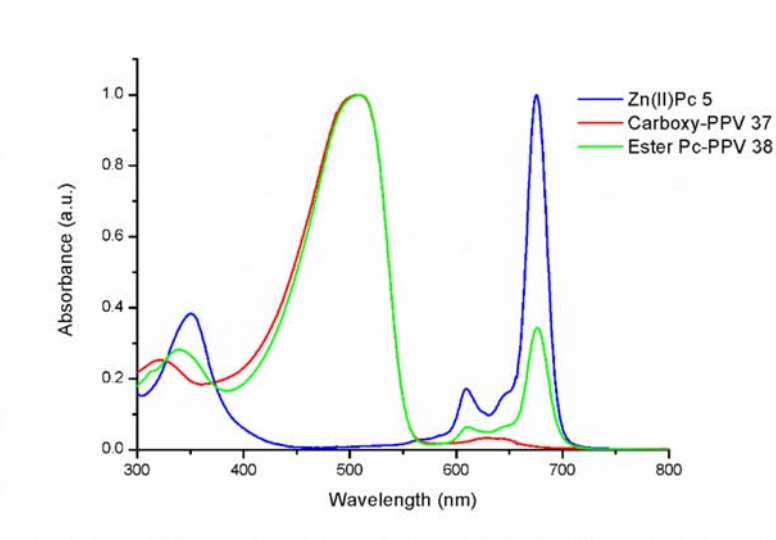

Figure 60.- Absorption spectra of Zn(II)Pc **5** (blue line), starting copolymer **37** (red line) and Zn(II)Pc-PPV **38** (green line), in THF.

Since the esterification of the COOH groups in **37** with Pc **5** was not complete, other chemical approaches were envisioned to improve the incorporation of Pcs into the polymeric skeleton as pendant moieties. A “click” reaction, which has been largely applied in materials science for the functionalization of polymers and surfaces, seems to be a good alternative. The well-known 1,3 Huisgen cycloaddition is one of the most popular reactions in the “click” chemistry family.[253] It is a 1,3-dipolar cycloaddition between an azide and an alkyne to give a 1,2,3-triazole.[254] When using a Cu(I) catalyst, a 1,4-disubstituted-1,2,3-triazole is selectively obtained from the alkyl or aromatic azide and the terminal alkyne. This “click” chemistry reaction proceeds with very high yields and has been largely applied to the side-chain functionalization of polymers and as a polymerization method,[255] and also exploited with success in the preparation of a range of elaborated mono- and multicomponent, Pc-based architectures.[256]

In the following cases, the well-known copper(I)-catalyzed 1,3-dipolar cycloaddition proceeded between an azide, Zn(II)Pc **7**, and conjugated copolymers properly functionalized with terminal triple bonds (**39**). These copolymers were synthesized at Hasselt University, from the previously obtained carboxy-MDMO-PPV **37**, through an optimized DCC/DMAP esterification reaction,[249] as shown in *Scheme 21* (GPC (THF): $M_W = 3.8 \cdot 10^5$ g/mol, PDI = 5.2). This copolymer contains 9% of triple bonds, as determined by ^{1}H-NMR.

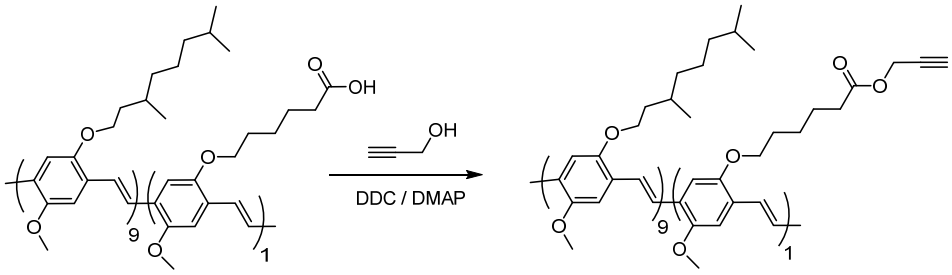

37 **39**

Scheme 21.- Synthesis of alkynyl-containing MDMO-PPV-type copolymer **39**.

[253] H. C. Kolb, M. G. Finn, K. B. Sharpless, *Angew. Chem. Int. Ed*. **2001**, *40*, 2004.
[254] V. V. Rostovtsev, L. G. Green, V. V. Fokin, K. B. Sharpless, *Angew. Chem. Int. Ed*. **2002**, *41*, 2596.
[255] a) W. H. Binder, R. Sachsenhofer, *Macromol. Rapid Commun*. **2008**, *29*, 952; b) P. L. Golas, K. Matyjaszewski, *Chem. Soc. Rev*. **2010**, *39*, 1338; c) K. Kempe, A. Krieg, C. R. Becer, U. S. Schubert, *Chem. Soc. Rev*. **2012**, *41, 176.*
[256] S. Campidelli, B. Ballesteros, A. Filoramo, D. D. Diaz, G. de la Torre, T. Torres, G. M. A. Rahman, C. Ehli, D. Kiessling, F. Werner, V. Sgobba, D. M. Guldi, C. Cioffi, M. Prato, J.-P. Bourgoin, *J. Am. Chem. Soc*. **2008**, *130*, 11503.

Also, poly(3-alkylthiophene) (PT) copolymer containing terminal alkynes was synthesized at Hasselt laboratories. After the copolymerization of adequately functionalized thiophenes using the Rieke method[257,258] (*Scheme 22*, steps 1 and 2), the ester functionalities in the alkyl side chains (one every ten repeating units) were converted into carboxylic acids (*Scheme 22*, step 3). The acid functional groups were reacted in a final step with propargyl alcohol using the DCC/DMAP protocol,[259] to obtain alkynyl-PT **40** (GPC (THF): $M_W = 3.2 \cdot 10^4$ g·mol^{-1}, PDI = 1.9), as shown in *Scheme 22*. This copolymer contains 8% of alkynyl moieties, as determined by ^{1}H-NMR.

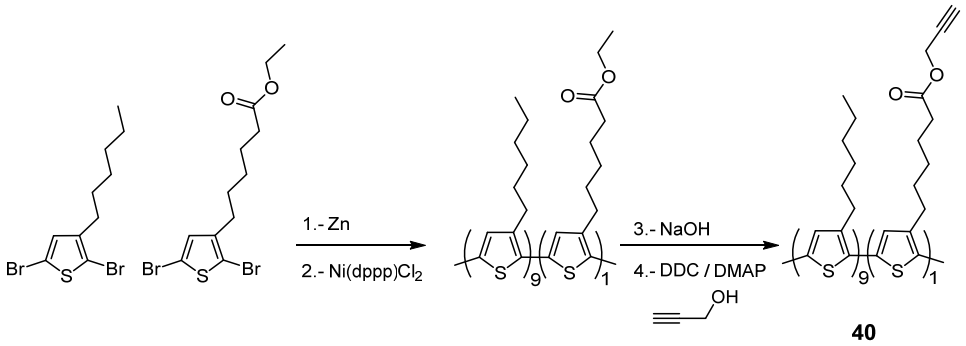

Scheme 22.- Synthesis of alkyne-containing PT-type copolymer.

Typical "click" chemistry conditions for the reaction between Zn(II)Pc **7** and copolymers **39** and **40** (*Scheme 23*) were applied: CuI as source of copper(I), and 2,6-lutidine as N-ligand. THF was chosen as the solvent because both copolymers and Zn(II)Pc **7** are well soluble in it.

[257] B. Campo, W. D. Oosterbaan, J. Gilot, T. J. Cleij, L. Lutsen, R. A. J. Janssen, D. Vanderzande, *Proc. SPIE* **2009**, 7416.
[258] B. J. Campo, D. Bevk, J. Kesters, J. Gilot, H. J. Bolink, J. Zhao, J.-C. Bolsee, W. D. Oosterbaan, S. Bertho, J. D'Haen, J. Manca, L. Lutsen, G. Van Assche, W. Maes, R. A. J. Janssen, D. Vanderzande, *Org. Electron*. **2013**, *14*, 523.
[259] B. Neises, W. Steglich, *Angew. Chem. Int. Ed*. **1978**, *17*, 522.

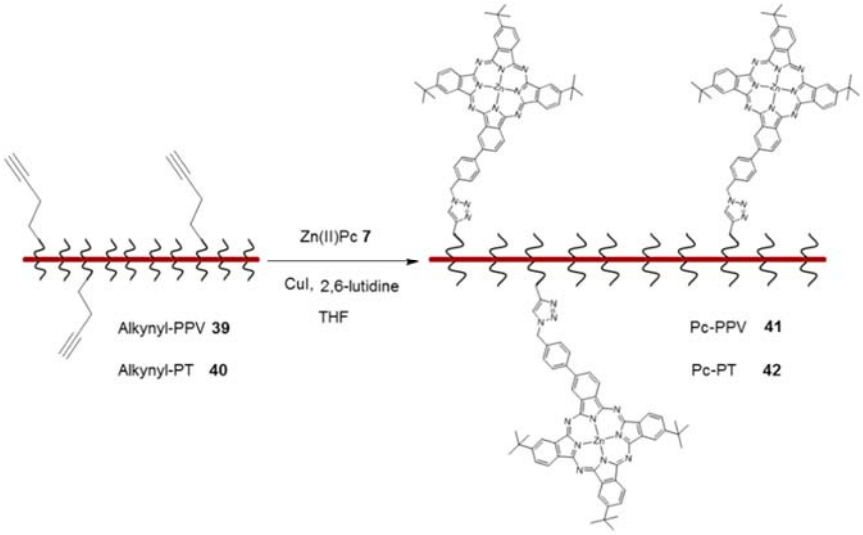

Scheme 23.- Schematic representation of the "click" reaction of alkynyl-copolymers with Zn(II)Pc **7** to obtain Pc-PPV **41** and Pc-PT **42**.

In an attempt to maximize the number of Zn(II)Pc molecules incorporated to the polymer, different ratios of Pc **7**, CuI or 2,6-lutidine, as well as different concentrations, were explored. The experimental results are summarized in *Table 1*.

Entry	Pc 7 (eq)	CuI (eq)	2,6-lutidine (eq)	THF (mL)
1	2.5	2.5	0.2	10
2	1.5	2.5	0.2	10
3	1.1	1.1	0.2	20
4	1.1	1.1	0.2	10

Table 1.- Screening of different ratios and concentrations for the "click" reaction between Zn(II)Pc **7** and alkynyl-MDMO-PPV **39** and alkynyl-PT **40**. Equivalents are calculated with respect to the number of alkyne functions present in 50 mg of the copolymer (**39** or **40**).

In all the cases, the resulting copolymer was filtered off and extensively washed with acetone to remove the excess of Pc **7**. After work up and verification by TLC of the absence of starting material, a UV-Vis spectrum was recorded for each sample. In the

case of alkynyl-MDMO-PPV **39** as starting copolymer, the UV-Vis spectra of the different batches of Pc-PPV **41**, together with those of the starting materials,are displayed in *Figure 61*.

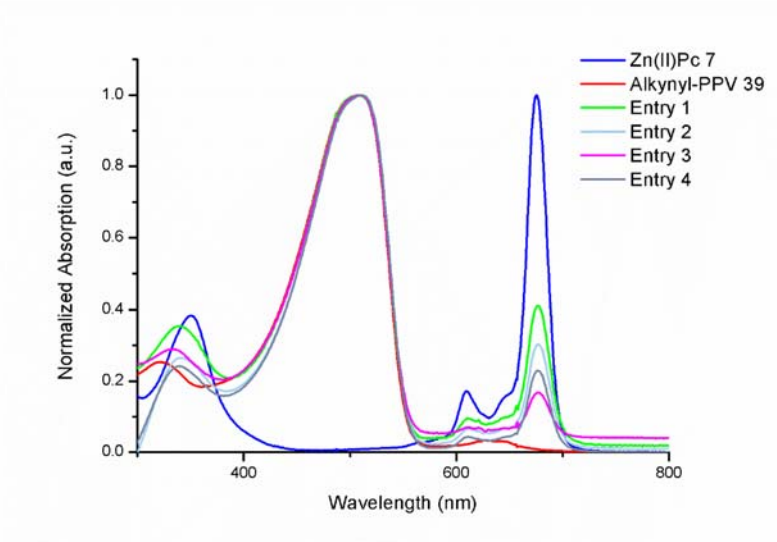

Figure 61.- UV-vis spectra of Pc-PPV **41** obtained under different conditions (entries 1-4) compared with the spectra of starting materials Zn(II)Pc **7** and alkynyl-MDMO-PPV **39**.

As could be deduced from the comparison of the spectra, increasing the equivalents of Pc **7** (entries 1 and 2) and also the concentrations (entries 3 and 4) led to a more efficient funcitionalization of the copolymer with Pc **7**. Also, sodium ascorbate was tested as reducing agent in combination with Cu(II) salts under optimized reaction conditions, but no improvement was observed. Full derivatization of the acetylene groups in the starting copolymer was archived with conditions depicted in entry 1. According to these experiments, the use of 2.5 equivalents of Pc **7**, CuI (2.5 eq) and 2,6-lutidine (0.2 eq) were found to be the optimum conditions for the proposed reaction. Analytical SEC of Pc-PPV **41** was performed using polystyrene standards. The observed M_w value in THF solutions is $3.0 \cdot 10^5$ g/mol, which is comparable to the platform copolymer alkynyl-MDMO-PPV **39**, with a M_w value of $3.8 \cdot 10^5$ g/mol. Consequently, no significant increase in the average molecular weight occurs during the functionalization with Zn(II)Pc **7**. However, it should be observed that there is a moderate decrease in the polidispersity upon functionalization, in contrast to what we observed in the case of the Pc-PPV polymer **38**. Whereas alkynyl-MDMO-PPV **39** copolymer presents a polydispersity value of 5.2, for Pc-PPV **41** the polydispersity is 4.0, reflecting, in this case, a narrowing of the molecular weight distribution.

As shown in *Figure 61*, the quality of the conjugated system and the success of the “click” reaction of Pc **7** to copolymer alkynyl-MDMO-PPV **39**, are further confirmed

via UV-Vis measurements in THF. The peak (λ_{max}) of the π-π^* transitions of the post-functionalized copolymer Pc-PPV **41** is located at 509 nm, namely the same spectral region as the transition observed for the starting copolymer (λ_{max} = 507 nm). In addition to the peak positions, the shapes of the UV-Vis absorption of the conjugated backbone are also identical. The Q-band of the attached Zn(II)Pc is clearly visible at λ = 676 nm. On the other hand, proof of the full conversion of the triple bond into the 1,4-disubstituted-1,2,3-triazole moiety is provided by the ^{1}H-NMR spectrum of Pc-PPV **41** (*Figure 62*). All the characteristic peaks for the attached Zn(II)Pc units – namely aromatic protons resonating in the 9.6-8.0 range and the CH_2N(triazole) methylene in the 5.0-5.5 range – are present in the spectrum of copolymer Zn(II)Pc-PPV **41**, as well as the peak corresponding to the 1,2,3-triazole ring. Considering the relative intensity of the signals of the PPV alkyl side chains and those of the Pc and triazole, they indicated that the Zn(II)Pc content in the final copolymer **41** is 9%.

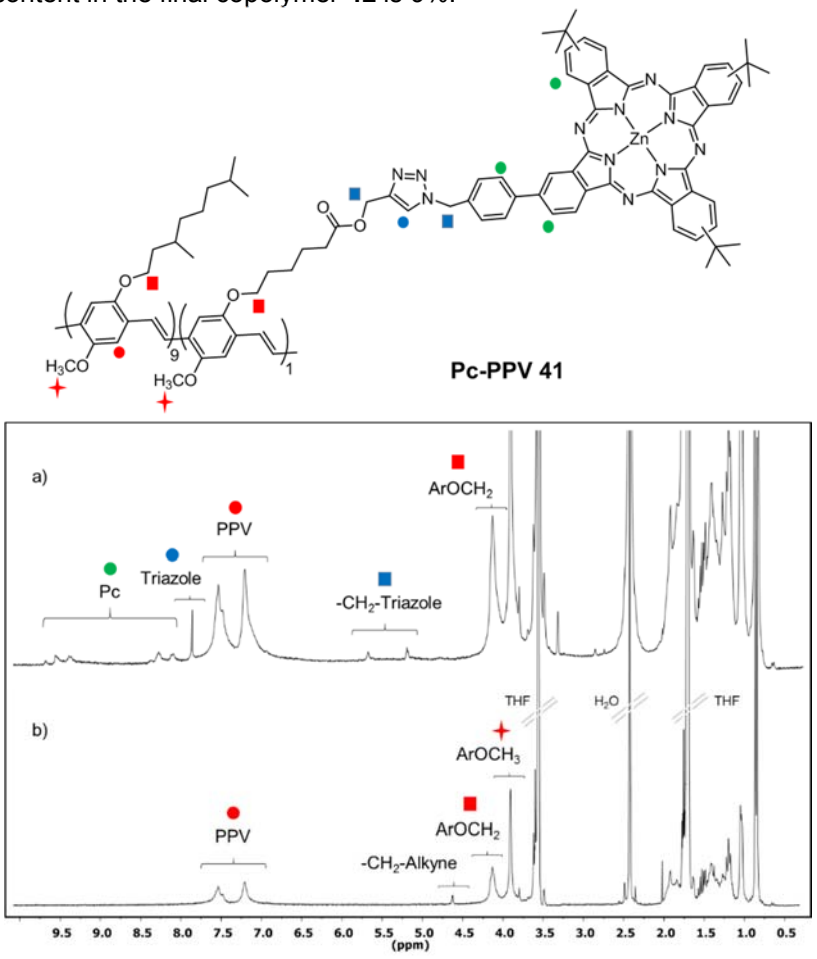

Figure 62.- ^{1}H-NMR (300 MHz) spectra of a) Zn(II)Pc-PPV **41** and b) alkynyl-PPV **39** in THF-d_8.

Regarding the synthesis of Zn(II)Pc-PT **42** by a click chemistry protocol, the conditions summarized in *Table 1* were also tested with copolymer alkynyl-PT **40** and and Zn(II)Pc **7** as starting materials, and the findings were the same: increasing the equivalents of Zn(II)Pc **7** and the concentration leads to the full derivatizacion of the acetylene groups in the copolymer. As can be deduced from comparison of the spectra (*Figure 63*), entry 1 of the table affords the optimal conditions for the proposed reaction.

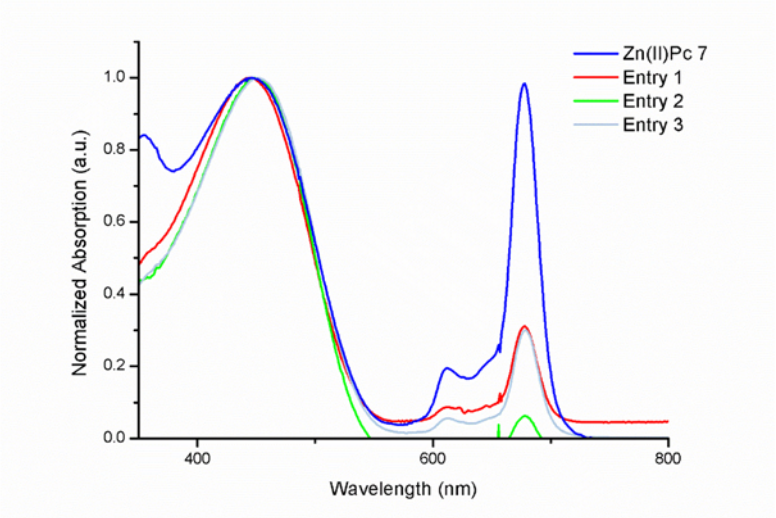

Figure 63.- UV-vis spectra of Pc-PPV **42** obtained under different conditions (entries 1-3) compared with the spectra of starting materials Zn(II)Pc **7**

Analytical SEC of Pc-PT **42** was performed using polystyrene standards in THF. It could be observed that there is an increase in the observed M_w value in THF solutions: Alkynyl-PT **40** copolymer presents a M_w value of $3.2 \cdot 10^4$ g/mol and a PDI of 1.9, whereas Pc-PT **42** shows a M_w value of $5.9 \cdot 10^4$ g/mol and a PDI of 1.8. As shown in *Figure 63*, the quality of the conjugated system and the success of the "click" reaction of Pc **7** to copolymer alkynyl-PT **40**, are confirmed by UV-Vis measurements in THF. The λ_{max} of the π-π^* transitions does not change after the linkage of Pc units, appearing at 450 nm in the spectra of both Pc-PT **42** and the starting copolymer. Also, the Q-band of the attached Zn(II)Pc is clearly visible at λ = 676 nm. Once again, the success of the reaction was confirmed by ^{1}H-NMR spectroscopy. The signal of the methylene protons next to the alkyne function is shifted downfield, indicating that all present alkyne moieties have reacted with a Pc molecule. Also, new signals from the incorporated Zn(II)Pc units together with the signal of the triazole ring are visible. Considering the signals of the alkyl side chains, the functionalization of the PT skeleton with Zn(II)Pc was estimated to be around 8%.

Polymers with electron-acceptor phthalocyanines : Double-Cable approach

As mentioned in the objectives section, we also decided to embark on the incorporation of electron-acceptor Zn(II)Pcs to a MDMO-PPV skeleton in a "double-cable" architecture, using "click" chemistry. In this approach, Zn(II)Pc is not only performing as absorbing material, but fully participating in the charge separation process and electron transport as the electron-acceptor component. To achieve this goal, Pcs funtionalized with electron-withdrawing groups have to be linked to the MDMO-PPV skeleton. On the other hand, it is necessary to prepare a PPV copolymer holding alternated functional groups able to react with appropriately functionalized electron-accepting Pcs. In particular, we undertook the preparation of a copolymer bearing azide moieties in alternated phenylene positions, which could react in a further step with an alkynyl-containing Zn(II)Pc by a "click"reaction. The precursor of this copolymer had been previously synthesized in our group[260] by a Wittig-Horner condensation reaction of adequate aromatic diphosphonates and dialdehydes, the latter containing protected hydroxyethoxy chains (*Scheme 24*, step 1 and 2). Analatycal SEC of the polymer gave a $M_W = 1.4 \cdot 10^4$ g/mol and a PDI = 2.9. Then we proceeded to convert the hydroxyl functions into azide moieties. First, a mesylation reaction was carried out to turn the hydroxyl moiety into a good leaving group (*Scheme 24*, step 3). This reaction procceeded successfully, using standard conditions, to give the polymer derivative **43.** The S_N2 reaction between the mesylate derivative **43** and an excess of NaN_3 yielded copolymer **44**.

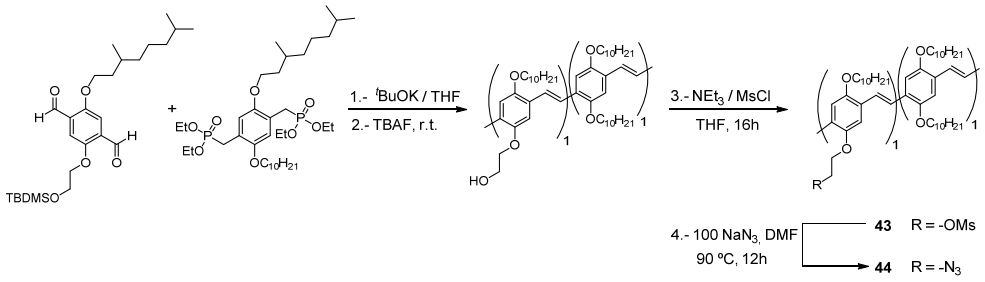

Scheme 24.- Synthesis of conjugated hydroxyl-PPV copolymer, and its consecutive transformation into the PPV containing azide groups (**44**).

[260] J.-J. Cid, *PhD Thesis* **2008**, Universidad Autónoma de Madrid, Spain.

The chemical transformations over the PPV-copolymer were quantified by ^{1}H-NMR, as shown in *Figure 64*. All the characteristic peaks for the aromatic units (PPV) are resonating in the 7.8-6.5 range and the methylene close to oxigen ($ArOCH_2$) methylene in the 4.2-3.6 range. For the mesylate derivative **43**, two additional signals corresponding to the methylene linked to the mesylate group could be observed. In the spectrum of the azide derivative **44,** obviously, there are no present, so it was concluded that around 90% of the former hydroxyl groups had been transformed into azide moieties.

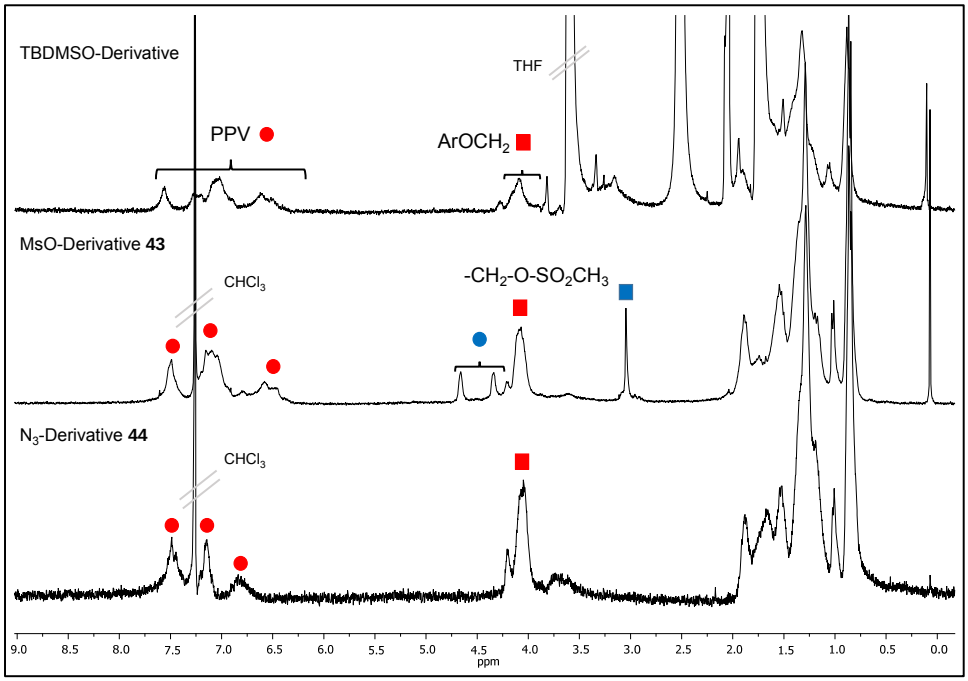

Figure 64.- ^{1}H-NMR (300 MHz) spectra of TBDMSO-PPV derivative (THF-d_8), mesylate-PPV **43** ($CDCl_3$-*d*), and azide-PPV **44** ($CDCl_3$).

First attempt to link the electron-acceptor Zn(II)Pc **18** to the polymer was made by the catalyzed version of the Huisgen 1,3-dipolar cycloaddition using the previously tested conditions. Azide PPV derivative **44** was treated with a 1.5 equivalents of alkylsulfonyl-Zn(II)Pc **18** with regard to the relative content of azide groups present in the copolymer. The reaction was performed in refluxing dry THF, using catalytic amounts of CuI and 2,6-lutidine as hindered base. However, the resulting material was impossible to analyze by UV/Vis spectroscopy or ^{1}H-NMR because of its insolubility. Probably a large quantity of Pcs was incorporated into the polymer, this fact largely reducing the solubility of the material. Considering that solubility is essential, not only for characterization but

also for the proposed preparation and study of BHJ devices, we decided to rule out the double cable approach.

Main-chain Pc-copolymers: Testing copolymerization conditions

Another plausible route towards the preparation of conjugated polymers containing Pc units for BHJ devices is the incorporation of the macrocycle into the main chain of the polymer. Aiming at keeping as much as possible the conjugation pathways, we have planned to incorporate the Pc in an edge-fused fashion, considering the remarkable results obtained with related Por-containing copolymers.[230,231,232] For that reason our final objective is the preparation of a copolymer incorporating Pcs and other electroactive units such as, for instance, BDT and DPP, which have been succesfully incorporated in low-band gap polymers and in small-molecule structures for BHJ (*Scheme 25*). Following this strategy the Pc units will be incorporated into the main chain, but connected through the exterior benzene unit.

The copolymerization of Pc monomers with DPP and BDT (or other analogous) species will be performed by the group of Iain McCulloch at Imperial College in the framework of EU-funded network, since they have a demonstrated expertise in the polymerization of different units by metal-catalyzed coupling reactions to obtain low bandgap polymers. We have provided them with Pc **21** (*Scheme 26)* to perform copolymerizations with DPP/BDT organometallic and halogenated derivatives in different conditions and ratio of the comonomers.

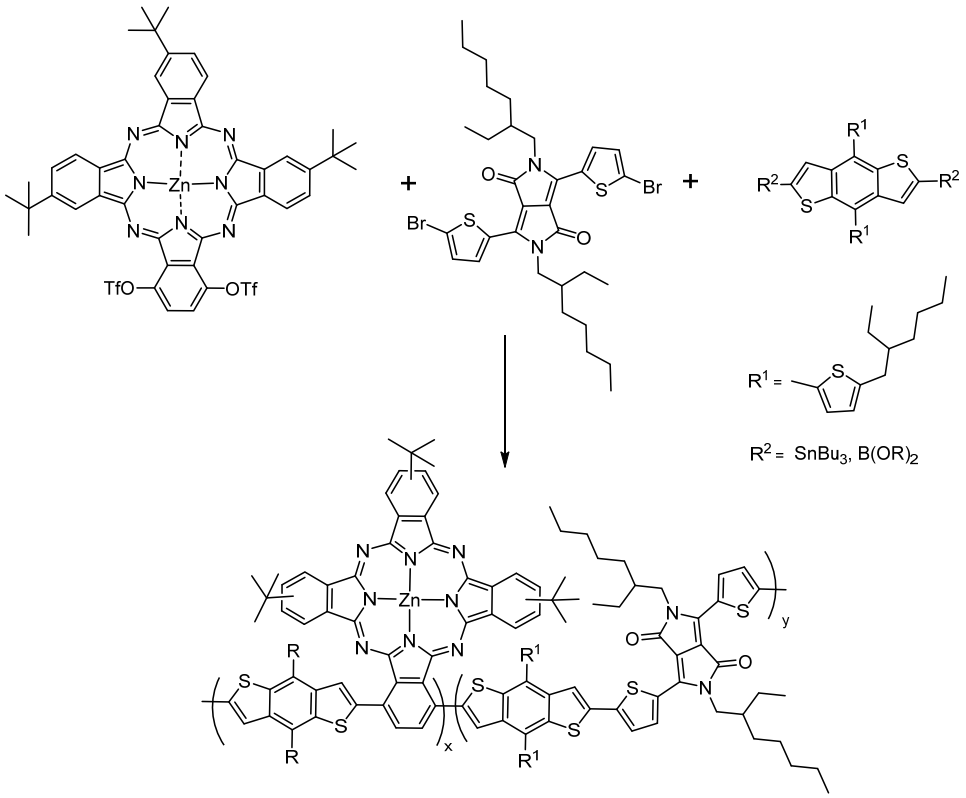

Scheme 25.- Proposed synthesis of a Zn(II)Pc-BDT-DPP copolymer.

However, we performed in our laboratories an optimization of the coupling condition with simple organometallic thiophenes in order to find the optimal conditions to be applied in the polymerization reactions (*Scheme 26*). Among the immense variety of Suzuki conditions, the ones depicted in *Scheme 26* and *Table 2* were selected because they worked successfully with Pcs in other related coupling reactions. The use of $Pd(PPh_3)_4$ in DME resulted in a clean transformation, providing the dithiophene derivative **43** in 47% isolated yield (*Scheme 26* and *Table 2, entry 1*), whereas the use of DMF as solvent (*Table 2, entry 2*) was found to be less effective, because the starting Zn(II)Pc **21** was not completely consumed after 24h. Interestingly, $Pd_2(dba)_3$ (*Table 2, entry 3*) resulted to be totally ineffective, affording just starting material. In an attempt to improve the yield of this cross-coupling reaction, a higher reactive form of thiophene derivative, 2-(tributylstannyl)thiophene. The Stille conditions used (*Scheme 26*) gave **43** in a better yield (64%).

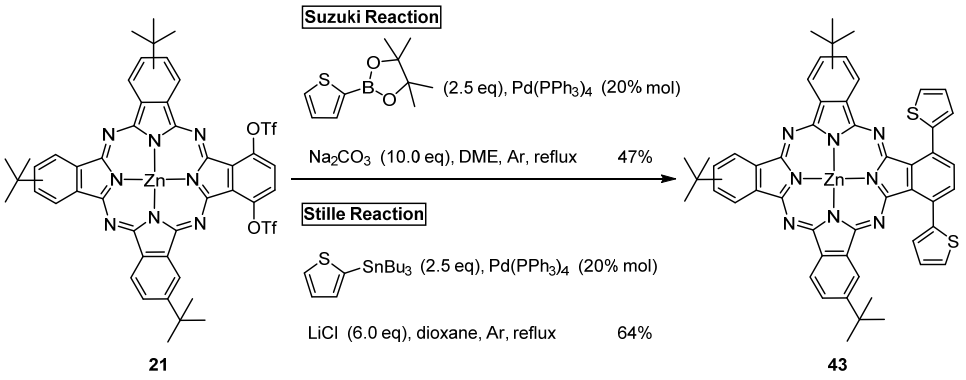

Scheme 26.- Two possible palladium-catalyzed reactions for the synthesis of Zn(II)Pc **43**.

With this preliminary conditions in hand, the first attempts to obtain co-polymers with derivative **21** as building block are currently being done in the laboratories of Iain McCulloch. Worth mentioning that the coupled tiophene-Pc derivative **43** can also be used for copolymerization experiments.

Entry	Pd source	Base	Solvent	Others
1	$Pd(PPh_3)_4$	Na_2CO_3	DME	-
2	$Pd(PPh_3)_4$	Na_2CO_3	DMF	-
3	$Pd_2(dba)_3$	K_3PO_4	Toluene	S-Phos

Table 2.- Different conditions for the Suzuki reaction Zn(II)Pc **21** and thiophene-2-boronic acid pinacol ester.

1.2.4.3 Photovoltaic studies of Pc-containing copolymers in bulk heterojunction solar cells

In order to study the effect of built-in Pc macrocycles in PPV and PT conjugated polymers in the efficiency of polymeric solar cells, BHJ devices based on Pc-PPV **37**, formed by esterification with Pc **5**, and Pc-PPV **41** and Pc-PT **42**, prepared by click reaction with Pc **7**, were prepared in the group Prof. R. A. J. Janssen (Eindhoven University of Technology) in the framework of an RTN-collaborative research project. Before buiding the devices, some optical and electrochemical studies of the active materials have been performed.

Uv-Vis Spectroscopy Measurements. Morphological Study of the Active Layer

First, the optical behaviour of the active Pc-PPV and Pc-PT materials is studied, both in solution and in film. The UV-vis spectra of the thin films provide valuable information about their morphology, which may be of help for the interpretation of the conversion efficiencies of the final devices. Thin films are prepared by drop-casting from solutions of the compounds in the corresponding solvents.

The UV-Vis absorption spectra of Zn(II)Pc-PPV **41** solutions in THF and CB are displayed in *Figure 65a*. In THF and CB, the λ_{max} of the Q band is at 676 nm and 691 nm, respectively. Red-sifting of the Q band in solutions of Pcs in aromatic solvents has been previously observed and rationalized in terms of stabilization of the LUMO level of the Pc through coordination of the aromatic solvent. In fact, precursor azido-phthalocyanine **7** shows a λ_{max} of its Q band in CB at 684 nm, whereas this Pc exhibits a λ_{max} at 675 in THF solution. A solvent-induced interaction between the Pc moiety and the conjugated PPV backbone can explain the additional red-shifting observed in CB solution of Zn(II)Pc-PPV **41** with regard to that of Pc **7**.

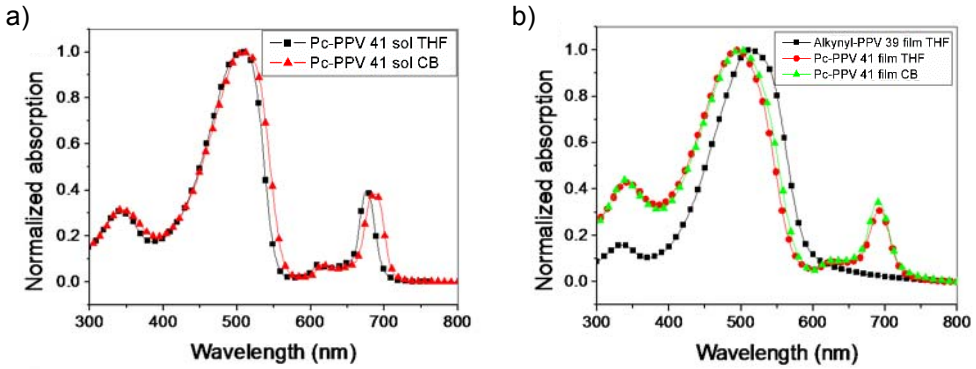

Figure 65.- UV-Vis absorption of: a) a solution of Pc-PPV **41** in THF (squares) and in CB (triangles); b) a film of alkynyl-PPV **39** drop-cast from a solution in THF (squares) and films of Pc-PPV **41** drop-cast from a solution in THF (circles) or CB (triangles).

In *Figure 65b*, the UV-Vis spectra of alkynyl-PPV **39** and Zn(II)Pc-PPV **41** in film are given. The absorption of **39** is comparable to the absorption of PPV between 400 and 550 nm with λ_{max} at 512 nm. In the Pc-PPV **41** film, the Pc absorption is visible with λ_{max} at 692 nm, while the λ_{max} of the PPV decreases to 494 nm. The shift to lower wavelengths of the PPV absorption in Pc-PPV **41** as compared to alkynyl-PPV **39** indicates that the presence of the Pc in the side chains disturbs the polymer organization and lowers effective conjugation length. The λ_{max} of the Pc Q band in the Pc-PPV **41** film almost

coincide with that obtained in CB solution, this fact being an indication of the interaction between the conjugated PPV backbone and the Pc molecules, which produces a stabilization of the LUMO level of the Pc as in the case of dilution in aromatic solvents.

Regarding the Zn(II)Pc-PT **42** copolymer, the polythiophene absorption has a λ_{max} around 450 nm. In THF solution, the Pc absorption appears at λ_{max} 677 nm, while in CB solution the λ_{max} of the Pc was at 691 nm for Pc-PT **42** (*Figure 66a*). The UV-Vis spectra of Pc-PT **42** films drop-cast from solutions in CB and THF are displayed in *Figure 66b*, together with the absorption of regio-regular PT in CB. Although the spectra are affected by scattering, they show that, compared to the spectrum in solution, the absorption of the polymer backbone in Pc-PT **42** broadens relative to the Q band of the Pc, as a consequence of the π-π stacking of the conjugated chains of the PT skeleton. The PT absorption is also red-shifted compared to the spectrum in solution, with maximum absorptions at 523 nm for the film drop-cast from CB and 564 nm for the film drop-cast from THF, respectively. The absorption at 600 nm, in both THF- and CB-drop-casted films is due to the ordering of regioregular PT chains.[261] The contribution of the absorption in the visible of the Pc was found at around 690 nm. The higher λ_{max}, together with the higher relative intensity of the shoulder at 600 nm, of the polymeric backbone in the film drop-cast from THF compared to the corresponding values of the film drop-cast from CB, seem to indicate that the former presents a better stacking of the PT chains.[262] Therefore, THF seems to be a better solvent than CB to induce a better organization of the polymer chains in the film: THF appears to minimize the impact of the large Pc molecules in the alkyl side chains on the structural ordering of the polymer chains.

[261] P. J. Brown, D. S. Thomas, A. Kohler, J. S. Wilson, J.-S. Kim, C. M. Ramsdale, H. Sirringhaus, R. H. Friend, *Phys. Rev. B* **2003**, *67*, 064203.
[262] F. C. J. Spano, *Chem. Phys*. **2005**, *122*, 234701.

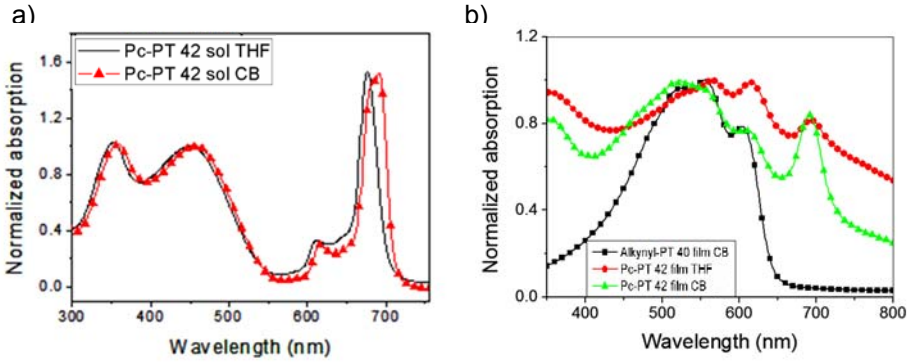

Figure 66.- UV-Vis absorption of: a) a solution of Pc-PT **42** in THF (black line) and CB (triangles); b) a film of alkynyl-PT **40** drop-cast from a solution in CB (square) and films of Pc-PT **42** drop-cast from a solution in THF (circles) or CB (triangles).

HOMO and LUMO Levels

In order to study the role of the Zn(II)Pcs in the copolymers, in terms of light absorption and charge separation, electrochemical experiments have been done to determine the HOMO and LUMO energy levels of each component in the Pc-PPV (**41**) and Pc-PT (**42**) materials.

First, the molecular orbitals of bromo Pc **6**, which was used as reference compound, were determined. Electrochemical data (V *vs*. Fc/Fc^+) of the redox process of Pc **6** were obtained from cyclic voltammetry in 0.1 M $TBAPF_6$ in *o*-DCB solution. The measured potentials of the onsets of the redox waves are: E_{red}^1 = -1.373 V, E_{ox}^1 = 0.005 V, and E_{ox}^2 = 0.749 V. The first oxidation and reduction potentials are used to estimate the energy of the HOMO and LUMO levels using the redox pair value of Fc/Fc^+ = -5.23 eV with respect to the vacuum level. The HOMO and LUMO energy levels of Pc **6** were found to be -5.2 eV and -3.9 eV, respectively. In *Figure 67*, the energy levels of the Pc reference compound are schematically represented in comparison with those determined for PPV, PT (electron donor role in the final device), and PCBM (electron acceptor role in the final device) under similar conditions. Considering the relative position of the LUMO levels, the Pc molecules could also act as electron acceptor relative to PT and as electron donor relative to PCBM. The same situation applies to the combination with PPV. The fact that the HOMO level of Pc **6** is similar to that of PT and PPV is advantageous as the Pc molecule in Zn(II)Pc-PPV **41** and Zn(II)Pc-PT **42** will not act as a hole trap.

In addition, the small HOMO-HOMO offset will likely result in energy transfer from the PT and PPV polymers to the Pc molecule, followed by electron transfer to PCBM. These events are plausible, since photoexcited charge transfer from the Pc component

to C_{60} or PCBM has been widely demonstrated in many different BHJ solar cells comprising Pcs and fullerene derivatives.[213,214,215,216,217,218,219,220,221,222] On the other hand, some previous studies in solution performed by our group with related covalent Pc-PPV short oligomers reveal a photosensitization of the Pc units when exciting the PPV chains.[233]

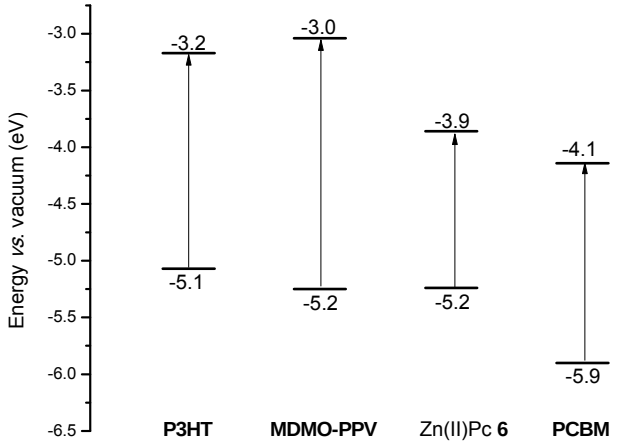

Figure 67.- Energy scheme of the absorbing materials in Zn(II)Pc-PPV **41**:PCBM and Zn(II)Pc-PT **42**:PCBM combinations.

Preparation and studies of bulk heterojunction devices

Devices with the configuration ITO/PEDOT:PSS/polymer:PCBM/LiF/Al were prepared (*Figur*e *68*), in which de active layer is constituted by the PPV or PT derivative as the donor and PCBM as the acceptor in a ratio of 1:4 respectively, for PPV derivatives, and 1:1 and 1:2 (w/w) blends for PT. The active layer is spin-coated from a mixed solution in chlorobenzene at different spinning speeds to obtain varying active layer thicknesses, in order to study the relationship between thickness and the corresponding performance of the different solar cells. It is worth mentioning that the use of chlorobenzene as solvent, is compulsory to dissolve a sufficient amount of PCBM, thus limitating the choice of different solvents to study their influence in the morphology of the active layer and therefore, the performance. As we have seen in the UV-Vis spectra section, THF would be a more convenient solvent.

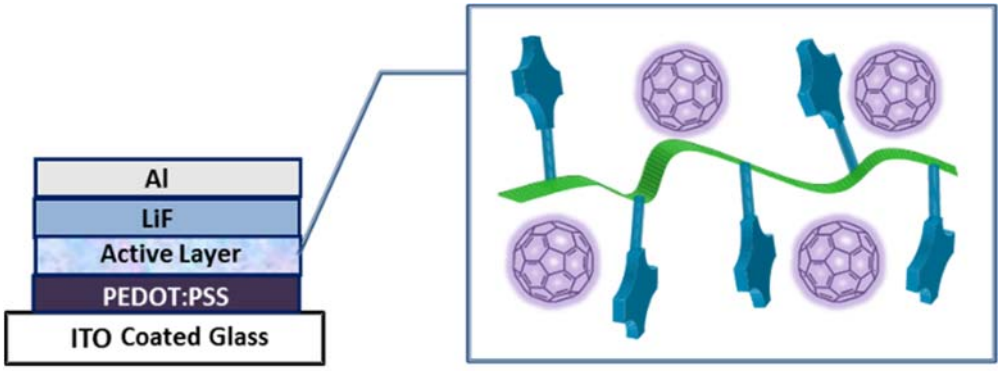

Figure 68.- Schematic structure of the bulk-heterojunction solar cells realized with Pc-PPV **35**, Pc-PPV **36** and Pc-PT **37**.

First, to investigate whether the attached Pc molecules contribute to the generation of photocurrent, the spectral response of the solar cells has been measured. EQE curves of Pc-PPV **38**, Pc-PPV **41** Pc-PT **42** are depicted in *Figure 69*. In the spectral response of the BHJ solar cells with functionalized PPVs (*Figure 69a*), there is a clear contribution of the PPV backbone around 500 nm, whereas the contribution of the Pc is visible around 700 nm. Comparing the EQE of both copolymers, ester Pc-PPV **38** and triazole Pc-PPV **41**, with the UV-Vis absorption spectrum of a Pc-PPV **41** solution in THF, one can observe that the absorption peak of the PPV backbone remains at the same wavelength, whereas there is a clear red-shift of the peaks corresponding to the Pcs as a result of the interaction between the individual Pc entities in the thin film. The height of the Pc Q-band in the EQE spectrum of derivative **41** is larger than in Pc-PPV **38**, owing to the fact that the relative amount of attached Zn(II)Pc units is higher in the former (9% in **41** *versus 7%* in **38**), due to the effectiveness of the click reaction

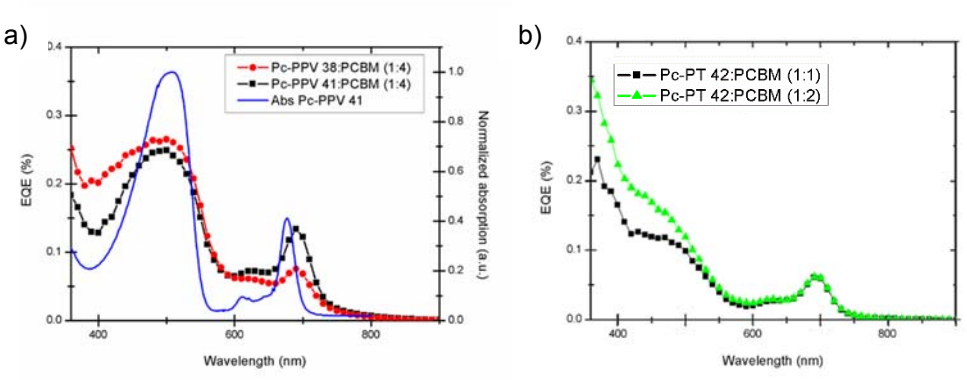

Figure 69.- EQE of solar cells with a) ester Pc-PPV **38**:PCBM (1:4) active layer (circles), triazole Pc-PPV **41** in blends with PCBM in a (1:4) weight ratio (squares) and UV-Vis absorption of triazole Pc-PPV **41** in THF (line); b) triazole Pc-PT **42** in blends with PCBM in a (1:1) (squares) and (1:2) (triangles) weight ratio.

In the spectral response of Pc-PT **42**:PCBM solar cells (*Figure 69b*), the EQE due to the Pc component is clearly present around 700 nm, indicating that the light absorbed by the Pc moiety leads to charge transfer, and that generated charges are extracted. The low values of the EQE between 350-550 nm, also indicates a lack of crystalline ordering of the PT part in spin-coated films as compared to drop cast films (see Figure 66), which is important for high conversion efficiencies in PT:PCBM solar cells.

A clear conclusion which can be obtained from the EQE is that that the absorption of the synthesized materials matches significantly better with the AM 1.5 solar spectrum due to the covalent attachment of Zn(II)Pcs. In this way, more sunlight ca be efficiently absorbed and therefore transformed in an external current by these functionalized copolymers.

After establishing the contribution of the Pcs to the EQE of the solar cells, the performance of the solar cells was investigated. The J-V curves of alkynyl-PPV **37**:PCBM (*Figure 70a*), ester Pc-PPV **38**:PCBM, triazole Pc-PPV **41**:PCBM *(Figure 70a*), alkynyl-PT **40**:PCBM (*Figure 70b*), Pc-PT **42**:PCBM (*Figure 70b*) were obtained, and therefore, the most important photovoltaic parameters as V_{OC} (V), J_{SC} (mA/cm^2), FF (%) and PCE (%) were determined for devices with different active layer thicknesses (*Figure 71;* the results of Pc-PT **42**:PCBM are omitted in this graphics, however, their best results are summarized in *Table 3*).

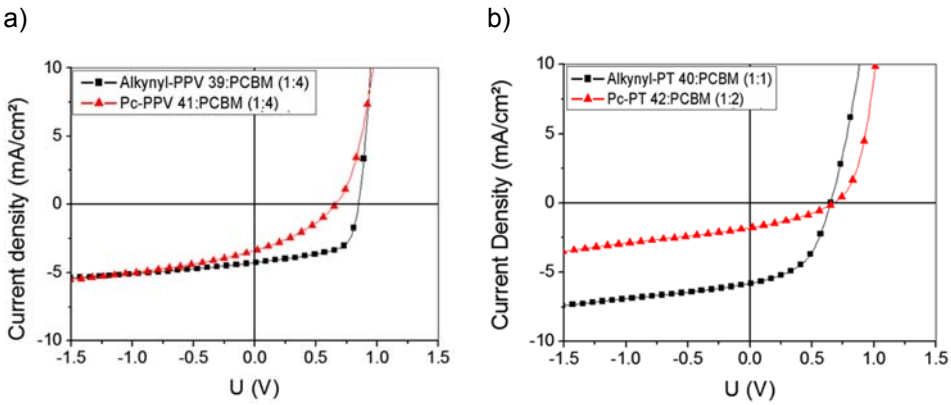

Figure 70.- *J-V* curve of ITO/PEDOT:PSS (~50nm)/polymer:PCBM/LiF/Al devices with a) alkynyl-PPV **39** (1:4) (squares) and Pc-PPV **41**:PCBM (triangles); b) alkynyl-PT **40**:PCBM (1:1) (squares) and Pc-PT **42**:PCBM (1:2) (triangles).

Regarding Pc-PPV copolymers, it is worth pointing out that the values of these parameters for the two different Pc-PPV copolymers, **38** and **41**, are lower than those found for the reference copolymer alkynyl-PPV **39**, being the latter quite comparable to what is reported for MDMO-PPV:PCBM (1:4) BHJ solar cells.[152] The detrimental effect of the Pc molecules on the solubility of the polymer in CB could be largely responsible for the poor performance, since it causes a poor polymer organization. All the measured solar cells exhibited a strong radial spreading over the sample, which indicates that poor quality thin films have been formed. Hence, it is not entirely surprising that this results in an inferior performance. The above mentioned absorption studies have illustrated how the election of a more convenient solvent, THF, can induce a better structural order of the polymer chains in a film, and therefore, a more regular layer; this would cause a favourable morphology and higher hole mobility in the blend, and consequently, high J_{SC} and FF, but the solubility of PCBM in this solvent was too low for device preparation.

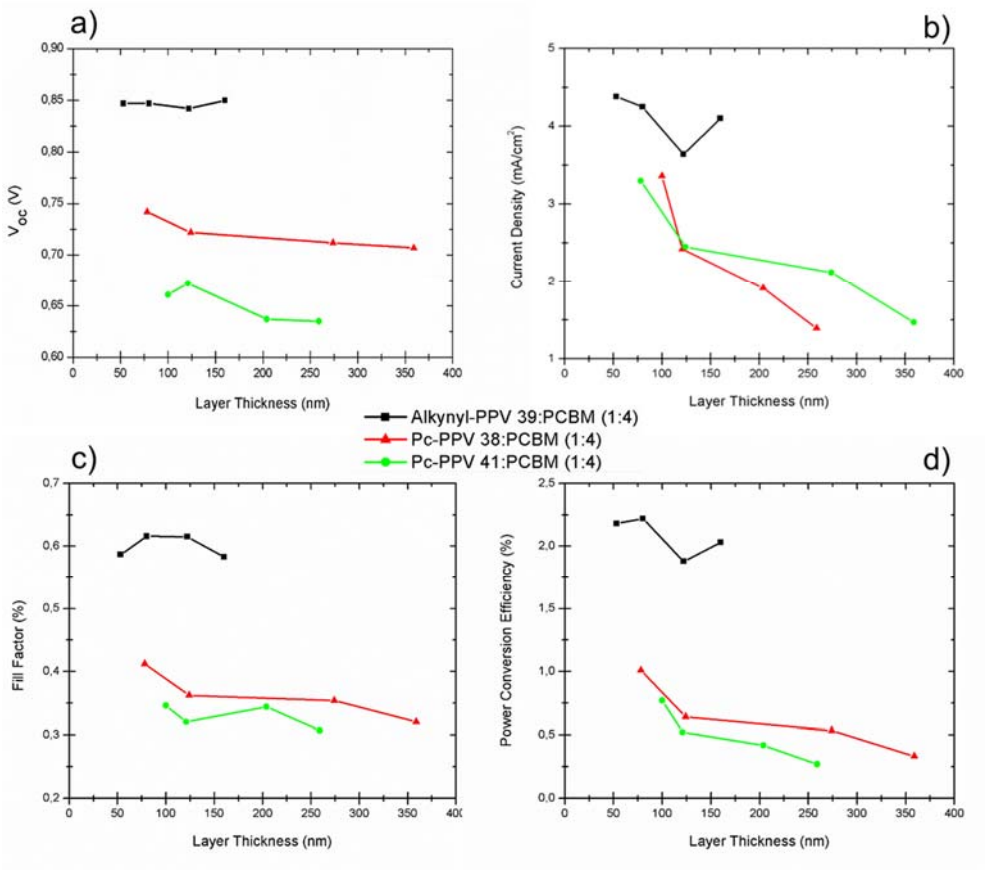

Figure 71.- Solar cell parameters of BHJ devices with different active layer thicknesses of alkynyl-PPV **39** (squares), Pc-PPV **38** (triangles) and Pc-PPV **41** (circles).

The best solar cells made with these copolymers are summarized in *Table 3*. These results correspond to active layers thicknesses of less than 100 nm. Focusing on both Pc-PPV derivatives, the solar cell performance of copolymer ester Pc-PPV **38** is better than the the performance of the solar cell of triazole Pc-PPV **41**. At first glance, this result is contradictory with the EQE spectra (*Figure 69a*). However, once again, this result can be explained in terms of morphology. The fact that copolymer **38** is functionalized with less Pc molecules than copolymer **41** makes it slightly more soluble in CB, which results in a better morphology of the active layer for the former.

Polymer:PCBM		J_{SC} (mA/cm^2)	V_{OC} (V)	FF(%)	PCE (%)	Layer thickness (nm)
PPV 39	(1:4)	4.25	0.85	0.62	2.22	80
Pc-PPV 38	(1:4)	3.30	0.74	0.41	1.01	75
Pc-PPV 41	(1:1)	3.36	0.66	0.35	0.77	100
PT 40	(1:1)	5.81	0.65	0.49	1.86	73
Pc-PT 42	(1:2)	1.79	0.67	0.34	0.41	42
Pc-PT 42	(1:1)	1.46	0.68	0.33	0.32	33

Table 3.- Solar cell parameters of the best devices of each polymer:PCBM combination.

The above observations are valid for all studied layer thicknesses, although thin devices perform better than devices containing thicker active layers. Apparently, although a thicker layer potentially will lead to more light harvesting, this does not offset the impact of a decrease in transport properties.

The J-V curves of the best alkynyl-PT **40**:PCBM and Pc-PT **42**:PCBM solar cells are shown in *Figure 70b*. The performance of the device with alkynyl-PT **40** as donor component was comparable to the performance of P3HT:PCBM solar cells prepared following the same procedure. The best performing Pc-PT **42**:PCBM solar cells (*Table 3*) were obtained using a relatively thin layer (42 nm). Better current densities and efficiencies were achieved with higher amounts of PCBM. The low J_{SC} values of Pc-PT **42**:PCBM solar cells compared to PT:PCBM solar cells, together with the fact that the best current densities were obtained for very thin layers (thickness < 50 nm), indicated that the charge transport properties in the blend were unfavourable. The low FF of the devices and the need of more PCBM to improve the extraction of charges indicate that also the morphology of the blended layer is poor. Thermal treatment of PT:PCBM solar cells has been reported to result in better hole transport in the polymer phase because of closer stacking of the conjugated polymers backbones.[263] However, annealing treatments of the Pc-PT **42** devices did not lead to better results. The Pc molecules in the side chains may prevent the PT chains from self-organizing, this fact explaining why no better results are obtained after annealing. A better π-π stacking would be obtained

[263] F. Padinger, R. S. Rittberger, N. S. Sariciftci, *Adv. Funct. Mater*. **2003**, *13*, 85.

by processing from THF, but, as mentioned above the solubility of PCBM in this solvent was too low for device preparation. A better solubility in the processing solvent might lead to an enhanced polymer organization in the blend and to an improved morphology, both increasing the PCE.

1.3 Dye-sensitized solar cells (DSSCs)

At the moment, dye-sensitized solar cells offer a lower-cost alternative to silicon photovoltaics because they are based on cheap materials and inexpensive manufacturing technology. A dye-sensitized solar cell can generally be described as a photoelectrochemical cell where the working electrode consists of photon-absorbing dyes (sensitizers) anchored onto mesoporous surfaces of semiconducting nanoparticles. Depending on the electronic nature of the semiconductor, electron acceptors (n-type) or donors (p-type), two generations of semiconductors and therefore, of DSSCs technologies, can be distinguished The first generation, that is the n-type or Grätzel cells,[116,117,264] which is based on the sensitization of a wide-band-gap n-type semiconductor oxide like ZnO or TiO_2, marches ahead of the race with photoconversion efficiencies over 13.0%.[119] A typical n-type cell consists of four main components: 1) A mesoporous semiconductor layer[265] (usually TiO_2 anatase,[116a,266] but also ZnO,[267,268] SnO_2[268,269] and Nb_2O_5[270]) deposited onto a transparent conducting glass substrate, 2) a dye sensitizer, 3) a redox electrolyte (typically I^-/I_3^- or cobalt complexes)[271] and 4) a counter electrode. Upon photoexcitation, the sensitizer promotes the electron injection in the TiO_2 CB. The oxidized dye is regenerated by the electrolyte, and finally the circuit is closed at the counter electrode where the reduction of the oxidized mediator occurs. To further improve the efficiency, much effort has been devoted to the optimization of these

[264] M. Gratzel, *Inorg. Chem*. **2005**, *44*, 6841.
[265] a) R. Jose, V. Thavasi, S. Ramakrishna, *J. Am. Ceram. Soc*. **2009**, *92*, 289; b) N. Sharifi, F. Tajabadi, N. Taghavinia, *ChemPhysChem* **2014**, *15*, 3902.
[266] a) P. M. Sommeling, B. C. O'Regan, R. R. Haswell, H. J. P. Smit, N. J. Bakker, J. J. T. Smits, J. M. Kroon, J. A. M. van Roosmalen, *J. Phys. Chem. B* **2006**, *110*, 19191; b) J. M. Kroon, N. J. Bakker, H. J. P. Smit, P. Liska, K. R. Thampi, P. Wang, S. M. Zakeeruddin, M. Gratzel, A. Hinsch, S. Hore, U. Wurfel, R. Sastrawan, J. R. Durrant, E. Palomares, H. Pettersson, T. Gruszecki, J. Walter, K. Skupien, G. E. Tulloch, *Prog. Photovoltaics* **2007**, *15*, 1; c) M. Kapilashrami, Y. Zhang, Y.-S. Liu, A. Hagfeldt, J. Guo, *Chem. Rev*. **2014**, *114*, 9662.
[267] a) K. Keis, E. Magnusson, H. Lindstrom, S.-E. Lindquist, A. Hagfeldt, *Sol. Energy Mater. Sol. Cells* **2002**, *73*, 51; b) K. Keis, C. Bauer, G. Boschloo, A. Hagfeldt, K. Westermark, H. Rensmo, H. Siegbahn, *J. Photochem. Photobiol. A* **2002**, *148*, 57.
[268] K. Tennakone, G. R. R. A. Kumara, I. R. M. Kottegoda, V. P. S. Perera, *Chem. Comm.* **1999**, 15.
[269] a) B. V. Bergeron, A. Marton, G. Oskam, G. J. Meyer, *J. Phys. Chem. B* **2005**, *109*, 937; b) S. Chappel, A. Zaban, *Sol. Energy Mater. Sol. Cells* **2002**, *71*, 141; c) A. Y. El-Etre, S. M. Reda, *Appl. Surf. Sci*. **2010**, *256*, 6601.
[270] a) K. Sayama, H. Sugihara, H. Arakawa, *Chem. Mater*. **1998**, *10*, 3825; b) P. Guo, M. A. Aegerter, *Thin Solid Films* **1999**, *351*, 290.
[271] J. Wu, Z. Lan, J. Lin, M. Huang, Y. Huang, L. Fan, G. Luo, *Chem. Rev*. **2015**, *115*, 2136.

components,[116] and undoubtedly the dye represents one of the keys to achieve better results.[272] Record efficiencies exceeding 11% have been obtained using ruthenium polypyridyl complexes as molecular sensitizers, the first and the most extensively investigated class of dyes, mainly by the group of M. Grätzel. Among them, N719,[273] black dye (also called N749),[274] and CYC-B11,[275] present the best reported efficiencies: 11.18%, 11.10%, and 11.50%, respectively (*Figure 72*). However, the high cost of Ru metal and the low extinction coefficients of Ru-based complexes (usually < 2.50 x 10^4 $M^{-1}\cdot cm^{-1}$ in the visible region) have restrained the research on DSSCs based on Ru-dyes.

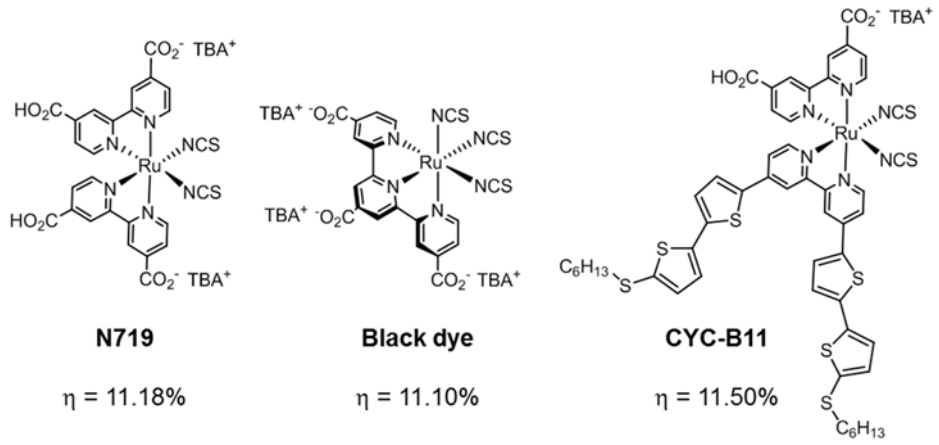

Figure 72.- Structures of Ru-sensitizers used in DSSCs.

In the search for ideal metal-free sensitizers, many different organic dyes have been reported.[276,277] This alternative has been extensively explored with the basic D-π-A structure, and more recently the D-A-π-A configuration. Various kinds of aromatic units

[272] C.-P. Lee, R. Y.-Y. Lin, L.-Y. Lin, C.-T. Li, T.-C. Chu, S.-S. Sun, J. T. Lin, K.-C. Ho, *RSC Adv*. **2015**, *5*, 23810.

[273] M. K. Nazeeruddin, F. De Angelis, S. Fantacci, A. Selloni, G. Viscardi, P. Liska, S. Ito, B. Takeru, M. Gratzel, *J. Am. Chem. Soc*. **2005**, *127*, 16835.

[274] a) Y. Chiba, A. Islam, Y. Watanabe, R. Komiya, N. Koide, L. Han, *Jpn. Appl. Phys.* **2006**, *45*, L638; b) M. K. Nazeeruddin, P. Pechy, M. Gratzel, *Chem. Comm*. **1997**, 1705; c) M. K. Nazeeruddin, P. Pechy, T. Renouard, S. M. Zakeeruddin, R. Humphry-Baker, P. Comte, P. Liska, L. Cevey, E. Costa, V. Shklover, L. Spiccia, G. B. Deacon, C. A. Bignozzi, M. Gratzel, *J. Am. Chem. Soc*. **2001**, *123*, 1613.

[275] C.-Y. Chen, M. Wang, J.-Y. Li, N. Pootrakulchote, L. Alibabaei, C.-h. Ngoc-le, J.-D. Decoppet, J.-H. Tsai, C. Gratzel, C.-G. Wu, S. M. Zakeeruddin, M. Gratzel, *ACS Nano* **2009**, *3*, 3103.

[276] J. N. Clifford, E. Martinez-Ferrero, A. Viterisi, E. Palomares, *Chem. Soc. Rev*. **2011**, *40*, 1635.

[277] a) A. Mishra, M. K. R. Fischer, P. Bauerle, *Angew. Chem. Int. Ed*. **2009**, *48*, 2474; b) Y. Uemura, S. Mori, K. Hara, N. Koumura, *Chem. Lett*. **2011**, *40*, 872; c) Y. Ooyama, Y. Harima, *ChemPhysChem* **2012**, *13*, 4032. See references cited therein; d) Y.-S. Yen, H.-H. Chou, Y.-C. Chen, C.-Y. Hsu, J. T. Lin, *J. Mater. Chem*. **2012**, *22*, 8734; e) M. Liang, J. Chen, *Chem. Soc. Rev*. **2013**, *42*, 3453; f) Y. Wu, W. Zhu, *Chem. Soc. Rev*. **2013**, *42*, 2039.

and functional groups have been combined to generate these patterns, and among them, arylamines, thiophene derivatives and the cyanoacrylic acid moiety are the most common subunits that act as electron donor, π-linker, and electron acceptor/anchoring groups, respectively. In terms of HOMO/LUMO levels, the duality of electron-acceptor/anchoring group makes sense because upon photoexcitation, the dye promotes the electron injection from its LUMO to the TiO_2 CB, and the LUMO is mainly localized in the electron acceptor group, which playing also as anchoring group, is located close to the semiconductor surface. In general, efficiencies consistently remain in the range of 6.0-8.0% with a few exceptions, and thus far only a few D/A organic dyes have achieved PCEs over 10.0% (C219 and C257 for instance, *Figure 51*). The successful implementation of the typical moieties present in low-band-gap polymers, like carbazoles, cyclopentadithiophenes, fluorenes, and benzothiadiazoles, has allowed to overcome this barrier a couple of times.[278] The current efficiency record for pure organic dyes, 12.5%, has been achieved by a *N*-annulated indenoperylene electron-donor, decorated with an electron-acceptor benzothiadiazole moiety (C275, *Figure 73*).[279] Further explorations of other exotic polycyclic aromatic materials seem to be steps in the right direction.

Ru-free sensitizers with large π-conjugated systems such as porphyrins and phthalocyanines, which efficiently absorb photons and promote electron-transfer processes, are receiving considerable attention.[280]

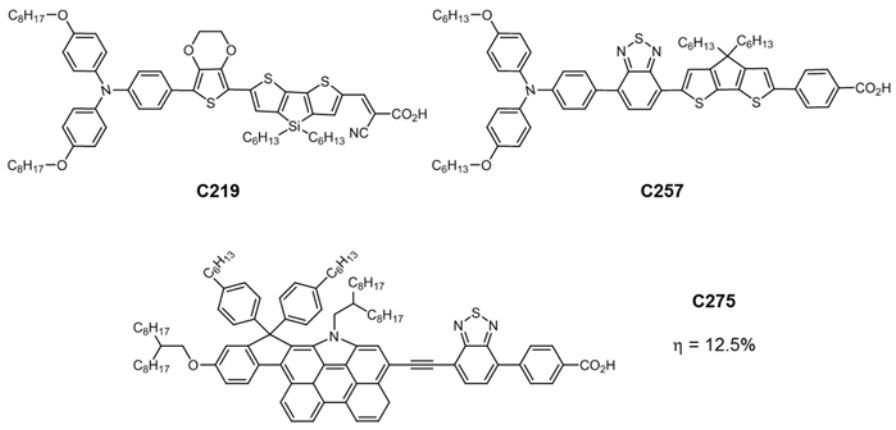

Figure 73.- Structures of metal-free organic dyes used in DSSCs.

[278] Some examples; a) M. Zhang, Y. Wang, M. Xu, W. Ma, R. Li, P. Wang, *Energy Environ. Sci*. **2013**, *6*, 2944; b) K. Kakiage, Y. Aoyama, T. Yano, T. Otsuka, T. Kyomen, M. Unno, M. Hanaya, *Chem. Comm*. **2014**, *50*, 6379.

[279] Z. Yao, M. Zhang, H. Wu, L. Yang, R. Li, P. Wang, *J. Am. Chem. Soc*. **2015**, DOI: 10.1021/jacs.5b01537.

[280] H. Imahori, T. Umeyama, S. Ito, *Acc. Chem. Res.* **2009**, *42*, 1809.

Porphyrins, in particular, have been successfully used in the past few years due to their strong absorption in the visible region and excellent flexibility in tuning photophysical and electrochemical properties through structural changes.[281] Furthermore, the D-π-A configuration of dye molecules has emerged as a premium model for high-efficient porphyrin dyes. The integration of a porphyrin chromophore as a π-bridge into a D-π-A structure,[282] has provided efficiencies comparable to the best ruthenium polypyridyl dyes; for instance push-pull porphyrin YD-2 (PCE = 11.0%)[283] and the improved YD2-oC8 (PCE = 11.9%, and 12.3% in co-sensitized cells),[284] in which the 3,5-bis(*tert*-butyl)phenyl substituents in YD-2 are replaced by 2,6-dioctoxyphenyl groups, as shown in *Figure 74*. Further structural optimization of porphyrins dyes involved the introduction of a benzothiadiazole ring between the porphyrin and the anchoring group, which yielded the porphyrins GY50 (PCE = 12.75%)[285] and SM315 (PCE = 13.0%),[119] being the latter the figure of merit for state-of-the art devices (*Figure 74*). The addition of the benzothiadiazole was successful in filling the gap between the Soret band and the Q band in the absorption spectrum, giving rise to panchromatic sensitizers.

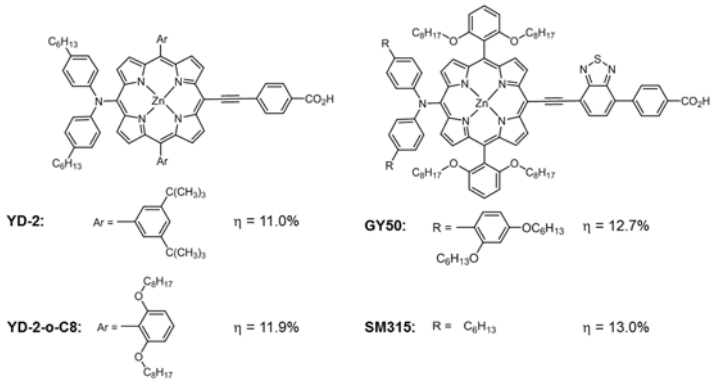

Figure 74.- Structures of porphyrin dyes used in DSSCs.

[281] a) L.-L. Li, E. W.-G. Diau, *Chem. Soc. Rev*. **2013**, *42*, 291; b) M. Urbani, M. Gratzel, M. K. Nazeeruddin, T. Torres, *Chem. Rev*. **2014**, *114*, 12330; c) T. Higashino, H. Imahori, *Dalton Trans*. **2015**, *44*, 448.

[282] a) H.-P. Lu, C.-Y. Tsai, W.-N. Yen, C.-P. Hsieh, C.-W. Lee, C.-Y. Yeh, E. W.-G. Diau, *J. Phys. Chem. C* **2009**, *113*, 20990; b) C.-P. Hsieh, H.-P. Lu, C.-L. Chiu, C.-W. Lee, S.-H. Chuang, C.-L. Mai, W.-N. Yen, S.-J. Hsu, E. W.-G. Diau, C.-Y. Yeh, *J. Mater. Chem.* **2010**, *20*, 1127.

[283] T. Bessho, S. M. Zakeeruddin, C.-Y. Yeh, E. W.-G. Diau, M. Gratzel, *Angew. Chem. Int. Ed*. **2010**, *49*, 6646.

[284] A. Yella, H.-W. Lee, H. N. Tsao, C. Yi, A. K. Chandiran, M. K. Nazeeruddin, E. W.-G. Diau, C.-Y. Yeh, S. M. Zakeeruddin, M. Gratzel, *Science* **2011**, *334*, 629.

[285] A. Yella, C.-L. Mai, S. M. Zakeeruddin, S.-N. Chang, C.-H. Hsieh, C.-Y. Yeh, M. Gratzel, *Angew. Chem. Int. Ed*. **2014**, *53*, 2973.

Regarding Pc-sensitized solar cells, performances have not yet achieved the values of porphyrin-based device. However tremendous progress has taken place, with the obtained efficiencies growing from 1% in the seminal report[286] to the recently published 6.4%.[287] The main advantages of porphyrins in comparison with Pcs are: 1) Their many reaction sites, *i.e.* four meso and eight β positions, available for functionalization, and 2) the easy synthesis of highly unsymmetrical structures. For their part, Pcs are important players in n-type sensitizers due to their impressive light-harvesting properties (better than porphyrins) in the far red/near IR spectral region and their extraordinary robustness.[288] On the other hand, the flat nature and large π-system induce in these molecules a strong tendency to stack, which dramatically diminishes their efficiencies when used in DSSCs due to the rapid deactivation of the dye excited state. In any case, there are strategies to control the formation of molecular aggregates onto the semiconductor nanoparticles: 1) Introduction of bulky groups in the periphery of the scaffold; 2) us of axially substituted Pcs, and 3) addition of co-adsorbents,[289] that strongly bind to the surface and displace a certain number of dye molecules from the TiO_2, reducing their probability of aggregation. Chenodeoxycolic acid (CHENO)[286] is the most common and broadly used co-adsorbent in Pc-based DSSCs, but there are also examples where 1-decylphosphonic (DPA)[290] or ω-guanidinoalkyl acids[291] are successfully used.

Regarding the use of bulky substituents, Grätzel and Torres reported Pc PCH001[292] and TT1,[293] which reached 3.05% and 3.50% overall efficiencies, respectively, employing *tert*-butyl groups at the β positions of the isoindoles (*Figure 75*). The utilization of even bulkier diphenylphenoxy substituents, brought about a significant

[286] M. K. Nazeeruddin, R. Humphry-Baker, M. Gratzel, D. Wohrle, G. Schnurpfeil, G. Schneider, A. Hirth, N. Trombach, *J. Porphyrins Phthalocyanines* **1999**, *3*, 230.
[287] T. Ikeuchi, H. Nomoto, N. Masaki, M. J. Griffith, S. Mori, M. Kimura, *Chem. Comm*. **2014**, *50*, 1941.
[288] a) M.-E. Ragoussi, M. Ince, T. Torres, *Eur. J. Org. Chem*. **2013**, *29*, 6475; b) L. Martin-Gomis, F. Fernandez-Lazaro, A. Sastre-Santos, *J. Mater. Chem. A* **2014**, *2*, 15672; c) V. K. Singh, R. K. Kanaparthi, L. Giribabu, *RSC Adv*. **2014**, *4*, 6970.
[289] V. S. Manthou, E. K. Pefkianakis, P. Falaras, G. C. Vougioukalakis, *ChemSusChem* **2015**, *8*, 588.
[290] A. Morandeira, I. Lopez-Duarte, B. O'Regan, M. V. Martinez-Diaz, A. Forneli, E. Palomares, T. Torres, J. R. Durrant, *J. Mater. Chem*. **2009**, *19*, 5016.
[291] Z. Zhang, N. Evans, S. M. Zakeeruddin, R. Humphry-Baker, M. Gratzel, *J. Phys. Chem. C* **2007**, *111*, 398.
[292] P. Y. Reddy, L. Giribabu, C. Lyness, H. J. Snaith, C. Vijaykumar, M. Chandrasekharam, M. Lakshmikantam, J.-H. Yum, K. Kalyanasundaram, M. Gratzel, M. K. Nazeeruddin, *Angew. Chem. Int. Ed*. **2007**, *46*, 373.
[293] J.-J. Cid, J.-H. Yum, S.-R. Jang, M. K. Nazeeruddin, E. Martinez-Ferrero, E. Palomares, J. Ko, M. Gratzel, T. Torres, *Angew. Chem. Int. Ed*. **2007**, *46*, 8358.

boost in the performances, first with PcS6[294] yielding a 4.60% PCE and later with TT40, [295] showing a 6.1% value (*Figure 75*). Replacement of the phenyl radicals by *n*-butoxy chains led to the most successful Pc dye to date, PcS20 (*Figure 75*). An excellent 6.4% PCE under 1 sun illumination was reported, which was attributed to an increased adsorption density of the dye on the TiO_2.[287] However, this shorter chain is not enough to totally suppress aggregation of dye molecules, and some stacking could be detected. On the other hand, the substitution at the α positions of the Pc isoindoles with bulky and rigid aryl groups coud lead to molecules with totally inhibited aggregation features, but this approach has been less studied mainly due to synthetic difficulties.[294,296]

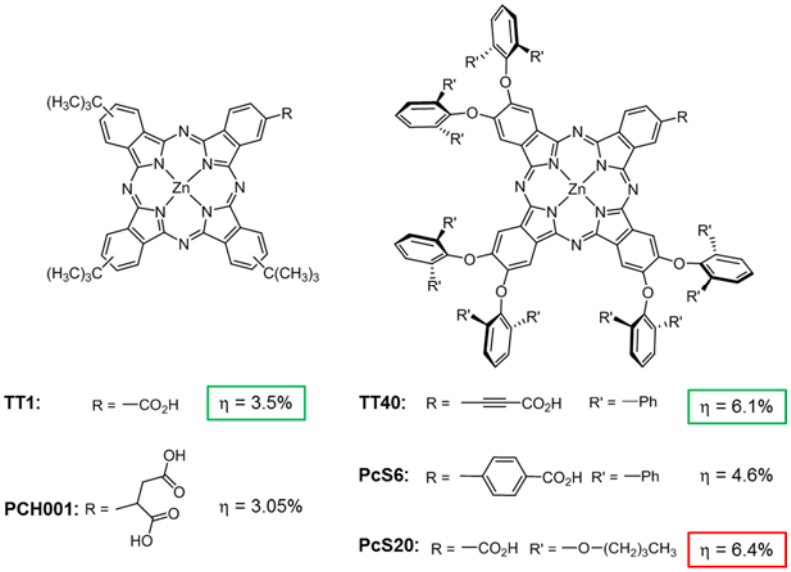

Figure 75.- Structures of porphyrin dyes used in DSSCs.

Another synthetic approach to reduce the aggregation behavior of Pcs is the use of axial substitution. In this regard the replacement of the central metal, usually Zn(II),[297]

[294] S. Mori, M. Nagata, Y. Nakahata, K. Yasuta, R. Goto, M. Kimura, M. Taya, *J. Am. Chem. Soc*. **2010**, *132*, 4054.

[295] a) M.-E. Ragoussi, J.-J. Cid, J.-H. Yum, G. de la Torre, D. Di Censo, M. Gratzel, M. K. Nazeeruddin, T. Torres, *Angew. Chem. Int. Ed*. **2012**, *51*, 4375; b) M.-E. Ragoussi, J.-H. Yum, A. K. Chandiran, M. Ince, G. de la Torre, M. Gratzel, MM. K. Nazeeruddin, T. Torres, *ChemPhysChem* **2014**, *15*, 1033.

[296] L. Tejerina, M. V. Martinez-Diaz, T. Torres, *Org. Lett*. **2015**, *17*, 552.

[297] Zn(II)Pcs presents the most favorable photohysical properties for their application in solar cells. Moreover, their synthesis is easier due to the good fit of the metal into the Pc cavity.

by Ti(IV),[298] Ru(II)[290],[299] or Si(IV) [300] offers this possibility. Our group has explored this approach, but efficiencies obtained were lower than 1%. An important lesson to be learnt from these results is that the parallel arrangement of the Pc and the TiO_2 surface induced by the anchoring group in the axial positions leads to unacceptable efficiencies, but even if the group is located on the peripheral positions, the results are not good enough.

The influence of the anchoring group on the final efficiency is other important issue in Pc sensitized solar cells. The number (mono and dicarboxy derivatives),[301,302] and nature (α-cyanoacrylic group[301] and phosphinic acid[303]) of the anchoring groups were systematically checked and compared with TT1 by Torres' group. Also, the spacers between the anchoring group and the Pc play a crucial role. An extensive study carried out by Torres *et al.* on tri-*tert*-butylPcs[295,301,304] leads to the conclusion that the selected spacer must be rigid and π-conjugated in order to present a directional character and preserve the electronic coupling between the Pc and the semiconductor surface. Combining both factors, the nature of the anchoring group and the spacer, a carboxylic acid directly linked to the Pc through an ethynyl spacer has turned out to be the best option. More elaborated linkers have been very recently used to prepare efficient Pc-sensitized cells, borrowed from reported molecular engineering of champion

[298] a) E. Palomares, M. V. Martinez-Diaz, S. A. Haque, T. Torres, J. R. Durrant, *Chem. Comm*. **2004**, 2112; b) E. Seikel, B. Oelkers, J. Sundermeyer, *Inorg. Chem*. **2012**, *51*, 2709; c) M. S. Rodriguez-Morgade, L. Pelleja, T. Torres, E. Palomares, *J. Porphyrins Phthalocyanines* **2013**, *17*, 814.

[299] a) M. Yanagisawa, F. Korodi, J. Bergquist, A. Holmberg, A. Hagfeldt, B. Akermark, L. Sun, *J. Porphyrins Phthalocyanines* **2004**, *08*, 1228; b) A. Morandeira, I. Lopez-Duarte, M. V. Martinez-Diaz, B. O'Regan, C. Shuttle, N. A. Haji-Zainulabidin, T. Torres, E. Palomares, J. R. Durrant, *J. Am. Chem. Soc*. **2007**, *129*, 9250; c) B. C. O'Regan, I. Lopez-Duarte, M. V. Martinez-Diaz, A. Forneli, J. Albero, A. Morandeira, E. Palomares, T. Torres, J. R. Durrant, *J. Am. Chem. Soc*. **2008**, *130*, 2906; d) A. Listorti, I. Lopez-Duarte, M. V. Martinez-Diaz, T. Torres, T. DosSantos, P. R. F. Barnes, J. R. Durrant, *Energy Environ. Sci*. **2010**, *3*, 1573.

[300] a) L. Martin-Gomis, E. M. Barea, F. Fernandez-Lazaro, J. Bisquert, A. Sastre-Santos, *J. Porphyrins Phthalocyanines* **2011**, *15*, 1004; b) K.-C. Lin, T. Doane, L. Wang, P. Li, S. Pejic, M. E. Kenney, C. Burda, *Sol. Energy Mater. Sol. Cells* **2014**, *126*, 155.

[301] M. Garcia-Iglesias, J.-J. Cid, J.-H. Yum, A. Forneli, P. Vazquez, M. K. Nazeeruddin, E. Palomares, M. Gratzel, T. Torres, *Energy Environ. Sci*. **2011**, *4*, 189.

[302] D. Sharma, G. Steen, J. P. Korterik, M. Garcia-Iglesias, P. Vazquez, T. Torres, J. L. Herek, A. Huijser, *J. Phys. Chem. C* **2013**, *117*, 25397.

[303] I. Lopez-Duarte, M. Wang, R. Humphry-Baker, M. Ince, M. V. Martinez-Diaz, M. K. Nazeeruddin, T. Torres, M. Gratzel, *Angew. Chem. Int. Ed*. **2012**, *51*, 1895.

[304] a) J.-J. Cid, M. Garcia-Iglesias, J.-H. Yum, A. Forneli, J. Albero, E. Martinez-Ferrero, P. Vazquez, M. Gratzel, M. K. Nazeeruddin, E. Palomares, T. Torres, *Chem. Eur. J*. **2009**, *15*, 5130; b) F. Silvestri, M. Garcia-Iglesias, J.-H. Yum, P. Vazquez, M. V. Martinez-Diaz, M. Gratzel, M. K. Nazeeruddin, T. Torres, *J. Porphyrins Phthalocyanines* **2009**, *13*, 369.

porphyrins.[305] Thus, a [7-(40-carboxyphenyl)-2,1,3-benzothiadiazole-4-yl]ethynyl-functionalized analogous of TT40 has been synthesized, with the aim of using the benzothiadiazole as an electron acceptor and extending the absorption spectral response. However, only a 3.29% efficiency was recorded, which was attributed to lower LUMO levels of the former compared to that of TT40.

1.3.1 p-type DSSCs: Architecture and operation principle

The second generation DSSCs uses a p-type metal oxide such as NiO[120,306] instead of TiO_2, but it has been much less investigated than Grätzel cells, and the efficiencies are still much lower (nowadays the best efficiency is 2.51%).[121] Moreover, the investigation of p-type DSSCs, besides being important in itself, opens the possibility to design n-p tandem DSSCs, in which both electrodes are photoactive. The main goal of these tandem devices is to absorb more photons, thereby increasing the efficiency. Presently, the best energy conversion efficiency from tandem DSSCs is 2.42%,[307] which is far below the maximum theoretical power-conversion efficiency (~40%) and also from the record from a single n-type DSSCs mentioned above. For this reason, there is a strong need for an improvement of appropriate semiconductors and dyes of the p-type devices.

In 1999, Lindquist and co-workers reported the first model of p-type, NiO-based DSSC[308] and, since then, the architecture and working principle have remained unchanged. As illustrated in *Figure 76*, the p-type DSSC is a sandwich- structured device composed of a photoactive working electrode (cathode), a passive counter electrode (anode), and a redox electrolyte. The main components are: 1) A fluorine-doped SnO_2 (FTO) glass substrate, 2) a nanostructured p-type semiconductor layer, 3) a light-absorbing layer, normally the dye, 4) a platinized (Pt) conducting glass counter electrode, and 5) the electrolyte.

[305] M. Ince, J.-H. Yum, Y. Kim, S. Mathew, M. Gratzel, T. Torres, M. K. Nazeeruddin, *J. Phys. Chem. C* **2014**, *118*, 17166.
[306] F. Odobel, L. Le Pleux, Y. Pellegrin, E. Blart, *Acc. Chem. Res*. **2010**, *43*, 1063.
[307] A. Nattestad, A. J. Mozer, M. K. R. Fischer, Y.-B. Cheng, A. Mishra, P. Bauerle, U. Bach, *Nat. Mater*. **2010**, *9*, 31.
[308] J. He, H. Lindstrom, A. Hagfeldt, S.-E. Lindquist, *J. Phys. Chem. B* **1999**, *103*, 8940.

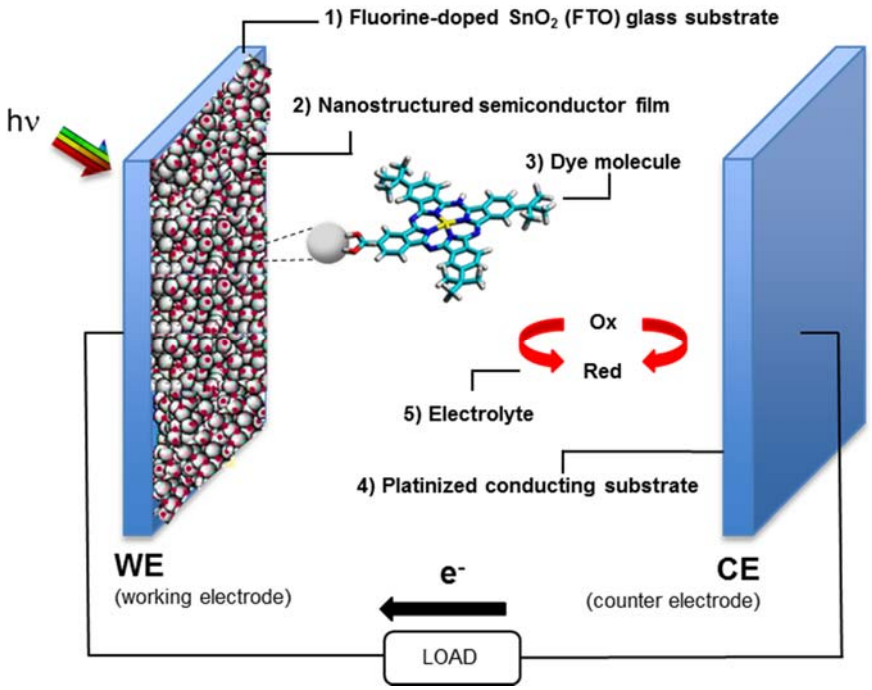

Figure 76.- Schematic illustration of a p-type DSSC.

In p-type DSSCs, visible light absorption by the sensitizer promotes an electron from the HOMO to the LUMO, which triggers a change of the redox potentials of the excited state, enabling a hole injection into the semiconductor valence band, or in other words, electron transfer from the valence band of the semiconductor to the dye (process 2 in *Figure 77*). The hole is transported through the network of nanoparticles in the semiconductor until it reaches the transparent conducting substrate and passes into the external electrical circuit through the working electrode. The reduced sensitizer is then regenerated by the oxidized redox mediator to restore its ground state (process 3 in *Figure 77*). The reduced redox mediator diffuses at the counter electrode where it is oxidized back to its initial state (process 4 in *Figure 77*). This charge collection gives rise to cathodic photocurrent in the external circuit.

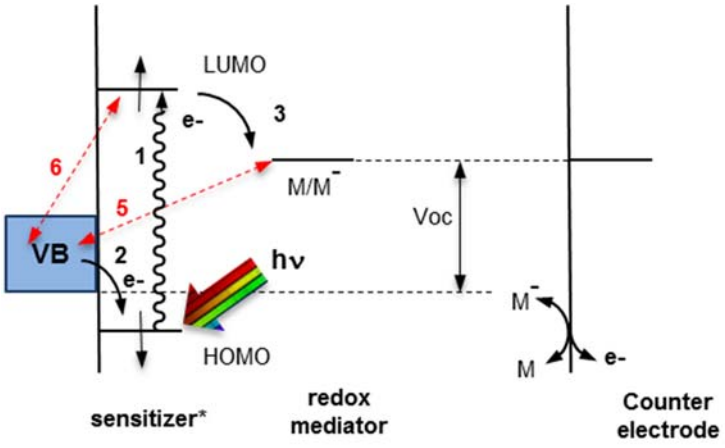

Figure 77.- Schematic diagram illustrating the key processes (black arrows) and the energy wasting processes (red dashed arrows) in a p-type DSSC under illumination.

The above operation principle is just the reverse of that occurring in n-DSSCs. There are some obvious similarities between n-DSSCs and p-DSSCs, but there are also some fundamental differences making this field of research a specific theme in itself. A major force that counteracts the electricity production in p-DSSCs is the charge recombination of electrons at the electrolyte interface (process 5 in *Figure 77*). The fast geminate recombination rate constant observed for process 6 is another major hurdle that needs to be taken into account when optimizing p-DSSCs. These particularities of p-DSSCs force the chemist to think differently when one aims at designing efficient photocathodes.

1.3.2 p-Type metal oxide semiconductors

A suitable choice of the p-type semiconductor may have a decisive impact on the performance of p-type DSSCs. The candidates for the fabrication of photocathodes are p-type semiconductors that are resistant to photocorrosion. The semiconductor must be easily synthesized as nanoparticles or other adequate nanostructures, in order to be transformed into mesoporous films that exhibit large surface area. Also, the surface of the p-semiconductor must exhibit high chemical affinity to an organic functional group in order to promote the chemisorption of the sensitizers on its surface by a simple self-assembling reaction. Finally, the position of the valence band potential is another fundamental parameter of the semiconductor because it governs the maximum V_{OC} that the cell can deliver (the theoretical V_{OC} of a p-type DSSC depends on the valence band

edge of the p-type semiconductor and the redox potential of the electrolyte (*Figure 77*). Unlike n-DSSCs, there are fewer metal oxides that exhibit p-type semiconductivity. The scarcity of p-type semiconducting nature in metal oxides has been explained on the basis of their electronic band structure.[309] Since the upper edge of the valence band in metal oxides is strongly localized on the oxide ions, the holes created in the valence band cannot be easily transported through the material. This is reflected in the typical lower conductivity values of p-type semiconductors than n-type ones.

The most frequently reported semiconductor in p-DSSCs is undoubtedly NiO,[120,310] which has a wide bandgap (3.6-4.0 eV) but a shallow VB potential (around 0.54 V vs NHE at pH = 7)[308] and low hole mobility (between 10^{-8} and 10^{-7} cm^2/S,[311] more than 2 orders of magnitude lower than the electron diffusion coefficient in TiO_2), this fact limiting the performance of the cell. Moreover, the slow diffusion of the injected holes within the nanoporous network of the NiO film increases the probability of losses by charge recombination with the reduced sensitizer and/or the reduced redox mediator in the electrolyte.[312] Also, the theoretical maximum V_{OC} is around 150−200 mV when NiO is combined with the classical iodide/tri-iodide electrolyte. Other drawbacks of NiO are its low transparency, which limits the thickness of the photocathode, and its ability to catalyze oxidation reactions. Therefore, it is of high importance to find alternatives to NiO, that is, materials showing better transparency, deeper VB potentials, higher hole mobilities and with kinetically blocked capacity to oxidize the reduced form of the redox mediator.

To sort out some of these problems, the synthesis of binary NiXO semiconductors, were X is cobalt, have recently evolved. The VB engineering of NiO upon doping with a cobalt ion was investigated by Wu and co-workers, [311c] who found outthat the VB potentials can be gradually increased with increasing amounts of cobalt in $Ni_{1-x}Co_xO_y$ from the value of 0.37 V vs NHE (undoped NiO) to 0.41 V vs NHE with a 6% molar ratio of cobalt, and the V_{OC} of the respective p-DCSSs moves from 118 to 159 mV. However, the photocurrent decreases as the concentration of cobalt is raised

[309] H. Kawazoe, M. Yasukawa, H. Hyodo, M. Kurita, H. Yanagi, H. Hosono, *Nature* **1997**, *389*, 939.
[310] a) G. Boschloo, A. Hagfeldt, *J. Phys. Chem. B* **2001**, *105*, 3039; b) I. Hod, Z. Tachan, M. Shalom, A. Zaban, *Phys. Chem. Chem. Phys*. **2013**, *15*, 6339; c) F. Odobel, Y. Pellegrin, *J. Phys. Chem. Lett*. **2013**, *4*, 2551; d) L. D'Amario, G. Boschloo, A. Hagfeldt, L. Hammarstrom, *J. Phys. Chem. C* **2014**, *118*, 19556.
[311] a) S. Mori, S. Fukuda, S. Sumikura, Y. Takeda, Y. Tamaki, E. Suzuki, T. Abe, *J. Phys. Chem. C* **2008**, *112*, 16134; b) L. Li, E. A. Gibson, P. Qin, G. Boschloo, M. Gorlov, A. Hagfeldt, L. Sun, *Adv. Mater*. **2010**, *22*, 1759; c) G. Natu, P. Hasin, Z. Huang, Z. Ji, M. He, Y. Wu, *ACS Appl. Mater. Interfaces* **2012**, *4*, 5922.
[312] L. D'Amario, L. J. Antila, B. P. Rimgard, G. Boschloo, L. Hammarstrom, *J. Phys. Chem. Lett*. **2015**, *6*, 779.

(from.417 to 0.392 mA/cm^2) because the cobalt cations in NiO act as scattering centers and reduce 0the hole mobility. As a result, the overall gain is modest, but this study has the merit to demonstrate that NiO doping can be used to tune its electronic properties, suggesting that other dopants may give more satisfactory outputs.

Other emergent materials are delafossite $CuMO_2$ (M = Al, Ga, In, Cr…) which feature excellent optical transparency in the visible range and high electrical conductivity owing to the hybridization of the occupied copper 3d states with the oxygen 2p states at the top of the VB, leading to more delocalized holes and thus higher mobility.[309,313,314,315] Moreover, V_{OC} of the reported cells based on delafossites proved 50-150 mV higher than that of NiO, as a consequence of their deeper valance band edge positions. Cheng and co-workers[316] first reported the fabrication of a p-type DSSC using $CuAlO_2$. The authors proved that the Fermi level of $CuAlO_2$ lies 0.2 eV above that of NiO, explaining thus the increase of the V_{OC} of the cells from 218 (with NiO) to 333 mV (with $CuAlO_2$). Unfortunately, the photocurrent density delivered by the cell was very low (0.33 mA/cm^2), owing to a very weak surface area (1.7 m^2/g). One year later, the groups of Wu[317] and Jobic[318] independently reported the successful utilization of $CuGaO_2$ in p-DSSCs. The higher conductivity and transparency of $CuGaO_2$ over $CuAlO_2$ and the possibility to prepare this material by hydrothermal synthesis represent attractive features to prepare better-performing semiconductors. However, gallium is much less abundant on the Earth's crust than aluminum. Moreover, $CuGaO_2$ tends to form nanoplates rather than nanoparticles, making it more difficult to obtain large surface areas; however a recent report describes a way to control the size and nature of $CuGaO_2$ nanoplates.[319] In addition, $CuGaO_2$ presents a significant thermal instability as it decomposes into CuO and $CuGa_2O_4$ upon heating under ambient atmosphere above 350 °C.

More recently, a new delafossite material, $CuCrO_2$, that is thermally stable under ambient atmosphere up to 400 °C, has been successfully employed to fabricate

[313] M. Yu, T. I. Draskovic, Y. Wu, *Phys. Chem. Chem. Phys*. **2014**, *16*, 5026.
[314] R. Nagarajan, A. D. Draeseke, A. W. Sleight, J. Tate, *J. Appl. Phys*. **2001**, *89*, 8022.
[315] R. Guillen, J. Robertson, *Phys. Rev. B* **2011**, *84*, 035125.
[316] A. Nattestad, X. Zhang, U. Bach, Y.-B. Cheng, *J. Photonics Energy* **2011**, *1*, 011103.
[317] M. Yu, G. Natu, Z. Ji, Y. Wu, *J. Phys. Chem. Lett*. **2012**, *3*, 1074.
[318] A. Renaud, B. Chavillon, L. Le Pleux, Y. Pellegrin, E. Blart, M. Boujtita, T. Pauporte, L. Cario, S. Jobic, F. Odobel, *J. Mater. Chem*. **2012**, *22*, 14353.
[319] a) Z. Xu, D. Xiong, H. Wang, W. Zhang, X. Zeng, L. Ming, W. Chen, X. Xu, J. Cui, M. Wang, S. Powar, U. Bach, Y.-B. Cheng, *J. Mater. Chem. A* **2014**, *2*, 2968; b) M. Yu, T. I. Draskovic, Y. Wu, *Inorg. Chem*. **2014**, *53*, 5845.

photocathodes for p-DSSC.[320,321] $CuCrO_2$ was prepared as nanoparticles (12 nm average particle size) with significantly high surface area (~90 m^2/g). Interestingly, the VB position of $CuCrO_2$ lies by 280 mV deeper than that of NiO, and the hole diffusion constant is around 10^{-5} cm^2/S, which is 2 orders of magnitude superior.

Another interesting approach is based on the long overlooked copper(II) oxide, which has interesting photovoltaic, electrochemical, and catalytic properties. This p-type semiconductor has a band gap of 1.21–1.51 eV, lying in an acceptable range for solar energy conversion, and presents several more advantages: 1) Availability and abundance, 2) non-toxic nature, and 3) low production costs. Moreover CuO films feature higher conductivity, better charge carrier mobility, and comparable valence band energy relative to NiO films.[322] Still, the most recent report on CuO based p-type DSSCs is dated from 2008.[323] Very likely, state-of-the-art efficiencies as low as 0.011% resulted in a moderate interest. Other CuO nanostructures like, for example, nanorods (*Figure 78*),[324] nanoplates, etc. have been less explored to date as photocathode in DSSCs.

1.3.2.1 Morphology of the photocathode

The capability to rationally control morphology provides a route for high-efficiency materials for p-type DSSCs and tandem solar energy devices. Since the effect of photocathode morphology on the performance of p-type DSSCs is very high, the nanostructure of the semiconductor should be taken into account in a way that is really going to serve the needs of the device: have large surface areas, low recombination and reproducibility. However, the morphology of p-type semiconductors has been much less studied, including that of NiO.[322a,325,326] On the other hand, the lessons learned from n-

[320] D. Xiong, Z. Xu, X. Zeng, W. Zhang, W. Chen, X. Xu, M. Wang, Y.-B. Cheng, *J. Mater. Chem*. **2012**, *22*, 24760.
[321] S. Powar, D. Xiong, T. Daeneke, M. T. Ma, A. Gupta, G. Lee, S. Makuta, Y. Tachibana, W. Chen, L. Spiccia, Y.-B. Cheng, G. Gotz, P. Bauerle, U. Bach, *J. Phys. Chem. C* **2014**, *118*, 16375.
[322] a) S. A. Makhlouf, M. A. Kassem, M. A. Abdel-Rahim, *J. Mater. Sci*. **2009**, *44*, 3438; b) D. M. Jundale, P. B. Joshi, S. Sen, V. B. Patil, *J. Mater. Sci. Mater. Electron*. **2012**, *23*, 1492.
[323] S. Sumikura, S. Mori, S. Shimizu, H. Usami, E. Suzuki, *J. Photochem. Photobiol. A Chem*. **2008**, *194*, 143.
[324] a) T. Yu, X. Zhao, Z. X. Shen, Y. H. Wu, W. H. Su, *J. Cryst. Growth* **2004**, *268*, 590; b) S. Anandan, X. Wen, S. Yang, *Mater. Chem. Phys.* **2005**, *93*, 35.
[325] Q. Wu, Y. Shen, L. Li, M. Cao, F. Gu, L. Wang, *Appl. Surf. Sci*. **2013**, *276*, 411.
[326] a) S. Powar, Q. Wu, M. Weidelener, A. Nattestad, Z. Hu, A. Mishra, P. Bauerle, L. Spiccia, Y.-B. Cheng, U. Bach, *Energy Environ. Sci*. **2012**, *5*, 8896; b) L. X. Song, Z. K. Yang, Y. Teng, J. Xia, P. Du, *J. Mater. Chem. A* **2013**, *1*, 8731; c) H. B. Yang, B. Liu, S. Y. Khoo, L. N. Zhu, C. X. Guo, Y. Q. Dong, C. M. Li, *Adv. Mater. Interfaces* **2014**, *1*, 1300110; d) C. J. Flynn, E. E. Oh, S. M. McCullough, R. W.

type semiconductors have established an effective basis. The various nanostructures in DSSCs[327] can be classified as 1) nanoparticles,[322,327] 2) shell structures,[328] and 3) 1D[329,330,331,332] and 3D nanostructures.[333,334,335,336]

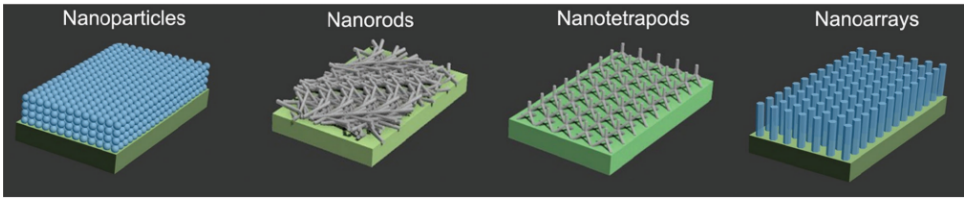

Figure 78.- Schematic illustration of four typical architectures of photoelectrodes constructed from different nanoscale building blocks for solar energy conversion devices.

Nanoparticles offer large surface area for dye adsorption but have recombination problems due to considerable grain boundaries (*Figure 78*). Shell structures are nanoparticles coated with a shell to reduce charge recombination, but they have not proved effective and lack reproducibility. 1D nanostructures[327] such as nanowires[329,332] and nanotubes,[330,331] theoretically provide direct pathways for electron transport but face the drawback of insufficient internal surface area of the photoelectrode films. 3D nanostructures consist of structures such as nanotetrapods (*Figure 56*),[333] branched nanowires or nanotubes,[334-336] and oxide aggregates. Among these structures, aggregates could simultaneously provide high surface area and generate light scattering, and therefore could allow for thinner photoelectrode films that would reduce charge recombination in DSSCs.

Call, C. L. Donley, R. Lopez, J. F. Cahoon, *J. Phys. Chem. C* **2014**, *118*, 14177; e) X. L. Zhang, Z. Zhang, F. Huang, P. Bauerle, U. Bach, Y.-B. Cheng, *J. Mater. Chem.* **2012**, *22*, 7005.

[327] Q. Zhang, G. Cao, *Nano Today* **2011**, *6*, 91.

[328] Y. Diamant, S. Chappel, S. G. Chen, O. Melamed, A. Zaban, *Coord. Chem. Rev*. **2004**, *248*, 1271.

[329] H. Wang, Z. Guo, S. Wang, W. Liu, *Thin Solid Films* **2014**, *558*, 1.

[330] O. K. Varghese, M. Paulose, C. A. Grimes, *Nat. Nanotechnol*. **2009**, *4*, 592.

[331] K. Shankar, J. Bandara, M. Paulose, H. Wietasch, O. K. Varghese, G. K. Mor, T. J. LaTempa, M. Thelakkat, C. A. Grimes, *Nano Lett*. **2008**, *8*, 1654.

[332] M. Law, L. E. Greene, J. C. Johnson, R. Saykally, P. Yang, *Nat. Mater*. **2005**, *4*, 455.

[333] a) Y. F. Hsu, Y. Y. Xi, C. T. Yip, A. B. Djurisic, W. K. Chan, *J. Appl. Phys.* **2008**, *103*, 083114; b) W. Chen, Y. Qiu, S. Yang, *Phys. Chem. Chem. Phys*. **2012**, *14*, 10872.

[334] J. Qiu, X. Li, X. Gao, X. Gan, B. Weng, L. Li, Z. Yuan, Z. Shi, Y.-H. Hwang, *J. Mater. Chem*. **2012**, *22*, 23411.

[335] W.-Q. Wu, H.-L. Feng, H.-S. Rao, Y.-F. Xu, D.-B. Kuang, C.-Y. Su, *Nat. Commun*. **2014**, *5*, 3968.

[336] S. L. Mensah, A. Prasad, J. Wang, Y. K. Yap, *J. Nanosci. Nanotechnol*. **2008**, *8*, 233.

1.3.3 Electrolytes

The electrolyte is a crucial element to ensure the proper operation of the device because it is implied in many pivotal processes.The role of the redox mediator in p-type DSSC is to regenerate the reduced sensitizer after the hole injection to the p-type semiconductor and to transport the electrons to the counter electrode. It should fulfill a certain number of criteria to be used in p-DSSCs: 1) The redox potential must be more negative than that of the valance band edge of the semiconductor, to ensure a decent V_{OC}; 2) the redox mediator must be transparent in the major part of the solar spectrum (400–800 nm), so that the dye can utilize the sunlight more efficiently; 3) the electron self-exchange rate and diffusion coefficient of the redox couple must be high, in order to ensure a quick transport of the charges to the counter electrode. The regeneration of the photoreduced chemisorbed sensitizer by harvesting its extra electron is crucial, because the lifetime of the interfacial charge-separated states is usually very short in most p-type sensitized cathodes. Also, the oxidation reaction of the reduced form of the mediator, must be slow on the p-semiconductor surface to avoid current losses. This is another fundamental point in p-DSSCs, as the interfacial charge recombination with the electrolyte is currently a key issue to raise the PCE of these devices. Finally, the M/M^- couple imposes the equilibrium potential at the counter electrode, following the Nernst equation. Because the output photopotential is equal to the difference between the potentials of the photocathode and the counter electrode, it must have the most possible negative redox potential to obtain the maximum photovoltage. Just from this latter consideration, the most useful redox couples to attain a large V_{OC} in p-DSSCs may not be stable under ambient atmosphere, imposing the preparation cells under an inert atmosphere.

Inherited from its extensive use in classical n-DSSCs, the iodide/triiodide electrolyte was the first redox couple used in p-DSSCs and still remains the most popular one. However, its drawbacks are evident and it is certainly not the most suitable redox shuttle for p-DSSCs. Besides its corrosive nature, tri-iodide is unfortunately a strongly colored substance, especially in case of a relatively high concentration of iodine, and displays a complex multielectron electrochemistry.[337] But the biggest issue should be assigned to the close proximity of the redox potential of I^-/I_3^- (+0.32 V vs NHE; *Figure 57*), with the VB of most p-semiconductors, which limits the maximal achievable V_{OC} of the device to 100-200 mV. Another characteristic of triiodide is its propensity to associate with the sensitizer, which was already proposed in n-DSSCs to explain the important

[337] E. A. Gibson, L. Le Pleux, J. Fortage, Y. Pellegrin, E. Blart, F. Odobel, A. Hagfeldt, G. Boschloo, *Langmuir* **2012**, *28*, 6485.

interfacial charge recombination sometimes observed.[338] The binding of triiodide to the sensitizer increases it local concentration in the vicinity of the TiO_2 surface and enhances the charge recombination with the injected electrons. Pre-association of tri-iodide with the sensitizer is one of the most valid explanations to rationalize the effective photocurrent production in p-DSSCs despite the generally very fast geminate recombination.[339] The lifetime of the charge-separated state in a p-DSSC is usually very short (less than 1 ns) and faster than diffusion; therefore, the effective interception of the reduced sensitizer by the redox shuttle is unfavorable. The high IPCE measured with some simple sensitizers featuring fast charge recombination is strong support for this interpretation.

Among the few other redox shuttles tested in p-DSSC, cobalt complexes are certainly the most successful ones. Tris-bipyridine cobalt(III/II) derivatives were first investigated as alternative redox couples.[340,341] Their tunable redox potentials through modification of the substituents on the bipyridine ligands, and their compatibility with TiO_2-based DSSCs, make them a powerful alternative to their iodine-based analogues. One example of useful structural modification is the incorporation of bulky moieties *e.g. tert*-butyl groups on the bipyridine, which hinder the approach of the redox mediator to the semiconductor surface, thus decreasing the interfacial charge recombination.[340] Boschloo and co-workers reported a series of polypyridyl cobalt complexes with different substituents, which were applied as redox mediators in p-type DSSC based on PMI-NDI (*Figure 80*) dye sensitized NiO.[341]

Moreover, cobalt(III/II) polypyridyl redox shuttles have lower visible light absorption and more negative redox potentials than the I_3^-/I^- system (*Figure 79*). On the other hand, the two drawbacks of these complexes are due to their large hydrodynamic volume, which restricts the diffusion coefficient, and their unusually large reorganization energy, owing to the spin change upon reduction of Co(III) into Co(II), which makes them slow electron acceptors. As a consequence, the use of these complexes required a

[338] a) M. Miyashita, K. Sunahara, T. Nishikawa, Y. Uemura, N. Koumura, K. Hara, A. Mori, T. Abe, E. Suzuki, S. Mori, *J. Am. Chem. Soc*. **2008**, *130*, 17874; b) B. C. O'Regan, K. Walley, M. Juozapavicius, A. Anderson, F. Matar, T. Ghaddar, S. M. Zakeeruddin, C. Klein, J. R. Durrant, *J. Am. Chem. Soc*. **2009**, *131*, 3541; c) H. Kusama, K. Sayama, *J. Phys. Chem. C* **2012**, *116*, 1493.

[339] a) A. Morandeira, G. Boschloo, A. Hagfeldt, L. Hammarstrom, *J. Phys. Chem. B* **2005**, *109*, 19403; b) A. Morandeira, G. Boschloo, A. Hagfeldt, L. Hammarstrom, *J. Phys. Chem. C* **2008**, *112*, 9530.

[340] E. A. Gibson, A. L. Smeigh, L. Le Pleux, J. Fortage, G. Boschloo, E. Blart, Y. Pellegrin, F. Odobel, A. Hagfeldt, L. Hammarstrom, *Angew. Chem. Int. Ed*. **2009**, *48*, 4402.

[341] E. A. Gibson, A. L. Smeigh, L. Le Pleux, L. Hammarstrom, F. Odobel, G. Boschloo, A. Hagfeldt, *J. Phys. Chem. C* **2011**, *115*, 9772.

particularly long-lived charge-separated states because the regeneration reaction is slow.[340,342] With p-DSSCs, this condition is particularly demanding.

Recently, Bach and co-workers employed a $Co^{III/II}(en)_3$ (en = diaminoethane) redox mediator in conjunction with the very efficient Thioph-PMI sensitizer, reporting a V_{OC} of 709 mV and leading to a PCE up to 1.3%.[343] This large V_{OC} is due to a more negative reduction potential of the mediator (−0.025 V vs NHE) (*Figure 79*), but also to the reduction of the interfacial recombination through the increase of the steric bulkiness of the selected dye, enhancing the charge collection efficiency. A more negative reduction potential has been recently obtained for a electrolyte based on the tris(acetylacetonato) iron(III)/(II) redox couple ($[Fe(acac)_3]^{0/1-}$ = -0.20 V vs NHE).[121] This brand new redox couple, together with the Thioph-PMI dye, has led to the highest reported J_{SC} (7.65 mA/cm^2) and PCE (2.51%) for p-type DSSCs.

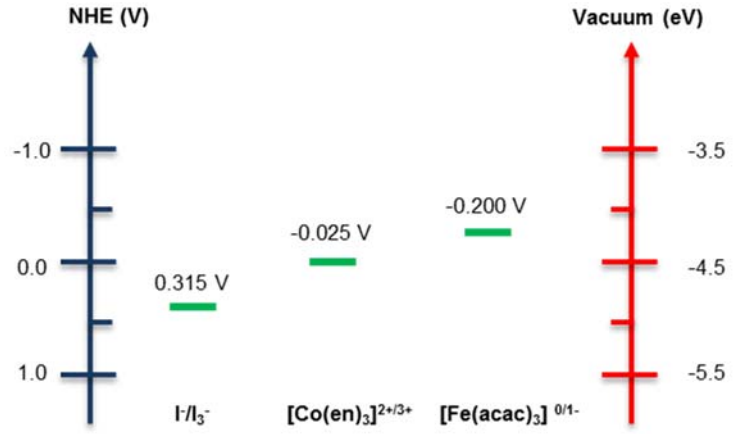

Figure 79.- Redox potentials of the most popular electrolytes relative to the NHE.

[342] L. Le Pleux, A. L. Smeigh, E. Gibson, Y. Pellegrin, E. Blart, G. Boschloo, A. Hagfeldt, L. Hammarstrom, F. Odobel, *Energy Environ. Sci*. **2011**, *4*, 2075

[343] S. Powar, T. Daeneke, M. T. Ma, D. Fu, N. W. Duffy, G. Gotz, M. Weidelener, A. Mishra, P. Bauerle, L. Spiccia, U. Bach, *Angew. Chem. Int. Ed*. **2013**, *52*, 602.

1.3.4 Sensitizers

As the field of p-DSSCs is relatively young, the diversity of dyes screened in p-DSSCs is much less than that tested on TiO_2-based Grätzel cells. A myriad of different organic and inorganic sensitizers, including triphenylamines,[311b,344,345,346] perylene imides,[342,347,348] porphycenes,[349] ruthenium[350] and iridium[351] complexes, coumarins,[311a,339] porphyrins[308,352] and a combination of the above.[121,343,353] A selection of the best performing sensitizers is given in *Figure 80*.

[344] a) P. Qin, H. Zhu, T. Edvinsson, G. Boschloo, A. Hagfeldt, L. Sun, *J. Am. Chem. Soc*. **2008**, *130*, 8570; b) P. Qin, M. Linder, T. Brinck, G. Boschloo, A. Hagfeldt, L. Sun, *Adv. Mater*. **2009**, *21*, 2993; c) P. Qin, J. Wiberg, E. A. Gibson, M. Linder, L. Li, T. Brinck, A. Hagfeldt, B. Albinsson, L. Sun, *J. Phys. Chem. C* **2010**, *114*, 4738; d) Y.-S. Yen, W.-T. Chen, C.-Y. Hsu, H.-H. Chou, J. T. Lin, M.-C. P. Yeh, *Org. Lett*. **2011**, *13*, 4930.

[345] a) L. Zhu, H. B. Yang, C. Zhong, C. M. Li, *Dyes Pigments* **2014**, *105*, 97; b) H.-B. Li, J. Zhang, Y. Wu, J.-L. Jin, Y.-A. Duan, Z.-M. Su, Y. Geng, *Dyes Pigments*, **2014**, *108*, 106.

[346] J. Cui, J. Lu, X. Xu, K. Cao, Z. Wang, G. Alemu, H. Yuang, Y. Shen, J. Xu, Y. Cheng, M. Wang, *J. Phys. Chem. C* **2014**, *118*, 16433.

[347] C. Li, H. Wonneberger, *Adv. Mater*. **2012**, *24*, 613.

[348] a) A. Morandeira, J. Fortage, T. Edvinsson, L. Le Pleux, E. Blart, G. Boschloo, A. Hagfeldt, L. Hammarstrom, F. Odobel, *J. Phys. Chem. C* **2008**, *112*, 1721; b) A. L. Smeigh, L. Le Pleux, J. Fortage, Y. Pellegrin, E. Blart, F. Odobel, L. Hammarstrom, *Chem. Comm*. **2012**, *48*, 678; c) S. Feihl, R. D. Costa, S. Pflock, C. Schmidt, J. Schonamsgruber, S. Backes, A. Hirsch, D. M. Guldi, *RSC Advances* **2012**, *2*, 11495.

[349] S. Feihl, R. D. Costa, W. Brenner, J. T. Margraf, R. Casillas, O. Langmar, A. Browa, T. E. Shubina, T. Clark, N. Jux, D. M. Guldi, *Chem. Comm*. **2014**, *50*, 11339.

[350] a) Y. Pellegrin, L. Le Pleux, E. Blart, A. Renaud, B. Chavillon, N. Szuwarski, M. Boujtita, L. Cario, S. Jobic, D. Jacquemin, F. Odobel, *J. Photochem. Photobiol. A* **2011**, *219*, 235; b) Z. Ji, G. Natu, Z. Huang, O. Kokhan, X. Zhang, Y. Wu, *J. Phys. Chem. C* **2012**, *116*, 16854; c) J. C. Freys, J. M. Gardner, L. D'Amario, A. M. Brown, L. Hammarstrom, *Dalton Trans*. **2012**, *41*, 13105; d) Z. Ji, Y. Wu, *J. Phys. Chem. C* **2013**, *117*, 18315; e) Z. Ji, G. Natu, Y. Wu, *ACS Appl. Mater. Interfaces* **2013**, *5*, 8641; f) M. He, Z. Ji, Z. Huang, Y. Wu, *J. Phys. Chem*. **2014**, *118*, 16518; g) C. J. Wood, K. C. D. Robson, P. I. P. Elliott, C. P. Berlinguette, E. A. Gibson, *RSC Adv*. **2014**, *4*, 5782; h) C. D. Ertl, D. P. Ris, S. C. Meier, E. C. Constable, C. E. Housecroft, M. Neuburger, J. Zampese, *Dalton Trans*. **2015**, *44*, 1557.

[351] M. Gennari, F. Legalite, L. Zhang, Y. Pellegrin, E. Blart, J. Fortage, A. M. Brown, A. Deronzier, M.-E. Collomb, M. Boujtita, D. Jacquemin, L. Hammarstrom, F. Odobel, *J. Phys. Chem. Lett*. **2014**, *5*, 2254.

[352] a) M. Borgstrom, E. Blart, G. Boschloo, E. Mukhtar, A. Hagfeldt, L. Hammarstrom, F. Odobel, *J. Phys. Chem. B* **2005**, *109*, 22928; b) H. Tian, J. Oscarsson, E. Gabrielsson, S. K. Eriksson, R. Lindblad, B. Xu, Y. Hao, G. Boschloo, E. M. J. Johansson, J. M. Gardner, A. Hagfeldt, H. Rensmo, L. Sun, *Sci. Rep*. **2014**, *4*, 4282; c) A. Maufroy, L. Favereau, F. B. Anne, Y. Pellegrin, E. Blart, M. Hissler, D. Jacquemin, F. Odobel, *J. Mater. Chem. A* **2015**, *3*, 3908.

[353] a) M. Weidelener, A. Mishra, A. Nattestad, S. Powar, A. J. Mozer, E. Mena-Osteritz, Y.-B. Cheng, U. Bach, P. Bauerle, *J. Mater. Chem*. **2012**, *22*, 7366; b) J. Warnan, J. Gardner, L. Le Pleux, J. Petersson, Y. Pellegrin, E. Blart, L. Hammarstrom, F. Odobel, *J. Phys. Chem. C* **2014**, *118*, 103;

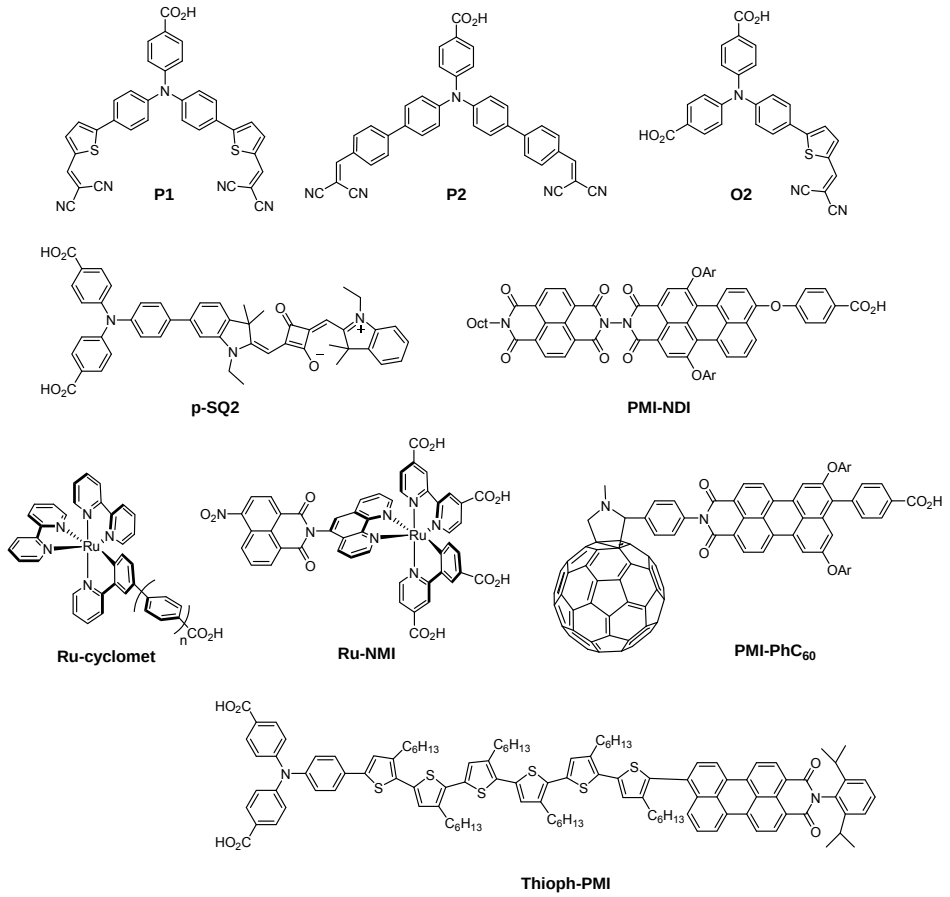

Figure 80.- Structures of some of the most efficient sensitizers for p-type DSSCs.

Naturally, efficient p-type sensitizers should possess the following features: 1) Photochemical and electrochemical stability to ensure the durability of the cell over a long period of time. 2) A broad absorbance to overlap the largest portion of the solar spectrum (panchromatic dye) in order to harvest the greatest number of photons. 3) High extinction coefficients to harvest more solar light within a thinner photocathode, allowing the holes to diffuse a shorter path length to reach the charge collection substrate. The optimal thickness of the p-semiconductor films (generally around 2−3 μm) is much lower than

c) Z. Liu, W. Li, S. Topa, X. Xu, X. Zeng, Z. Zhao, M. Wang, W. Chen, F. Wang, Y.-B. Cheng, H. He, *ACS Appl. Mater. Interfaces* **2014**, *6*, 10614; d) K. A. Click, D. R. Beauchamp, B. R. Garrett, Z. Huang, C. M. Hadad, Y. Wu, *Phys. Chem. Chem. Phys*. **2014**, *16*, 26103; e) C. J. Wood, M. Cheng, C. A. Clark, R. Horvath, I. P. Clark, M. L. Hamilton, M. Towrie, M. W. George, L. Sun, X. Yang, E. A. Gibson, *J. Phys. Chem. C* **2014**, *118*, 16536; f) M. Weidelener, S. Powar, H. Kast, Z. Yu, P. P. Boix, C. Li, K. Mullen, T. Geiger, S. Kuster, F. Nuesch, U. Bach, A. Mishra, P. Bauerle, *Chem. Asian J*. **2014**, *9*, 3251; g) C. J. Wood, G. H. Summers, E. A. Gibson, *Chem. Comm*. **2015**, *51*, 3915.

that of the TiO_2 in Grätzel cells (rarely lower than 10 µm). 4) The dye must as well exhibit significant oxidizing power in the excited state, in other words, having a HOMO positioned below the VB of the p-semiconductor to ensure an exergonic hole driving force (*Figure 77*). 5) The reducing power of the reduced sensitizer must be also significant, especially when the iodide/tri-iodide electrolyte is used because the redox potential of the couple $I_3^-/I_2^{-\bullet}$ (−0.08 V vs NHE)[354] because I_2^- is relatively cathodic. The energetics are indeed essential to achieve both thermodynamically downhill hole injection and dye regeneration reactions.

A sufficient driving force for charge-transfer reactions is essential; however, the kinetics are also relevant to the overall performances. Hole injection into the oxide must be fast compared to ground-state relaxation of the dye excited state. After hole injection, dye regeneration by the oxidized redox species should be much faster than recombination with holes in the p-semiconductor. Fast hole injection dynamics require a strong electronic coupling with the density of the VB states energetically accessible from the dye excited state. The magnitude of this coupling is primarily determined by the energy spacing and the overlap between the HOMO orbitals of the dye excited state and the VB orbitals of the p-type semiconductor. This wave function overlap is dependent on both the distance of the dye HOMO orbital from the p-semiconductor surface and the nature of the anchoring group. The attachment of the dye to the surface via a chemical bond also induces the formation of a new orbital between the dye and the semiconductor surface. This enables electronic coupling, which is the key to the fast injection rates observed for many of these dyes. Carboxylic acid groups have been shown to favor electron injection in TiO_2 by draining and localizing the LUMO of the dye close to the TiO_2 surface, thereby ensuring a large overlap with the conduction band.[116a,350a] Accordingly, carboxylic acid may not be the optimal choice to promote electronic coupling with p-semiconductors. However, it is a good option as a first step towards a more rational design. In future, new anchoring groups exhibiting electron-rich character must be tested because they may better assist hole injection by allowing the delocalization of HOMO orbital of the dye over the anchoring group towards the metal oxide surface.[346,350a] Another essential difference of p-DSSCs stems from the very fast geminate charge recombination as compared to the rates measured in sensitized TiO_2 films. Detailed ultrafast transient absorption spectroscopy studies have demonstrated that hole injection in the NiO VB is usually fast (picosecond time scale), but charge recombination is also very fast too (nanosecond time scale).[344c,348a,339a,b,352a]

Other parameters being equal, the charge recombination between the injected hole and the reduced sensitizer depends on the spatial separation of the dye anion (which

[354] G. Boschloo, E. A. Gibson, A. Hagfeldt, *J. Phys. Chem. Lett*. **2011**, *2*, 3016.

can be represented in a first approximation by the LUMO) from the p-semiconductor surface, with a rate constant decaying exponentially with distance, consistent with electron tunnelling theory.[355] Push−pull dyes with an electron-acceptor moiety localized at the opposite extremity of the anchoring groups proved to be particularly well-suited in NiO-based DSSCs, as demonstrated with sensitizers such as P1, P4, O2, p-SQ2, or Thioph-PMI in *Figure 58*. It is important to state here that the dipolar moment of the sensitizer for the p-DSSC must be oriented in the opposite direction as that for TiO_2 DSSCs. Indeed, the electron should shift from the anchoring group to the extremity of the dye in order to bend upward the VB of the semiconductor and to move the electron density far away from the surface upon hole injection. Another powerful strategy to reduce the geminate recombination is to append a secondary electron acceptor to the sensitizer to move the negative charge further away from the p-semiconductor surface. This is typical of the PMI-NDI[348b,340] and Thioph-PMI[121,343] systems (*Figure 80*), which indeed feature particularly long-lived charge-separated states in the range of the microsecond time scale. However, each additional charge-transfer step results in an increased spatial separation of electron/hole pair increasing the lifetime of the charge-separated state but at the expense of reducing power stored in the final state.

Overall, key factors for the design of good sensitizers for p-DCSSs is the spatial location of the HOMO orbital close to the surface, to ensure a large electronic coupling and to assist hole injection, and the localization of the LUMO orbital away from the metal oxide surface, which decreases the extremely fast, geminate charge recombination.

Different classes of dyes have been tested in NiO-based DSSCs but to a lower extent compared to those investigated in conventional Grätzel cells; therefore, there is significant room for discovering better-performing systems. *Figure 80* gathers a selection of the most efficient systems published until now. Push−pull organic D−π-A dyes have shown relatively high performances because they offer large molar absorptivities and widely tunable electronic properties by changing the substituents, as was shown in n-type DSSCs. One of the most efficient and relatively simple sensitizers is the push−pull P1 dye reported by Sun and co-workers[311b,344a,b] (V_{OC} = 84 mV, J_{SC} = 5.48 mA/cm^2, and FF = 33% for a PCE = 0.15% and max IPCE = 63%). Variation around this type of structure led to dyes P4 and O2, which gave similar PCEs.[356,344c,d]

Another interesting compound that absorbs far in the low energy region is the push−pull squaraine derivative p-SQ2 that gives a similar PCE as P1.[357] Interestingly, co-

[355] P. Bonhote, J.-E. Moser, R. Humphry-Baker, N. Vlachopoulos, S. M. Zakeeruddin, L. Walder, M. Gratzel, *J. Am. Chem. Soc*. **1999**, *121*, 1324.
[356] Z. Ji, G. Natu, Z. Huang, Y. Wu, *Energy Environ. Sci*. **2011**, *4*, 2818.
[357] C.-H. Chang, Y.-C. Chen, C.-Y. Hsu, H.-H. Chou, J. T. Lin, *Org. Lett*. **2012**, *14*, 4726.

adsorption of p-SQ2 with P1 yields a slightly higher overall PCE than cells sensitized with a single chromophore, showing the first implementation of the co-sensitization concept in p-DSSCs. However, it should be noted that, if the electricity production is extended toward the red region with the presence of p-SQ2, the IPCE on the absorption band of P1 is significantly diminished upon coadsorption of p-SQ2. Recently, Hupp and co-workers proposed an interesting explanation of such phenomenon for n-DSSCs. They showed that the efficiency of mixed co-sensitization is highly dependent on the effective electron collection length of the less-performing sensitizer and of the relative disposition of the sensitizers.[358] Similar rules certainly govern cosensitization in p-DSSCs.

Other efficient systems are composed of a sensitizer connected to a secondary electron acceptor, which pulls the electron far away from the anchoring group to retard charge recombination. PMI-NDI, PMI-PhC60,[348a,b,340], Ru-NMI[350c] dyads, and Thioph-PMI,[121,326a,e353a,359] (*Figure 80*) are examples of such systems. On NiO photocathodes, these sensitizers exhibit a charge separated lifetime of tenths of microseconds owing to the large electronic decoupling and the long distance between the charge carriers. The great success of Thioph-PMI probably stems from a combination of several features: first, a high extinction coefficient, second the presence of alkyl chains on the thienyl units, which avoid dye aggregation and certainly protect the NiO surface from the approach of the electrolyte (reducing thus the current leakage), and last but not least, a long-lived charge-separated state owing to the large distance of the ion pair (the hole in NiO and electron on PMI).

Another approach to sensitize a wide-band-gap semiconductor is to use semiconductor nanocrystals, commonly referred as quantum-dot-sensitized solar cells. There has been intense research activity in the use of quantum dots in classical Grätzel cells,[360,361] and interest is now growing for their utilization in p-DSSCs.[362]

---

[358] N. C. Jeong, H.-J. Son, C. Prasittichai, C. Y. Lee, R. A. Jensen, O. K. Farha, J. T. Hupp, *J. Am. Chem. Soc*. **2012**, *134*, 19820.
[359] X. L. Zhang, Z. Zhang, D. Chen, P. Bauerle, U. Bach, Y.-B. Cheng, *Chem. Comm*. **2012**, *48*, 9885.
[360] M. R. Kim, D. Ma, *J. Phys. Chem. Lett*. **2015**, *6*, 85.
[361] a) P. V. Kamat, *Acc. Chem. Res*. **2012**, *45*, 1906; b) F. Hetsch, X. Xu, H. Wang, S. V. Kershaw, A. L. Rogach, *J. Phys. Chem. Lett*. **2011**, *2*, 1879.
[362] a) X. Wu, E. K. L. Yeow, *Chem. Comm*. **2010**, *46*, 4390; b) I. Barcelo, E. Guillen, T. Lana-Villarreal, R. Gomez, *J. Phys. Chem. C* **2013**, *117*, 22509; c) K. Zheng, K. Zidek, M. Abdellah, W. Zhang, P. Chabera, N. Lenngren, A. Yartsev, T. Pullerits, *J. Phys. Chem. C* **2014**, *118*, 18462.

1.3.5 Objectives

Dyes for p-type solar cells are gaining popularity in the field of photovoltaics and Pcs can constitute ideal alternatives. In the the past decade, a lot of effort was paid to the synthesis of Pc-sensitizers for Grätzel cells, with the aim of studying in detail the structure-property relationships and fulfilling the essential requirements for efficient sensitization.

Up to know there are no reports on p-type Pc-based DSSCs, in spite of the proven n-type semiconductor properties of some Pcs functionalized with strong electron-withdrawing groups at peripheral and/or non-peripheral positions, including F,[238,239] Cl,[238] CN,[238] CO_2R,[240] and SO_2R.[241] Regarding charge separation processes, electron-accepting A_3B Pcs functionalized with alkylsulfonyl groups, Zn(II)[$Pc(SO_2R)_6X$], have been linked to graphene and the resulting hybrid material studied in terms of photoinduced donor-acceptor interactions. In this hybrid system, the Zn(II)Pcs are able to accept electron from the graphene surface after photoexcitation.[363] Therefore, these substituents seem to be the best choice for the preparation of Pc sensitizers for p-type DSSCs, since they effectively decrease the HOMO and LUMO energy levels of the Pc, favouring the hole injection into p-type semiconductors after photoexcitation

Then, the main purpose here is to synthesize two novel electron-acceptor Zn(II)Pcs, having six electron-withdrawing alkylsulfonyl groups at three isoindoles and an adequate anchoring group at the other (*Figure 81*), as sensitizers for p-type DSSCs. It is worth mentioning that the branched alkylsulfonyl chains (i.e. 2-ethylhexyl) can play the threefold role of decreasing the HOMO/LUMO levels, protecting the semiconductor surface from the approach of the electrolyte and inhibiting aggregation. Regarding the anchoring groups, although at first sight carboxylic acids would not be ideal anchoring moieties for hole injection from the dye to the semiconductor, the lack of background with other type of anchors make us select COOH as the first option to test the capabilities of Pcs as p-type sensitizers. Regarding the type of linkage between the carboxylic acid and the Pc core, we will use the optimal connectors found in TiO_2, Pc-sensitizers, namely, a direct linkage of the COOH to the Pc, or through a conjugated ethynyl spacer (*Figure 81)*.

[363] a) M.-E. Ragoussi, G. Katsukis, A. Roth, J. Malig, G. de la Torre, D. M. Guldi, T. Torres, *J. Am. Chem. Soc*. **2014**, *136*, 4593; b) A. Roth, M.-E. Ragoussi, L. Wibmer, G. Katsukis, G. de la Torre, T. Torres, D. M. Guldi, *Chem. Sci*. **2014**, *5*, 3432.

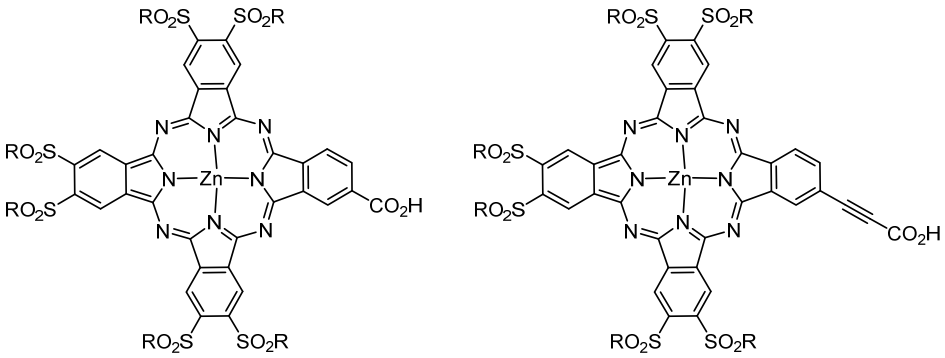

Figure 81.- Structure of the two proposed electron-acceptor phthalocyanines for p-type DSSCs.

The inmediate precursors for the preparation of the target carboxy-containing, alkynylsulfonyl Zn(II)Pcs shown in *Figure 59* are, in all the cases, the corresponding hydroxymethyl derivatives that will be oxidized in a further step using a well-established methodology..

The new dyes will be evaluated as photosensitizers in p-DSSCs with nanorod like CuO electrodes, which have not been explored to date. To offset the shortage of n-type semiconductors, we proposed the use CuO, whose films feature higher conductivity, better charge carrier mobility, and comparable valence band energy relative to the widely used NiO films.

1.3.6 Results and discussion

1.3.6.1 Synthesis of electron-acceptor Pc sensitizers

First, hydroxymethyl phthalonitrile was synthesized according to a procedure previously described by our group (*Scheme 27*).[364]Bromination of 4-methylphthalonitrile, using NBS and AIBN, under UV lamp, gave a mixture of mono-, di-, and tribrominated compounds at the benzylic positions in a 1:2:1 ratio, respectively (determined by ^{1}H-NMR analysis). Treatment of the mixture with and excess of diethyl phosphite and DIPEA yielded 4-(bromomethyl)phthalonitrile **44** in a 67% yield. Reaction of **44** with calcium carbonate in a refluxing aqueous solution of dioxane led to 4-(hydroxymethyl)phthalonitrile (**45**) in moderate yield (64%). Subsequently, protection of the alcohol group was performed by stirring *tert*-butyldimethylsilyl chloride in THF at room temperature for 16h, using triethylamine as base, with an overall yield of 39%.

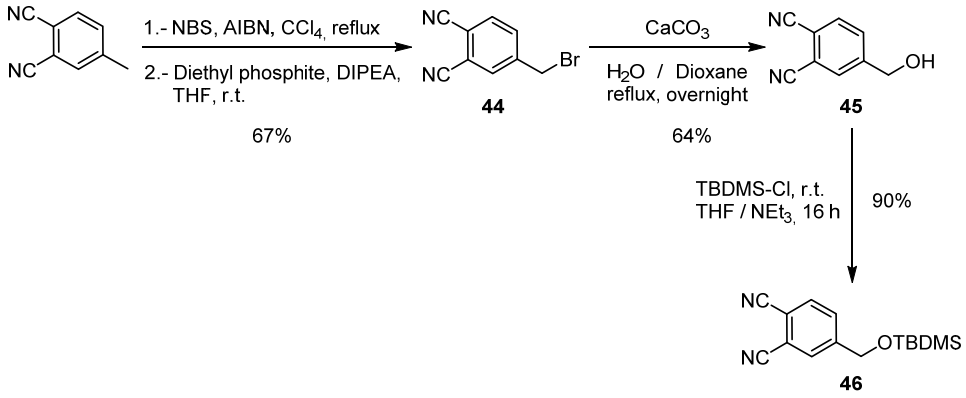

Scheme 27.- Synthesis of 4-[(*tert*-butyldimethylsilyloxy)methyl]phthalonitrile **(46)**.

The synthesis of Zn(II)Pc **47** bearing (2-ethyl)hexylsulfonyl groups and one hydroxymethyl peripheral substituent, was accomplished by condensation of phthalonitriles **13** and **46** (3:1) in presence of $Zn(OAc)_2$ in *o*-DCB / DMF (3:1). (*Scheme 28*).When the reaction was completed, the alcohol moiety was deprotected by addition of TBAF before chromatographic purification, just to facilitate the separation of the target compound from the symmetric octa(2-ethylhexyl)Zn(II) Pc **14**.The latter compound was

[364] R. F. Enes, J.-J. Cid, A. Hausmann, O. Trukhina, A. Gouloumis, P. Vazquez, J. A. S. Cavaleiro, A. C. Tomé, D. M. Guldi, T. Torres, *Chem. Eur. J.* **2012**, *18*, 1727.

isolated in 19%, while the target Pc **47** could only be isolated in a poor 4%. It is worth mentioning that previous unsuccessful attempts to obtain Zn(II)Pc **47** had been performed using the deprotected hydroxymethyl phthalonitrile **45**, and only symmetrical Pc **14** had been detected in that cases.

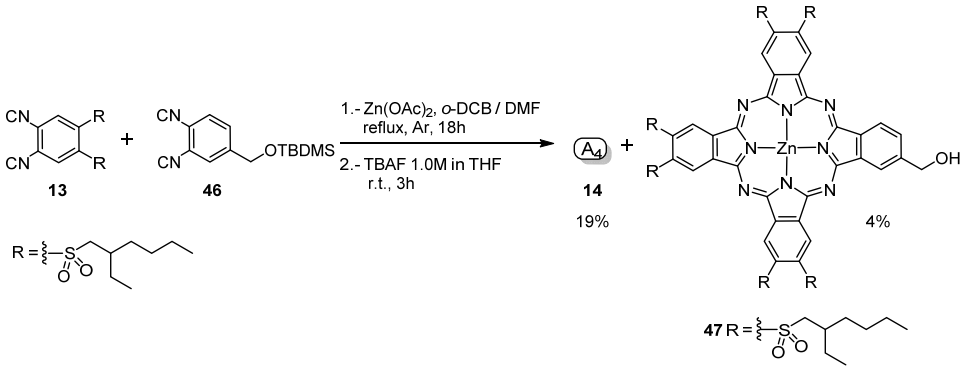

Scheme 28.- Synthesis of Pc **47**.

On the other hand, the synthetic route for hydroxypropynyl Zn(II)Pc **48** (*Scheme 29)* employed as starting compound iodo Zn(II)Pc **15**, which was already described in the section 1.2.4.1. This compound was subjected to a Sonogashira coupling reaction with propargylic alcohol in the presence of bis(triphenylphosphine)palladium(II) dichloride and a catalytic amount of copper(I)iodide, to give compound **48** in a moderate 50% yield.

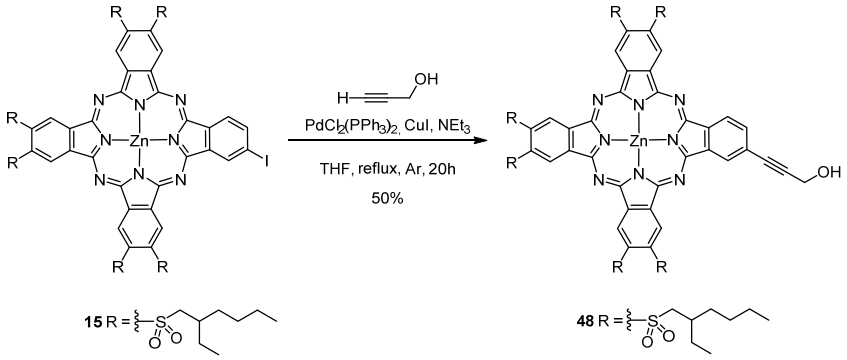

Scheme 29.- Synthesis of hydroxypropynyl Zn(II)Pc **48**.

To obtain the two target compounds, two consecutives oxidation steps were necessary to transform the initial alcohols **47** and **48** into the carboxylic acids (*Scheme*

30),[293,295a] namely a reaction with periodinane derivative, IBX,[365] in THF / DMSO to afford formyl derivatives **49** and **50**, respectively, and treatment with $NaClO_2$ in water in the presence of sulfamic acid, used as a hypochlorite scavenger. The carboxy Pcs, **51** and **52**, were obtained in good yields.

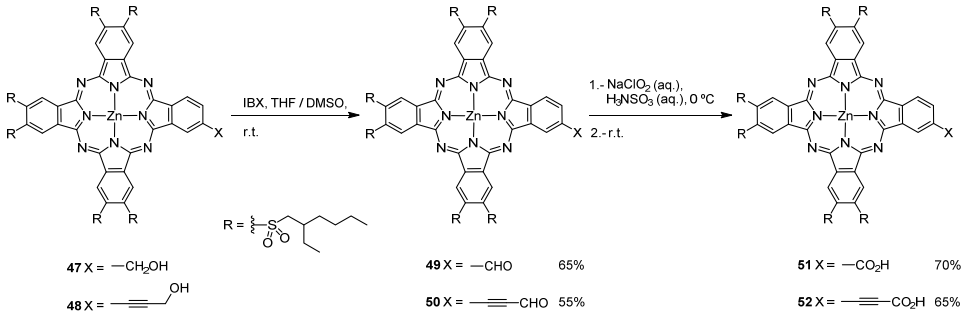

Scheme 30.- Synthesis of carboxyhepta[(2-ethylhexyl)sulfonyl]Zn(II)Pcs **51** and **52**.

Regarding Pc **52**, the three-step strategy starting from iodoPc **15** afforded the compound in relative good yield, but it is quite time-consuming and requires multiple and arduous column chromatography purification steps. Therefore, a second direct route using propargylic acid,[366] instead of propargyl alcohol, was tested using similar Sonogashira conditions. However, we did not succeeded in obtaining compound **52** and, it was no possible even to recover the starting iodo Pc **15**. Previous attempts of coupling propargylic acid to other iodoPcs performed in the group had proven also unsuccessful.

Finally, all the final products and their corresponding intermediates were fully characterized by spectroscopic and electrochemical means. As depicted in *Figure 82*, the absorption spectra of Zn(II)Pcs **51** and **52** show split Q bands as a result of the asymmetric functionalization of the Pc, with maxima at 609 nm and 703 nm.

[365] a) A. Duschek, S. F. Kirsch, *Angew. Chem. Int. Ed*. **2011**, *50*, 1524; b) M. Frigerio, M. Santagostino, S. Sputore, *J. Org. Chem*. **1999**, *64*, 4537; c) V. Satam, A. Harad, R. Rajule, H. Pati, *Tetrahedron* **2010**, *66*, 7659.

[366] This route have been previously employed on porphyrins: a) C.-W. Lee, H.-P. Lu, C.-M. Lan, Y.-L. Huang, Y.-R. Liang, W.-N. Yen, Y.-C. Liu, Y.-S. Lin, E. W.-G. Diau, C.-Y. Yeh, *Chem. Eur. J*. **2009**, *15*, 1403; b) C.-F. Lo, S.-J. Hsu, C.-L. Wang, Y.-H. Cheng, H.-P. Lu, E. W.-G. Diau, C.-Y. Lin, *J. Phys. Chem. C* **2010**, *114*, 12018.

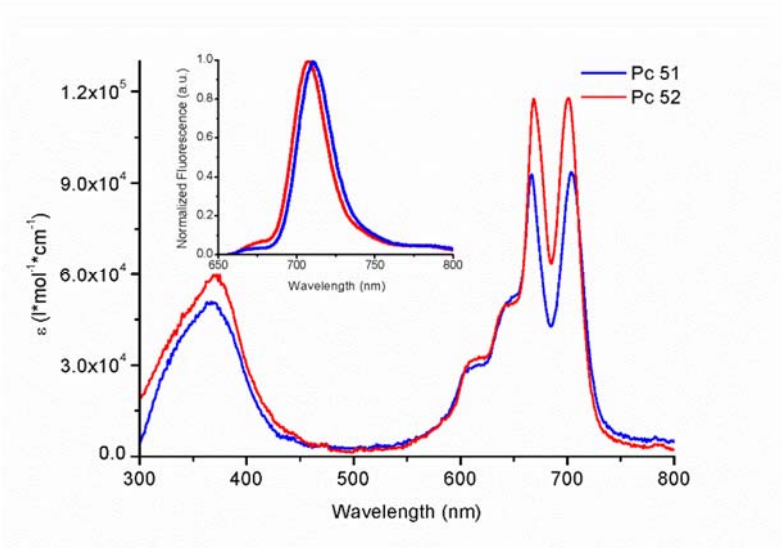

Figure 82.- Comparison of absorption and fluorescence (inset) spectra of Zn(II)Pc **51** (blue line) and Zn(II)Pc **52** (red line) in EtOH ($2.3 \cdot 10^{-7}$ M).

Moreover, cyclic voltammetry experiments were performed to probe the electron accepting character of carboxy derivatives **51** and **52** (*Figure 83*). They were carried out in CH_2Cl_2 solutions containing 0.1 M tetrabutylammonium hexafluorophosphate, using a glassy carbon electrode as working electrode, $Ag/AgNO_3$ as reference electrode and platinum wire as auxiliary electrode. Ferrocene was chosen as internal reference.

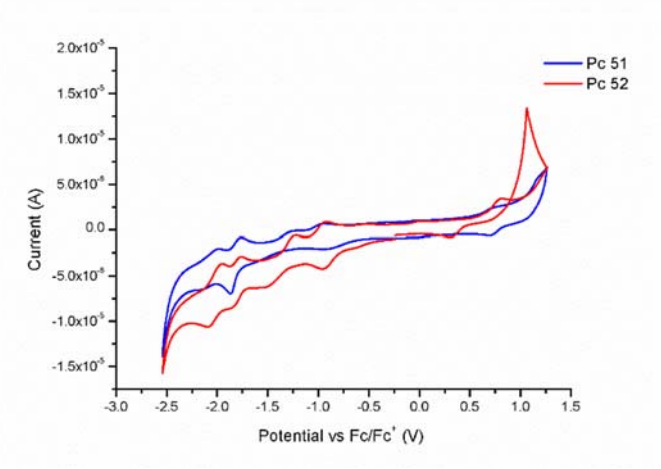

Figure 83.- Cyclic voltammetry of Zn(II)Pc **51** (blue line) and Zn(II)Pc **52** (red line) in dichloromethane; Fc / Fc^+ was used as an external reference.

Four quasi-reversible reductions for each electron-acceptor Pc, are complemented by one quasi-reversible oxidation (*Table 4*). A comparison with Pc **4** [Pc(^{t}Bu)$_4$], which is a prototype

electron-donating counterpart, render **51** and **52** better electron-acceptor (or in other words, easier to be reduced) but poorer electron-donors (more difficult to be oxidized). Compared to the related Pc[$(SO_2R)_6$-C_6H_4-CH_2N_3] previously reported and used as electron acceptor *versus* graphene, both Pcs present very similar first reduction and oxidation waves. From the aforementioned, we determined a LUMO energy of -0.30 V vs. NHE for both Pc **51** and Pc **52**.[367]

	Pc 51	**Pc 52**	**Pc[$(SO_2R)_6$-C_6H_4-CH_2N_3]**	**Pc(^{t}Bu)$_4$ (4)**
E_{1red}	-0.94	-0.94	-1.1	-1.4
E_{2red}	-1.45	-1.36	-	-
E_{3red}	-1.82	-1.82	-	-
E_{4red}	-2.06	-2.03	-	-
E_{1ox}	+0.72	+0.77	+0.6	+0.1

Table 4.- Reduction (E_{nred}) and oxidation (E_{nox}) of Pc **51**, Pc **52**, Pc[$(SO_2R)_6$-C_6H_4-CH_2N_3] and Pc(^{t}Bu)$_4$ **(4)**.

1.3.6.2 Photovoltaic studies of new electron-acceptor Pc dyes in p-type DSSCs

In order to study the new Pcs as dyes in solar cells, p-type DSSCs were assembled consisting of nanorod-like CuO as p-type electrode material with carboxy Pcs **51** and **52** as photosensitizers. These studies were performed in collaboration with Prof. D. M. Guldi (Friedrich-Alexander-Universität Erlangen-Nürnberg).

Electrodes were prepared by doctor-blading a paste of nanorod-like CuO diluted with ethylcellulose in ethanol followed by sintering at 300 ºC.[368] A crack-free mesoporous morphology and a rod-like shape of CuO after calcination were corroborated by scanning electron microscopy (*Figure 84*).

[367] C. M. Cardona, W. Li, A. E. Kaifer, D. Stockdale, G. C. Bazan, *Adv. Mater*. **2011**, *23*, 2367.
[368] S. Ito, T. N. Murakami, P. Comte, P. Liska, C. Gratzel, M. K. Nazeeruddin, M. Gratzel, *Thin Solid Films* **2008**, *516*, 4613.

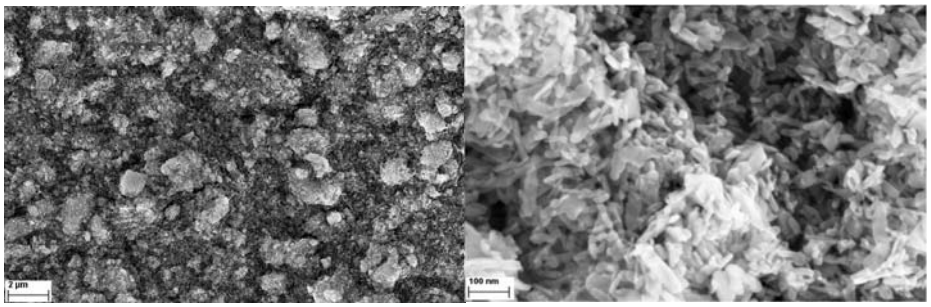

Figure 84.- SEM images with 5k magnification (left) and 100k magnification (right) of a CuO electrode after calcination.

To determine the Fermi energy level of the mesoporous CuO, Kelvin Probe microscopic experiments were performed, and a value of 0.55 V was obtained. As an approximation, we used the latter, in agreement with the literature, as the valence band energy.[369] Furthermore, diffuse reflectance assays were used to determine the bandgap energy of around E_g = 1.61 eV (*Figure 85*).[370] With this information in hand, we calculated the energy position of the conduction band, CB, via $E_{CB} = E_{VB} – E_g = 0.55 – 1.61 = -1.06$ V.

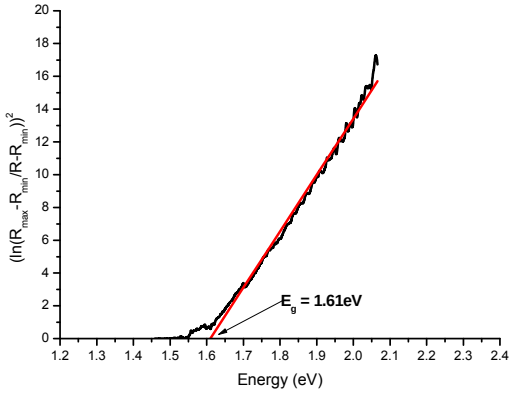

Figure 85.- Determination of the bandgap of CuO electrodes by diffuse reflectance assays.

Figure 86 illustrates an energy diagram depicting the HOMO/LUMO levels of dyes Zn(II)Pcs **51** and **52** with regard to other components of p-type DSSCs. Firstly, the

[369] C.-Y. Chiang, K. Aroh, N. Franson, V. R. Satsangi, S. Dass, S. Ehrman, *Int. J. Hydrogen Energy* **2011**, *36*, 15519.
[370] V. Kumar, S. K. Sharma, T. P. Sharma, V. Singh, *Opt. Mater*. **1999**, *12*, 115.

HOMOs are placed at 0.81 V (**51**) and 0.86 V (**52**) below the VB of the electrode (0.55 V). Such driving forces ensure an efficient electron flow from the electrode to the photoexcited Zn(II)Pcs. Secondly, upon excitation, electron recombination from the LUMOs to the CB should be suppressed. Finally, considering the redox potential of the I^-/I^-_3 and Co^{2+}/Co^{3+} couples as 0.34 V and 0.22 V vs. NHE,[341] respectively, Zn(II)Pc **51** and Zn(II)Pc **52** should be effectively regenerated because the electrolyte levels are 0.5 to 0.6 V below those of their LUMOs.

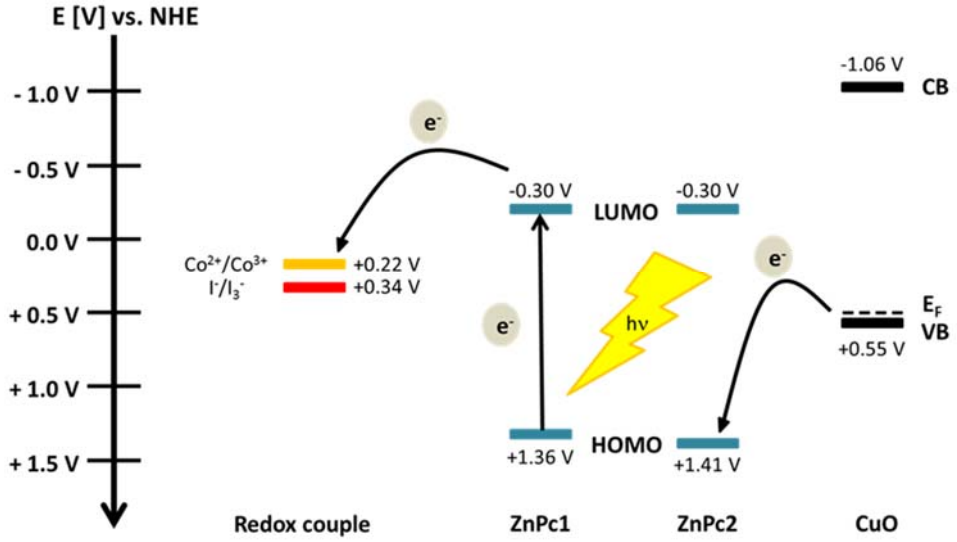

Figure 86.- Schematic diagram of the HOMO / LUMO levels of Pc **51** and Pc **52** with respect to the VB / CB energy of CuO and the redox potential of the electrolytes.

Based on the aforementioned thermodynamics, the CuO electrodes were immersed into ethanol solutions of the dyes. In resulting, p-type DSSCs were completed with Pt counterelectrodes and either with LiI/I_2 (1 M:0.4 M) in a 50:50 (v/v) mixture of acetonitrile/3-methoxypropionitrile, or with Co^{2+}/Co^{3+} (0.01 M:0.1 M) of $[Co(dtb\text{-}bpy)_3][PF_6]_{2/3}$ in acetonitrile as electrolytes. In this context, as we will see, the time dependences on the adsorption kinetics are important. For example, the efficiency starts to rise before plateauing at around 60 minutes of ZnPc uptake (*Figure 87*). The same trends are observed for J_{sc} and V_{oc}. From desorption experiments, similar concentrations of $1.38 \cdot 10^{-8}$ and 1.39×10^{-8} M were derived for **51** and **52**, respectively, which ensures comparability of the figures-of-merit.

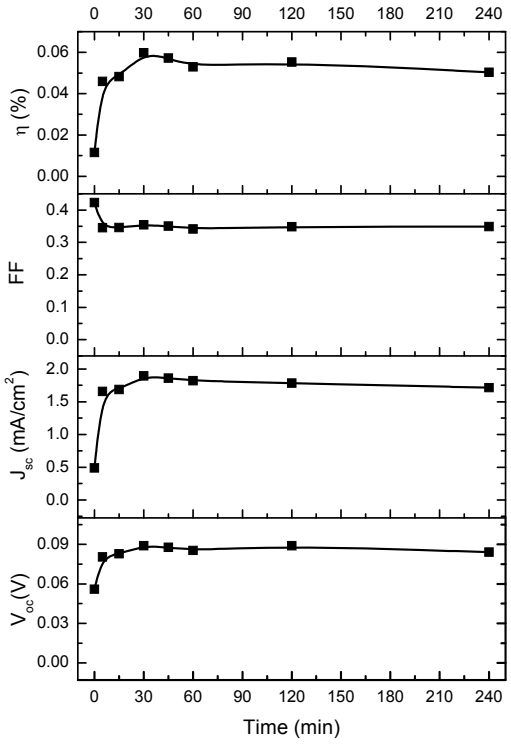

Figure 87.- Figures-of-merit vs. dye soaking time of a device with a LiI:I_2 (1M:0.2M) electrolyte in acetonitrile and the Zn(II)Pc **52** dye.

As starting point, we probed I^-/I^-_3 devices under 1 sun illumination and AM 1.5 conditions (*Figure* 88, Table *5*). **52** devices show higher V_{OC} and J_{SC} relative to **51** devices. Please compare 102 with 93 mV and 2.78 with 1.93 mA/cm^2. In contrast, the fill factors were nearly the same in both devices, leading to overall efficiencies of 0.103% and 0.067% for Pc **52** and Pc **51**, respectively. In line with the aforementioned, the EQE values are around 78% higher for **52** (27.4%) compared to **51** (15.4%) at 670 nm.

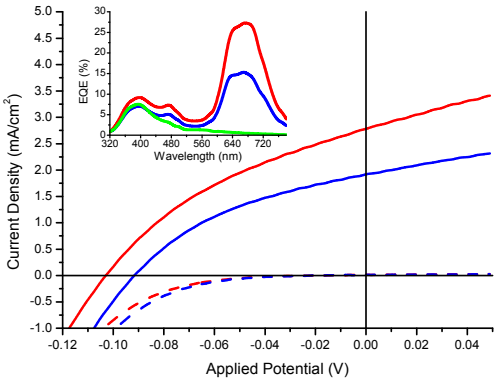

Figure 88.- J-V curves under 1 sun and AM 1.5 (line) and dark (dashed) conditions for carboxy derivatives **51** (blue) and **52** (red) devices with iodine-based electrolyte. Inset – EQE spectra of both kind of devices compared to a non-sensitized cell (green).

Dye	**Voc** (mV)	**Jsc** (mA/cm^2)	**FF**	**PCE**	**EQE (%)** at 670nm
51	93	1.93	0.38	0.067	15.4
52	102	2.78	0.36	0.103	27.4

Table 5.- Summarized device performance under 1 sun and AM 1.5 conditions for the iodine-based devices.

Comparable conditions, in terms of dye loading, electrode thickness, and electrolyte composition, as well as differences in J_{sc} and EQE obtained with **51** and **52**, point to a linker-dependent injection and/or recombination processes. **52** features the carboxylic linker connected to the Pc *via* a carbon-carbon triple bond, while the linker is directly connected in the case of **51**. In general, the nature of the linker determines both the dye-electrode distance and the orientation of the dye relative to the surface.[371] Both govern the injection and recombination kinetics, as seen in previous and our own results, where thermodynamic differences between the dyes are ruled out. Notably, the efficiency

[371] a) A. S. Hart, C. B. KC, H. B. Gobeze, L. R. Sequeira, F. D'Souza, *ACS Appl. Mater. Interfaces* **2013**, *5*, 5314.

trend found for these compounds in p-type DSSCs is in line with that observed in n-type devices sensitized by electron-donor Zn(II)Pc dyes featuring the same carboxylic linkers.[295b]

Considering that the CuO electrode opaqueness prohibited transient absorption spectroscopy assays, we turned to electrochemical impedance spectroscopy (EIS). Applying different voltages to change between short-circuit current density and open-circuit voltage conditions assists in probing the aforementioned processes in p-type DSSCs.[372,373] As an illustration, the Nyquist plots under V_{oc} and J_{sc} conditions are shown in *Figure 89*. Two semicircles, which relate to the resistance across the platinum/electrolyte interface in the high frequency region and the dye/electrode/electrolyte interface in the low frequency region are discernable.[372] From the corresponding electrical circuit model, which is illustrated also in *Figure 89*, the resistances and capacitances are derived. EIS measurements under dark conditions give insights into the electrode to electrolyte recombination.[372] To this end, *Figure 90* documents that the recombination resistance (R_{rec}) in both devices increases with decreasing voltage. Within the voltage range, slightly lower resistances towards recombination with the I^-/I_3^- redox couple are noted for Zn(II)Pc **52** devices. In the latter, larger dye to electrode distances facilitate interactions with the redox couple, as the electrode surface is more exposed to the polyiodide species. A closer look at the EQE spectra in *Figure 88* further substantiates this trend. Here, Zn(II)Pc **52** devices feature in the high-energy region, which is dominated by excitation of CuO and/or the redox couple, slightly higher EQEs (≤ 2%) compared to devices made of **51**.

[372] Z. Huang, G. Natu, Z. Ji, P. Hasin, Y. Wu, *J. Phys. Chem. C* **2011**, *115*, 25109.
[373] Z. Huang, G. Natu, Z. Ji, M. He, M. Yu, Y. Wu, *J. Phys. Chem. C* **2012**, *116*, 26239.

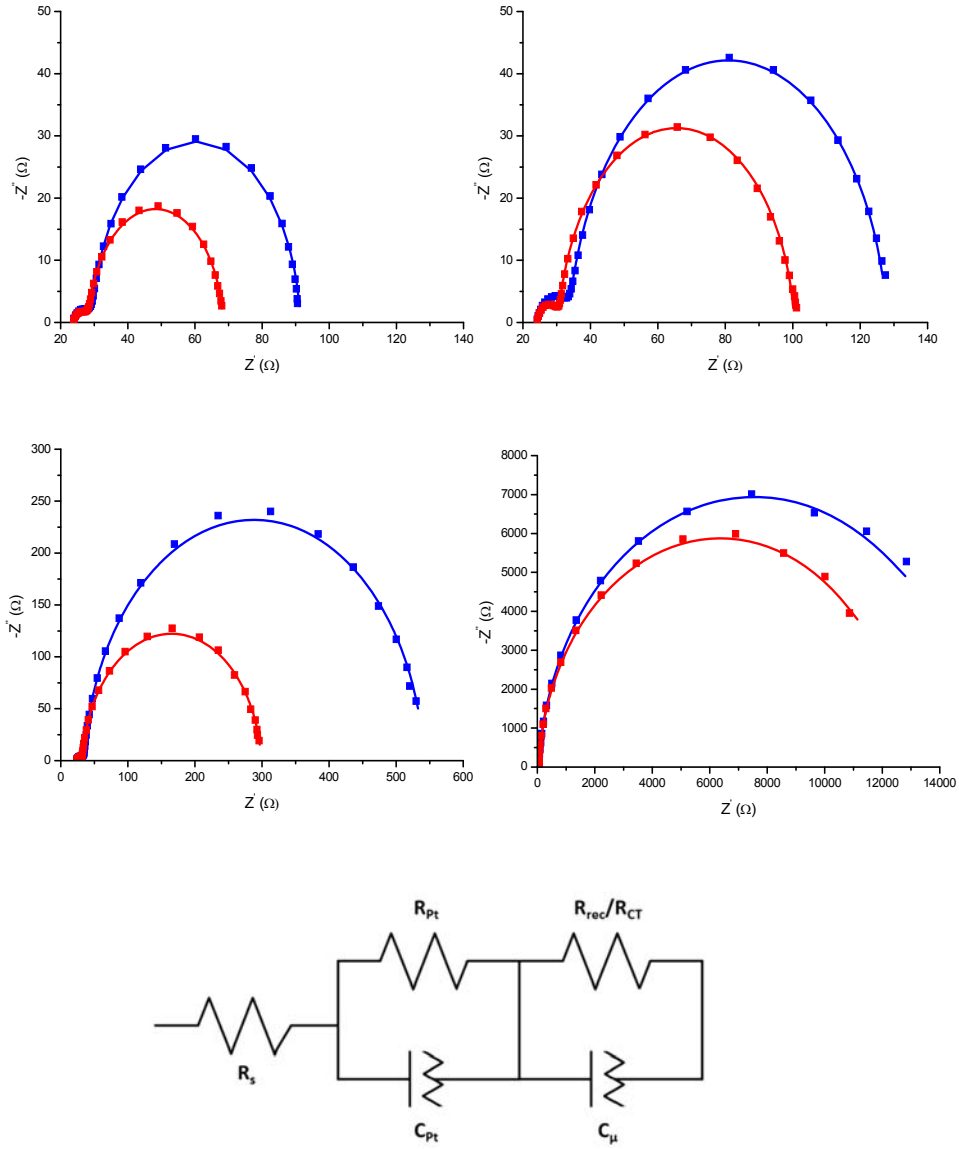

Figure 89.- Nyquist plots (solid squares) with the corresponding circuit model fits (line) for Pc **51** (blue) and Pc **52** (red) devices under V_{OC} (top) and J_{SC} (botton) conditions, as well as under 1 sun and AM 1.5 (left) and dark (right) conditions for the iodine-based devices. Also, it is represented the electrical circuit model used to obtain the determined EIS parameter.

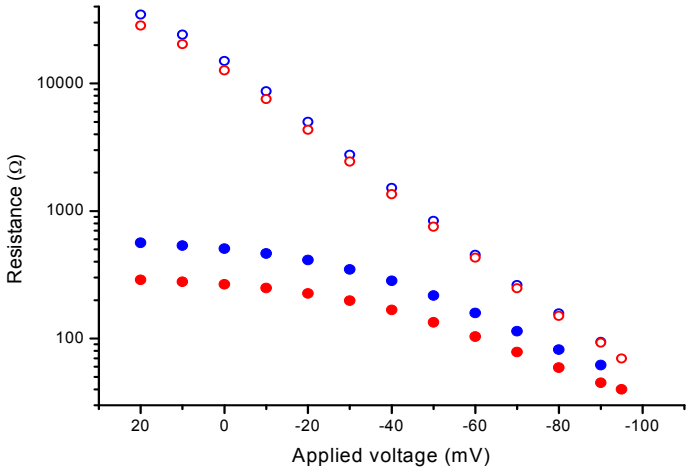

Figure 90.-. Resistance vs. applied voltage for Zn(II)Pc **51** (blue) and **52** (red) devices under dark (open circles) and illumination (closed circles) conditions.

More interesting are the EIS measurements under illumination. Here, several contributions impact the charge-transfer resistance (R_{CT}). Besides the electrode to redox couple recombination, charge injection from the electrode to the dye and transport processes in the electrode play the major roles.[374] Again, a linear increase of R_{CT} with decreasing voltage is noted before it plateaus at around J_{SC} conditions (*Figure 90*). A similar trend has recently been reported for NiO-based DSSCs.[373]

Overall, **52** devices give rise to lower R_{CT} throughout the entire voltage range in direct comparison to **51** devices, indicating better charge injection and charge transport in the former. At V_{OC} conditions, the recombination across the electrode/electrolyte interface is the most prominent process, since no external current flows. Here, in line with EIS observations in the dark, the resistance towards recombination with I^-/I^-_3 is slightly lower for Pc **52** (40.0 Ω) than for Pc **51** (61.8 Ω). At J_{SC} and under forward conditions, the lack of recombination allows the relation of R_{CT} to the charge injection from the electrode to the dye. From a comparison between **51** (506.3 Ω) and **52** (266.4 Ω), a nearly two times lower R_{CT} in the latter devices prompts to better charge injection. The EQE spectra are helpful in this regard, since the photocurrents due to dye excitation at around 670 nm are nearly twice as high in the case of **52**. The lack of photoactivity of the electrolyte in

[374] H. Choi, S. O. Kang, J. Ko, G. Gao, H. S. Kang, M.-S. Kang, M. K. Nazeeruddin, M. Gratzel, *Angew. Chem. Int. Ed*. **2009**, *48*, 5938.

the low-energy region only leaves contributions from the charge injection to rationalize the superior performance of devices featuring Zn(II)Pc **52**.

Additional device properties, namely the chemical capacitance (C_μ), the charge collection efficiency (η_{cc}), the effective diffusion length (L_{eff}), and the effective diffusion coefficient (D_{eff}) have been determined for all devices and are summarized in *Figure 91*.[372,374] Briefly, C_μ directly correlates with the density of injected holes at the electrode. A higher rate of charge injection increases the hole density, affording high V_{oc} and C_μ.[375] In agreement with this notion is the fact that higher V_{OC}, higher C_μ, and superior charge injections were observed for **52**. This also explains the improved η_{cc} seen in devices with Zn(II)Pc **52**, since charge injection across the electrode/dye interface is twice as efficient in this kind of devices. This is also reflected in longer L_{eff} and higher D_{eff} compared to Zn(II)Pc **51** devices.

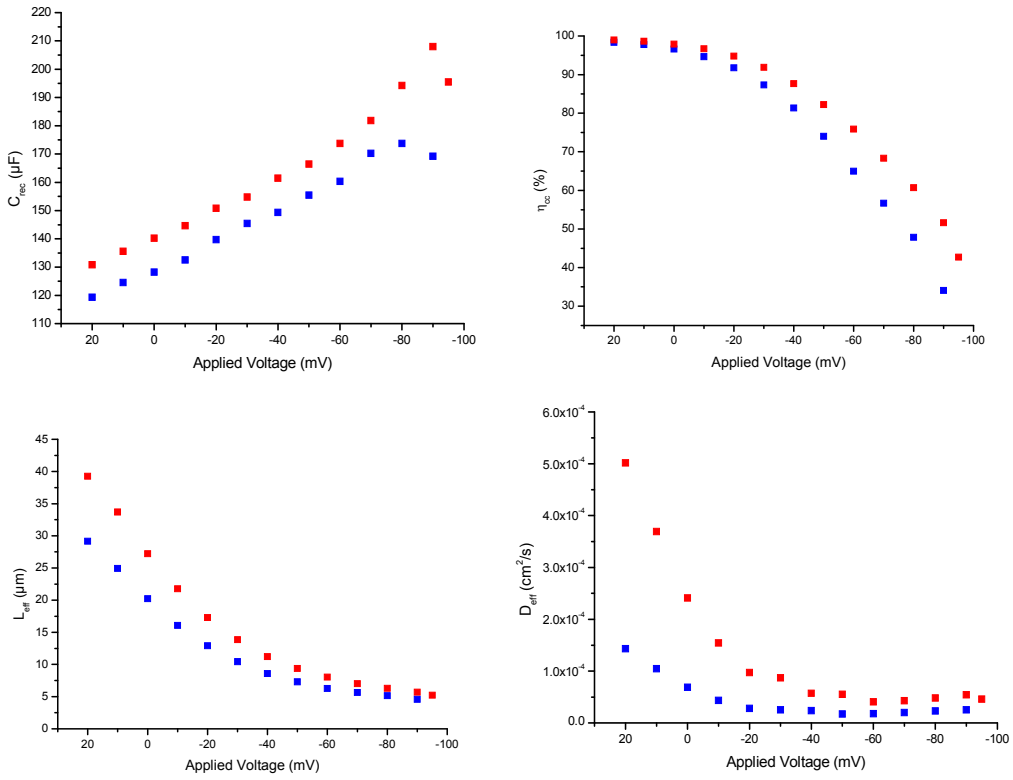

Figure 91.- Device parameters determined by EIS. C_{rec} (top left), η_{cc} (top right), L_{eff} (bottom left) and D_{eff} (bottom right) for Zn(II)Pc **51** (blue) and **52** (red).

[375] J. Bisquert, *Phys. Chem. Chem. Phys*. **2003**, *5*, 5360.

The major bottleneck of our devices evolves around the low V_{oc}, since J_{SC} values are comparable to those of $CuXO_2$ based DSSCs.[313] Using cobalt di-*tert*-butyl bipyridine hexafluorophosphate $[Co(dtb\text{-}bpy)_3][PF_6]_{2/3}$ as electrolyte is the most efficient way to overcome this limitation.[341] Under 1 sun illumination and AM 1.5 conditions, Pc **52** DSSC reveal higher V_{OC} and J_{SC} (251 mV and 2.35 mA/cm^2) than Pc **51** DSSC (224 mV and 1.99 mA/cm^2) (*Figure 92, table 6*). EQEs for macrocycle **52** at 670 nm are nearly 5.5% higher than for **51**. More importantly, the V_{OC} for both compunds increase by almost 150% when comparing iodine- and cobalt-based devices. As such, the efficiencies increase nearly by a factor of two, 0.191% and 0.141%, for dye **52** and derivative **51**, respectively.

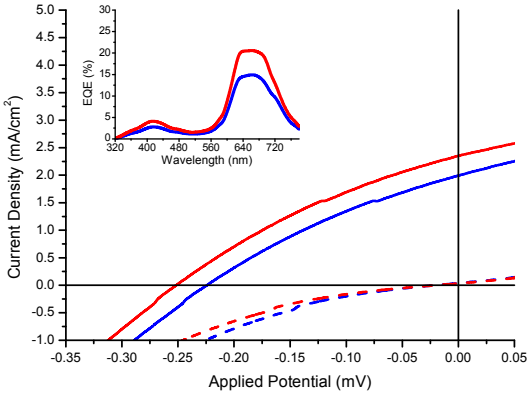

Figure 92.- J-V curves under 1 sun and AM 1.5 (line) and dark (dashed) conditions for carboxy derivatives **51** (blue) and **52** (red) devices with cobalt-based electrolyte. Inset – EQE spectra of both kind of devices. The EQE of the non-sensitized device is not shown, since a maximum of only 0.13% at 400 nm was measured.

Dye	**V_{oc}** (mV)	**J_{sc}** (mA/cm^2)	**FF**	**PCE**	**EQE (%)** at 670nm
51	224	1.99	0.32	0.141	14.9
52	251	2.35	0.32	0.191	20.5

Table 6.- Summarized device performance under 1 sun and AM 1.5 conditions for the cobalt-based devices.

EIS assays under V_{OC} and J_{SC} conditions are also in line with the trends noted for devices with iodine-based electrolytes (*Figure 93*). Zn(II)Pc **52** devices reveal, in

comparison to Zn(II)Pc **51** ones, a slightly higher recombination with the electrolyte as well as a better charge injection.

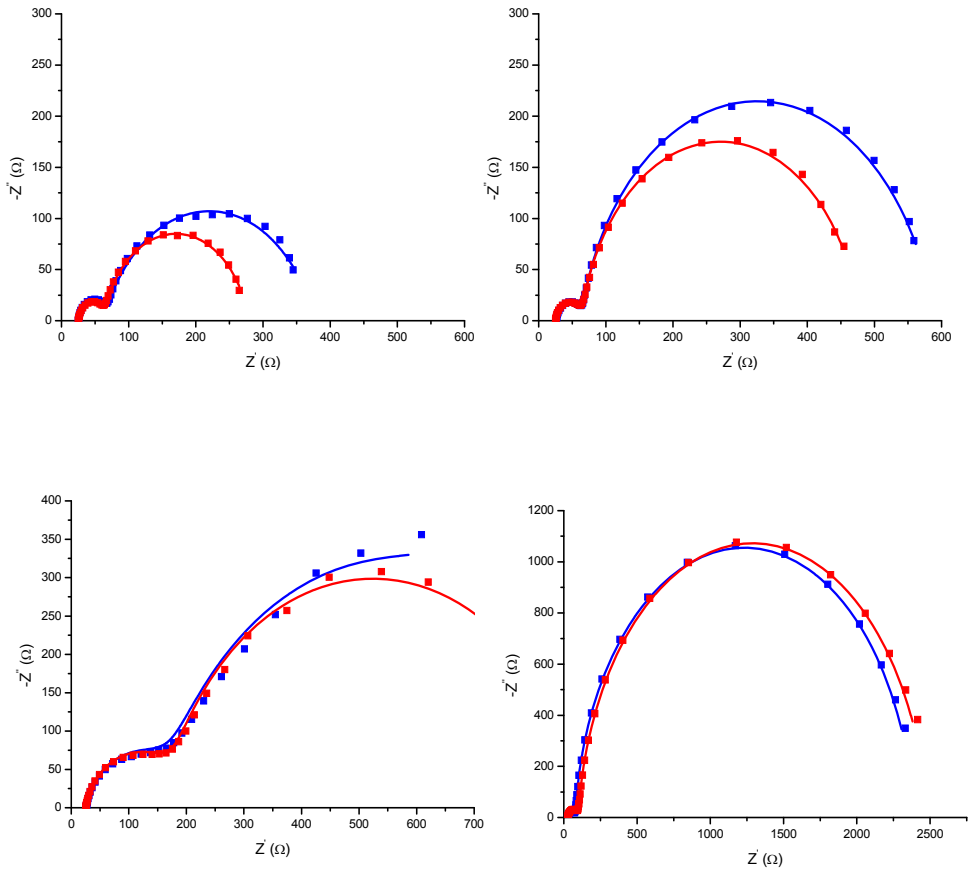

Figure 93.- Nyquist plots (solid squares) with the corresponding circuit model fits (line) for Pc **51** (blue) and Pc **52** (red) devices under V_{OC} (top) and J_{SC} (botton) conditions, as well as under 1 sun and AM 1.5 (left) and dark (right) conditions for the cobalt-based devices

1.4 Summary and conclusions

Lateral functionalization of conjugated polymers with Pcs have been performed following two approaches:

- Conjugated polyphenylenevinylene- and polythiophene type copolymers decorated with Pc molecules (Pc-PPV **38**, Pc-PPV **41** and Pc-PT **42**) have been successfully synthesizedd by post-polymerization procedures. Pc-PPV **38** has been synthesized through esterification of hydroxy Pc **5** and a copolymer comprising a 10% of CO_2H-containing monomers (**37**), whereas Pc-PPV **41** was prepared by a "click" 1,3-dipolar cycloaddition reaction between a copolymer (**39**) comprising a 10% of terminal alkyne-containing monomers and an azido-functionalized Pc **7**. The latter proved to be more effective than the esterification reaction and, therefore, the Pc ratio in Pc-PPV **41** was higher (9%) than in Pc-PPV **38** (7%). "Click" conditions were also applied for the incorporation of Pcs in a PT skeleton to obtain Pc-PT **42**. The Pc-containing polymers were applied in BHJ solar cells with PCBM. The contribution of the linked Pcs to the photocurrent was confirmed by EQE. However, solubility of the materials in CB, which use is compulsory for the solubilization of the PCBM, is not good enough to achieve a good morphology in the spin-coated film, this fact decreasing the PCE of the devices with regard to those prepared with the related polymers lacking the Zn(II)Pc units.

- A conjugated polymer holding electron acceptor Zn(II)Pcs in alternated monomer units has been prepared, in the search for new polymers with a "double-cable" architecture, that is, a material in which the donor (polymer) and acceptor (Pc) components are covalently linked instead of blended. For that purpose, a conjugated 1:1 PPV copolymer with *ca* 50% of units containing lateral azide moieties (**44**) has been prepared and reacted ethynyl Zn(II)Pc **18**, holding electron-withdrawing alkylsulfonyl groups at the peripheral positions. Unfortunately, a completely insoluble material was obteined, which make it impossible to characterize and to use this material for the preparation of devices. Therefore, the double-cable approach was discarded.

Additionally, polymers containing Pcs in the main chain, in combination with other high-performing electroactive subunits, have been also envisioned as an approach towards the preparation of highly-absorbing, active polymers for BHJ devices. For that purpose, a Pc with good leaving groups in two α positions of one isoindole, namely **21**,

has been synthesized and characterized. Then, optimization of coupling conditions for further co-polymerization with tiophene-containing organometallic species has been performed. Co-polymerization experiments are currently under study in the group of Prof. Iain McCulloch at Imperial College

Regarding p-type DSSCs, two new electron accepting Zn(II)Pcs, **51** and **52**, have been synthesized and characterized.Electrochemical measurements address their electron-acceptor behaviour. These chromophores have been used as photosensitizers in p-DSSCs based on nanorod-like CuO electrodes, which have been previously characterized to show their validity as p-type semiconductor. The efficiencies (%) found were 0.067 and 0.141 for Pc **51**, and 0.103 and 0.191 for Pc **52**, using iodine or cobalt-based electrolytes, respectively. The latter values represent the highest ever reported efficiencies for pure CuO p-type DSSCs. Regarding the dye, it was shown that the presence of an ethynyl bridge in the dye **52**, enhances the electronic coupling between the Zn(II)Pc dye and the CuO due to an optimum balance between the charge injection and charge recombination.

1.5 Experimental Section

Unless stated otherwise, all reagents and starting materials were used as obtained from commercial sources such as SDS, Fluka, Aldrich, Acros Organics and Merck, without further purification. Most of the solvents employed in this work were purchased from SDS. Monitoring of the reactions was carried out by thin layer chromatography (TLC), employing aluminium sheets coated with silica gel 60 F_{254} (Merck). The purification and isolation of most of the products was performed by column chromatography using silica gel Merck-60 (230-400 mesh, 0.040-0.063 mm). Size exclusion chromatography (SEC) was done using swollen Bio-beads S-X1 (200-400 mesh) from Bio-Rad.

Melting points were taken in open-end capillary tubes by using a Büchi 504392-S apparatus, and are uncorrected. NMR spectra (^{1}H, ^{13}C and ^{19}F) were recorded with a Bruker AC-300 (300 MHz, ^{1}H) instrument. In each case, the deuterated solvent employed is indicated in brackets, and its residual peak was used to calibrate the spectra using literature reference δ ppm values.[376] Infrared spectra were recorded on a Bruker Vector 22 spectrophotometer, in the employing solid samples (KBr pressed disks) or using KBr plates (films). UV-Vis absorption spectra were collected on a Hewlett-Packard 8453 spectrometer, employing spectroscopic grade solvents, purchased from Fluka Chemie. The logarithm of the absorption coefficient (ε, $dm^3 \cdot cm^{-1} \cdot mol^{-1}$) is indicated in brackets for each maximum. Mass spectra (MS) were recorded employing Electronic Impact (EI), Fast Atom Bombardment (FAB-MS) or Matrix Assisted Laser Desorption/Ionization-Time of Flight (MALDI-TOF), using a VG-AutoSpec spectrometer for EI and FAB-MS and a Bruker Reflex III spectrometer, with a laser operating at 337 nm, for MALDI-TOF. Elemental analyses were performed employing a Perkin Elmer 2400 CHNS/O analyzer.

In this *Experimental Section*, the preparation and characterization of the compounds has been organised following the order in which they appear in the text.

[376] G. R. Fulmer, A. J. M. Miller, N. H. Sherden, H. E. Gottlieb, A. Nudelman, B. M. Stoltz, J. E. Bercaw, K. I. Goldberg, *Organometallics* **2010**, *29*, 2176

1.5.1 Organic solar cells

1.5.1.1 Synthesis of phthalocyanines

Phthalocyanines for lateral functionalization of conjugated polymers

4-Aminophthalonitrile (1)

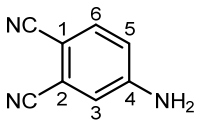

To a mixture of MeOH (450.0 mL) and concentrated HCl 37% (96.0 mL), 4-nitrophthalonitrile (1.0 eq, 115 mmol, 20.0 g) was added. Upon heating to reflux, total dissolution of the solid was observed and iron powder (3.4 eq, 394 mmol, 22.0 g) was added in small portions over 1 h. The brown solution was stirred at reflux for a further hour and allowed to warm up to room temperature. Cold water (600 mL) was then poured onto the mixture resulting in the precipitation of a yellow-green solid which was filtered on a fritted glass, washed with water (200 mL) and hexane (100 ml). Recrystallization from toluene led to 12.6 g (88.0 mmol) of **1** as ochre crystalline needles. Yield: 76%.

Mp: 171-173 ºC (reported:[164a] 172-174 ºC).

^{1}H-NMR (200 MHz, DMSO-d_6): δ (ppm) = 7.65 (d, $J_{o,5\text{-}6}$ = 8.7 Hz, 1H; H-6), 7.00 (d, $J_{m,3\text{-}5}$ = 2.5 Hz, 1H; H-3), 6.85 (dd, $J_{o,5\text{-}6}$ = 8.7 Hz, $J_{m,3\text{-}5}$ = 2.5 Hz, 1H; H-5), 6.70 (br s, 2H; NH_2).

FT-IR (KBr): ν (cm^{-1}) = 2230 (ν_{st} C≡N), 1515, 1380, 1255.

MS (EI): *m/z* = 143 $[M]^+$ (100%). $C_8H_5N_3$ (Exact mass: 143.05, molecular weight: 143.15).

4-Iodophthalonitrile (2)[164b]

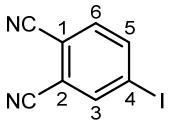

A suspension of 4-aminophthalonitrile (**1**) (1.0 eq, 35.0 mmol, 5.0 g) in H_2SO_4 2.5 M (70.0 mL) was cooled to -10 ºC and a solution of $NaNO_2$ (1.1 eq, 39.0 mmol, 2.8 g) in water (10.0 mL) was added dropwise under constant stirring. After total addition, the mixture was further stirred at 0 ºC for 30 min and then poured over a solution of KI (1.1 eq, 39.0 mmol, 6.5 g) in cold water (40 mL). The resulting mixture was stirred at room temperature for 45 min and the brown solid was filtered, washed with water (100 mL) and dissolved in $CHCl_3$ (200 mL). This solution was then washed with a saturated solution of $Na_2S_2O_3$ (3x30 mL) and water (2x30 mL), and dried over Na_2SO_4. After filtration of the drying agent, the solvent was vacuum-evaporated and the yellow solid obtained was subjected to column chromatography on silica gel using DCM as the eluent. In this way, 6.1 g (24.0 mmol) of **2** were obtained as a white solid. Yield: 69%.

Mp: 142-143 ºC (reported:[164b] 142-143 ºC).

^{1}H-NMR (300 MHz, $CDCl_3$): δ (ppm) = 8.17 (d, $J_{m,3-5}$ = 1.6 Hz, 1H; H-3), 8.12 (dd, $J_{o,5-6}$ = 8.2 Hz, $J_{m,3-5}$ = 1.6 Hz, 1H; H-5), 7.49 (d, $J_{o,5-6}$ = 8.6 Hz, 1H; H-6).

^{13}C-NMR (75.5 MHz, $CDCl_3$): δ (ppm) = 142.6 (C-5), 142.1 (C-3), 133.9 (C-6), 116.7 (2C; CN), 114.9 (C-2), 113.5 (C-1), 99.6 (C-4).

FT-IR (KBr): ν (cm^{-1}) = 2241 (ν_{st} C≡N), 1585, 940, 852.

MS (EI): *m/z* = 254 $[M]^+$ (84%), 127 $[M-I]^+$ (100%). $C_8H_3IN_2$ (Exact mass: 253.93, molecular weight: 254.03).

4-(4'-Hydroxymethyl)phenylphthalonitrile (3)

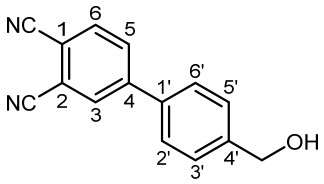

To a solution of 4-iodophthalonitrile (2) (1.0 eq, 3.93 mmol, 1.00 g) in dry THF (40.0 mL), $Pd(PPh_3)_4$ (10% mol, 0.39 mmol, 0.46 g) was added. After stirring the reaction mixture under argon for 20 min, K_2CO_3 (1.0 eq, 3.93 mmol, 0.54 g), 4-(hydroxymethyl)phenylboronic acid (1.0 eq, 3.93 mmol, 0.60 g) and water (10.0 mL) were added. The mixture was refluxed for 24 h, then cooled to room temperature and the THF evaporated. The suspended solid in water was filtered through a fritted glass funnel and washed with more water (50 mL) and hexane (70 mL). The residue was dissolved in THF and dried over anhydrous Na_2SO_4. After removing the solvent under reduced pressure, the crude product was purified by column chromatography in silica gel (hexane/THF, 2:1) to give compound **3** (0.74 g, 3.2 mmol) as a white solid. Yield: 80%.

Mp: 129-130 ºC (reported:[165] 129-130 ºC).

^{1}H-NMR (300 MHz, $CDCl_3$): δ (ppm) = 8.00 (d, $J_{m,3-5}$ = 1.8 Hz, 1H; H-3), 7.93 (dd, $J_{o,5-6}$ = 8.6 Hz, $J_{m,3-5}$ = 1.8 Hz, 1H; H-5), 7.87 (d, $J_{o,5-6}$ = 8.6 Hz, 1H; H-6), 7.59 (d, $J_{o,2'-3'}$ = 8.2 Hz, 2H; H-2', H-6'), 7.53 (d, J_o = 8.2 Hz, 2H; H-3', H-5'), 4.80 (s, 2H; Ar$\underline{H}_2$OH), 1.80 (br s, 1H, ArCH$_2$O$\underline{H}$).

^{13}C-NMR (75.5 MHz, $CDCl_3$): δ (ppm) = 146.3 (C-4), 142.9 (C-4'), 136.3 (C-1'), 134.1 (C-6), 132.0 (C-5), 131.5 (C-3), 128.0 (C-3', C-5'), 127.5 (C-2', C-6'), 116.7 (C-2), 115.6 (CN), 115.5 (CN), 114.8 (C-1), 64.7 (CH_2OH).

FT-IR (KBr): ν (cm^{-1}) = 3354 (ν_{st} O-H), 3105, 3072, 3047, 2231 (ν_{st} C≡N), 1567, 1382, 1163, 1099, 852, 747.

MS (EI): *m/z* = 235 $[M+H]^+$ (2%), 234 $[M]^+$ (11%), 233 $[M-H]^+$ (5%), 218 M_1 $[M-OH]^+$ (100%). $C_{15}H_{10}N_2O$ (Exact mass: 234.08, molecular weight: 234.26).

EA for $C_{15}H_{10}N_2O$ (%): calculated = C 76.91, H 4.30, N 13.66. Found = C 76.74, H 4.37, N 13.59.

2,9,16-Tri-*tert*-butyl-23-(4'-hydroxymethyl)phenyl-5,28:14,19-diimino-7,12:21,26-dinitrilo-tetrabenzo[*c,h,m,r*]-[1,6,11,16]tetraazacycloeicosinato-(2$^-$)-N^{29},N^{30},N^{31},N^{32} zinc (II) (only one regioisomer is named) (5)

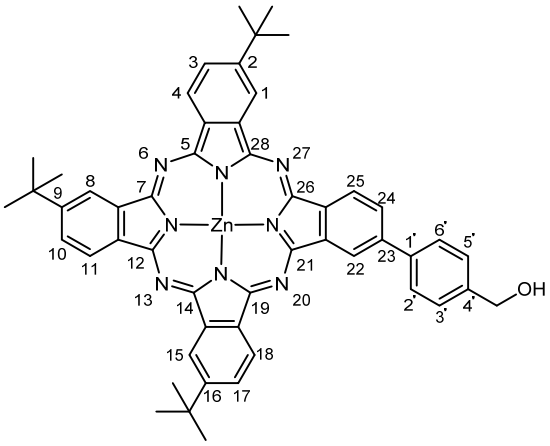

4-*tert*-butylphthalonitrile (3.0 eq, 3.84 mmol, 709 mg), phthalonitrile **3** (1.0 eq, 1.28 mmol, 300 mg) and $Zn(OAc)_2$ (1.3 eq, 1.66 mmol, 305 mg) in DMAE (5.0 mL) were heated to reflux under an argon atmosphere for 16 h. After cooling to room temperature, the reaction mixture was treated with MeOH/Water (3:1, 200 mL), and the solid obtained was filtered, washed with MeOH (75 mL) and vacuum dried. The resulting blue solid was purified by column chromatography on silica gel using hexane/dioxane (2:1) as the carrier phase. The symmetrically *tert*-butyl substituted phthalocyanine **4** was eluted first, and obtained as a blue solid (162 mg, yield: 21%). It was followed by the unsymmetrical derivative **5**, as a blue solid (273.0 mg, 0.32 mmol). Yield: 25%.

Mp: > 250 ºC.

^{1}H-NMR (300 MHz, DMSO-d_6): δ (ppm) = 9.4-8.9 (m, 8H; Pc-H), 8.4-8.1 (m, 6H; Pc-H, phenyl H-2', H-6'), 7.8-7.7 (m, 2H; phenyl-H H-3', H-5'), 5.45 (s, 1H; $CH_2O\underline{H}$), 4.75 (s, 2H; $C\underline{H}_2OH$), 1.81 (s, 27H; $C(CH_3)_3$).

FT-IR (KBr): ν (cm^{-1}) = 2959, 1728, 1607, 1483, 1090, 1047, 831, 764.

UV-Vis (THF): λ_{max} (nm) (log ε) = 675 (5.3), 609 (4.5), 350 (4.8).

HRMS (MALDI-TOF, DCTB+PMMANa600): *m/z* = 850.3055. $C_{51}H_{46}N_8OZn$ (Exact mass: 850.3081, molecular weight: 852.36).

2-(4'-Bromomethyl)phenyl-9,16,23-tri-*tert*-butyl-5,28:14,19-diimino-7,12:21,26-dinitrilo-tetrabenzo[*c,h,m,r*]-[1,6,11,16]tetraazacycloeicosinato-(2$^-$)-N^{29},N^{30},N^{31},N^{32} zinc (II) (only one regioisomer is named) (6)

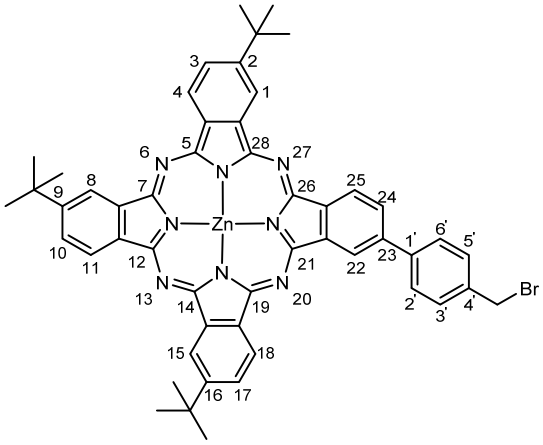

PPh_3 (3.3 eq, 0.97 mmol, 254 mg) and CBr_4 (3.3 eq, 0.97 mmol, 321 mg) were added to a solution of Pc **5** (1.0 eq, 0.29 mmol, 250 mg) in dry DCM (10.0 mL) under an argon atmosphere. After stirring at 50 ºC for 1 h, the reaction mixture was washed with a saturated aqueous solution of $NaHCO_3$ (2x150 mL), dried over $MgSO_4$, and vacuum concentrated. Purification by column chromatography on silica gel with hexane/dioxane (3:1) as the eluent, afforded Pc **6** as a blue solid (239 mg, 0.26 mmol). Yield: 89%.

Mp: > 250 ºC.

^{1}H-NMR (300 MHz, DMSO-d_6): δ (ppm) = 9.4-8.9 (m, 8H; Pc-H), 8.4-8.1 (m, 6H; Pc-H, phenyl-H H-2', H-6'), 7.8-7.7 (m, 2H; phenyl-H H-3', H-5'), 4.99 (s, 2H; C$\underline{H}_2$Br), 1.80 (s, 27H; $C(CH_3)_3$).

FT-IR (KBr): ν (cm^{-1}) = 2959, 1728, 1607, 1483, 1090, 1047, 831, 764.

UV-Vis (THF): λ_{max} (nm) (log ε) = 675 (5.3), 609 (4.6), 350 (4.9).

HRMS (MALDI-TOF, DCTB+PMMANa600): *m/z* = 912.2200. $C_{51}H_{45}BrN_8Zn$ (Exact mass: 912.2237, molecular weight: 915.26).

2-(4'-Azidomethyl)phenyl-9,16,23-tri-*tert*-butyl-5,28:14,19-diimino-7,12:21,26-dinitrilo-tetrabenzo[*c,h,m,r*]-[1,6,11,16]tetraazacycloeicosinato-(2$^-$)-N^{29},N^{30},N^{31},N^{32} zinc (II) (only one regioisomer is named) (7)

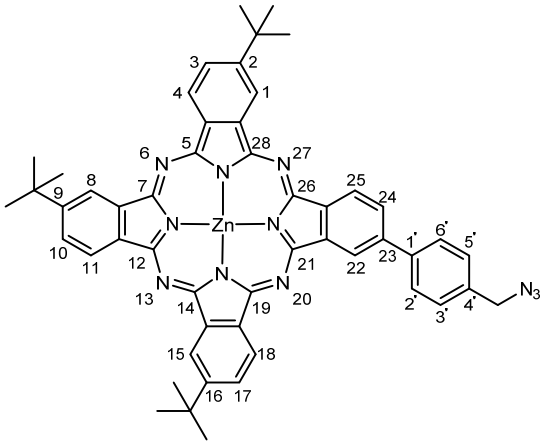

Sodium azide (100.0 eq, 26.11 mmol, 1.70 g) and Pc **6** (1.0 eq, 0.26 mmol, 239.0 mg) were dissolved in DMF/H_2O (10:1, 33.0 mL) and heated to 70 ºC for 4 h. After cooling down to room temperature, the solvent was removed and the crude product was extracted with DCM (3x100 mL) and dried over Na_2SO_4. The solvent was evaporated and the resulting solid was filtered and washed with hexane (100 mL) to give Pc **7** as a blue solid (207.0 mg, 0.24 mmol). Yield: 90%.

Mp: > 250 ºC.

^{1}H-NMR (300 MHz, THF-d_8): δ (ppm) = 9.5-9.1 (m, 9H; Pc-H, phenyl-H), 8.4-8.1 (m, 7H; Pc-H, phenyl-H), 4.61 (s, 2H; C$\underline{H}_2N_3$), 1.84 (s, 27H; $C(CH_3)_3$).

FT-IR (KBr): ν (cm^{-1}) = 2959, 2166 (νN_3), 1728, 1607, 1483, 1090, 1047, 831, 764.

UV-Vis (THF): λ_{max} (nm) (log ε) = 675 (5.6), 609 (4.9), 350 (5.2).

HRMS (MALDI-TOF, DCTB+PPGNa 1000): *m/z* = 875.3138. $C_{51}H_{45}N_{11}Zn$ (Exact mass: 875.3145, molecular weight: 877.38).

4,5-Dichlorophthalic anhydride (8)

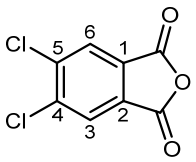

A solution of 4,5-dichlorophthalic acid (65.0 mmol, 15.3 g) in acetic anhydride (25.0 mL) was heated to reflux. After 5 h, the suspended solid was filtered and washed with hexane. The grey solid obtained was stirred in hexane over 12 h, obtaining a solid that was filtered and thoroughly washed with the same solvent (100 mL). In this way, 13.0 g of anhydride **7** (60.2 mmol) were obtained. Yield: 92%.

Mp: 181-183 ºC (reported:[166] 184-186 ºC).

^{1}H-NMR (300 MHz, $CDCl_3$): δ (ppm) = 8.12 (s, 2H; H-3, H-6).

^{13}C-NMR (75.5 MHz, $CDCl_3$): δ (ppm) = 160.6 (CO), 141.7 (C-4, C-5), 130.0 (C-1, C-2), 127.3 (C-3, C-6).

4,5-Dichlorophthalimide (9)

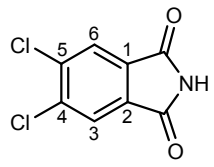

A mixture of 4,5-dichlorophthalic anhydride (**8**) (13.0 g, 60.2 mmol) and formamide (19.0 mL) was heated to 200 ºC over 3 h. After cooling to room temperature, the solid obtained was filtered, washed with water (40 mL) and vacuum-dried, yielding 12.0 g of 4,5-dichlorophthalamide (**9**) (55.5 mmol) as a white solid. Yield: 93%.

Mp: 193-195 ºC (reported:[166] 193-195 ºC).

^{1}H-NMR (300 MHz, $CDCl_3$): δ (ppm) = 8.12 (s, 2H; H-3, H-6).

^{13}C-NMR (75.5 MHz, $CDCl_3$): δ (ppm) = 160.6 (CONH), 141.7 (C-4, C-5), 130.0 (C-1, C-2), 127.3 (C-3, C-6).

4,5-Dichlorophthalamide (10)[166]

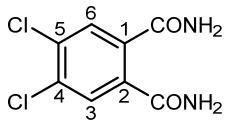

A suspension of 4,5-dichlorophthalimide (**9**) (12.0 g, 55.5 mmol) in 25% aqueous ammonia (168 mL) was stirred at room temperature for 24 h. At that time, a 33% ammonium hydroxide solution (56.0 mL) was added and the mixture was further stirred for 24 h. The white solid obtained was filtered, washed with water (50 mL) and vacuum-dried. In so doing, 11.4 g of 4,5-dichlorophthalamide (**10**) (48.9 mmol) were isolated as a white solid. Yield: 88%.

Mp: 240-242 ºC (reported:[166] 245-247 ºC).

^{1}H-NMR (300 MHz, DMSO-d_6): δ (ppm) = 7.95 (br s, 2H; NH_2), 7.72 (s, 2H; H-3, H-6), 7.45 (br s, 2H; NH2).

^{13}C-NMR (75.5 MHz, DMSO-d_6): δ (ppm) = 169.6 ($CONH_2$), 136.6 (C-4, C-5), 131.9 (C-1, C-2), 129.2 (C-3, C-6).

4,5-Dichlorophthalonitrile (11)[166]

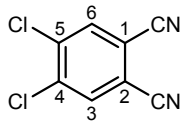

Thionyl chloride (41.0 mL) was cautiously poured over dry DMF (58.0 mL) at 0 ºC under argon atmosphere. The mixture was vigorously stirred at that temperature for 2 h and then 4,5-dichlorophthalamide (**10**) (48.9 mmol, 11.4 g,) was added. After stirring at room temperature for 12 h, the reaction mixture was poured onto crushed ice (100 mL), resulting in the precipitation of a slightly grey solid which was filtered and washed with

water (20 mL). Upon recrystallization from methanol, 8.4 g (42.5 mmol) of compound **11** were obtained. Yield: 87%.

Mp: 180-183 ºC (reported:[166] 182-184 ºC).

^{1}H-NMR (300 MHz, $CDCl_3$): δ (ppm) = 7.94 (s, 2H; H-3, H-6).

^{13}C-NMR (75.5 MHz, $CDCl_3$): δ (ppm) = 138.2 (C-4, C-5), 135.7 (C-3, C-6), 115.0, 114.6, 114.0 (C-1, C-2, CN).

MS (EI): *m/z* = 196 $[M]^+$ (100%). $C_8H_2Cl_2N_2$ (Exact Mass: 195.96, molecular weight: 197.02).

4,5-Bis(2-ethylhexylthio)phthalonitrile (12)

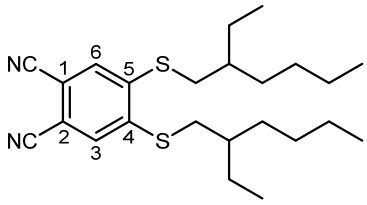

A solution of 4,5-dichlorophthalonitrile (**11**) (1.0 eq, 1.27 mmol, 0.25 g,) in freshly distilled DMAC (5 mL) was heated to 100ºC, and oven-dry K_2CO_3 (9.7 eq, 12.3 mmol 1.7 g) was added in five portions over 30 min. Then, 2-ethylhexane-1-thiol (2.4 eq, 3.1 mmol, 0.53 mL) was added, and the resulting mixture was stirred at 100 ºC for 10h. It was then allowed to reach room temperature, poured in water (15 mL) and extracted with DCM (3x15 mL). Combined organic layers were dried over $MgSO_4$ and evaporated. The residue was purified by column chromatography (SiO_2, hexane/DCM 1:1) to give **12** (0.42 g, 1.02 mmol) as a yellowish oil. Yield: 80%.

^{1}H-NMR (300 MHz, $CDCl_3$): δ (ppm) = 7.41 (s, 2H; H-3, H-6), 2.97 (m, 4H; SCH_2), 1.71 (m, 2H; $SCH_2C\underline{H}$), 1.4-1.3 (m, 16H; SCH_2CH ($C\underline{H}_2$)$C\underline{H}_2C\underline{H}_2C\underline{H}_2CH_3$), 0.94 (m, 12H; CH_3).

^{13}C-NMR (75.5 MHz, $CDCl_3$): δ (ppm) = 145.0 (C-4, C-5), 128.4 (C-3, C-6), 115.9 (CN), 111.01(C-1, C-2), 38.7 (SCH_2), 37.4 ($SCH_2\underline{C}H$), 32.7 ($SCH_2CH\underline{C}H_2$), 28.9 ($SCH_2CHCH_2\underline{C}H_2$), 26.0 ($SCH_2CH\underline{C}H_2CH_3$), 23.1 ($SCH_2CHCH_2CH_2\underline{C}H_2CH_3$), 14.2 (CH3), 10.9 ($CH_3$).

MS (MALDI-TOF, TCNQ): *m/z* = 417.3 $[M+H]^+$ (100%). $C_{24}H_{36}N_2S_2$ (Exact mass: 416.23, molecular weight: 416.69).

EA for $C_{24}H_{36}N_2S_2$ (%): calculated = C 69.18, H 8.71, N 6.72, S, 15.39. Found = C 69.64, H 8.81, N 6.68, S 15.28.

4,5-Bis(2-ethylhexylsulfonyl)phthalonitrile (13)

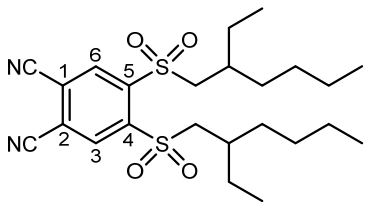

To a stirred solution of 4,5-bis(2-ethylhexylthio)phthalonitrile (**12**) (1.0 eq, 2.4 mmol, 1.0 g) in acetic acid (20.0 mL) at 90 ºC, a 33% H_2O_2 solution (11.2 mL) was slowly added. After stirring at 80 ºC for 3 h, the resulting cloudy mixture was allowed to warm up to room temperature, poured in water and extracted with DCM (3x15 mL). Combined organic layers were dried over $MgSO_4$ and evaporated. Compound **13** was purified by column chromatography on silica gel using a 6:1 mixture of hexane/ethyl acetate as eluent, and obtained as a yellowish oil (1.1 g, 2.3 mmol). Yield: 95%.

^{1}H-NMR (300 MHz, $CDCl_3$): δ (ppm) = 8.69 (s, 2H; H-3, H-6), 3.57 (m, 4H; SO_2CH_2), 2.15 (m, 2H; SO_2CH_2CHR), 1.4-1.2 (m, 16H; CH_2), 0.88 (m, 12H; CH_3).

^{13}C-NMR (75.5 MHz, $CDCl_3$): δ (ppm) = 145.4 (C-4, C-5), 137.3 (C-3, C-6), 121.3 (C-1, C-2), 113.3 (CN), 60.1 (SO_2CH_2), 34.7 (SO_2CH_2CH), 32.7 ($SO_2CH_2CHCH_2$), 28.2 ($SO_2CH_2CHCH_2CH_2$), 26.1 ($SO_2CH_2CHCH_2CH_3$), 22.9 ($SO_2CH_2CHCH_2CH_2CH_2CH_3$), 14.2 ($CH_3$), 10.3 ($CH_3$).

MS (FAB, *m*-NBA): m/z = 481.2 [M+H]+ (100%). $C_{24}H_{36}N_2O_4S_2$ (Exact mass: 480.21, molecular weight: 480.68).

EA: ($C_{24}H_{36}N_2O_4S_2$); calculated: C 59.97, H 7.55, N 5.83, S 13.34. Found: C 61.36, H 7.71, N 5.80, S 13.04.

Synthesis of phthalocyanines 14 and 15

A *o*-DCB/DMF (3:1, 2.4 mL, 0.8 mL) solution of 4,5-bis(2-ethylhexylsulfonyl)phthalonitrile (**13**) (3.0 eq, 0.52 mmol, 250 mg), 4-iodophthalonitrile (**2**) (2.0 eq, 0.35 mmol, 88.1 g) and $Zn(OAc)_2$ (1.2 eq, 0.024 mmol, 38.2 mg) was heated at 135 ºC under an argon atmosphere for 12 h. After cooling down to room temperature, the solvent was removed under reduced pressure and the crude was poured on water and extracted with DCM (3x15 mL). Combined organic layers were dried over $MgSO_4$ and evaporated. The mixture of Pcs formed was separated by column chromatography on silica gel using a mixture of $CHCl_3$/THF (40:1) as eluent. The unsymmetrically substituted Pc **15** was eluted first followed by derivative **14**.

2,3,9,10,16,17,23,24-Octakis(2-ethylhexylsulfonyl)-5,28:14,19-diimino-7,12:21,26-dinitrilo-tetrabenzo[*c, h, m, r*]-[1, 6, 11, 16]tetraazacycloeicosinato-(2$^-$)- *N*^{29}, *N*^{30}, *N*^{31}, *N*^{32} zinc (II) (14)

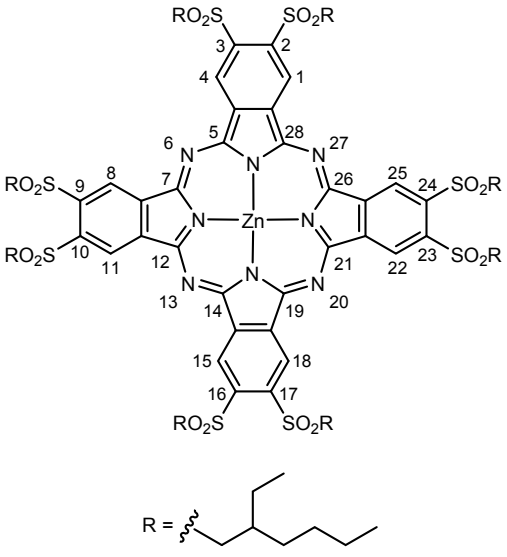

Compound **14** was obtained as a dark green solid (68.9 mg, 0.035 mmol). Yield: 20%

Mp: > 250 ºC.

^{1}H-NMR (300 MHz, $CDCl_3$): δ (ppm) = 10.5 (m, 8H; Pc-H), 3.9-3.6 (m, 16H; SO_2CH_2), 1.8-1.1 (m, 72H; CH_2), 0.86 (t, J = 7.2 Hz, 48H; CH_3).

FT-IR (film): ν (cm^{-1}) = 2956, 2922, 2852 (C-H), 1402, 1374 ($\nu_{st\ as}$ SO_2), 1066 ($\nu_{st\ sim}$ SO_2), 741.

UV-Vis (THF): λ_{max} (nm) (log ε) = 685 (5.4), 620 (4.6), 377 (4.7).

MS (MALDI-TOF, DCTB): *m/z* = 1987.8.

2,3,9,10,16,17-Hexakis(2-ethylhexylsulfonyl)-23-iodo-5,28:14,19-diimino-7,12:21,26- dinitrilo-tetrabenzo[*c, h, m, r*]-[1, 6, 11, 16]tetraazacycloeicosinato-(2$^-$)-*N*^{29}, *N*^{30}, *N*^{31}, *N*^{32} zinc (II) (15)

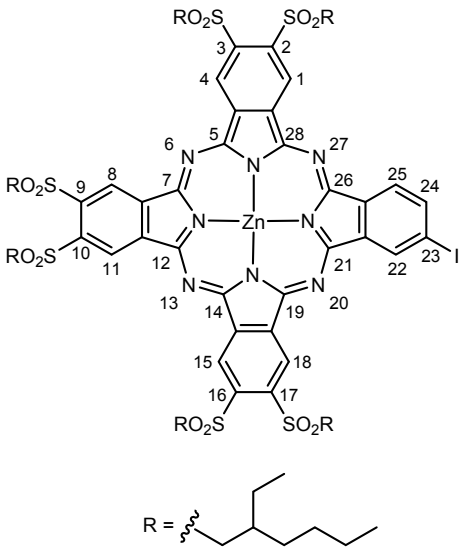

Compound **15** was obtained as a dark green solid. Yield: 25% (76.4 mg, 0.043 mmol).

Mp: > 250 ºC.

^{1}H-NMR (300 MHz, THF-d_8): δ (ppm) = 10.39 (m, 3H; Pc-H), 10.26 (s, 1H; Pc-H), 10.14 (s, 1H; Pc-H), 9.99 (s, 1H; Pc-H), 9.67 (s, 1H; Pc-H), 9.08 (s, 1H; Pc-H), 8.55 (s, 1H; Pc-H), 4.23-3.89 (m, 12H; SO_2CH_2-R), 2.73-2.48 (m, 6H; $SO_2CH_2C\underline{H}R$), 1.85-1.35 (m, 48H; CH_2), 1.15-0.92 (m, 36H; CH_3).

FT-IR (film): ν (cm^{-1}) = 2928, 2860, 1776, 1572, 1464, 1410, 1302 ($\nu_{st\ as}$ SO_2), 1140 ($\nu_{st\ sim}$ SO_2).

UV-Vis (THF): λ_{max} (nm) (log ε) = 701 (5.2), 672 (5.2), 640 (4.7), 608 (4.5), 371 (4.8).

HRMS (MALDI-TOF, DCTB+PPGNa 2000): *m/z* = 1758.4963. $C_{80}H_{111}IN_8O_{12}S_6Zn$ (Exact mass: 1758.4976, molecular weight: 1761.46).

Synthesis of phthalocyanines 16 and 17

A mixture of 4,5-bis(2-ethylhexylthio)phthalonitrile (**12**) (3.0 eq, 0.48 mmol, 200 mg,), 4-iodophthalonitrile (**2**) (1.0 eq, 0.16 mmol, 41.0 mg) and $Zn(OAc)_2$ (1.2 eq, 0.20 mmol, 35.2 mg) in DMAE (2 mL) was stirred at 140 ºC under an argon atmosphere for 16 h. After cooling down to room temperature, the crude was treated with methanol/water (3:1, 20 mL) and then filtered under vacuum. The resulting green solid was then purified by column chromatography on silica gel using hexane/dioxane (8:1) as eluent. The symmetrically substituted Pc **16** was eluted first followed by derivative **17**.

2,3,9,10,16,17,23,24-Octakis(2-ethylhexylthio)-5,28:14,19-diimino-7,12:21,26-dinitrilo-tetrabenzo[*c, h, m, r*]-[1, 6, 11, 16]tetraazacycloeicosinato-(2^-)- N^{29}, N^{30}, N^{31}, N^{32} zinc (II) (16)

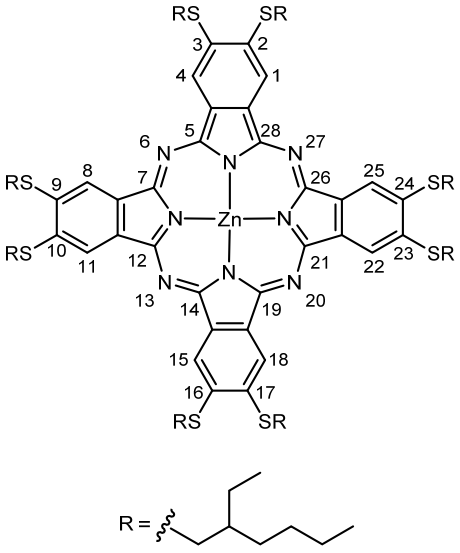

Compound **16** was obtained as a dark green solid (58.7 mg, 0.34 mmol). Yield: 21%

Mp: > 250 ºC.

^{1}H-NMR (300 MHz, $CDCl_3$): δ (ppm) = 9.5-9.0 (m, 8H; Pc-H), 3.54 (m, 16H; SCH_2), 2.05 (br s, 8H; CH), 1.8-0.8 (m, 112H; CH_2, CH_3).

FT-IR (KBr): ν (cm^{-1}) = 2957, 2925, 2856, 1404, 1371, 1066 (ν S-CH_2).

UV-Vis (THF): λ_{max} (nm) (log ε) = 704 (5.7), 640 (4.9), 365 (5.2).

MS (MALDI-TOF, Dithranol): *m/z* = 1731.8.

EA for $C_{96}H_{144}N_8S_8Zn$ (%): calculated = C 66.57, H 8.38, N 6.47, S 14.81. Found: C 66.03, H 8.51, N 6.22, S 13.84.

2,3,9,10,16,17-Hexakis(2-ethylhexylthio)-23-iodo-5,28:14,19-diimino-7,12:21,26-dinitrilo-tetrabenzo[*c, h, m, r*]-[1, 6, 11, 16]tetraazacycloeicosinato-(2$^-$)- N^{29}, N^{30}, N^{31}, N^{32} zinc (II) (17)

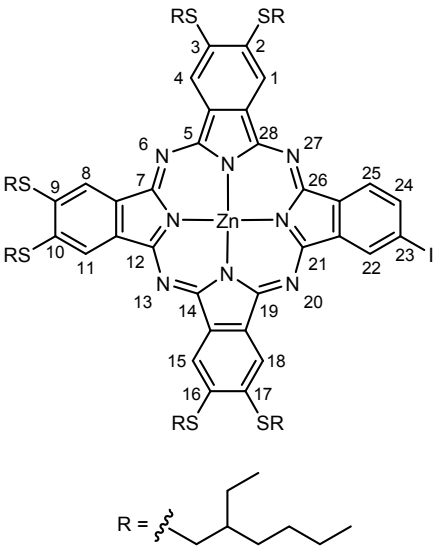

Compound **17** was obtained as a dark green solid. (40.5 mg, 0.026 mmol). Yield: 16%

Mp: > 250 ºC.

^{1}H-NMR (300 MHz, $CDCl_3$): δ (ppm) = 8.66 (m, 4H; Pc-H), 8.40 (m, 2H; Pc-H), 8.03 (m, 3H; Pc-H), 3.61 (m, 12H; SCH_2), 1.90-0.91 (m, 90H; CH, CH_2, CH_3).

FT-IR (KBr): ν (cm^{-1}) = 2960, 2871, 1308, 1143 (ν S-CH_2).

UV-Vis (THF): λ_{max} (nm) (log ε) = 697 (5.5), 672 (5.4), 643 (4.4), 611 (4.3), 375 (4.5).

MS (MALDI-TOF, Dithranol): *m/z* = 1762.5.

EA for $C_{80}H_{111}IN_8S_6Zn$ (%): calculated = C 61.22, H 7.13, N 7.14, S 12.26. Found: C 60.87, H 7.23, N 6.89, S 11.86.

2,3,9,10,16,17-Hexakis(2-ethylhexylsulfonyl)-23-ethynyl-5,28:14,19-diimino-7,12:21,26- dinitrilo-tetrabenzo[*c, h, m, r*]-[1, 6, 11, 16]tetraazacycloeicosinato-(2$^-$)-N^{29}, N^{30}, N^{31}, N^{32} zinc (II) (18)

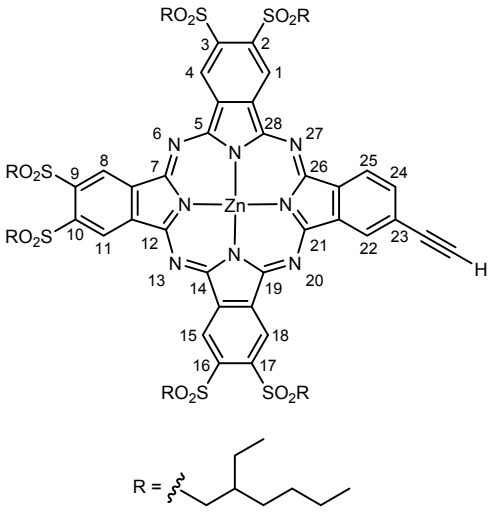

Pc **15** (1.0 eq, 0.044 mmol, 77.2 mg), $Pd(PPh_3)_2Cl_2$ (0.009 mmol, 6.2 mg) and CuI (0.018 mmol, 3.4 mg) were dissolved in a mixture of freshly distilled and deoxygenated NEt_3 (5 mL) and dry THF (5 mL), under an argon atmosphere. To this stirred solution, ethynyltrimethylsilane (1.5 eq, 0.066 mmol, 6.2 mg, 0.009 mL,) was added and the reaction was allowed to proceed at 90 ºC during 20 h. After that time, the solvent was removed under vacuum and the green solid obtained was dissolved in DCM (50 mL), washed with water (3 x 30 mL) and dried over Na_2SO_4.

After filtration of the drying agent, the solvent was vacuum-evaporated and the green solid obtained (0.159 g) was directly dissolved in THF (4 mL) for the next step. A solution of TBAF (2.8 eq, 0.121 mmol, 32.1 mg,) in THF (1 mL) was added to the above obtained THF solution of TMS-ethynyl phthalocyanine. The reaction mixture was stirred at room temperature for 4h. Then, the solvent was removed under vacuum and the solid obtained was submitted to column chromatography on silica gel using hexane/THF (4:1) as eluent to give **18** (14.5 mg, 0.009 mmol) of as a green solid. Yield: 21%,

Mp: > 250 ºC.

^{1}H-NMR (300 MHz, THF-d_8): δ (ppm) = 10.8 (s, 6H; Pc-H), 10.7 (br s, 1H; Pc-H), 10.4 (br s, 2H; Pc-H), 4.01 (s, 1H; alkynyl – H), 2.42 (m, 12H; SO_2CH_2), 1.5-0.8 (m, 90H; CH, CH_2, CH_3).

FT-IR (KBr): ν (cm^{-1}) = 3502 (ν alkynyl-H), 2977, 2893, 1354 ($\nu_{st\ as}$ SO_2), 1202 ($\nu_{st\ sim}$ SO_2), 699.

UV-Vis (THF): λ_{max} (nm) (log ε) = 697 (5.2), 675 (5.1), 640 (4.6), 617 (5.5), 370 (4.8).

HRMS (MALDI-TOF, DCTB+PPGNa 2000): *m/z* = 1592.6263. $C_{82}H_{112}N_8O_8S_6Zn$ (Exact mass: 1592.6275, molecular weight: 1595.59).

Phthalocyanines as monomers for copolymerization

3,6-Bis(trifluoromethanesulfonate)phthalonitrile (19) [377]

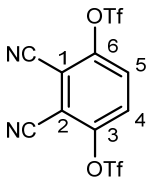

In a dried flask with a septum, 2,3-dicyanohydroquinone (1.0 eq, 3.12 mmol, 0.500 g) was dissolved in 85 mL of dry DCM under argon and dry pyridine (6.0 eq, 18.72 mmol, 1.50 mL) was added. After cooling to -78 ºC, trifluoromethane sulfonic anhydride solution (1M in DCM; 3.0 eq, 9.36 mmol, 9.4 mL) was added dropwise and stirred. The reaction mixture was warmed to room temperature overnight. The reaction mixture was poured into DCM (50 mL), 0.5 N HCl (1 mL) added, and the organic layer separated and evaporated under reduced pressure. The residue was subjected to column chromatography on silica gel with $CHCl_3$ as eluent to give target compound **19** (1.26 g, 2.97 mmol) as white powder. Yield: 95%

Mp: 104-107 ºC (reported: [?] 106-107 ºC).

[377] N. Kobayashi, H. Ogata, N. Nonaka, E. A. Luk'yanets, *Chem. Eur. J.* **2003**, *9*, 5123.

^{1}H-NMR (300 MHz, $CDCl_3$): δ (ppm) = 7.85 (s, 2H; H-4, H-5).

^{19}F-NMR (282 MHz, $CDCl_3$, CF_3COOH): δ (ppm) = -73.3 (s, 6F).

EA for $C_{10}H_2F_6N_2O_6S_2$ (%): calculated = C 28.31, H 0.48, N 6.60, S 15.12. Found = C 28.02, H 0.82, N 7.77, S 15.24.

9,16,23-Tri-*tert*-butyl-1,4-dihydroxy-7,12:21,26-diimino-5,28:14,19-dinitrilo-tetrabenzo[*c,h,m,r*]-[1,6,11,16]tetraazacycloeicosinato-(2$^-$)-*N*^{29},*N*^{30},*N*^{31},*N*^{32} zinc (II) (only one regioisomer is named) (20)

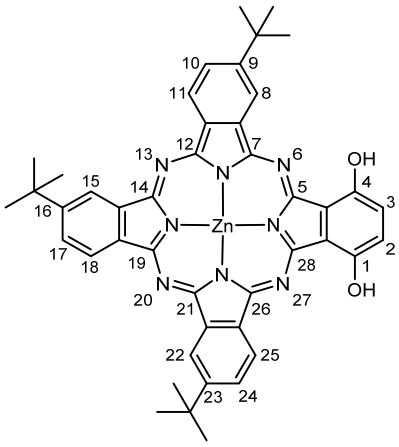

4-*tert*-butylphthalonitrile (3.0 eq, 3.26 mmol, 600.0 mg), 2,3-dicyanohydroquinone (1.0 eq, 1.09 mmol, 174 mg) and $Zn(OAc)_2$ (1.2 eq, 1.30 mmol, 240 mg) in a 3:1 *o*-DCB/DMF mixture (8 mL) were heated to reflux under an argon atmosphere for 16 h. After cooling to room temperature, the solvents were removed and the product was extracted into DCM (3x75 mL). The extract dried over anhydrous $MgSO_4$, filtered and evaporated. The resulting blue solid was purified by column chromatography on silica gel using hexane/dioxane (6:1, 5:1, 4:1) as the carrier phase. The symmetrically *tert*-butyl substituted phthalocyanine **4** was eluted first, and obtained as a blue solid (yield: 21%, 137.2 mg, 1.71 mmol). It was followed by the unsymmetrical derivative Pc **20** (42.3 mg, 0.05 mmol). Yield: 5%.

Mp: > 250 ºC.

^{1}H-NMR (300 MHz, THF-d_8): δ (ppm) = 9.60-9.51 (m, 1H; OH), 9.37 (m, 7H; Pc-H, OH), 8.32-8.17 (m, 3H; Pc-H), 7.52-7.40 (m, 2H; Pc-H), 1.98-1.90 (m, 27H; $C(CH_3)_3$).

UV-Vis (THF): λ_{max} (nm) (log ε) = 706 (4.9), 635 (4.5), 345 (4.7).

HRMS (MALDI-TOF, DCTB+PPGNa 2000): *m/z* = 776.2567. $C_{44}H_{40}N_8O_2Zn$ (Exact mass: 776.2584, molecular weight: 778.24).

9,16,23-Tri-*tert*-butyl-1,4-bis(trifluoromethanesulfonate)-7,12:21,26-diimino-5,28:14,19-dinitrilo-tetrabenzo[*c,h,m,r*]-[1,6,11,16]tetraazacycloeicosinato-(2⁻)-*N*^{29},*N*^{30},*N*^{31},*N*^{32} zinc (II) (only one regioisomer is named) (21)

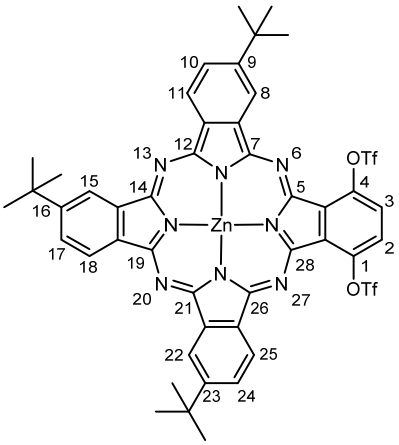

In a dried flask with a septum, Pc **20** (1.0 eq, 0.13 mmol, 100 mg) was dissolved in 2.0 mL of dry DCM under argon, and dry pyridine (6.0 eq, 0.77 mmol, 0.062 mL) was added. After cooling to -78 ºC, trifluoromethane sulfonic anhydride solution (1M in DCM; 3.0 eq, 0.385 mmol, 0.385 mL) was added dropwise. The reaction mixture was warmed to room temperature and stirred overnight. Then, it was poured into DCM (50 mL), 0.5 N HCl (0.1 mL) added, and the organic layer separated and evaporated under reduced pressure. The resulting blue solid was purified by column chromatography on silica gel using hexane/dioxane (4:1) as the carrier phase. The Pc **21** was obtained as a blue solid (87.1 mg, 0.084 mmol). Yield: 65%.

Mp: > 250 ºC.

^{1}H-NMR (300 MHz, THF-d_8): δ (ppm) = 9.58-9.50 (m, 1H; Pc-H), 9.36-8.89 (m, 5H; Pc-H), 8.41-8.16 (m, 3H; Pc-H), 7.98-7.94 (m, 2H; Pc-H), 1.94-1.88 (m, 27H; $C(CH_3)_3$).

^{19}F-NMR (282 MHz, THF-d_8, CF_3COOH): δ (ppm) = -73.7 (s, 6F).

UV-Vis (THF): λ_{max} (nm) (log ε) =688 (4.9), 654 (4.8) 593 (4.3), 354 (4.6).

HRMS (MALDI-TOF, DCTB+PPGNa 1000): *m/z* = 1040.1531. $C_{46}H_{38}F_6N_8O_6S_2Zn$ (Exact mass: 1040.1546, molecular weight: 1042.35).

3,6-Dimethoxyphthalonitrile (22)

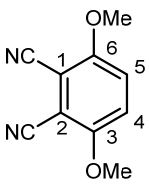

To a stirred solution of 2,3-dicyanohydroquinone (1.0 eq, 3.12 mmol, 0.50 g) in 2-butanone (15 mL), was added oven-dry potassium carbonate (9.0 eq, 28.1 mmol, 3.80 g). After stirring for 15min at room temperature, dimethyl sulphate (8.0 eq, 25.0 mmol, 2.4 mL) was added. The reaction mixture was refluxed for 18h, cooled to room temperature and the solid was filtered. Recrystallization from acetic acid gave **22** (0.582 g, 3.09 mmol) as a white solid. Yield: 99%.

Mp: 271-273 ºC (reported: 273-274 ºC).

^{1}H-NMR (300 MHz, $CDCl_3$): δ (ppm) = 7.18 (s, 2H; H-4, H-5), 3.93 (s, 6H; CH_3)

^{13}C-NMR (75.5 MHz, $CDCl_3$): δ (ppm) = 160.6 (C-3, C-6), 118.1 (C-4, C-5), 112.8 (CN), 105.3 (C-1, C-2), 53.5 (OCH_3).

MS (EI): *m/z* = 188 $[M]^+$ (100%). $C_{10}H_8N_2O_2$ (Exact mass: 188.06, molecular weight: 188.19).

3,6-Bis(4'-methylbenzenesulfonate)phthalonitrile (23)[378]

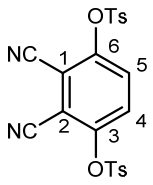

2,3-dicyanohydroquinone (1.0 eq, 3.1 mmol, 0.50 g), K_2CO_3 (4.2 eq, 13.1 mmol, 1.81 g), and tosyl chloride (2.3 eq, 7.13 mmol, 1.36 g) were dissolved in 5 mL of acetone and the mixture was stirred under reflux for 2 h. Then the mixture was poured into water (10 mL) and stirred for 1 h. The residue was filtered, washed with water and dried. The title compound was obtained as a pale brown powder (1.17 g, 2.50 mmol). Yield: 80%

^{1}H-NMR (300 MHz, $CDCl_3$): δ (ppm) = 7.81 (d, *J* = 8.0 Hz, 4H; tosyl-H), 7.78 (s, 2H; H-4, H-5), 7.39 (d, *J* = 8.0 Hz, 4H; tosyl-H) 2.48 (s, 6H; CH_3)

^{13}C-NMR (75.5 MHz, $CDCl_3$): δ (ppm) = 149.0, 147.4, 130.7, 130.5, 129.4, 128.8, 112.1, 110.6, 21.9 (CH_3).

FT-IR (KBr): ν (cm^{-1}) = 3432, 3239, 3085, 2243, 2226 (ν_{st} C≡N), 1504, 1449, 1315, 1279, 1204, 1174, 1142, 1021, 1004, 979, 934, 847, 749, 694, 638, 614.

9,16,23-Tri-*tert*-butyl-1,4-bis(4'-methylbenzenesulfonate)-7,12:21,26-diimino-5,28:14,19-dinitrilo-tetrabenzo[*c,h,m,r*]-[1,6,11,16]tetraazacycloeicosinato-(2$^-$)-*N*^{29},*N*^{30},*N*^{31},*N*^{32} zinc (II) (only one regioisomer is named) (25)

4-*tert*-butylphthalonitrile (3.0 eq, 2.71 mmol, 500 mg), phthalonitrile **23** (1.0 eq, 0.90 mmol, 424 mg) and $Zn(OAc)_2$ (1.2 eq, 1.08 mmol, 199.2 mg) in a 3:1 *o*-DCB/DMF mixture (8.0 mL) were heated to reflux under an argon atmosphere for 16 h. After cooling to room temperature, the solvents were removed and the product was extracted into DCM (3x75 mL). The extract dried over anhydrous $MgSO_4$, filtered and evaporated. The resulting green solid was purified by column chromatography on silica gel using hexane/dioxane (4:1) as the carrier phase. Pc **25** was obtained as a green solid (78.6 mg, 0.072 mmol). Yield: 8%.

[378] G. Mbambisa, P. Tau, E. Antunes, T. Nyokong, *Polyhedron* **2007**, *26*, 5355.

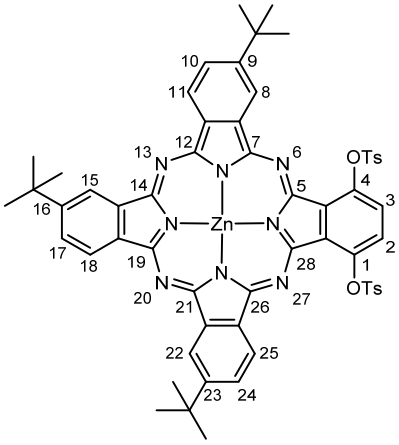

Mp: > 250 ºC.

^{1}H-NMR (300 MHz, THF-d_8): δ (ppm) = 9.58-9.50 (m, 1H; Pc-H), 9.36-8.89 (m, 5H; Pc-H), 8.41-8.16 (m, 3H; Pc-H), 7.98-7.94 (m, 2H; Pc-H), 1.94-1.88 (m, 27H; $C(CH_3)_3$).

UV-Vis (THF): λ_{max} (nm) (log ε) = 688 (4.9), 654 (4.8) 593 (4.3), 354 (4.6).

MS (MALDI-TOF, DCTB): *m/z* = 1084.3

1,4-Dimethoxy-2,3-dimethylbenzene (26)

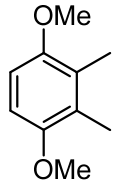

To a suspension of sodium hydride (60%, 3.0 eq, 109 mmol, 4.40 g) in 100 mL of freshly distilled DMF was added 5.00 g (1.0 eq, 36.2 mmol) of commercially available 2,3-dimethylhydro-*p*-benzoquinone. The mixture was stirred for 10 min and then cooled to 0 °C. A solution of 11.8 g (2.3 eq, 83.1 mmol, 5.2 mL) of methyl iodide in 50 mL of dry DMF was added dropwise at 0 °C. After 5 h at 0 °C and 2h at room temperature, the reaction mixture was poured into 1 L of water and filtered. Recrystallization of the residue from methanol gave 5.35 g (32.2mmol) of **26**. Yield: 89%.

Mp: 78-80 ºC (reported: 73-74 ºC).

^{1}H-NMR (300 MHz, $CDCl_3$): δ (ppm) = 6.67 (s, 2H; phenyl-H), 3.79 (s, 6H; OCH_3), 2.18 (s, 6H; CH_3).

^{13}C-NMR (75.5 MHz, $CDCl_3$): δ (ppm) = 152.1, 126.8, 107.9, 56.2 (OCH_3), 12.2 (CH_3).

FT-IR (film): ν (cm^{-1}) = 2922, 1481, 1257, 1117, 1099, 800.

HRMS (EI): *m/z* = 166.0990 $[M]^+$ (100%). $C_{10}H_{14}O_2$ (Exact mass: 166.0994, molecular weight: 166.22).

2,3-Bis(bromomethyl)-1,4-dimethoxybenzene (27)

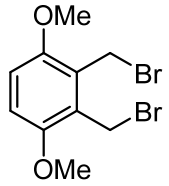

To a stirred mixture of compound **26** (1.0 eq, 32.2 mmol, 5.35 g) and NBS (2.5 eq, 80.6 mmol, 14.36 g) in CCl_4 (130 mL) was added a solution of benzoil peroxide (0.1 eq, 3.22 mmol, 0.78 g) in 15 mL of CCl_4 over 20 min. At that point, the mixture was refluxed during 3h. When the reaction was completed, the solution was cooled to room temperature, filtered and the residue washed with CCl_4. The filtrate was then

concentrated under vacuum, and the residue was purified by column chromatography (hexane/EtOAc, 10:1). The pale yellow solid was recrystallized from methanol to afford **27** (8.24 g, 25.4 mmol) as a white solid. Yield: 79%

Mp: 149-150 ºC (reported: 150-152 ºC).

^{1}H-NMR (300 MHz, $CDCl_3$): δ (ppm) = 6.84 (s, 2H; phenyl-H), 4.74 (s, 4H; CH_2Br), 3.86 (s, 6H; OCH_3).

^{13}C-NMR (75.5 MHz, $CDCl_3$): δ (ppm) = 151.9, 126.6, 112.3, 56.2 (OCH_3), 24.1.

3,4-Dibromothiophene-1,1-dioxide (29)

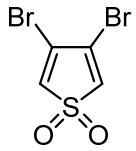

To a 250-mL three-neck round-bottom flask fitted with a dropping funnel and a thermometer was added 10 mL (100 mmol) of 33% H_2O_2 and the mixture was stirred in a $CaCl_2$-ice bath (-15 °C). Trifluoroacetic anhydride (185 mmol, 25.0 mL) was added dropwise so that the temperature was kept below 5 ºC. The solution was stirred for another 10 min, and 3,4-dibromothiophene (12.4 mmol, 3.0 g) in DCM (5 mL) was added. The mixture was stirred for 3h at room temperature. Then, the solution was transferred to an ice bath, and saturated Na_2CO_3 (250 ml) was slowly added to bring the pH up to around 5. The organic layer was separated and the aqueous layer was extracted with DCM (25 ml) four times. The organic solutions were combined and washed with saturated solution of Na_2CO_3 (2x20 ml) and water (2x20 ml), then dried over MgSO4. The solvent was evaporated and the remaining yellow oil was mixed with 10 mL of ethanol and stored at -5 ºC. After 12h, pale yellow crystals were washed with cold ethanol. Recrystallization from ethanol led to **29** (2.38 g, 8.68 mmol) as yellow crystals. Yield 70%.

Mp: 102-104 ºC (reported: 104-106 ºC).

^{1}H-NMR (300 MHz, $CDCl_3$): δ (ppm) = 6.83 (s, 2H).

^{13}C-NMR (75.5 MHz, $CDCl_3$): δ (ppm) = 130.7, 128.9.

6,7-Dibromonaphthalene-1,4-dione (30)

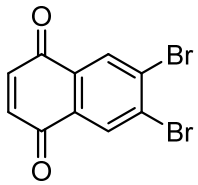

3,4-Dibromothiophene-1,1-dioxide (1.0 eq, 2.77 mmol, 0.76 g) and *p*-benzoquinone (10.0 eq, 27.7 mmol, 3.00 g) were dissolved in 140 mL of acetic acid and refluxed for 2 days. The solution was then poured into 100 mL of water. The resulting suspension was extracted with $CHCl_3$ (3x75 mL). The organic layers were separated, then washed with water (2x100 mL), dried over $MgSO_4$ and the solvent evaporated to

obtain the crude product. The product was purified by column chromatography on silica gel (hexane:DCM, 1:1) and recrystallized from ethanol to yield and ivory solid (0.44 g, 1.39 mmol). Yield: 50%

Mp: 171-173 ºC (reported: 171-172 ºC).

^{1}H-NMR (300 MHz, $CDCl_3$): δ (ppm) = 8.30 (s, 2H), 6.99 (s, 2H)

^{13}C-NMR (75.5 MHz, $CDCl_3$): δ (ppm) = 183.4 (C=O), 138.8, 132.1, 131.9, 131.2.

FT-IR (film): ν (cm^{-1}) = 2249, 1655 (ν_{st} C=O).

MS (EI): *m/z* = 315 $[M+H]^+$ (100%). $C_{10}H_4Br_2O_2$ (Exact mass: 313.86, molecular weight: 315.95).

6,7-Dibromo-1,4-dimethoxynaphthalene (31)

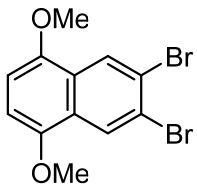

To a suspension naphthoquinone **30** (1.0 eq, 0.95 mmol, 300.0 mg) in AcOEt (1.8 mL), Et_2O (18.0 mL), and water (18.0 mL) at room temperature was added $Na_2S_2O_4$ (5.0 eq, 4.75 mmol, 998.0 mg) and the reaction mixture was stirred vigorously for 3h. Upon consumption of starting material (TLC, heptane:DCM), the biphasic reaction mixture was extracted with AcOEt (3x40 mL), the combined organic layers washed with brine (30 mL), dried ($MgSO_4$), and concentrated. The resulting oil was then dissolved in dry DMF (9 mL) and cooled to -15 ºC. 80.0 mg of sodium hydride (2.1 eq, 3.32 mmol) were added portionwise to the reaction mixture, and then MeI (2.2 eq, 2.08 mmol, 0.09 mL), was added dropwise over 5 min, and the reaction mixture was stirred at -15 ºC for 1h. The reaction mixture was then quenched with sat. aqueous NH_4Cl (20 mL) and the biphasic reaction mixture was extracted with AcOEt (3x20 mL), and the combined organic layers washed with brine (40 mL), dried ($MgSO_4$), and concentrated. Flash column chromatography (silica gel, heptane:DCM, 10:1) gave methyl-protected hydronaphtoquinone **31** as an off-white solid. The product was washed with MeOH to afford a white solid (246.4 mg, 0.71 mmol). Yield: 75%.

^{1}H-NMR (300 MHz, $CDCl_3$): δ (ppm) = 8.46 (s, 2H), 6.69 (s, 2H), 3.93 (s, 6H, OCH_3).

^{13}C-NMR (75.5 MHz, $CDCl_3$): δ (ppm) = 148.5, 127.1, 126.1, 122.4, 104.6, 55.9 (OCH_3).

5,8-Dimethoxynaphthalene-2,3-dicarbonitrile (32)

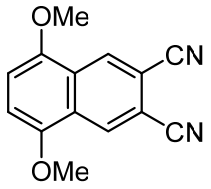

In a Schlenk tube under argon, compound **31** (1.0 eq, 0.751 mmol, 260 mg), $Pd(PPh_3)_4$ (33% mol, 0.248 mmol, 287 mg) and zinc(II) cyanide (2.0 eq, 1.502 mmol, 177 mg) were introduced. Freshly distilled DMF (8.0 mL) was added and the mixture was deaerated over 30min. After that, the mixture was stirred at 120 ºC during 12h. After this time, concentrated ammonia was added (50 mL), and the solid residues were filtered, dried, and directly purified by column chromatography of silica gel using hexane:DCM 2:1 as eluent, affording **32** (144 mg 0.601 mmol) as a yellow solid. Yied: 80%

Mp: 240-242 ºC.

^{1}H-NMR (300 MHz, $CDCl_3$): δ (ppm) = 8.59 (s, 2H), 6.98 (s, 2H), 3.99 (s, 6H, OCH_3).

^{13}C-NMR (75.5 MHz, $CDCl_3$): δ (ppm) = 149.1, 130.5, 125.8, 116.4, 109.7, 108.9, 56.2 (OCH_3).

MS (GC-EI): *m/z* = 238.7 $[M]^+$ (13%), 223.05 $[M\text{-}CH_3]^+$ (100%). $C_{14}H_{10}N_2O_2$ (Exact mass: 238.07, molecular weight: 238.25).

11,18,25-Tri-*tert*-butyl-2,5-dimethoxy-9,14:23,28-diimino-7,30:16,21-dinitrilo-tribenzo[*h,m,r*]-naphtho[*c*]-[1,6,11,16]tetraazacycloeicosinato-(2$^-$)-*N*^{29},*N*^{30},*N*^{31},*N*^{32} zinc (II) (only one regioisomer is named) (33)

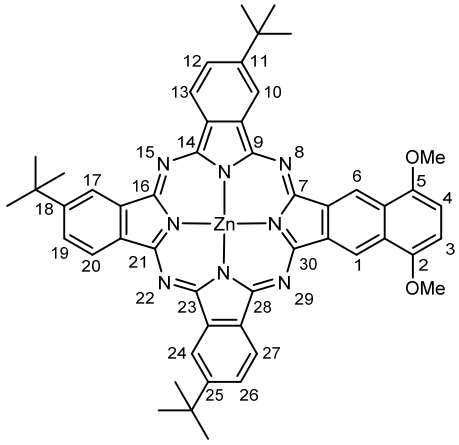

4-*tert*-butylphthalonitrile (3.0 eq, 1.76 mmol, 325 mg), compound **32** (1.0 eq, 0.59 mmol, 140 mg) and $Zn(OAc)_2$ (1.2 eq, 0.71 mmol, 130 mg) in DMAE (5.0 mL) and drops of DBU, were heated to reflux under an argon atmosphere for 16 h. After cooling to room temperature, the solvents were removed and the product was extracted into DCM (3x100 mL). The extract dried over anhydrous $MgSO_4$, filtered and evaporated. The resulting blue solid was purified by column chromatography on silica gel using hexane/dioxane (4:1) as the carrier phase. The symmetrically *tert*-butyl substituted phthalocyanine **4** was eluted first, and obtained as a green solid (yield: 25%, 88.5 mg, 0.11 mmol). It was followed by the unsymmetrical derivative Pc **33** (104.2 mg, 0.12 mmol). Yield: 21%.

Mp: > 250 ºC.

^{1}H-NMR (300 MHz, THF-d_8): δ (ppm) = 9.54 (m, 3H; Pc-H), 9.31 (m, 3H; Pc-H), 8.28 (m, 3H; Pc-H), 6.93 (m, 2H; Pc-H), 5.83 (m, 2H; Pc-H), 4.21-4.03 (m, 6H; OCH_3) 1.88 (m, 27H; $C(CH_3)_3$).

UV-Vis (THF): λ_{max} (nm) (log ε) = 697 (5.4), 628 (4.7), 347 (4.9).

HRMS (MALDI-TOF, Ditranol+PEGNa 600+PEGNa 1000): *m/z* = 854.3025. $C_{50}H_{46}N_8O_2Zn$ (Exact mass: 854.3030, molecular weight: 856.35).

11,18,25-Tri-*tert*-butyl-9,14:23,28-diimino-7,30:16,21-dinitrilo-tribenzo[*h,m,r*]-naphthoquinone[*c*]-[1,6,11,16]tetraazacycloeicosinato-(2$^-$)-*N*^{29},*N*^{30},*N*^{31},*N*^{32} zinc (II) (only one regioisomer is named) (35)

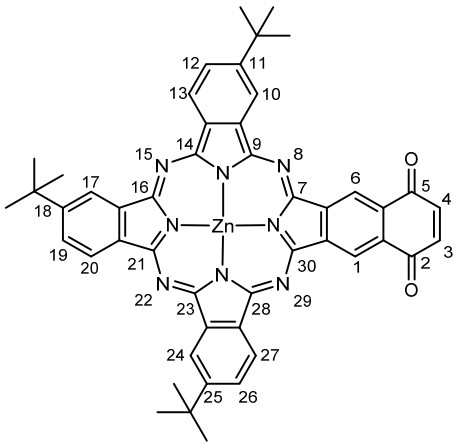

A 1M solution of BBr_3 in DCM (11.0 eq, 0.195 mmol, 0.2 mL) was slowly added to a solution of Pc **33** (1 eq, 0.018 mmol, 16.7 mg) in 1 mL of anhydrous DCM at -78 ºC under argon atmosphere. The green mixture was then stirred and allowed to cool to room temperature. After that, the reaction mixture was stirred at 30 ºC during 12h. Then, the mixture was poured over 10 mL of ice, and the product was extracted into DCM, and the organic layer dried over $MgSO_4$, filtered and evaporated. The title compound was obtained as a green solid (13.4 mg, 0.162 mmol). Yield: 83%

Mp: > 250 ºC.

^{1}H-NMR (300 MHz, THF-d_8): δ (ppm) = 9.60-9.51 (m, 1H; OH), 9.37 (m, 7H; Pc-H, OH), 8.32-8.17 (m, 3H; Pc-H), 7.52-7.40 (m, 2H; Pc-H), 1.98-1.90 (m, 27H; $C(CH_3)_3$).

UV-Vis (THF): λ_{max} (nm) (log ε) = 688 (4.9), 654 (4.8) 593 (4.3), 354 (4.6).

MS (MALDI-TOF, DCTB): *m/z* = 824.3

5,8-Dihydroxynaphthalene-2,3-dicarbonitrile (36)

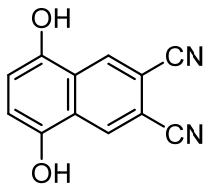

A solution of compound **32** (1.0 eq, 0.42 mmol, 100 mg) in 10 mL of dry DCM was slowly added to a 1M solution of BBr_3 (11.0 eq, 4.61 mmol, 4.6 mL) in DCM at -78 ºC. The mixture was then stirred at 0 ºC for 6h, and 8h at room temperature. Then, the mixture was poured over 25 mL of ice, and the product was extracted into chloroform, and the organic layer dried over MgSO4, filtered and evaporated. The title compound was obtained as a brown sticky solid (21.3 mg, 0.10 mmol). Yield: 24%

^{1}H-NMR (300 MHz, $CDCl_3$): δ (ppm) = 8.64 (s, 2H), 6.35 (s, 2H).

^{13}C-NMR (75.5 MHz, $CDCl_3$): δ (ppm) = 146.1, 127.5, 115.8, 110.4, 109.7, 108.9.

MS (GC-EI): *m/z* = 211.4 $[M+H]^+$ (100%). $C_{12}H_6N_2O_2$ (Exact mass: 210.04, molecular weight: 210.19).

1.5.1.2 Synthesis of Pc-containing, conjugated polymers

PPV- and PT-type copolymers with phthalocyanines as light-harvesting moieties

Pc-PPV 38

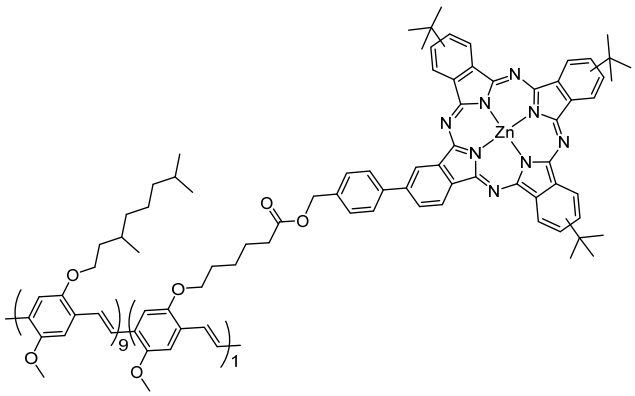

Copolymer **37** (50.0 mg, 0.018 mmol of carboxylic acid functionalities) was dissolved in dry DCM (12 mL) and cooled down to 0°C. Hydroxy-functionalized Zn(II)Pc **5** (18.0 mg, 0.022 mmol) and DCC (4.5 mg, 0.022 mmol) were added. Subsequently DMAP (3.0 mg, 0.022 mmol) in dry DCM (1 mL) was added dropwise over a period of 15 min under N_2 atmosphere. The reaction was allowed to proceed for 1h at 0 °C and, additionally, for 24h at room temperature, after which time the product was precipitated by dropwise addition of the crude into cold MeOH (200 mL). The resulting red copolymer was filtered off, washed extensively with cold MeOH and acetone and dried at room temperature under reduced pressure, giving a dark red-blue, fibrous polymer. Yield: 86%.

SEC (THF): Mw = $3.1 \cdot 10^5$ g·mol^{-1}, Mw/Mn = 4.4.

^{1}H-NMR (300 MHz, THF-d_8): δ (ppm) = 9.6–9.4 (Pc-H), 8.30 (Pc-H), 8.13 (Pc-H), 8.00 (Pc-H), 7.90 (Pc-H), 7.6–7.4 (PPV), 7.3–7.1 (PPV), 5.28 (Pc-CH_2O), 4.1–3.8, 2.4–2.3, 1.8-0.7.

UV-Vis (THF): λ_{max} (nm) = 676, 510 (0.28/1 absorption ratio).

FT-IR: ν (cm^{-1}) = 3058, 2953, 2926, 2868, 1733 (ν_{st} C=O), 1503, 1464, 1413, 1384, 1351, 1256, 1204 (ν_{as} C–O–C), 1092 (ν_s C–O–C), 1038, 968, 920, 860, 801.

Pc-PPV 41

Alkynyl-PPV **39** (50 mg) was dissolved before adding Zn(II)Pc **7** (0.036 mmol, 31.0 mg), distilled PMDETA (0.0017 mmol, 0.3 mg) and CuBr (0.0020 mmol, 0.3 mg). After purification, PPV-Pc **41** (60 mg) was isolated.

GPC (THF): Mw = $3.1 \cdot 10^5$ g·mol^{-1}, Mw/Mn = 4.0

^{1}H-NMR (300 MHz, THF-d_8): δ (ppm) = 9.58–9.38, 8.30, 8.11, 7.90, 7.55– 7.4, 7.3–7.1, 5.70, 5.21, 4.1–3.8, 2.4–2.3 and 1.8–0.7.

FT-IR: ν (cm^{-1}) = 3058, 2959, 2927, 2869, 1737, 1504, 1464, 1414, 1385, 1351, 1260, 1205, 1027, 970, 862 and 800.

UV-Vis: λ_{max} (THF, nm) = 676, 509, 352; λ_{max} (CB, nm) = 691, 510, 358; λ_{max} (thin film, nm) = 692, 494.

Pc-PT 42

Alkynyk-PT **40** (60 mg) was dissolved, and Pc **7** (0.070 mmol, 61 mg), PMDETA (0.0035 mmol, 0.6 mg) and CuBr (0.0035 mmol, 0.5 mg) were subsequently added. After purification, Pc-PT **42** (36 mg) was isolated.

GPC (THF): Iw = 58 600 g·mol-1, Mw/Mn = 1.8

^{1}H-NMR (300 MHz, THF-d_8): δ (ppm) = 8.14, 7.97, 7.76, 7.44, 7.35, 6.96, 6.89, 6.83, 6.79, 5.60, 5.06, 2.80, 2.67, 2.40, 2.04, 1.91, 1.77, 1.34, 1.27, 0.91.

FT-IR: ν (cm^{-1}) = 2957, 2927, 2856, 1739, 1644, 1511, 1487, 1456, 1390, 1363, 1331, 1261, 1231, 1186, 1152, 1092, 1048, 1024, 920, 820, 800, 748.

UV-Vis: λ_{max} (THF, nm) = 677, 459, 352; λ_{max} (CB, nm) = 691, 458, 358; λ_{max} (thin film, drop-cast from THF, nm) = 694, 564; λ_{max} (thin film, drop-cast from CB, nm) = 692, 523.

Polymers with electron-acceptor phthalocyanines: Double-cable approach

PPV-OMs 43

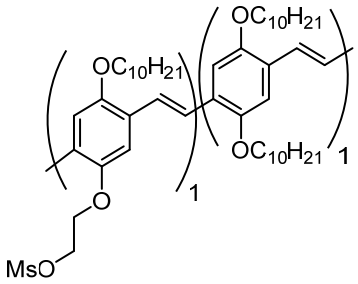

To a solution of hydroxy-PPV derivative (0.05 mmol, 44.2 mg) and triethylamine (0.138 mmol, 13.9 mg, 0.019 mL) in dry THF (2.7 mL), was added dropwise a solution of methanesulfonyl chloride (0.115 mmol, 13.1 g, 0.009 mL) in dry THF (0.9 mL). The mixture with stirred overnight at room temperature. Upon completion, the reaction was quenched with saturated aqueous NH_4Cl solution. The organic solvents were removed under vacuum and the left aqueous solution was extracted with $CHCl_3$. The combined organic portions were washed with brine and then dried over anhydrous Na_2SO_4. The filtered solution was concentrated under vacuum to give the product **43** as an orange solid.

^{1}H-NMR (300 MHz, THF-d_8): δ (ppm) = 7.6-6.9 (br s; aromatic-H PPV), 4.6-4.3 (m, 2H; C$\underline{H}_2$OSO$_2$CH$_3$), 4.05 (br s; alkenyl-H PPV, OCH$_2$), 3.03 (s, 3H; SO$_2$CH$_3$), 2.0-0.9 (m; CH$_2$, CH$_3$ PPV).

PPV-N_3 44

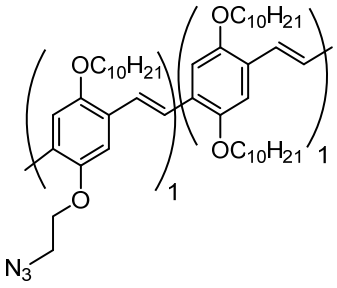

Sodium azide (3.80 mmol, 24.8 mg) and the mesylated polymer **43** (0.038 mmol, 31.0 mg) were dissolved in 7 mL of DMF and heated to 90 ºC for 12 h. After cooling down to room temperature, the crude polymer was treated with water, filtered, washed with methanol and vacuum-dried. The product was purified by size exclusion chromatography to give an orange polymer **44**.

^{1}H-NMR (300 MHz, THF-d_8): δ (ppm) = 7.6-6.6 (br s; aromatic-H PPV), 4.3 (br s; alkenyl-H PPV, OCH$_2$), 4.0 (m, 2H; C$\underline{H}_2$N$_3$), 3.0-0.9 (m; CH$_2$, CH$_3$ PPV).

Main-chain Pc-copolymers: Testing copolymerization conditions

9,16,23-Tri-*tert*-butyl-1,4-di(thiophen-2-yl)-7,12:21,26-diimino-5,28:14,19-dinitrilo-tetrabenzo[*c,h,m,r*]-[1,6,11,16]tetraazacycloeicosinato-(2$^-$)-N^{29},N^{30},N^{31},N^{32} zinc (II) (only one regioisomer is named) (43)

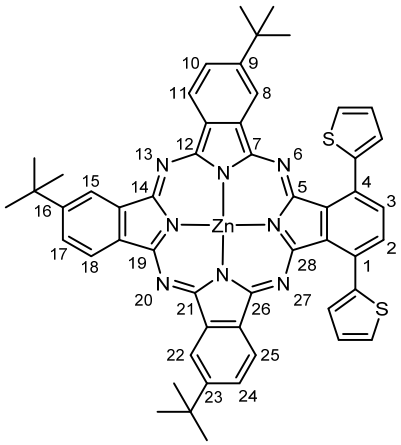

In a Schlenk tube under argon were introduced Pc **21** (1.0 eq, 0.029 mmol, 30.0 mg), $Pd(PPh_3)_4$ (20% mol, 0.015 mmol, 13.3 mg), and LiCl (6.0 eq, 0.172 mmol, 7.3 mg). Dry dioxane (1.0 mL) and 2-(tributylstannyl)thiophene (2.5 eq, 0.072 mmol, 0.023 mL) were added and the reaction mixture was stirred at 110 ºC during 8h. After cooling to room temperature, the solvents were removed and the product was extracted into DCM (3x50 mL). The extract dried over anhydrous $MgSO_4$, filtered and evaporated. The resulting blue solid was purified by column chromatography on silica gel using hexane/dioxane (4:1) as the carrier phase. The target compound **43** was obtained as a blue solid (16.8 mg, 0.018 mmol). Yield: 64%,

Mp: > 250 ºC.

^{1}H-NMR (300 MHz, THF-d_8): δ (ppm) = 9.53-9.30 (m, 4H), 9.07 (m, 1H), 8.95-8.91 (m, 1H), 8.48-8.15 (m, 7H), 7.93 (m, 2H), 7.72-7.65 (m, 2H), 1.81-1.70 (m, 27H; $C(CH_3)_3$,

UV-Vis (THF): λ_{max} (nm) (log ε) = 684 (4.9), 613 (4.3), 348 (4.6).

MS (MALDI-TOF, DCTB): *m/z* = 908.3

1.5.2 Dye-sensitized solar cells

Synthesis of electron-acceptor Pc sensitizers

4-(Bromomethyl)phthalonitrile (44)

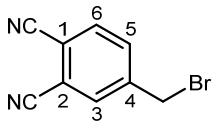

A mixture of 4-methylphthalonitrile (43.6 mmol, 6.20 g), NBS (130 mmol, 23.3 g), and AIBN (1.84 mmol, 0.30 g) in degassed CCl_4 (350 ml) was heated at reflux under argon for 4h under irradiation by a high-pressure 125 W mercury lamp (>300 nm). The reaction was monitored by ^{1}H-NMR until the disappearance of the starting material. After cooling down, succinimide as a by-product was filtered off and washed with CCl_4. Afterwards, the solvent was evaporated affording a red oil residue consisting of mono-, di-, and tribromination products (in an approximate 1:2:1 ratio by ^{1}H-NMR) at the benzylic position. The crude mixture was dissolved in dry THF (50 ml) and cooled at 0 ºC with an ice bath. Then, diethyl phosphite (17.9 mmol, 2.30 g) and DIPEA (17.0 mmol, 2.20 g) were added dropwise. The solution was allowed to reach room temperature and left stirring for 3h. The reaction was monitored by TLC and by ^{1}H-NMR until the disappearance of the di- and tribromination products. Then, the solvent was evaporated and the residue was dissolved in $CHCl_3$ (100 ml). The solution was washed with a 0.1M solution of HCl (3x50 ml), then with a saturated solution of $NaHCO_3$ (2x50 ml), and finally with brine (2x50 ml). After drying over Na_2SO_4 and filtration, the solvent was removed under vacuum affording a red oil that became solid upon standing. The crude was purified on silica gel column chromography (DCM) to yield 4-(bromomethyl)phthalonitrile (**44**) (6.46 g, 29.2 mmol) as a beige solid. Yield: 67%.

Mp: 65-67 ºC.

^{1}H-NMR (300 MHz, $CDCl_3$): δ (ppm) = 7.84 (d, $J_{m,3\text{-}5}$ =1.7 Hz, 1H; H-3), 7.80 (d, $J_{o,5\text{-}6}$ =8.1 Hz, 1H; H-6), 7.75 (dd, $J_{o,5\text{-}6}$ =8.1, $J_{m,3\text{-}5}$ =1.7 Hz, 1H; H-5), 4.48 (s, 2H; CH_2Br).

^{13}C-NMR (75.5 MHz, $CDCl_3$): δ (ppm) = 144.0 (C-5), 134.0 (C-4), 133.9 (C-6), 133.7 (C-3), 116.4 (C-1), 115.4 (C-2), 115.1 (CN), 115.0 (CN), 29.8 (CH_2Br).

MS (EI): *m/z* = 221 $[M+2]^+$ (4%), 219 $[M]^+$ (4%). $C_9H_5BrN_2$ (Exact mass: 219.96, molecular weight: 221.06).

4-(Hydroxymethyl)phthalonitrile (45)

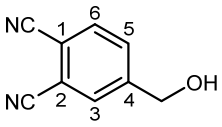

4-(Bromomethyl)phthalonitrile (**44**) (9.82 mmol, 2.17 g) was added to a suspension of calcium carbonate (3.92 g) in dioxane - water (1:1.5, 80 ml) and the mixture was stirred at reflux temperature for 24 h. The reaction mixture was allowed to cool, and then filtered from $CaCO_3$. The compound was extracted with Et_2O (3x150 ml). The combined organic layers were dried over Na_2SO_4 and concentrated under reduced pressure giving a pale yellow oil that became solid upon standing. Recrystallization from toluene (15 ml) afforded **45** (0.99 g, 6.28 mmol) as a white solid. Yield: 64%.

Mp: 49-51 ºC.

^{1}H-NMR (300 MHz, $CDCl_3$): δ (ppm) = 7.85 (bs, 1H; H-6), 7.80-7.70 (m, 2H; H-3, H-5), 4.84 (bs, 2H; CH_2OH).

^{13}C-NMR (75.5 MHz, $CDCl_3$): δ (ppm) = 147.4 (C-4), 133.6 (C-5), 131.1 (C-3), 130.7 (C-6), 116.1 (CN), 115.4 (CN), 114.4 (C-1), 114.3 (C-2), 63.1 (CH_2OH).

FT-IR (KBr): ν (cm^{-1}) = 3356 (ν_{st}O-H), 3106, 3071, 3047, 2230 (ν_{st}C≡N), 1567, 1381, 1163, 1097, 852, 749.

MS (EI): *m/z* = 158 $[M]^+$ (16%). $C_9H_6N_2O$ (Exact mass: 158.05, molecular weight: 158.16).

EA for $C_9H_6N_2O$ (%): calculated = C 68.35, H 3.82, N 17.71. Found = C 68.08, H 3.86, N 17.57.

4-[(*tert*-Butyldimethylsilyloxy)methyl]phthalonitrile (46)

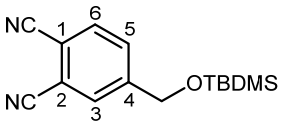

A mixture of phthalonitrile **45** (1.0 eq, 1.26 mmol, 200 mg) and *tert*-butyldimethylsilyl chloride (1.1 eq, 1.39 mmol, 210 mg) was dissolved in 3 mL of dry THF. To the stirred solution, dry triethylamine (0.70 mL) was slowly added at room temperature and the mixture was further stirred at that temperature for 16h. The solvent was then eliminated and the resulting brown solid was subjected to purification by flash column chromatography on silica gel using a 1:1 mixture of hexane:AcOEt as eluent. In that way, compound **46** obtained as a white solid (310 mg, 1.14 mmol). Yield: 90%.

^{1}H-NMR (300 MHz, $CDCl_3$): δ (ppm) = 7.78-7.76 (m, 2H; Ar-H), 7.68-7.65 (m, 1H; Ar-H), 4.81 (s, 2H; Ar-C$\underline{H}_2$O-TBDMS), 0.95 (s, 9H; Ar-CH_2O-Si-C(C$\underline{H}_3$)$_3$), 0.13 (s, 6H; Ar-CH_2O-Si-C(C$\underline{H}_3$)$_2$).

^{13}C-NMR (75.5 MHz, $CDCl_3$): δ (ppm) = 148.4, 133.5, 130.8, 130.2, 116.1, 115.7, 114.2, 63.5 (CH_2O-Si), 26.0, 18.5, -5.3.

2,3,9,10,16,17-Hexakis(2-ethylsulfonyl)-23-hydroxymethyl-5,28:14,19-diimino-7,12:21,26-dinitrilo-tetrabenzo[*c*, *h*, *m*, *r*]-[1, 6, 11, 16]tetraazacycloeicosinato-(2$^-$)-*N*^{29}, *N*^{30}, *N*^{31}, *N*^{32} zinc (II) (47)

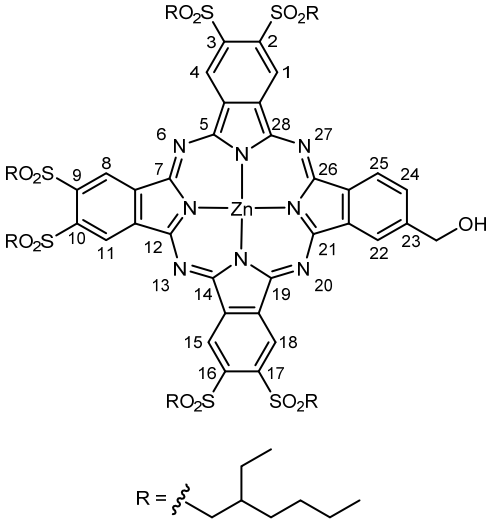

A solution of 4,5-bis(2-ethylhexylsulfonyl)phthalonitrile (**13**) (3.0 eq, 1.25 mmol, 600 mg), 4-[(*ter*t-butyldimethylsilyloxy)methyl]phthalonitrile (**46**) (1.0 eq, 0.416 mmol, 113 mg) and $Zn(OAc)_2$ (1.2 eq, 0.499 mmol, 91.6 mg) in 8 mL of *o*-DCB/DMF (3:1) was heated at 170 ºC under an argon atmosphere for 18h. After cooling down to room temperature, the solvent was removed under reduced pressure and the blue crude was dissolved in dry DCM (75.0 mL) for the next step. A 1.0 M solution of TBAF in THF (2.0 eq, 0.832 mmol, 0.83 mL) was added to de above DCM solution of protected phthalocyanine under an argon atmosphere. The reaction mixture was stirred at room temperature for 3 h. Then, the mixture was washed with brine (3 x 20 mL) and dried over $MgSO_4$. After filtration of the drying agent, solvent was removed under vacuum and the solid obtained was submitted to column chromatography on silica with gradient elution using toluene/AcOEt mixtures (starting from 4:1 and increasing proportions of AcOEt until the ratio of 1:1 was attained). The asymmetric phthalocyanine **47** was eluted, washed in an acetonitrile/water mixture (2:1, 10.0 mL), filtered and dried under vacuum, affording 28 mg (0.017 mmol) of the target compound as a blue powder. Yield: 4%.

^{1}H-NMR (300 MHz, THF-d_8): δ (ppm) = 10.35-10.11 (m, 4H; Pc-H), 9.91 (m, 2H; Pc-H), 9.14 (m, 2H; Pc-H), 8.11 (s, 1H; Pc-H), 5.24 (d, J = 5.5 Hz, 2H; C$\underline{H}_2$OH), 4.88 (t, J = 5.5 Hz, 1H; $CH_2O\underline{H}$), 4.32-3.77 (m, 12H; $SO_2C\underline{H}_2$-R), 2.73-2.48 (m, 6H; $SO_2CH_2C\underline{H}R$), 1.86-1.44 (m, 48H; $SO_2CH_2CH(C\underline{H}_2CH_3)C\underline{H}_2$ $C\underline{H}_2C\underline{H}_2CH_3$), 1.18-0.88 (m, 36H, C$\underline{H}_3$).

FT-IR (film): ν (cm^{-1}) = 3515 (ν_{st} O-H), 2957, 2930, 2862, 1851, 1776, 1563, 1460, 1409, 1293 ($\nu_{st\ as}$ SO_2), 1142 ($\nu_{st\ sim}$ SO_2).

UV-Vis (THF): λ_{max} (nm) (log ε) = 703 (5.20), 665 (5.10), 640 (4.72), 602 (4.41), 367 (4.77).

HRMS (MALDI-TOF, DCTB + PEGNa 1500): m/z calculated for $C_{81}H_{114}N_8O_{13}S_6Zn$ [M^+]: 1662.61; found: 1662.6102.

2,3,9,10,16,17-Hexakis(2-ethylsulfonyl)-23-(3'-hydroxypropyn-1-yl)--5,28:14,19-diimino-7,12:21,26-dinitrilo-tetrabenzo[*c*, *h*, *m*, *r*]-[1, 6, 11, 16]tetraazacycloeicosinato-(2$^-$)- N^{29}, N^{30}, N^{31}, N^{32} zinc (II) (48)

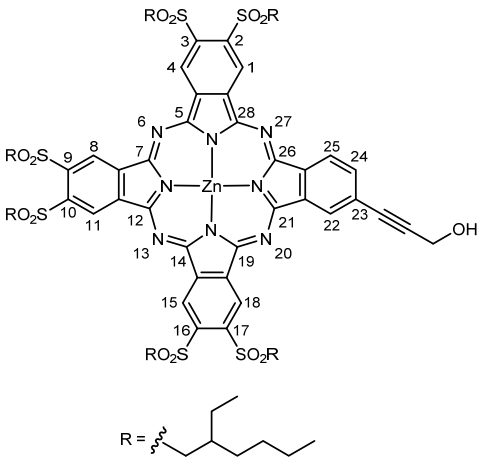

To a solution of Zn(II)Pc **15** (1.0 eq, 0.057 mmol, 100 mg), $Pd(PPh_3)_2Cl_2$ (10% mol, 0.006 mmol, 4.1 mg) and CuI (20% mol, 0.011 mmol, 2.2 mg) in dry THF (4.0 mL), freshly distilled TEA (0.4 mL) was added under an argon atmosphere. The mixture was deoxygenated by bubbling argon through it for 30 min. Propargyl alcohol (2.0 eq, 0.113 mmol, 7.0 μL) was subsequently added and the reaction was stirred at reflux for 20 h. The crude solution was then poured into aqueous HCl (0.1 M, 80.0 mL). The precipitate was collected by filtration over celite, washed with water and dried. The crude was recovered from the filtration agent by using THF, and then concentrated in vacuum. The solid was purified by column chromatography on silica gel ($CHCl_3$/THF, 40:1). The hydroxypropargyl derivative was purified by trituration in acetonitrile/water 2:1 and filtration, obtaining ZnPc **48** as a green solid (0.028 mmol, 48.3 mg). Yield: 50%.

^{1}H-NMR (300 MHz, THF-d_8): δ (ppm) = 10.38 (m, 4H; Pc-H), 9.75 (m, 2H; Pc-H), 9.05 (m, 2H; Pc-H), 7.96 (m, 1H; Pc-H), 4.73 (s, 2H; Pc-CCC$\underline{H}_2$OH), 4.13 (m, 12H; $SO_2C\underline{H}_2$-R), 2.84-2.34 (m, 6H; $SO_2CH_2C\underline{H}$R), 2.03-1.44 (m, 48H; $SO_2CH_2CH(C\underline{H}_2CH_3)C\underline{H}_2$ $C\underline{H}_2C\underline{H}_2CH_3$), 1.26-0.90 (m, 36H; $C\underline{H}_3$).

FT-IR (film): ν (cm^{-1}) = 3516 (ν_{st} O-H), 2935, 2868, 1771, 1558, 1464, 1410, 1302 ($\nu_{st\ as}$ SO_2), 1140 ($\nu_{st\ sim}$ SO_2).

UV-Vis (THF): λ_{max} (nm) (log ε) = 700 (5.25), 670 (5.21), 640 (4.68), 608 (4.50), 373 (4.83).

HRMS (MALDI-TOF, DCTB + PPGNa 2000): m/z calculated for $C_{83}H_{114}N_8O_{13}S_6Zn$ [M^+]: 1686.6116; found: 1686.6097.

2,3,9,10,16,17-Hexakis(2-ethylsulfonyl)-23-formyl-5,28:14,19-diimino-7,12:21,26-dinitrilo-tetrabenzo[*c*, *h*, *m*, *r*]-[1, 6, 11, 16]tetraazacycloeicosinato-(2$^-$)- N^{29}, N^{30}, N^{31}, N^{32} zinc (II) (49)

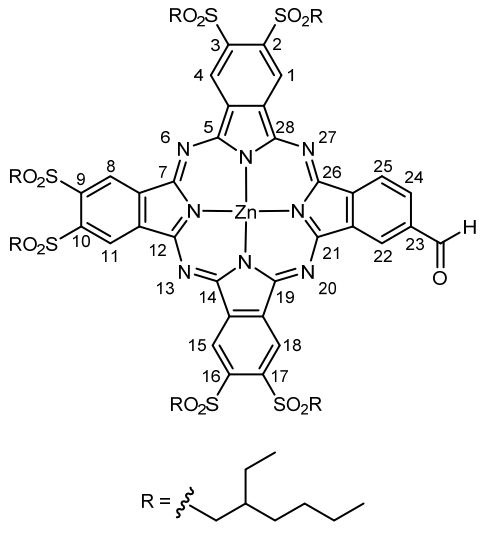

To a well-stirred and colorless solution of IBX (2.0 eq, 0.216 mmol, 61 mg) in DMSO (0.9 mL) was added a solution of Zn(II)Pc **47** (1.0 eq, 0.108 mmol, 180 mg) in THF/DMSO (2:1, 1.8 mL, 0.9 mL). The mixture was left under stirring at room temperature overnight. The reaction was monitored by TLC until all the starting material was consumed. It was then poured into brine (100 mL) and extracted with ether (3x100 mL). The combined organic layers were washed with $NaHCO_3$ (100 mL) and brine (100 mL), dried over $MgSO_4$ and concentrated. The solid residue was purified by column chromatography on silica gel (toluene/AcOEt, 4:1), and the isolated compound was washed with an acetonitrile/water (2:1, 60 mL) mixture, filtered and dried under vacuum, to afford formyl derivative **6** (0.070 mmol, 116 mg) as a blue solid. Yield: 65%.

^{1}H-NMR (300 MHz, THF-d_8): δ (ppm) = 10.62 (s, 1H; Pc-CHO), 10.37-10.29 (m, 4H; Pc-H), 10.03 (m, 2H; Pc-H), 9.73 (m, 1H; Pc-H), 9.47 (m, 1H; Pc-H), 8.69 (m, 1H; Pc-H), 4.16-3.97 (m, 12H; $SO_2C\underline{H}_2$-R), 2.61 (m, 6H; $SO_2CH_2C\underline{H}R$), 1.86-1.43 (m, 48H; $SO_2CH_2CH(C\underline{H}_2CH_3)C\underline{H}_2$ $C\underline{H}_2C\underline{H}_2CH_3$), 1.17-0.93 (m, 36H; $C\underline{H}_3$).

FT-IR (film): ν (cm^{-1}) = 2961, 2934, 2866, 1772, 1705 (ν_{st} CO), 1570, 1462, 1408, 1300 ($\nu_{st\ as}$ SO_2), 1138 ($\nu_{st\ sim}$ SO_2).

UV-Vis (THF): λ_{max} (nm) (log ε) = 694 (5.23), 672 (5.17), 638 (4.58), 609 (4.48), 372 (4.77).

HRMS (MALDI-TOF, DCTB + PEGNa 1500): m/z calculated for $C_{81}H_{112}N_8O_{13}S_6Zn$ [M^+]: 1660.5959; found: 1660.5977.

2,3,9,10,16,17-Hexakis(2-ethylsulfonyl)-23-formylethynyl-5,28:14,19-diimino-7,12:21,26-dinitrilo-tetrabenzo[*c*, *h*, *m*, *r*]-[1, 6, 11, 16]tetraazacycloeicosinato-(2$^-$)-*N*^{29}, *N*^{30}, *N*^{31}, *N*^{32} zinc (II) (50)

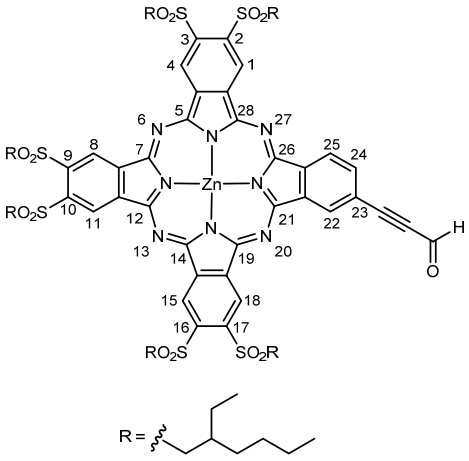

To a well-stirred and colorless solution of IBX (4.0 eq, 0.292 mmol, 82 mg) in DMSO (2.0 mL) was added a solution of Zn(II)Pc **48** (1.0 eq, 0.073 mmol, 123 mg) in THF/DMSO (1:1, 2.0 mL, 2.0 mL). The mixture was left under stirring at room temperature overnight. The reaction was monitored by TLC until all the starting material was consumed. It was then poured into brine (100 mL) and extracted with ether (3x100 mL). The combined organic layers were washed with $NaHCO_3$ (100 mL) and brine (100 mL), dried over $MgSO_4$ and concentrated. The solid residue was purified by column chromatography on silica gel (chloroform/THF, 40:1), and the isolated compound was washed with an acetonitrile/water (2:1, 60 mL) mixture, filtered and dried under vacuum, to afford formylethynyl derivative **8** (0.040 mmol, 68 mg) as a green solid. Yield: 55%.

^{1}H-NMR (300 MHz, THF-d_8): δ (ppm) = 10.40 (m, 5H; Pc-CHO, Pc-H), 9.89-9.76 (m, 2H; Pc-H), 9.51-9.15 (m, 2H; Pc-H), 8.22 (bs, 1H; Pc-H), 4.26-3.82 (m, 12H; $SO_2C\underline{H}_2$-R), 2.87-2.45 (m, 6H; $SO_2CH_2C\underline{H}R$), 1.84-1.30 (m, 48H; $SO_2CH_2CH(C\underline{H}_2CH_3)C\underline{H}_2$ $C\underline{H}_2C\underline{H}_2CH_3$), 1.19-0.91 (m, 36H; $C\underline{H}_3$).

FT-IR (film): ν (cm^{-1}) = 2932, 2864, 2195, 1771, 1661(ν_{st} CO), 1464, 1302 ($\nu_{st\ as}$ SO_2), 1142 ($\nu_{st\ sim}$ SO_2).

UV-Vis (THF): λ_{max} (nm) (log ε) = 696 (5.25), 675 (5.21), 638 (4.58), 612 (4.51), 374 (4.80).

HRMS (MALDI-TOF, DCTB + PPGNa 2000): m/z calculated for $C_{83}H_{112}N_8O_{13}S_6Zn$ [M^+]: 1684.5959; found: 1684.5980.

23-Carboxy-2,3,9,10,16,17-hexakis(2-ethylsulfonyl)-5,28:14,19-diimino-7,12:21,26-dinitrilo-tetrabenzo[*c*, *h*, *m*, *r*]-[1, 6, 11, 16]tetraazacycloeicosinato-(2$^-$)- N^{29}, N^{30}, N^{31}, N^{32} zinc (II) (51)

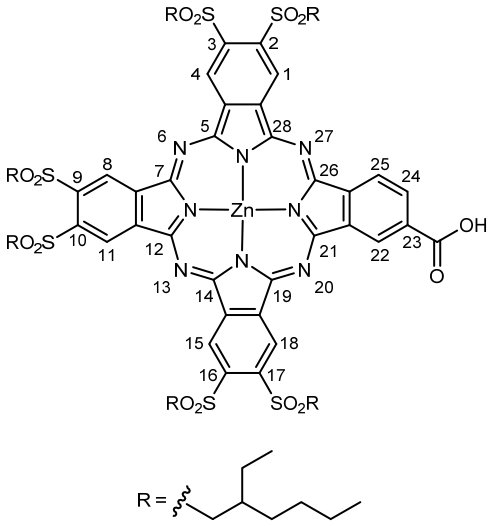

To a well-stirred solution of formyl Zn(II)Pc **49** (1.0 eq, 0.096 mmol, 160 mg) in THF (15.0 mL) at 0 ºC was added dropwise a solution of $NaClO_2$ (2.0 eq, 0.192 mmol, 17 mg) in Milli-Q-grade deionized water (1.5 mL). A solution of sulfamic acid (2.5 eq, 0.241 mmol, 23 mg) in water (1.5 mL) was added to the mixture while the reaction mixture was vigorously stirred at 0 ºC. After the addition was complete, the solution was brought to room temperature and left under stirring until the starting material was consumed. The crude solution was then poured into water (70 mL) and extracted several times with DCM (3x100 mL). The organic extracts were washed with water (100 mL), dried over MgSO4 and concentrated in vacuum. The solid was washed with a mixture an acetonitrile/water (2:1, 60 mL) mixture and filtered and dried under vacuum. In this way, compound **51** was obtained as a dark blue solid (0.067 mmol, 113 mg). Yield: 70%.

^{1}H-NMR (300 MHz, THF-d_8): δ (ppm) = 10.41 (m, 3H; Pc-COOH, Pc-H), 10.26 (m, 1H; Pc-H), 10.06 (m, 2H; Pc-H), 9.88-9.65 (m, 2H; Pc-H), 9.33-9.13 (m, 1H; Pc-H), 8.76-8.64 (m, 1H; Pc-H), 4.25-3.92 (m, 12H; $SO_2C\underline{H}_2$-R), 2.69-2.38 (m, 6H; $SO_2CH_2C\underline{H}R$), 1.88-1.45 (m, 48H; $SO_2CH_2CH(C\underline{H}_2CH_3)C\underline{H}_2$ $C\underline{H}_2C\underline{H}_2CH_3$), 1.07-0.83 (m, 36H; $C\underline{H}_3$).

FT-IR (film): ν (cm^{-1}) = 3433 (ν_{st} O-H), 2957, 2930, 2862, 1776, 1695 (ν_{st} CO), 1560, 1466, 1398, 1290 ($\nu_{st\ as}$ SO_2), 1142 ($\nu_{st\ sim}$ SO_2).

UV-Vis (THF): λ_{max} (nm) (log ε) = 697 (4.99), 670 (4.93), 638 (4.43), 607 (4.26), 370 (4.56).

HRMS (MALDI-TOF, DCTB + PPGNa 2000): m/z calculated for $C_{81}H_{112}N_8O_{14}S_6Zn$ [M^+]: 1676.5908; found: 1676.5891.

23-Carboxyethynyl-2,3,9,10,16,17-hexakis(2-ethylsulfonyl)-5,28:14,19-diimino-7,12:21,26-dinitrilo-tetrabenzo[*c*, *h*, *m*, *r*]-[1, 6, 11, 16]tetraazacycloeicosinato-(2$^-$)-*N*^{29}, *N*^{30}, *N*^{31}, *N*^{32} zinc (II) (52)

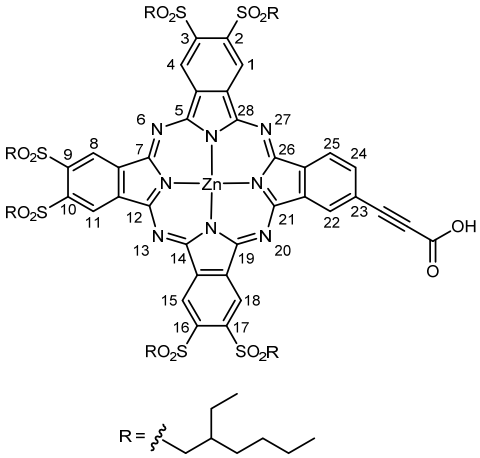

To a well-stirred solution of formyl Zn(II)Pc **50** (1.0 eq, 0.032 mmol, 55 mg) in THF (5.0 mL) at 0 ºC was added dropwise a solution of $NaClO_2$ (2.0 eq, 0.065 mmol, 5.8 mg) in Milli-Q-grade deionized water (1.0 mL). A solution of sulfamic acid (2.5 eq, 0.081 mmol, 7.8 mg) in water (1.0 mL) was added to the mixture while the reaction mixture was vigorously stirred at 0 ºC. After the addition was complete, the solution was brought to room temperature and left under stirring until the starting material was consumed. The crude solution was then poured into water (30 mL) and extracted several times with DCM (3x40 mL). The organic extracts were washed with water (60 mL), dried over MgSO4 and concentrated in vacuum. The solid was washed with a mixture an acetonitrile/water (2:1, 60.0 mL) mixture and filtered and dried under vacuum. In this way, compound **52** was obtained as a dark green solid (0.021 mmol, 36 mg). Yield: 65%.

^{1}H-NMR (300 MHz, THF-d_8): δ (ppm) = 10.76-10.04 (m, 6H; Pc-H), 9.47 (m, 2H; Pc-H), 8.34 (m, 1H; Pc-H), 8.07 (m, 1H; Pc-H), 4.26-3.82 (m, 12H; $SO_2C\underline{H}_2$-R), 2.87-2.45 (m, 6H; $SO_2CH_2C\underline{H}R$), 1.73-1.30 (m, 48H; $SO_2CH_2CH(C\underline{H}_2CH_3)C\underline{H}_2$ $C\underline{H}_2C\underline{H}_2CH_3$), 1.18-0.81 (m, 36H; $C\underline{H}_3$).

FT-IR (film): ν (cm^{-1}) = 3406 (ν_{st} O-H), 2961, 2920, 2866, 1732, 1597 (ν_{st} CO), 1570, 1462, 1300 ($\nu_{st\ as}$ SO_2), 1142 ($\nu_{st\ sim}$ SO_2).

UV-Vis (THF): λ_{max} (nm) (log ε) = 700 (5.02), 676 (4.97), 639 (4.43), 612 (4.30), 373 (4.57).

HRMS (MALDI-TOF, DCTB + PPGNa 2000): m/z calculated for $C_{83}H_{112}N_8O_{14}S_6Zn$ [M^+]: 1700.5908; found: 1700.5924.

Chapter 2. *New Tb(III) bis(phthalocyanine) as single-molecule magnets*

2.1 Introduction

2.1.1 Magnetism

Magnetism is certainly one of the most important physical phenomena in the universe. It is ubiquitous in both natural and technological matters, from the earth´s magnetic field to many components of electronic devices which are part of our everyday life. The history of magnetism dates back to earlier than the 6th century B.C., but it is only in the twentieth century that scientists have begun to understand it, and develop technologies based on this understanding. Magnetism was most probably first observed in a form of the mineral magnetite called lodestone, a naturally magnetized piece of magnetite (Fe_3O_4), found in Magnesia, in ancient Thessaly, Greece, which explains the origin of the word "magnet".[382] The observation of the attraction of lodestone to iron was repeated over centuries by an incredible number of scientists, but it took centuries for lodestone to pass from a scientific curiosity to an actual functional material. Indeed, it was not until the 12th century D.C. that the Chinese used a lodestone based compass for navigation, which was the first milestone of a long series of scientific discoveries leading to the exploitation of magnetism as a more general fundamental tool. Ever since the early example of the compass, magnetic materials have been little by little incorporated in our everyday life. Permanent magnets can be found in our hard-disk drives and credit cards as recording media and are also present in electromechanical transductor devices such as electric motors, audio speakers or microphones.

2.1.1.1 Magnetization hysteresis

A magnet is a material that can be magnetized and can present a permanent magnetic moment in the absence of any exterior magnetic field. The main characteristics of a magnet are the parameters of its hysteresis of magnetization, which are its remnant magnetization and its coercive field (*Figure 94*). Magnets are in essence bistable systems which can be magnetized along one particular z direction or the opposite direction –z. When applying a sufficiently high magnetic field along z, magnets are magnetized at a saturation magnetization value M_s. When the external magnetic field is removed, hard magnets maintain a non zero permanent magnetization called remnant magnetization M_r. If one applies an external magnetic field in the opposite direction, along –z, then the magnet saturates at a magnetization value of $-M_s$ and when removing the magnetic field, the remnant magnetization value is now $-M_r$. For an ideal magnet the magnitude of the

[382] G. L. Verschuur, *Hidden attraction: The history and mystery of magnetism*, Oxford University Press, Oxford, **1993**.

remnant magnetization M_{ri} is equal to the saturation magnetization M_s, nevertheless in a real hard magnet, the from one magnet to the other. Simply put, the value of M_r is the relative amount of magnetization that the magnet maintains when in the absence of an external magnetic field.

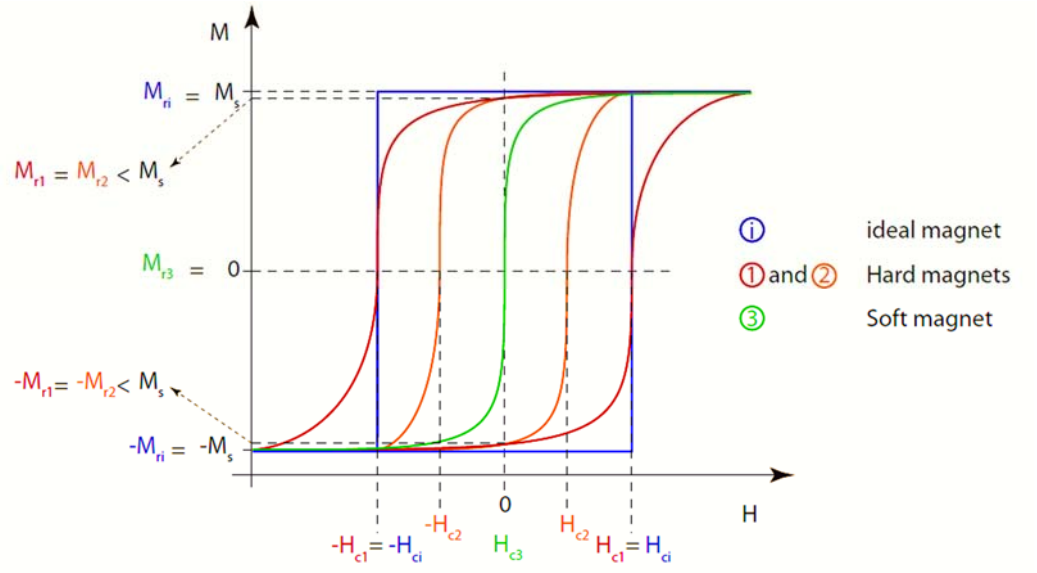

Figure 94.- Magnetization hysteresis plots of four model magnets indicating their coercive fields H_c and remnant magnetizations M_r.

In order to flip the magnetization of a hard magnet from positive to negative value, it is necessary to apply a magnetic field strong enough to destroy the cohesion of the magnet. The field at which such a flipping occurs is therefore called the coercive field (H_c). This is the other important parameter of the magnetization hysteresis curves of hard magnets. Finally, a soft magnet is a material that can be magnetized but shows no magnetization hysteresis, which translates into $H_c = 0$ and $M_r = 0$. *Figure 94* illustrates the magnetization versus field curves obtained for an ideal magnet (i), two hard magnets with different values of H_c (1 and 2) and a soft magnet (3).

2.1.1.2 Molecular magnetic materials

Traditionally, magnetic materials are bulk materials based on atoms with *d* or *f* orbital based spin sites and has extended network bonding in three dimensions. However, a new field of research emerged, around the end of the 20th century, to

investigate the properties of molecular magnetic materials.[383,384,385,386,387] In the 80s, a new research field, the Molecular Magnetism,[388] envisaged an essentially multidisciplinary field that aims at combining the knowledge of chemists with those of theoretical chemists and physicists in order to design molecular magnetic materials and predict and rationalize their physical properties. The research activity of the field was conducted in several directions. While some groups investigated the possibility to obtain purely organic ferromagnets, others tried to push up the ordering temperatures, which are typically below the boiling point of liquid nitrogen.

The first examples of molecular ferro- and ferrimagnets were reported in the late 1980s. In 1987, Miller and his team successfully produced ferromagnets using the tetracyanoethylene (TCNE) anion.[389] For instance, they reported that $[Fe(C_5Me_5)_2][TCNE]$ showed spontaneous ferromagnetic ordering below 4.5 K.[390] Only one year later, Kahn *et al*. presented a new ferromagnetically ordering system at approximately the same temperature (4.6 K) based on bimetallic Cu(II)-Mn(II) chains.[391] In 1991 two more breakthroughs occurred. On one hand Miller *et al*. reported the first room temperature molecular magnet,[392] $V(TCNE)_2$, whose structure remains unknown to date. $V(TCNE)_2$ orders ferrimagnetically above room temperature due to the antiferromagnetic coupling between the V^{2+} ions (S = 3/2) and the radical anions $TCNE^{\bullet-}$ (S = 1/2). On the other hand, Kinoshita and coworkers reported the first all-organic ferromagnet,[393] a compound of the well known nitronyl nitroxide family of stable radicals. While the compound ordered at only 0.6 K, it demonstrated the possibility to obtain molecular magnets in which the magnetic orbitals were purely of type *s* or *p* and not *d* or *f* as is the case for third and fourth row transition metals (3d or 4d), lanthanides (4f) and actinides (5f) used in classical bulk magnets. Nevertheless, these magnets are soft

[383] J. S. Miller and M. Drillon, *Magnetism: Molecules to Materials I*, *Models and Experiments,* Wiley-VCH, **2001**.
[384] J. S. Miller and M. Drillon*, Magnetism: Molecules to Materials II, Molecule-based Materials,* Wiley-VCH, **2001**.
[385] J. S. Miller and M. Drillon, *Magnetism: Molecules to Materials III, Nanosized Magnetic Materials,* Wiley-VCH, **2002**.
[386] J. S. Miller and M. Drillon, *Magnetism: Molecules to Materials* IV, Wiley-VCH, **2003**.
[387] J. S. Miller and M. Drillon, *Magnetism: Molecules to Materials V,* Wiley-VCH, **2005**.
[388] O. Kahn, *Molecular Magnetism*, VCH Publishers, **1993**.
[389] J. S. Miller, *Inorg. Chem*. **2000**, *39*, 4392.
[390] J. S. Miller, J. C. Calabrese, H. Rommelmann, S. R. Chittipeddi, J. H. Zhang, W. M. Reiff, A. J. Epstein, *J. Am. Chem. Soc*. **1987**, *109*, 769.
[391] O. Kahn, Y. Pei, M. Verdaguer, J. P. Renard, J. Sletten*, J. Am. Chem. Soc*. **1988**, *110*, 782.
[392] J. M. Manriquez, G. T. Yee, R. S. McLean, A. J. Epstein, J. S. Miller, *Science* **1991**, *252*, 1415.
[393] M. Tamura, Y. Nakazawa, D. Shiomi, K. Nozawa, Y. Hosokoshi, M. Ishikawa, M. Takahashi, M. Kinoshita, *Chem. Phys. Lett*. **1991**, *186*, 401.

magnets with almost no coercive field due to the lack of anisotropy of the *s* and *p* orbitals. The highest ordering temperature in a purely organic magnet to date is 36 K,[394] which is quite an improvement when compared to the compound by Kinoshita and coworkers, but is still too low to envisage any practical application as a permanent magnet. The development of a purely organic molecular magnet provides exciting possibilities because apart from being magnetic, the molecule would also have properties specific to the organic compounds.

Despite the novelty of preparing bulk molecular magnets ordering around room temperature, it was soon realized that one of the great advantages of molecular materials in magnetism is the possibility to control the dimensionality of the magnetic structure. Indeed, the control of the reaction conditions and the chemical nature of the compounds used to prepare molecular magnetic materials allows the preparation of strictly 3D bulk ferro- or ferrimagnets, but also in lower dimensionalities, with 2D, 1D or strictly 0D magnetic materials, in which the magnetic interactions are propagated in a plane, in only one direction, or confined to an independent nanometric magnetic cluster. An extensive amount of research was done in order to prepare such materials, eventually leading to the discovery of the first compound behaving as a single-molecule magnet, which is a compound that, below a blocking temperature, exhibits stable magnetization purely of molecular origin, and not caused by long-range ordering of magnetic moments in the bulk.[395]

Molecular magnets have several potential uses, including the use in high capacity magnetic storage media[396] and quantum bits (qubits) applicable to quantum computers.[397]

---

[394] F. Palacio, G. Antorrena, M. Castro, R. Burriel, J. Rawson, J. N. B. Smith, N. Bricklebank, J. Novoa, C. Ritter*, Phys. Rev. Lett*. **1997**, *79*, 2336.

[395] D. Gatteschi, R. Sessoli, J. Villain, *Molecular Nanomagnets,* Oxford University Press*,* Oxford, UK, **2006**.

[396] a) L. Bogani, W. Wernsdorfer, *Nat. Mater*. **2008**, *7*, 179; b) J. J. L. Morton, A. M. Tyryshkin, R. M. Brown, S. Shankar, B. W. Lovett, A. Ardavan, T. Schenkel, E. E. Haller, J. W. Ager, S. A. Lyon, *Nature* **2008**, *455*, 1085.

[397] a) J. Ahn, T. C. Weinacht, P. H. Bucksbaum, *Science* **2000**, *287*, 463; b) M. N. Leuenberger, D. Loss, *Nature* **2001**, *410*, 789; c) R. E. P. Winpenny, *Angew. Chem. Int. Ed*. **2008**, *47*, 7992; d) J. Lehmann, A. Gaita-Ariño, E. Coronado, D. Loss, *J. Mater. Chem*. **2009**, *19*, 1672.

2.1.2 Single-molecule magnets. Concepts

The 90s were characterized by an intense research on a new class of molecular materials, known as single-molecule magnets (SMMs).[395,398] These compounds are, in general, polynuclear coordination compounds of paramagnetic metal ions held together by suitable ligands, which often provide an effective shielding between adjacent molecules in the solid. The magnetic centers can be transition-metal or rare-earth ions,[399] or even organic radicals. The most interesting aspect is that a few of these molecular clusters, featuring a combination of a large spin and an easy axis magnetic anisotropy, are characterized by a dramatic slowing down of the fluctuations of the magnetization at low temperature, and in some cases a magnetic hysteresis is observed.[400] At variance with more conventional magnetic materials, this type of hysteresis has a pure molecular origin and does not imply long range order. It was soon recognized that SMMs hold great potential to store information at the molecular level, even if the temperatures at which the hysteresis is observed remains prohibitive for technological applications. In fact, it is still confined to liquid helium region despite the many synthetic efforts. This, however, has not diminished the interest in SMMs as model systems to investigate magnetism at the nanoscale and, in particular, the coexistence of quantum phenomena with the classical hysteretic behaviour.[401] A key issue that has emerged in the last years is the possibility to address the magnetism of a single molecule, indeed a mandatory step to fully exploit the potential of SMMs. In its circular pathway, molecular magnetism is therefore focussing again on isolated magnetic objects. However, the environment is no longer a crystal lattice but a nanostructured surface or a miniaturized electronic device built using a single magnetic molecule. This gives the possibility to combine the rich quantum dynamics of SMMs with transport properties, in the emerging field known as molecular spintronics.[402] The first step in this direction has been the organization of isolated SMMs on conducting and semiconducting surfaces[403] as a means of imaging single molecules and of measuring their transport properties with scanning probes techniques.

---

[398] a) A. Caneschi, D. Gatteschi, R. Sessoli, A.-L. Barra, L.-C. Brunel, M. Guillot, *J. Am. Chem. Soc*. **1991**, *113*, 5873; b) R. Sessoli, H. L. Tsai, A. R. Schake, S. Wang, J. B. Vincent, K. Folting, D. Gatteschi, G. Christou, D. N. Hendrickson, *J. Am. Chem. Soc*. **1993**, *115*, 1804.

[399] D. N. Woodruff, R. E. P. Winpenny, R. A. Layfield, *Chem. Rev*. **2013**, *113*, 5110.

[400] S. M. Holmes, G. S. Girolami, *J. Am. Chem. Soc*. **1999**, *121*, 5593.

[401] D. Gatteschi, R. Sessoli, *Angew. Chem. Int. Ed*. **2003**, *42*, 268.

[402] S. Sanvito, *Nat. Mater*. **2007**, *6*, 803.

[403] A. Cornia, A. F. Constantino, L. Zobbi, A. Caneschi, D. Gatteschi, M. Mannini, R. Sessoli, *Struct. Bonding* **2006**, *122*, 133.

Single-molecule magnets (SMMs)[404] are characterized by high spin ground state (S), high zero field splitting and an easy axis of the magnetization (which correspond to high and negative zero field splitting parameter D). If we exclude the case of mononuclear lanthanide complexes of high symmetry, *e.g.* double decker compounds, that have been described in the last part of this introduction, all other molecules presenting slow relaxation of the magnetization are constituted by polynuclear complexes of paramagnetic metal ions. Usually in this case only interactions between nearest neighboring magnetic sites are considered and the effective Spin Hamiltonian (SH) can be write as:

$$H_{ex} = \sum_{i>j}^{J_{ij}} S_i \cdot S_j \qquad \textit{Eq. 6}$$

where *i* and *j* run over all metal sites of the cluster. The energy of the different S_T states can be calculated analytically in some high symmetry cases, in particular when a central spin exhibits the same exchange interaction with the neighboring ones. This is also known as the Kambe approach[405] and spin systems comprising up to 13 coupled spins have been handled in this way.[406]

The spin structure of the SMM is strongly correlated to the dynamics of the magnetization and can be considered as a sort of fingerprint of the SMM. On the other hand, the occurrence of a large spin ground state is a necessary, although not sufficient, condition to observe slow relaxation of the magnetization. The second key ingredient in SMM is magnetic anisotropy. In traditional magnets, three factors give equally important contributions to the anisotropy, namely surface, strain, and magnetocrystalline contributions. In SMM, the only significant role is played by magnetocrystalline anisotropy and is brought in by a combination of spin-orbit coupling with the low-symmetry environment around the metal centers constituting the SMM. Dipolar contributions are in most cases negligible. A quantitative treatment of the magnetic anisotropy is based on the effective spin-hamiltonian approach where only the spin variables appear, while the orbital contributions are introduced through parameters. For a system with no symmetry at all, the SH can be written as:

$$H_{an} = S \cdot \widehat{D} \cdot S = D[S_z^2 - \tfrac{1}{3}S(S+1)] + E(S_x^2 - S_y^2) \qquad \textit{Eq. 7}$$

[404] G. Christou, D. Gatteschi, D. N. Hendrickson, R. Sessoli, *MRS Bull*. **2000**, *25*, 66.
[405] K. Kambe, *J. Phys. Soc. Jpn*. **1950**, *5*, 48.
[406] J. van Slageren, P. Rosa, A. Caneschi, R. Sessoli, H. Casellas, Y. V. Rakitin, L. Cianchi, F. Del Giallo, G. Spina, A. Bino, A.-L. Barra, T. Guidi, S. Carretta, R. Caciuffo, *Phys. Rev. B* **2006**, *73*, 014422.

Where $D = D_{zz} - \frac{1}{2}D_{xx} - \frac{1}{2}D_{yy}$ represents the axial anisotropy, and $E = {}^{1}/_{2}\left(D_{xx} - D_{yy}\right)$ the transverse (or rhombic) one. The value of *E* is intrinsically limited to ${}^{1}/_{3}\,D$ because going going beyond this limit indeed corresponds to a change in the axis of the leading anisotropy. The effect of the magnetic anisotropy on the $(2S+1)$ states of the spin multiplet is that of removing their degeneracy even in the absence of an external field, and thus is also named Zero Field Splitting (ZFS).

The effect of a negative D in *Eq. 7* is that the system can be magnetized much more easily when the field is applied along the principal, *i.e.* z, axis. Moreover, a system showing easy axis magnetic anisotropy, $D < 0$, has the ground doublet characterized by $m = \pm S$, which corresponds to two potential wells separated by an energy barrier, U_{eff}, as we will see in next section. In the case of a spin system constituted by a single paramagnetic center carrying $2S$ unpaired electrons, the value of D can be experimentally determined through electron paramagnetic spectroscopy (EPR),[407] or alternatively through inelastic neutron scattering.[408] Also magnetometry, especially if performed on a single crystal sample, can provide accurate values. The magnetic anisotropy can also be estimated theoretically, with a great variety of approaches. These range from simple perturbation theory, starting from a spectroscopic estimation of the energy separation of the partially filled *d* orbitals,[409] to a ligand field treatment based on the Angular Overlap Model.[410] More recently ab initio calculations, either based on Density Functionals or on post Hartree-Foch approaches[411] have also shown a good predictive capability. The situation is more complicated in the case of a polynuclear metal system.

2.1.2.1 $[Mn_{12}O_{12}(CH_3COO)_{16}(H_2O)_4]$

The first single-molecule magnet ever reported and the most studied one is undoubtedly $[Mn_{12}O_{12}(CH_3COO)_{16}(H_2O)_4]$, from now on called Mn_{12}ac, depicted in *Figure 95*.

---

[407] a) A. Bencini, D. Gatteschi, *Transition Metal Chemistry*, **1982**, *8*, 1; b) D. Gatteschi, A.-L. Barra, A. Caneschi, A. Cornia, R. Sessoli, L. Sorace, *Coord. Chem. Rev*. **2006**, *250*, 1514; c) A.-L. Barra, A. Caneschi, D. Gatteschi, R. Sessoli, *J. Magn. Magn. Mater*. **1998**, *177*, 709.

[408] R. Caciuffo, G. Amoretti, A. Murani, R. Sessoli, A. Caneschi, D. Gatteschi, *Phys. Rev. Lett*. **1998**, *81*, 4744.

[409] a) A.-L. Barra, D. Gatteschi, R. Sessoli, G. L. Abbati, A. Cornia, A. C. Fabretti, M. G. Uytterhoeven, *Angew. Chem. Int. Ed*. **1997**, *36*, 2329; b) D. P. Goldberg, J. Telser, J. Krzystek, A. G. Montalban, L.-C. Brunel , A. G. M. Barrett, B. M. Hoffman, *J. Am. Chem. Soc*. **1997**, *119*, 8722.

[410] A. Bencini, I. Ciofini, M. G. Uytterhoeven, *Inorg. Chim. Acta* **1998**, *274*, 90.

[411] L. F. Chinotaru, L. Ungur, A. Soncini, *Angew. Chem. Int. Ed*. **2008**, *47*, 4126.

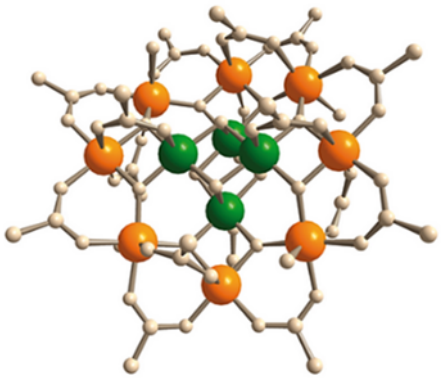

Figure 95.- Crystal structure of the Mn_{12}ac complex. Green atoms correspond to Mn(II) and yellow ones to Mn(III).

The first synthesis and crystal structure of the Mn_{12}ac cluster as we know it was reported by Lis in 1980.[412] At the time, the author performed only dc magnetic measurements and limited his observations mostly to describing the structure of the cluster. Eight years later, Boyd *et al.* presented the magnetic properties of the benzoate equivalent of the Mn_{12} cluster,[413] and concluded on the possibility to build bulk molecular magnetic materials using these complexes as a building block and finding a way to link them together. Finally, in 1991, the true nature of Mn_{12}ac was recognized. When measuring the ac magnetic susceptibility of the cluster, Caneschi *et al*. noticed that the temperature dependant imaginary part of the ac magnetic susceptibility presented a peak whose position depended on the frequency of the applied field (*Figure 96*).[398a] The presence of a peak in the imaginary part of the susceptibility meant that the complex was lagging with respect to the applied oscillating magnetic field, which in turn meant that it showed a slow magnetic relaxation below 10 K. Moreover, the fact that the position of the maximums of the peaks was frequency dependent allowed the researchers to discard the possibility that this was produced by a bulk magnetic ordering, and the complex was attributed a multiplet splitted $S = 10$ ground state with a zero field splitting parameter D = -0.50 cm^{-1}.

[412] T. Lis, *Acta Crystallog. B* **1980**, *36*, 2042.
[413] P. D. W. Boyd, Q. Li, J. B. Vincent, K. Folting, H. R. Chang, W. E. Streib, J. C. Huffman, G. Christou, D. N. Hendrickson, *J. Am. Chem. Soc*. **1988**, *110*, 8537.

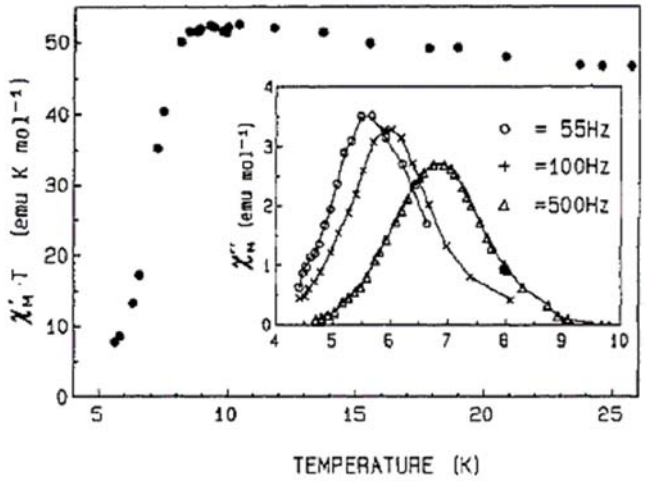

Figure 96.- First ac magnetic susceptibility data recorded on Mn_{12}ac. The inset shows the imaginary part of the magnetic susceptibility *vs*. T measured at 55, 100 and 500 Hz.

These values were confirmed a few years later by Sessoli *et al.* in an in depth study of the interactions in the cluster.[398b]

At the time, the authors pointed out that even though Mn_{12}ac was much smaller than the previously reported superparamagnets, it presented a similar behavior (temperature dependent blocking of the magnetic relaxation), and it was tempting to assume that the reason for its peculiar behavior laid in its high magnetic anisotropy originating from its high spin ground state and the anisotropy of the component metal ions.

In 1993, it was shown that the complex shows magnetic hysteresis (*Figure 97*) of purely molecular origin since no 3D ordering could be observed in either magnetization, susceptibility or specific heat measurements.[414] The discovery of the possibility of magnetization hysteresis in a single-molecule, that is of the possibility of making single-molecule magnets, created quite an excitement, but more was to come since Mn12ac was soon to provide the experimental observation of a quantum phenomenon: quantum tunneling of magnetization.

[414] R. Sessoli, D. Gatteschi, A. Caneschi, M. A. Novak, *Nature* **1993**, *365*, 141.

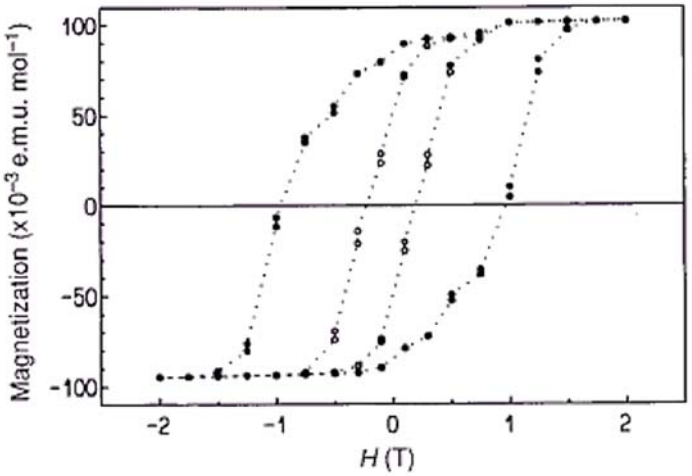

Figure 97.- First magnetization hysteresis recorded on a polycristalline sample of Mn_{12}ac.[414]

Mn_{12}ac, as previously mentioned, is a polynuclear transition metal cluster that combines a high spin $(S = 10)$ ground state with a strong easy axis of magnetic anisotropy. In the case of Mn_{12}ac, the complex is made up of an outer ring of eight Mn(III) ions $(S = 2)$ and a core of four Mn(II) ions $(S = 3/2)$. The manganese ions of the outer ring are ferromagnetically coupled together, and so are the core manganese ions. Nevertheless, the core and the ring are coupled antiferromagnetically which altogether accounts for the $S = 10$ ground state. The complex presents an axial symmetry, and it was shown that it presents a strong Ising anisotropy, which means that it presents an easy axis (or hard plane) of magnetization.

In a first approximation, the Mn_{12}ac complexes are described by the following Hamiltonian, taking into account the axial zero field splitting and the Zeeman splitting:

$$H = -DS_z^2 - g\mu_B S H_f \qquad \textit{Eq. 8}$$

where D is the axial zero field splitting parameter, g is the g-factor of the compound, μ_B is the Bohr magneton, H_f is the applied magnetic field, S is the total spin of the system and S_z is its projection on the easy axis direction. The energies of the different m_s states are therefore given by the following expression:

$$E(m_s) = -Dm_s^2 - g\mu_B m_s H_{fz} \qquad \textit{Eq. 9}$$

where H_{fz} is the projection of the magnetic field on the easy axis direction and m_s are the spin microstates projected on the same axis. In zero field the Zeeman term is equal to zero and the energy diagram of the system is given in *Figure 98*. In this situation the two

states with quantum number S and $-S$ are equal in energy and the ground state is therefore degenerate and in principle the two states $m_s = S$ and $m_s = -S$ are equally populated.

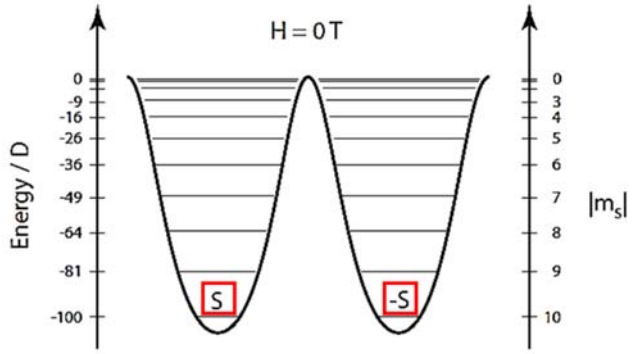

Figure 98.- Energy diagram of the multiplets of the $S = 10$ compound in zero applied field.

On the contrary, when applying a component H_{fz} along the easy axis of magnetization, the Zeeman term is non zero and the degeneracy is removed. In this case, the energies of one well are stabilized with respect to those of the other (*Figure 99*). The state $|S>$ with $m_s = S$, is now metastable and it starts to depopulate to the benefit of the $|-S>$ state with $m_s = -S$ which is now a true non degenerate ground state. The relaxation can occur in two ways. The compounds that are in a state $|S>$ can overcome the anisotropy barrier by populating thermally the upper $|S+n>$ states and therefore reach the state $|0>$ and relax to the $|-S>$ state in a thermally activated process following an Arrhenius-like behavior, with a relaxation rate τ^{-1} given by:

$$\tau^{-1} = \tau_0^{-1} exp\left(-\frac{U_{eff}}{k_B T}\right) \qquad \textit{Eq. 10}$$

where U_{eff} is the effective barrier of reversal and k_B is the Boltzmann constant. Alternatively, if the applied magnetic component along the easy axis H_{fn} is such that the $|S>$ state coincides in energy with a $|-S+n>$ state, then resonant tunneling occurs between the two states and the compounds in state $|S>$ tunnel to state $|-S+n>$ and relax to the $|-S>$ state. This process is called quantum tunneling of magnetization (QTM) and is a temperature independent process.

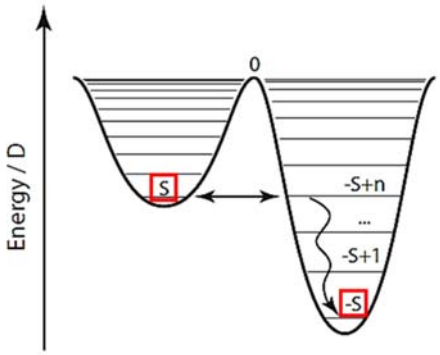

Figure 99.- Energy diagram of the multiplets of the $S = 10$ compound applying a non zero magnetic field component H_{fn} along the easy axis which makes the energy of the $|S>$ and $|-S+n>$ states coincide.

The occurrence of QTM happens at discrete values of magnetic field H_{fn} for which the energies of $|m>$ and $|-m+n>$ are equal. This in turn means that QTM occurs at evenly spaced values of H_f which depend only on the zero field splitting parameter D and the g factor of the compound. QTM provides an alternative route to the thermal relaxation of the superparamagnetic clusters, which was first evidenced in Mn_{12}ac and translate in a staircase hysteresis curve of magnetization with a step at the values of H_{fn} at which resonant tunneling occurs (*Figure 100*). While the effect of QTM was already visible in the first recorded magnetization hysteresis of Mn_{12}ac (*Figure* 97),[414] it was not identified at the time, and only a few years later was it recognized as such.[401,415,416,417,418] In Mn_{12}ac the magnetization hysteresis curves (*Figure 100*) present steps that are evenly spaced by approximately 0.46 T, which corresponds to D/g = 0.21 cm^{-1} which is in good agreement with the values of D and g (0.5 cm^{-1} and 1.9, respectively) experimentally determined in an independent way from high field EPR experiments.[398b,414] The steps can clearly be seen in *Figure 100*, and upon changing the temperature, the position of the steps is unchanged, but when lowering the temperature the hysteresis loop broadens and some steps that were so far undetectable can be observed.

[415] J. R. Friedman, M. P. Sarachik, J. Tejada, R. Ziolo*, Phys. Rev. Lett.* **1996***, 76*, 3830.
[416] L. Thomas, F. Lionti, R. Ballou, D. Gatteschi, R. Sessoli, B. Barbara, *Nature* **1996***, 383*, 145.
[417] J. R. Friedman, M. P. Sarachik, J. Tejada, J. Maciejewski, R. Ziolo, *J. Appl. Phys*. **1996***, 79*, 6031.
[418] J. Tejada, R. F. Ziolo, X. X. Zhang, *Chem. Mater***. 1996***, 8*, 1784.

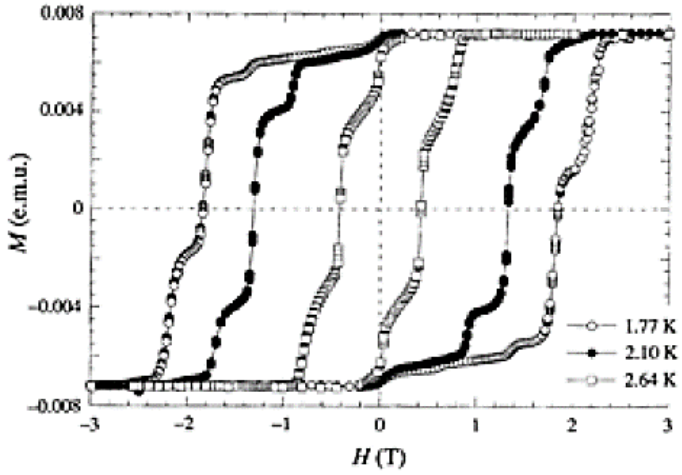

Figure 100.- Magnetization hysteresis curve measured on a single-crystal of Mn_{12}ac measured at 1.77 K, 2.10 K and 2.64 K.

Following the discovery of the Mn_{12} clusters, a great number of systems were prepared and showed SMM behavior. But, while a lot of new compounds have been synthesized, the general trends are the same, and most SMMs are still metallic clusters with a high spin ground state and a strong uniaxial anisotropy. In this group of new single-molecule magnets based on transition metal there are a variety of systems, including

others manganese clusters[419] of various nuclearity (Mn_2,[420] Mn_4,[421] Mn_6,[422] Mn_{84},[423] among others), iron (ferric wheels,[424] Fe_4,[425] Fe_8,[426] among others), V_4,[427] and $CrNi_6$.[428]

2.1.2.2 Single-ion magnets[429]

As we have seen in the last section, the aim of the scientific community for years has been to obtain polynuclear transition metal clusters with a high magnetic anisotropy, and to achieve a high spin ground state by engineering the exchange coupling between the different metal ions constituting the clusters. Nevertheless, in 2003, this vision of single-molecule magnet was revised due to the appearance of the first mononuclear

[419] a) E. K. Brechin, *Chem. Comm*. **2005**, 5141; b) G. Rogez, B. Donnio, E. Terazzi, J.-L. Gallani, J.-P. Kappler, J.-P. Bucher, M. Drillon, *Adv. Mater*. **2009**, *21*, 4323.
[420] a) Z. Lu, M. Yuan, F. Pan, S. Gao, D. Zhang, D. Zhu, *Inorg. Chem*. **2006**, *45*, 3538; b) H. Miyasaka, R. Clerac, W. Wernsdorfer, L. Lecren, C. Bonhomme, K.-i. Sugiura, M. Yamashita, *Angew. Chem. Int. Ed*. **2004**, *43*, 2801.
[421] a) S. M. J. Aubin, N. R. Dilley, L. Pardi, J. Krzystek, M. W. Wemple, L.-C. Brunel, M. B. Maple, G. Christou, D. N. Hendrickson, *J. Am. Chem. Soc*. **1998**, *120*, 4991; b) J. Yoo, E. K. Brechin, A. Yamaguchi, M. Nakano, J. C. Huffman, A. L.. Maniero, L.-C. Brunel, K. Awaga, H. Ishimoto, G. Christou, D. N. Hendrickson, *Inorg. Chem*. **2000**, *39*, 3615; c) A. Bhattacharjee, Y. Miyazaki, M. Nakano, J. Yoo, G. Christou, D. N. Hendrickson, M. Sorai, *Polyhedron* **2001**, *20*, 1607.
[422] a) C. J. Milios, R. Inglis, R. Bagai, W. Wernsdorfer, A. Collins, S. Moggach, S. Parsons, S. P. Perlepes, G. Christou, E. K. Brenchin, *Chem. Comm*. **2007**, 3476; b) C. J. Milios, A. Vinslava, W. Wernsdorfer, A. Prescimone, P. A. Wood, S. Parsons, S. P. Perlepes, G. Christou, E. K. Brechin, *J. Am. Chem. Soc*. **2007**, *129*, 6547; c) C. J. Milios, A. Vinslava, P. A. Wood, S. Parsons, W. Wernsdorfer, G. Christou, S. P. Perlepes, E. K. Brechin, *J. Am. Chem. Soc*. **2006**, *129*, 8.
[423] A. J. Tasiopoulos, A. Vinslava, W. Wernsdorfer, K. A. Abboud, G. Christou, *Angew. Chem. Int. Ed*. **2004**, *43*, 2117.
[424] a) A. Caneschi, A. Cornia, A. C. Fabretti, D. Gatteschi, *Angew. Chem. Int. Ed*. **1996**, *34*, 2716; b) A. Caneschi, A. Cornia, A. C. Fabretti, D. Gatteschi, *Angew. Chem. Int. Ed*. **1999**, *38*, 1295.
[425] a) A. L. Barra, A. Caneschi, A. Cornia, F. Fabrizi de Biani, D. Gatteschi, C. Sangregorio, R. Sessoli, L. Sorace, *J. Am. Chem. Soc*. **1999**, *121*, 5302; b) A. Cornia, L. Gregoli, C. Danieli, A. Caneschi, R. Sessoli, L. Sorace, A.-L. Barra, W. Wernsdorfer, *Inorg. Chim. Acta* **2008**, *361*, 3481; c) A. Cornia, A. C. Fabretti, P. Garrisi, C. Mortalo, D. Bonacchi, D. Gatteschi, R. Sessoli, L. Sorace, W. Wernsdorfer, A.-L. Barra, *Angew. Chem. Int. Ed*. **2004**, *43*, 1136.
[426] a) K. Wieghardt, K. Pohl, I. Jibril, G. Huttner, *Angew. Chem. Int. Ed*. **1984**, *23*, 77; b) A.-L. Barra, P. Debrunner, D. Gatteschi, C. E. Schulz, R. Sessoli, *Europhys. Lett*. **1996**, *35*, 133.
[427] S. L. Castro, Z. Sun, C. M. Grant, J. C. Bollinger, D. N. Hendrickson, G. Christou, *J. Am. Chem. Soc*. **1998**, *120*, 2365.
[428] T. Mallah, C. Auberger, M. Verdaguer, P. Veillet, *J. Chem. Soc., Chem. Commun*. **1995**, 61.
[429] The term single-ion magnet is used in this section in order to mark a difference with polynuclear clusters; however, the compounds mentioned here are also called single-molecule magnets in the literature.

SMM $TbPc_2$ (*Figure 101*), described by Ishikawa *et al*.[430], in which obviously no intramolecular exchange coupling between metals could take place.

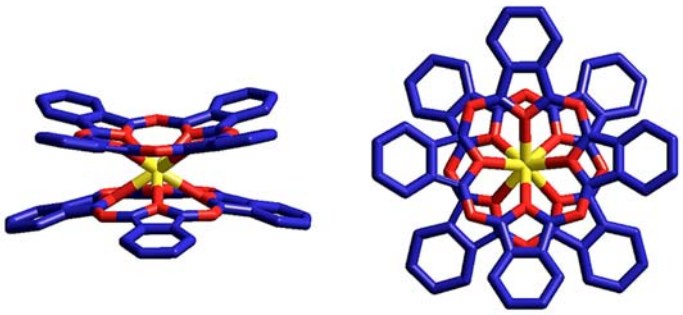

Figure 101.- Structure of $TbPc_2$, with Pcs in blue and Tb(III) atom in yellow. Nitrogen atoms are in red to show the square-antiprismatic coordination environment of the lanthanide.

These new systems were first limited to double-decker terbium(III) phthalocyanine complexes, and were extended recently to erbium polyoxometalates and to the first mononuclear transition metal SMM, a high spin iron (II) complex.[431] In this section, we will first review briefly the magnetic lanthanide polyoxometalates and we will then discuss, in more detail, the history and the magnetic behavior of lanthanide phthalocyanine double-decker complexes.

Magnetic polyoxometalates[432]

Polyoxometalates (POMs) are robust ligands capable of encapsulating lanthanides in high-symmetry coordination environments, making them well suited to SMM applications. Recently, Coronado *et al.* reported two families of monolanthanide polyoxometalates compounds[433,434] that behave as single-ion magnets: $[Ln(W_5O_{18})_2]^{9-}$ (for Ln^{3+} = Tb, Dy, Ho, and Er) and $[Ln(SiW_{11}O_{39})_2]^{13-}$ (for Ln^{3+} = Tb, Dy, Ho, Er, Tm and Yb). Out of all the prepared complexes, only the Ho and Er complexes of the form $[Ln(W_5O_{18})_2]^{9-}$ and the Dy, Ho, Er and Yb complexes of the form $[Ln(SiW_{11}O_{39})_2]^{13-}$ presented a slow magnetic relaxation characteristic of SMMs. Finally $[Er(W_5O_{18})_2]^{9-}$ was

[430] N. Ishikawa, M. Sugita, T. Ishikawa, S.-y. Koshihara, Y. Kaizu, *J. Am. Chem. Soc*. **2003**, *125*, 8694.
[431] a) W. H. Harman, C. J. Chang, *J. Am. Chem. Soc*. **2007**, *129*, 15128; b) D. E. Freedman, W. H. Harman, T. D. Harris, G. J. Long, C. J. Chang, J. R. Long, *J. Am. Chem. Soc*. **2010**, *132*, 1224.
[432] J. M. Clemente-Juan, E. Coronado, A. Gaita-Ariño, *Chem. Soc. Rev*. **2012**, *41*, 7464, and references therein.
[433] M. A. AlDamen, J. M. Clemente-Juan, E. Coronado, C. Martí-Gastaldo, A. Gaita-Ariño, *J. Am. Chem. Soc.* **2008**, *130*, 8874.
[434] M. A. AlDamen, S. Cardona-Serra, J. M. Clemente-Juan, E. Coronado, A. Gaita-Ariño, C. Martí-Gastaldo, F. Luis, O. Montero, *Inorg. Chem.* **2009**, *48*, 3467.

the only species exhibiting SMM behavior above 2 K. The symmetry of these polyoxometalate clusters is in principle the same as that of the double-decker lanthanide complexes (*Figure 102*), providing a similar environment to the lanthanide ion.

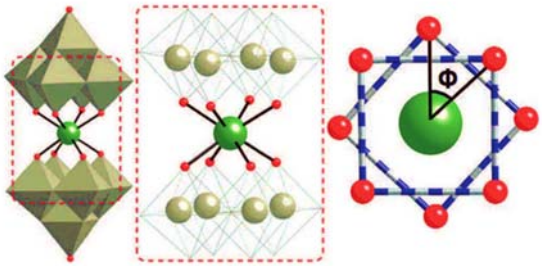

Figure 102.- Structure of $[Er(W_5O_{18})_2]^{9-}$ and projection showing the Er^{3+} ion square-antiprismatic coordination site.

It is worth noting that $TbPc_2$ and $[Er(W_5O_{18})_2]^{9-}$ are SMMs, but $[Tb(W_5O_{18})_2]_{9-}$ and $ErPc_2$ are not, possibly suggesting some sort of relationship. This apparently surprising result was interpreted using a detailed ligand field analysis of the POM complexes, which revealed that the ground state of Tb POM is not bistable ($m_J = 0$). In contrast, the ground state of Er POM derivative has $m_J = \pm 13/2$ and can display easy-axis magnetization. In terms of molecular structure, the main difference is the substitution of the nitrogen (Pc) by oxygen atoms (POM) in the coordination sphere of the lanthanide and a slight compression of the square antiprism defined by the lanthanide ion and the eight oxygen atoms with respect to the geometry of Ishikawa's compounds, in other words, the POM complexes are axially compressed and the Pc complexes are axially relatively elongated. These slight differences are enough to completely perturb the ligand field splitting parameters and thus the energy level of the ground-state multiplets.

More recently, this group has described a new family of magnetic polyoxometalates with a 5-fold symmetry: $[LnP_5W_{30}O_{110}]^{12-}$ (for Ln^{3+} = Tb, Dy, Ho, Er, Tm and Yb), and for the Dy and Ho derivatives, slow relaxation of the magnetization has been found.[435]

2.1.3 Lanthanide and yttrium phthalocyanine compounds

The lanthanides comprise the group of elements from La to Lu in the periodic table and they are characterized by the gradual filling of the 4f sub-shell. The electronic configurations of the neutral atoms show some irregularities, particularly for the stable $4f^7$

[435] S. Cardona-Serra, J. M. Clemente-Juan, E. Coronado, A. Gaita-Ariño, A. Camon, M. Evangelisti, F. Luis, M. J. Martinez-Perez, J. Sese, *J. Am. Chem. Soc*. **2012**, *134*, 14982.

configurations found in Eu and Gd. The trivalent cations of the lanthanides however, show strict regularity, all having the $4f^n5d^06s^0$ electronic configuration.[436] The chemistry of yttrium is usually reported with that of the lanthanides because it lies above lanthanum in group 3 of the periodic table; it has no 4f electrons, but forms a +3 ion with the Kr noble gas core and the size of both its atomic and ionic radii are comparable to Tb and Dy. It is also generally found in nature along with the lanthanides and resembles the Tb(III) and Dy(III) compounds in its compounds.[437] The absence of 4f electrons and the closed shell of Y(III) ion means the metallic core of its compounds are diamagnetic in nature and they therefore provide a good comparative study of magnetic phenomena in the lanthanides. The characteristic oxidation state of the lanthanides is the +3, but the +2 oxidation state is also important with the Eu^{+2} and Yb^{+2} being the most stable of the di-positive ions. Although higher oxidation states occur, they are not usual. Cerium forms a stable +4 species in aqueous solution. Dy, Tb, Pr, and Nd also form the +4 species.[438] There is a reduction in atomic size with an increase in atomic number in the lanthanides, the so called lanthanide contraction.[439] This trend is even more apparent in the radii of the trivalent ions. The reduction in size is due to the poor shielding of the 4f electrons as the nuclear charge increases. The electrons responsible for the properties of the lanthanide ions are the 4f electrons and the 4f orbitals are effectively shielded from the influence of external forces by the overlying $5s^2$ and $5p^6$ shells.[437] The result is that the electronic states arising from the various 4f n configurations are not significantly affected by surrounding ions and do not vary much for a given ion in all its compounds.

The Russell-Saunders[437,440] coupling gives a good approximation for the electronic states of the 4f n configurations. Spin-orbit coupling is present in lanthanide ions with non-zero orbital angular momentum. The spin-orbit couplings are also very large. This result in most of the lanthanide ions having ground states with well-defined values of total angular momentum, J, and the next lowest J state at energies many times the product of Boltzmann constant and temperature ($k_B \cdot T$). The magnetic susceptibilities and magnetic moments are for most part calculated from the well defined ground state and are in good agreement with experiment. For the lanthanides, the external fields do not either appreciably split the free ion terms or quench orbital angular momentum.[437] In

[436] J. E. Huheey, *Inorganic chemistry: principles of structure and reactivity* (2nd ed.), John Wiley and Sons, New York, **1978**.
[437] F. A. Cotton, G. Wilkinson, *Advanced inorganic chemistry: a comprehensive text* (4th ed.), John Wiley and Sons, New York, **1980**.
[438] T. Moeller, *J. Chem. Educ*. **1970**, *47*, 417.
[439] K. S. Pitzer, *Acc. Chem. Res*, **1979**, *12*, 271.
[440] J. G. Conway, B. G. Wybourne, *Phys. Rev*. **1963**, *130*, 2325.

forming complexes the lanthanides have a preference for coordination numbers greater than 6, being the most common co-ordination numbers of the Ln^{3+} ions, 8 and 9.[437]

Three general subgroups of the lanthanide phthalocyanines derivatives are known: lanthanide monophthalocyanines, bisphthalocyanines and dilanthanide trisphthalocyanines.[441] For the monophthalocyanines, the Ln^{3+} is coordinated to one dianionic tetradentate phthalocyanine ligand and can have axial ligands which are monoanionic and can be either mono- or bi-dentate. Other neutral ligand(s) can then complete coordination environment which is often 8 (*Figure 103*). The bisphthalocyanine, sometimes called double-decker or sandwich complexes consists of two Pc ligands. For the Ln^{3+} ion, one of the Pc ligands is dianionic and the other can be radical anionic. It has been argued that some of the lanthanides may form the Ln^{4+} and is instead coordinated to two dianionic Pc ligands.[442] The dilanthanide tris-phthalocyanines have two metal cations sandwiched between three Pc rings. This would make the regular Pc ligands dianionic.

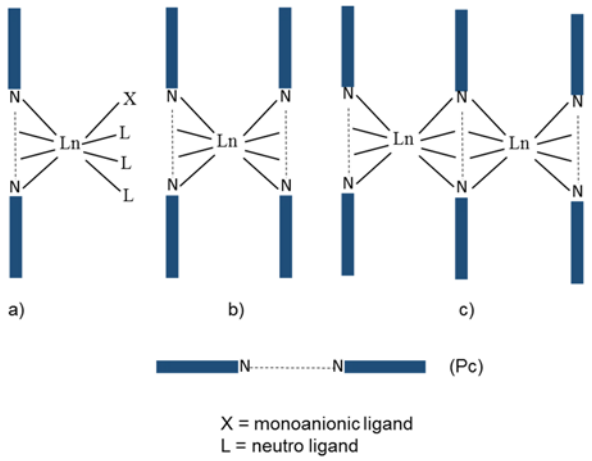

Figure 103.- Schematic representation of different possibilities of coordination for the lanthanides.

Several variations in the double deckers and triple deckers are possible.[441] For example, sandwich complexes have been synthesized with dissimilar Pc rings. That is, each ring has different substituents attached to it, and such bisphthalocyanines have been called heteroleptic. Dilanthanide tris-phthalocyanines, with the same two cations are referred to as homonuclear and with different cations, heteronuclear. These triple deckers can also be heteronuclear and heteroleptic (*Figure 104*).

[441] R. Weiss, J. Fischer, *Lanthanide Phthalocyanine Complexes*, Academic Press: San Diego, Vol. 16, p 171-246, **2003**.
[442] L. G. Tomilova, K. M. Dyumaev, O. P. Tkachenko, *Russ. Chem. Bull*. **1995**, *44*, 410.

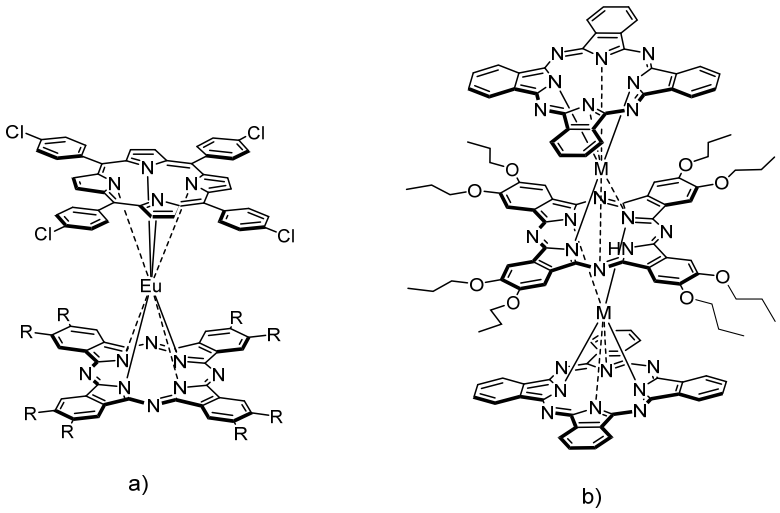

Figure 104.- a) porphyrin-phthalocyanine double-decker; b) porphyrin-phthalocyanine triple-decker.

2.1.3.1 Synthesis methods

There have been several reported methods for the preparation of bisphthalocyanines.[443] A popular method of synthesis is the solid state reaction of the substituted or un-substituted phthalonitriles and the lanthanide salt such as the acetate, as is shown in *Scheme 30*.

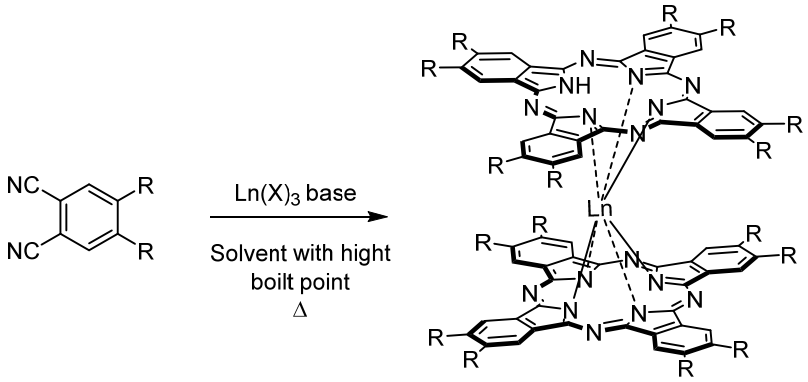

Scheme 30.- Synthethic procedure to obtain homoleptic compounds.

[443] a) V. E. Pushkarev, L. G. Tomilova, Y. V. Tomilov, *Russ. Chem. Rev*. **2008**, *77*, 875; b) J. Jiang, D. K. P. Ng, *Acc. Chem. Res*. **2009**, *42*, 79.

These reactions are a template reaction resulting in cyclic tetramerization of the phthalonitrile using the metal center. Reported difficulties with purifying the products of the solid state reaction, probably led to the development of solution reactions in which cyclotetramerization of the phthalonitrile occurred in alcohol with the presence of DBU[444,445] or in dimethylethanolamine.[445] The sandwich molecules can also be prepared from metal insertion into the metal free phthalocyanine analogues.[446] There are several established methods for the synthesis of metal free phthalocyanines. These also involve the cyclotetramerization of the respective phthalonitrile and include methods such as the cerium promoted synthesis,[447] lithium metal in alcohol (followed by acid work-up),[448] and the use of ionic liquids such as 1,1,3,3-tetramethylguaninidinium trifluoracetate.[449] The synthesis of the heteroleptic double deckers poses a greater challenge. It can be achieved by the reaction of one LnPc′ and the phthalonitrile necessary for the second substituted lanthanide phthalocyanine ring (Pc″), forming the (Pc′)Ln(Pc″) complex. The reaction of an alkali metal salt, with two different macrocycles and the lanthanide salt produces the heteroleptic as well as homoleptic species.[450,451]

2.1.3.2 Oxidized and reduced bisphthalocyanines

The lanthanide phthalocyaninate anions, $[(LnPc_2)]^-$ was first made by Konami *et al*.[452] This synthesis method used was cyclic tetramerization of phthalonitrile in the presence of the lanthanide salt and sodium carbonate. Separation of the sodium salts $Na[Pc_2Ln]$ and the addition of NBu_4Br yielded the TBA salts $NBu_4[LnPc_2]$. The sandwich compound has been reduced with hydrazine in the presence of tetrabutylammonium perchlorate and it yielded $NBu_4[LnPc_2]$.[453] The oxidized double decker $[LnPc_2]+$ species has been reportedly synthesized as the compound $[LnPc_2]SbCl_6$.This complex is

[444] A. De Cian, M. Moussavi, J. Fischer, R. Weiss, *Inorg. Chem*. **1985**, *24*, 3162.
[445] J. Sleven, C. Gorller-Walrand, K. Binnemans, *Mat. Sci. Eng. C* **2001**, *18*, 229.
[446] M. L´Her, Y. Cozien, J. Courtot-Coupez, *J. Electroanal. Chem. Interfacial Electrochem*. **1983**, *157*, 183.
[447] C.-H. Lee, D. K. P. Ng, *Tetrahedron Lett*. **2002**, *43*, 4211.
[448] M. J. Cook, A. J. Dunn, S. D. Howe, A. J. Thomson, K. J. Harrison, *J. Chem. Soc., Perkin Trans. 1* **1988**, *8*, 2453.
[449] A. Shaabani, A. Maleki, *J. Porphyrins Phthalocyanines* **2006**, *10*, 1253.
[450] W. Liu, J. Jiang, N. Pan, D. P. Arnold, *Inorg. Chim. Acta* **2000**, *310*, 140.
[451] V. E. Pushkarev, M. O. Breusova, S. E. Nefedov, L. G. Tomilova, *Mendeleev Commun*. **2007**, *17*, 220.
[452] H. Konami, M. Hatano, A. Taijiri, *Chem. Phys. Lett*. **1989**, *160*, 163.
[453] M. Moussavi, A. De Cian, J. Fischer, R. Weiss, *Inorg. Chem*. **1988**, *27*, 1287.

expected to contain two Pc radical anionic macrocycles.[454] The synthesis and characterization of the $SbCl_6^-$ precursor has been reported.[455,456]

2.1.3.3 Properties and applications

While the SMM behavior of double-decker pthalocyanine lanthanide complexes have been reported only recently, these systems have been known for many years. Indeed, the first synthesis of a lanthanide double-decker complex dates back to 1965,[457] and the lutetium(III) complex was structurally characterized as early as 1985.[444] Lu double-decker phthalocyanine complexes were also among the first molecular compound behaving as semi-conductors,[458] and have even been studied for field effect transistor applications.[459] In 1989, Belarbi *et al*. obtained a series of alkoxy functionalized double-decker phthalocyanine complexes and demonstrated their mesomorphic properties.[460] The phase behavior of functionalized lanthanide DD phthalocyanine complexes would later be the subject of many articles, demonstrating the versatility of the property.[461]

One of the most interesting reported characteristics of functionalized double-decker complexes towards nanotechnological applications is their ability to form well packed self-assembled monolayers over a graphite surface. This was demonstrated by STM experiments performed at the liquid-graphite interface.[462] This, combined with the single-molecule magnet behavior of the complexes, allows in principle to prepare a 2D-

[454] S. Takamatsu, N. Ishikawa, *Polyhedron* **2007**, *26*, 1859.
[455] N. Carnieri, A. Harriman, *Inorg. Chim. Acta* **1982**, *62*, 103.
[456] P. Gans, G. Buisson, E. Duee, J.-C. Marchon, B. S. Erler, W. F. Scholz, C. A. Reed, *J. Am. Chem. Soc*. **1986**, *108*, 1223.
[457] I. S. Kirin, P. N. Moskalev, Y. A. Makashev, *Russ. J. Inorg. Chem*. **1965**, *10*, 1065.
[458] a) M. Maitrot, G. Guillaud, B. Boudjema, J.-J. Andre, H. Strzelecka, J. Simon, R. Even, *Chem. Phys. Lett*. **1987**, *133*, 59; b) P. Turek, P. Petit, J.-J. Andre, J. Simon, R. Even, B. Boudjema, G. Guillaud, M. Maitrot, *J. Am. Chem. Soc*. **1987**, *109*, 5119; c) A. T. Chang, J.-C. Marchon, *Inorg. Chim. Acta* **1981**, *53*, 241.
[459] a) N. B. Chaure, J. L. Sosa-Sanchez, A. N. Cammidge, M. J. Cook, A. K. Ray, *Org. Elec*. **2010**, *11*, 434; b) G. Chaidogiannos, F. Petraki, N. Glezos, S. Kennou, S. Nespurek, *Mat. Sci. Eng. B* **2008**, *152*, 105.
[460] Z. Belarbi, C. Sirlin, J. Simon, J.-J. Andre, *J. Phys. Chem*. **1989**, *93*, 8105.
[461] a) C. F. van Nostrum, S. J. Picken, A.-J. Schouten, R. J. M. Nolte, *J. Am. Chem. Soc*. **1995**, *117*, 9957; b) K. Ban, K. Nishizawa, K. Ohta, A. M. van de Craats, J. M. Warman, I. Yamamoto, H. Shirai, *J. Mater. Chem*. **2001**, *11*, 321; c) K. Binnemans, C. Gorller-Walrand, *Chem. Rev*. **2002**, *102*, 2303; d) A. G. Gurek, T. Basova, D. Luneau, C. Lebrun, E. Koltsov, A. K. Hassan, V. Ahsen, *Inorg. Chem*. **2006**, *45*, 1667.
[462] a) K. Binnemans, J. Sleven, S. De Feyter, F. C. De Schryver, B. Donnio, D. Guillon, *Chem. Mater*. **2003**, *15*, 3930; b) A. S. Klymchenko, J. Sleven, K. Binnemans, S. De Feyter, *Langmuir* **2006**, *22*, 723.

array of independent nanometric units, which could represent individual data bits of a hypothetical ultra high density storage device (albeit at very low temperature).[463]

Finally, another interesting property of double-decker complexes is their electroactivity.[464,465] Indeed, these complexes can be oxidized or reduced to a variety of oxidation states ranging from -5 to +2. This is yet another degree of freedom added to the possibilities of the system in order to study its magnetic behavior, since the magnetic properties of the different oxidation states are likely to be different from one another. It has already been shown above that Ishikawa, and coworkers have reported how upon oxidation to the neutral complex, the magnetic properties of the anionic double-decker Tb(III) phthalocyanine complex are strongly modified, and present a higher effective barrier.[466]

2.1.4 Terbium(III) bisphthalocyaninato complexes

In 2002, after working with double and triple decker phthalocyanine complexes for several years,[467,468,469,470,471] Ishikawa *et al.* established a new method to determine the ligand field parameters of a series of neutral triple decker lanthanide complexes by theoretical analysis of their magnetic susceptibility and their ^{1}H-NMR spectra. Therefore, they could extract the energy diagram of the ground-state multiplets of the complexes.[472] The method was then applied to the determination of the ligand-field parameters of the closed-shell anionic double-decker lanthanide complexes, extracting again the groundstate multiplets energy diagram (*Figure 105*).[473]

[463] J. Gomez-Segura, I. Diez-Perez, N. Ishikawa, M. Nakano, J. Veciana, D. Ruiz-Molina, *Chem. Comm*. **2006**, 2866.
[464] P. Zhu, F. Lu, N. Pan, D. P. Arnold, S. Zhang, J. Jiang, *Eur. J. Inorg. Chem*. **2004**, *2004*, 510.
[465] K. M. Kadish, T. Nakanishi, A. Gurek, V. Ahsen, I. Yilmaz, *J. Phys. Chem. B* **2001**, *105*, 9817.
[466] N. Ishikawa, M. Sugita, N. Tanaka, T. Ishikawa, S.-y. Koshihara, Y. Kaizu, *Inorg. Chem*. **2004**, *43*, 5498.
[467] N. Ishikawa, Y. Kaizu, *J. Phys. Chem.* **1996**, *100*, 8722.
[468] N. Ishikawa, T. Okubo, Y. Kaizu, *Inorg. Chem.* **1999**, *38*, 3173.
[469] N. Ishikawa, Y. Kaizu, *J. Phys. Chem. A* **2000**, *104*, 10009.
[470] N. Ishikawa, *J. Porphyrins Phthalocyanines* **2001**, *5*, 87.
[471] N. Ishikawa, T. Iino, Y. Kaizu, *J. Am. Chem. Soc.* **2002**, *124*, 11440.
[472] N. Ishikawa, T. Iino, Y. Kaizu, *J. Phys. Chem. A* **2002**, *106*, 9543.
[473] N. Ishikawa, M. Sugita, T. Okubo, N. Tanaka, T. Iino, Y. Kaizu, *Inorg. Chem.* **2003**, *42*, 2440.

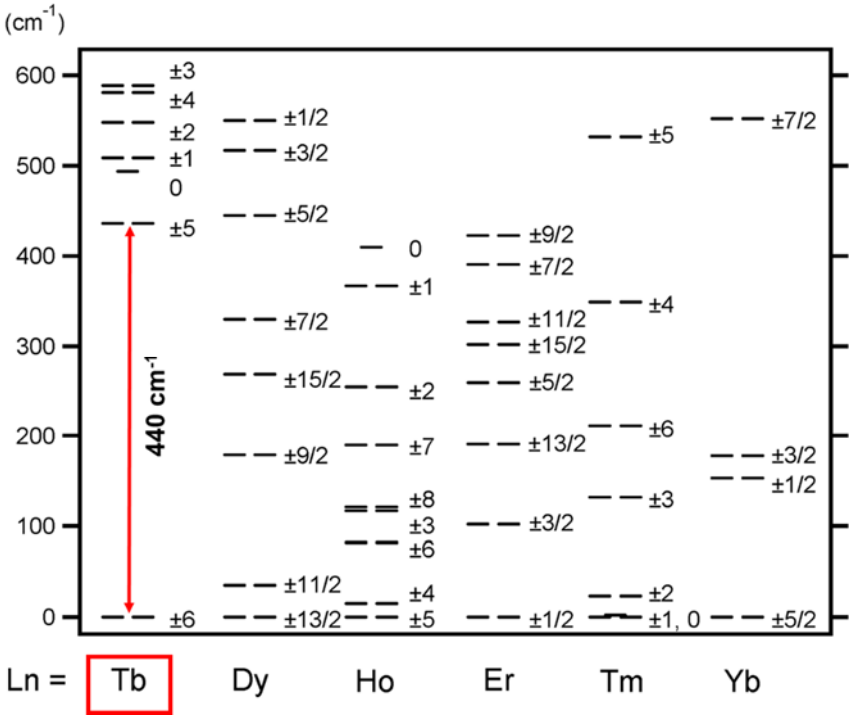

Figure 105.- Energy diagram of the substates of the ground multiplets of TBA[$LnPc_2$] (Ln = Tb, Dy, Ho, Er, Tm, or Yb). The *J* value of each substrate is indicated to the rightof the corresponding energy level.

Upon doing so, the energy diagram of the terbium(III) complex appeared to be a very appealing case. Indeed, the complex presents a $J = 6$ ground state, where $J = S + L$ is the total angular momentum, and the $m_J = 5$ multiplet was found to lay about 440 cm^{-1} or 633 K above the ground state, far too high to be populated thermally, which altogether predicted an outstanding behavior as a single-molecule magnet. In order to demonstrate the SMM behavior of the $[TbPc_2]^-$ complex, the ac magnetic susceptibility was recorded on a pure sample and on a 2% solid solution of the magnetic complex in the isomorphic diamagnetic yttrium(III) complex.[430] As expected, the ac magnetic susceptibility of the complex showed a peak in the imaginary component at a much higher temperature than those observed for the previously described SMMs. Indeed, while Mn_{12}ac has an ac magnetic susceptibility peak at 6 K at an oscillating field of 100 Hz, $[TbPc_2]^-$ in the same conditions presents a peak at 33 K (*Figure 106*).

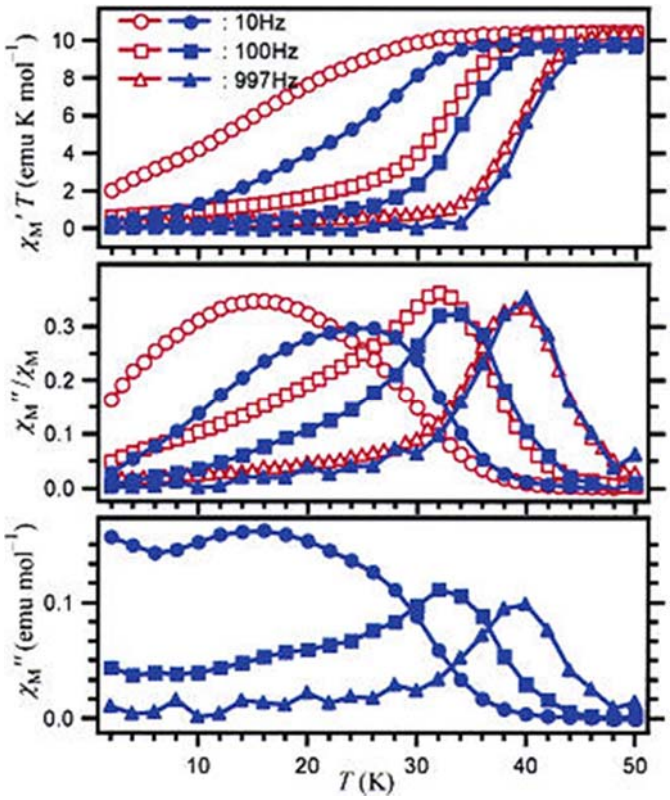

Figure 106.- Real χ_M' (above) and imaginary χ_M'' (middle and below) components of the ac magnetic susceptibility of $[TbPc_2]^-$ (open symbols) and of a 2% dilution of the same in the diamagnetic $[YPc_2]^-$ complex (solid symbols).

It is also interesting to notice that upon dilution, the characteristics of the complex were not lessened, but that on the contrary, the blocking temperature observed in the ac magnetic susceptibility curves were even increased. This was taken as a demonstration that the magnetic behavior was effectively an intramolecular one and that the weak intermolecular interactions were actually detrimental.

These data were completed later by magnetic hysteresis measurements done in the same solid solution conditions (*Figure 107*).[474]

[474] N. Ishikawa, M. Sugita, T. Ishikawa, S.-y. Koshihara, Y. Kaizu, *J. Phys. Chem. B* **2004**, *108*, 11265.

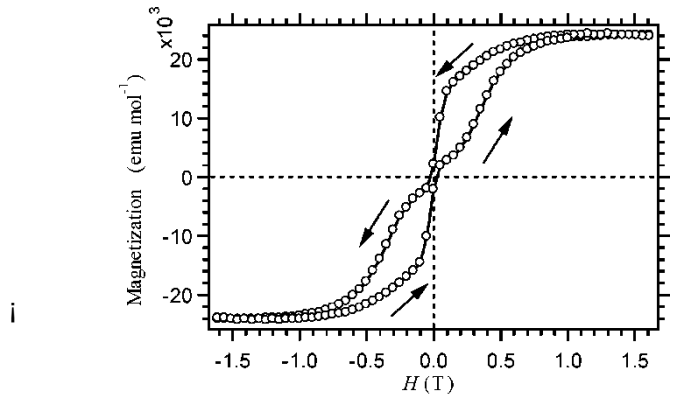

Figure 107.- Magnetization vs field plot measured at 1.7 K for a powder sample of $[TbPc_2]^-TBA^+$ diluted at a concentration of 2% in $[YPc_2]^-TBA^+$.

Despite the very high blocking temperature seen in the ac magnetic susceptibility of the $[TbPc_2]^-$ complex, the magnetization hysteresis was observed only at quite a low temperature (1.7 K), and it proved to be quite narrow close to zero-field (*i.e.* it presented a very small coercive field and a very small remnant magnetization). The magnetization hysteresis of the Dy complex was even narrower close to zero-field than that of the Tb complex.

The relaxation mechanisms involved in the $[TbPc_2]^-$ complexes were studied via Arrhenius analysis of the relaxation rate $1/\tau$ and the results are shown in *Figure 108*. In a non-Kramer system, that is when there is an even number of electrons like in Tb^{3+} ($4f^8$), the relaxation time of the paramagnetic ion is given by the spin-lattice relaxation and obeys:[475]

$$\tau^{-1} = R_{d(h\nu)} \coth(h\nu/2kT) + R_{or}\Delta^3[exp(\Delta/kT) - 1]^{-1} + R_r T^7 \qquad \textit{Eq. 11}$$

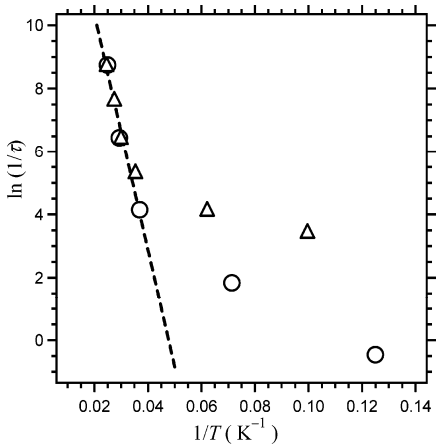

Figure 108.- Arrhenius plot of $ln(\tau^{-1})$ as a function of $1/T$ for the anionic terbium double-decker phthalocyanine complex (triangles) and the diluted sample of the same in the yttrium diamagnetic equivalent matrix (circles).

[475] A. Abragam, B. Bleaney, Electron Paramagnetic Resonance,*Chapter 10*, Clarandon press, Oxford, **1970**.

Where the first term corresponds to a direct spin-phonon coupling, the second term corresponds to an Orbach process (a two phonon process where the energy transferred to the lattice is given by the energy difference between the absorbed and emitted phonons for a low lying excited state) and the third one corresponds to a Raman process (a two phonon process where the energy transferred to the lattice is given by the energy difference between the absorbed and emitted phonons for a virtual excited state). The three type of processes are illustrated in *Figure 109*.

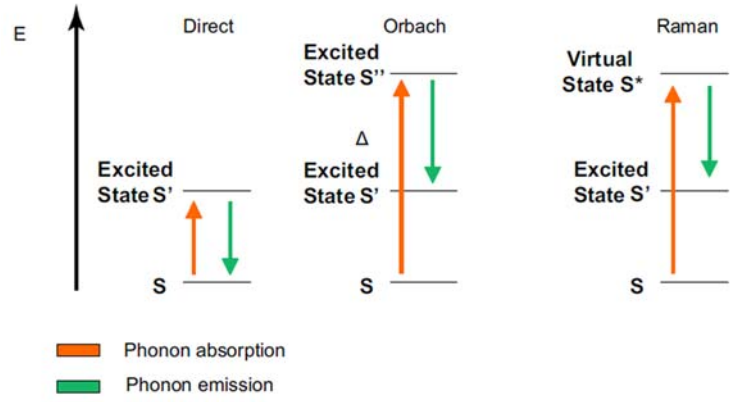

Figure 109.- Illustration of the three spin-lattice relaxation mechanisms: the direct spin-phonon coupling, the Orbach process and the Raman process.

It was shown that at high temperature (above 25 K), the response of the complex response occurs through a thermally activated Orbach regime with an activation barrier of about 260 cm^{-1} which was consistent in principle with the order of magnitude of the difference in energy between the ground state J = 6 to the first excited state J = 5 (440 cm^{-1}). At lower temperatures, below 25 K, another process occurred which was attributed to either a Raman process or a direct spin-phonon coupling. At the time, the authors concluded on the absence of quantum tunneling of magnetization steps in the magnetization hysteresis curve, and explained this absence by the huge energy difference between the ground-state and the first excited state of J = 5 (*Figure 110*). Nevertheless, after recording a low temperature hysteresis of magnetization on a monocrystal of formula TBA[$Pc_2Tb_{0.02}Y_{0.98}$], it was observed that the compound presents a staircase-like hysteresis, which is the trace of quantum tunneling of magnetization.[476]

[476] N. Ishikawa, M. Sugita, W. Wernsdorfer, *Angew. Chem. Int. Ed.* **2005**, *44*, 2931.

Since the J = 6 and the J = 5 states are too far apart, the observed resonant tunneling could not be due to a transition between them.

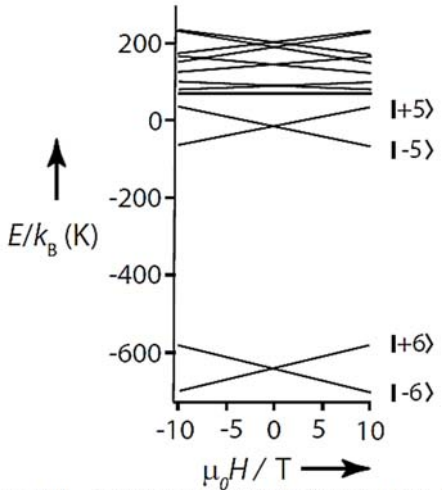

Figure 110.- Zeeman energy diagram for the J = 6 ground-state multiplet.

Instead, it was realized that terbium presents a nucleus with I = 3/2 in 100% natural abundance. Therefore, taking into account the interaction between the nucleus and the $4f^8$ system, the appropriate Hamiltonian for the system still contains the ligand field terms but one should add two additional terms corresponding to the hyperfine interaction $A_{hf}\boldsymbol{JJ}$ and the nuclear quadrupole interaction. Taking into account all of these parameters, it was therefore possible to assign the tunneling steps in the magnetization hysteresis curve to QTM between |±J>|±I> substates of the J = 6 ground-state in the range of a few mK (*Figure 111*). This nuclear spin driven quantum tunneling of magnetization was also demonstrated in a Holmium double-decker phthalocyanine complex.[477]

[477] N. Ishikawa, M. Sugita, W. Wernsdorfer, *J. Am. Chem. Soc.* **2005**, *127*, 3650.

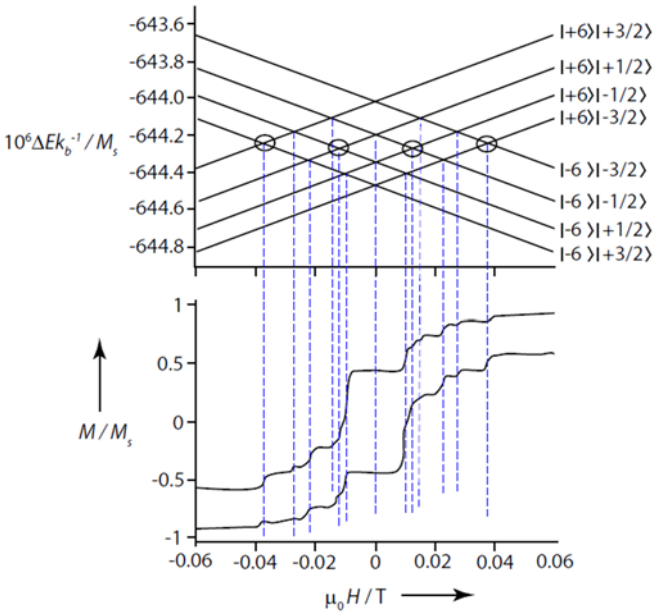

Figure 111.- Zeeman energy diagram (above) taking into account the ligand field splitting, the hyperfine interaction and the quandrupole interaction. Magnetization hysteresis measured at 0.04 K (below).

Finally, in 2004, it was shown that the neutral species $[TbPc_2]^0$ which is the one electron oxidation product of $[TbPc_2]^-$ and therefore presents an unpaired electron delocalized over the whole complex and can be written as $[Pc^{2-}Tb^{3+}Pc^{\bullet -}]$, also presents single-molecule magnet behavior.[466] Moreover, the neutral complex showed out of phase ac magnetic susceptibility peaks at higher temperature than the corresponding anionic compound (*Figure 112*). This suggests that this oxidation state might be a better single-molecule magnet than its parent anionic compound. Nevertheless, surprisingly, no hysteresis of magnetization was reported on this oxidation state at the beginning of the work toward this PhD thesis.

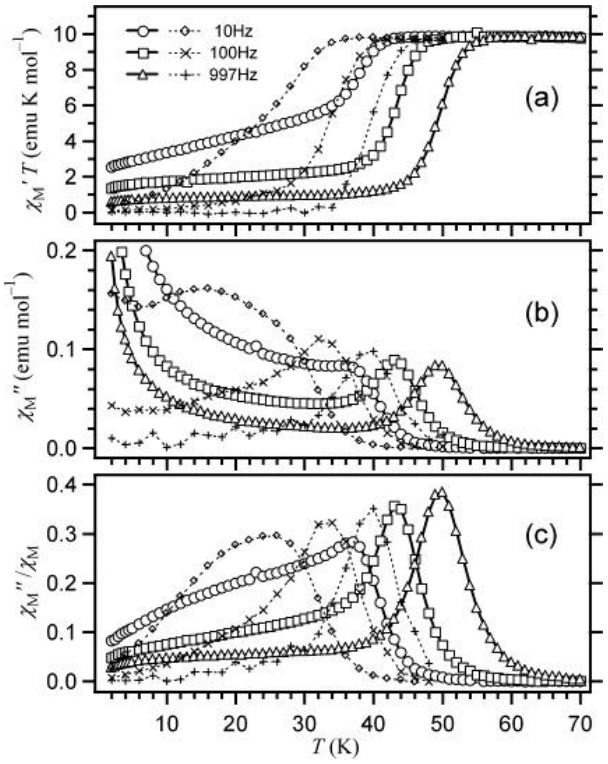

Figure 112.- Real χ_M' (above) and imaginary χ_M'' (middle and below) components of the ac magnetic susceptibility of $[TbPc_2]^0$ (full line) and $[TbPc_2]^-$ (dotted line).

In principle, the double-decker complexes can be found in a variety of oxidation states, and at the beginning of this work, the magnetic behavior of the cationic state and the polyanionic states had not yet been studied either, and only the magnetic behavior of the cationic species has been reported since then,[454,478] showing a further increase in the temperature of the peaks of the out of phase ac magnetic susceptibility plots.

[478] S. Takamatsu, T. Ishikawa, S.-y. Koshihara and N. Ishikawa, *Inorg. Chem.* **2007**, *46*, 7250-7252.

2.2 Objectives

The main goal of the present section of *chapter 1* is the preparation and in depth structural and magnetic characterization of a series of Tb(III) bisphthalocyaninato complexes in their neutral or anionic forms (as tetraalkylammonium salts), holding different peripheral substituents in either one or two of the Pc ligands. Therefore we aim to prepare various homoleptic and heteroleptic Tb(III) double-decker complexes, which will allow us to estimate the possible influence of the number and electronic nature of the peripheral substituents, as well as the presence or not of an unpaired electron at the Pc ligands, on the SMM behavior of these type of complexes.

Synthesis of homoleptic and heteroleptic Tb(III) bisphthalocyaninato

The magnetic behavior of lanthanide double-decker has been studied only on the archetypal $LnPc_2$, without substitution of the macrocyclic rings. By chemical modification of the phthalocyanine ligands, the objective of this work is to synthesize new functionalized homoleptic and heteroleptic Tb(III) double-decker (*Figure 113*), both as neutral forms as anionic derivatives, in order to produce functional magnetic material.

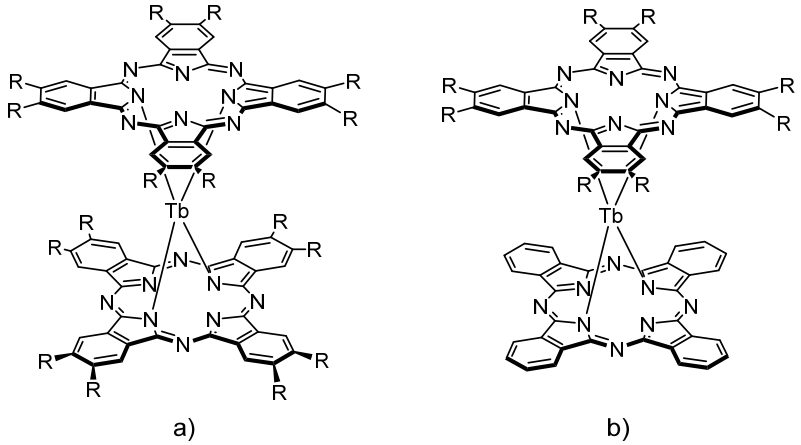

Figure 113.- Molecular structure of a) homoleptic and b) heteroleptic terbium(III) bisphthalocyanine complexes.

Synthesis of dimeric Tb(III) bisphthalocyaninato

The study of interaction between terbium(III) atoms in this type of structure has been carried out principaly in triple-decker complexes. However, our approach is focus on studying these interactions in dimeric double-decker, where two double-deckers are covalently linked. In this case, the selected linker must offer some flexibility due to these structures tend to be very rigid. Therefore, a triple bond seems to be the best option (*Figure 114*).

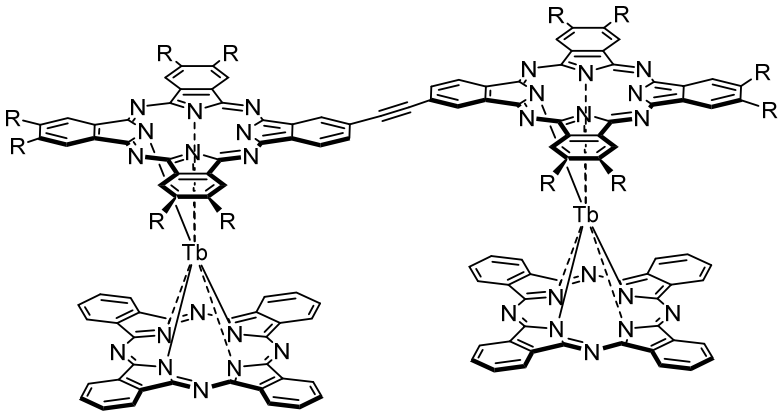

Figure 114.- Molecular structure of an heteroleptic dimeric terbium(III) bisphthalocyanine complex. Other possibility is to obtain an heteroleptic derivative where the terbium atoms are not in the same plane.

Magnetic studies of double-decker complexes

Finally, all of the new magnetic material will be magnetically characterized in collaboration with Prof. E. Coronado at ICMOL. Typical magnetic parameters such as U_{eff} and τ^{-1} will be achieved and compared to obtain a rational relationship between structure and magnetic response.

2.3 Results and discussion

2.3.1 Terbium(III) bisphthalocyaninato complexes

Neutral homoleptic and heteroleptic Tb(III) double-deckers with electron-donor substituents

The classical method for the preparation of homoleptic sandwich compounds involves the self-condensation of phthalonitriles in the presence of metal salts.[479] With this purpose, the synthesis of 4,5-bis[(*para-tert*-butyl)phenoxy]phthalonitrile (**53**) was carried out in one step by reaction of 4,5-dichlorophthalonitrile (**11**) in a DMSO / K_2CO_3 medium, in *ca*. 83% yield (*Scheme 32*).

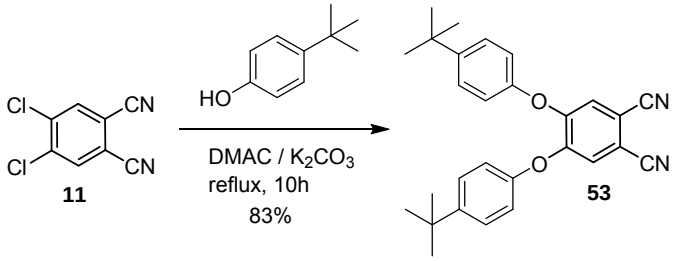

Scheme 32.- Synthesis of phthalonitrile **53**.

Following the classical approach, homoleptic terbium(III) bis(phthalocyaninate) complex **54** was prepared by heating the corresponding terbium(III) acetylacetonate salt ([Tb(acac)$_3$]·*n*H_2O) at reflux in the presence of 4,5-bis[(*para-tert*-butyl)phenoxy]phthalonitrile (**53**), with 1-pentanol as solvent and DBU as a basic catalyst (*Scheme 33*). At this stage, the crude product of the reaction contained a mixture of free radical [Tb(Pc)$_2$] (**54**) and its corresponding reduced protonated complex, [Tb(Pc)$_2$H]. To fully convert this mixture into the free-radical neutral form (**54**), DDQ was added to oxidize the reduced [Tb(Pc)$_2$H] species in solution. Further chromatographic purification yielded compound **54** in 51% yield.

The structure of this neutral homoleptic compound **54** was confirmed by using various spectroscopic methods: MS, FT-IR, UV-Vis and ^{1}H-NMR. The spectrum of the

[479] a) A. Pondaven, Y. Cozien, M. L'Her, *New. J. Chem.* **1991**, *15*, 515; b) N. Ishikawa, O. Ohno, Y. Kaizu, *Chem. Phys. Lett*. **1991**, *180*, 51; c) A. Pondaven, Y. Cozien, M. L'Her, *New. J. Chem.* **1992**, *16*, 711; d) N. Ishikawa, Y. Kaizu, *Chem. Phys. Lett*. **1993**, *203*, 472; e) F. Guyon, A. Pondaven, P. Guenot, M. L'Her, *Inorg. Chem.* **1994**, *33*, 4784.

latter could be recorded upon the addition of hydrazine hydrate to a solution of this compound in a mixture of DMF-d_7 and CCl_4. In this way, the π-radical form was transformed into the reduced form, which is the active specie in NMR.

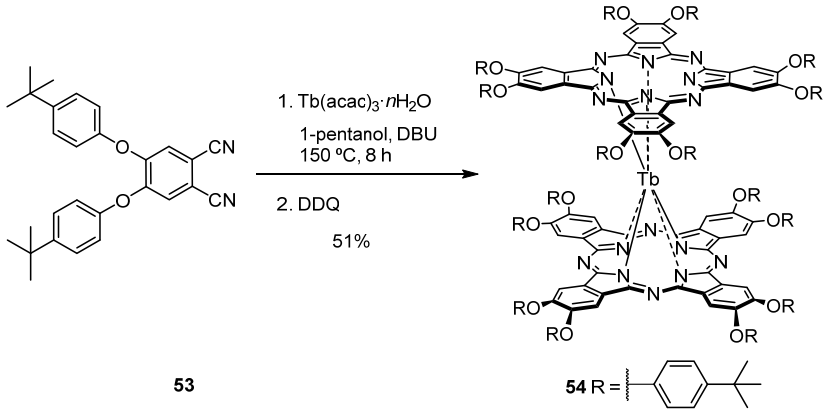

Scheme 33.- Synthesis of homoleptic double-decker **54** in its neutral form.

In *Figure 115* are exhibited the large negative chemical shifts for the aromatic protons on the Pc ligands of compound **54**, as a consequence of the strong, upfield paramagnetic shifts that are induced by the terbium(III) ion.[480]

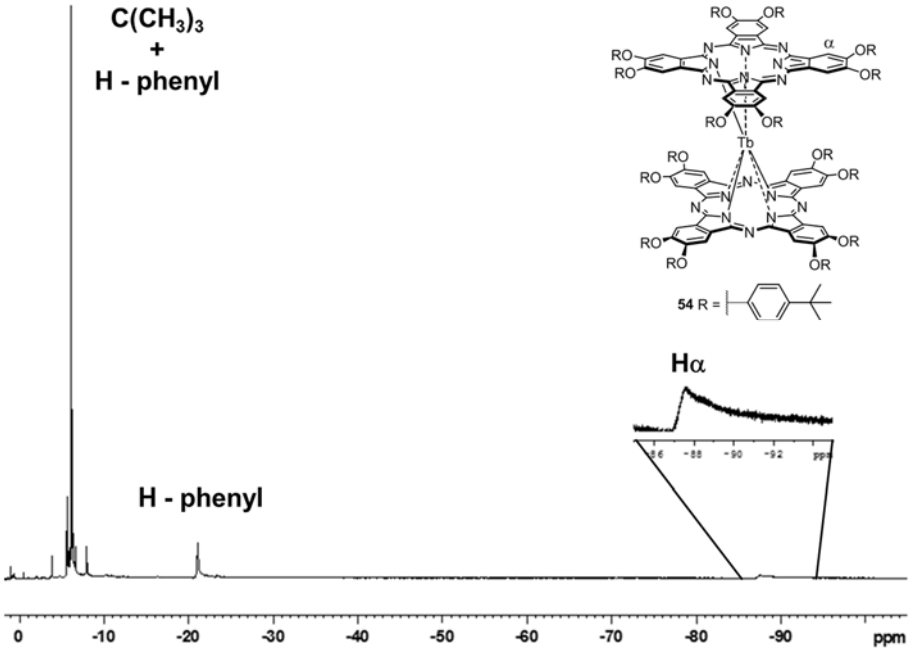

Figure 115.- ^{1}H-NMR spectrum of compound **54** in DMF-d_7/CCl_4.

[480] N. Ishikawa, T. Iino, Y. Kaizu, *J. Phys. Chem. A* **2003**, *107*, 7879.

Regarding heteroleptic rare-earth-metal bis(phthalocyaninate) compounds, the most convenient method in terms of simplicity and product conversion, involves the formation of an intermediate mononuclear lanthanide(III) Pc complex, starting from the free-base macrocycle, followed by cyclic tetramerization of the phthalonitrile (or naphthaloitrile) around the terbium(III) center of the preformed monophthalocyaninate.[481,482] The synthesis of the free-base **55** and **56** was carried out employing the corresponding phthalonitriles **53** and the commercially available 4-*tert*-butylphthalonitrile, respectively:

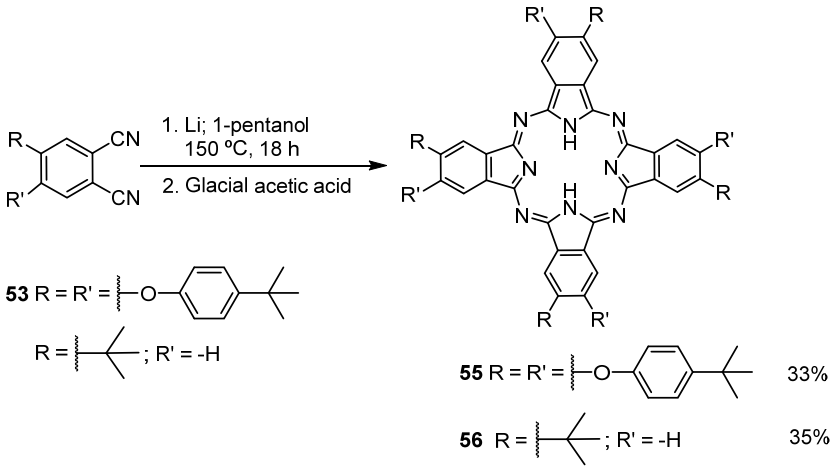

Scheme 34.- Synthesis of symmetrically substituted metal-free Pc **55** and **56**.

Compounds **55** and **56** were obtained following the standard procedure depicted in *Scheme 34*. The purified phthalonitrile **53** was cyclized in a refluxing mixture of 1-pentanol and lithium metal. In these conditions, a dilithium phthalocyaninate ($PcLi_2$) was obtained, which was further converted in the metal-free Pc **55** by addition of glacial acetic acid. Purification by column chromatography led to the isolation of metal-free Pc **55** in 33% yield. The same procedure was followed for macrocycle **56** (35%). Afterwards, the preparation of heteroleptic Tb(III) bis(phthalocyaninatos) compounds **57** and **58** began with the reaction of their metal-free Pc derivatives (**57**, **58**) and ($[Tb(acac)_3]\cdot nH_2O$ at *ca*. 170 ºC in *o*-DCB. The formation of the corresponding mononuclear Tb(III)acetylacetonate-Pc intermediates (**57 intermediate**, **58 intermediate**) was

[481] a) G. Lu, M. Bai, R. Li, X. Zhang, C. Ma, P.-C. Lo, D. K. P. Ng, J. Jiang, *Eur. J. Inorg. Chem*. **2006**, *18*, 3703; b) J. Jiang, W. Liu, W.-F. Law, J. Lin, D. K. P. Ng, *Inorg. Chim. Acta* **1998**, *268*, 141; c) N. Sheng, R. Li, C.-F. Choi, W. Su, D. K. P. Ng, X. Cui, K. Yoshida, N. Konayashi, J. Jiang, *Inorg. Chem.* **2006**, *45*, 3794.

[482] B. Ballesteros, G. de la Torre, A. Shearer, A. Hausmann, M. A. Herranz, D. M. Guldi, T. Torres, *Chem. Eur. J.* **2010**, *16*, 14.

monitored by UV-vis experiments, where one can appreciate a decrease in the intensity of the two distinctive bands of the low-symmetry metal-free Pc derivatives and the growing of a new band in between them (*Figure 116*).

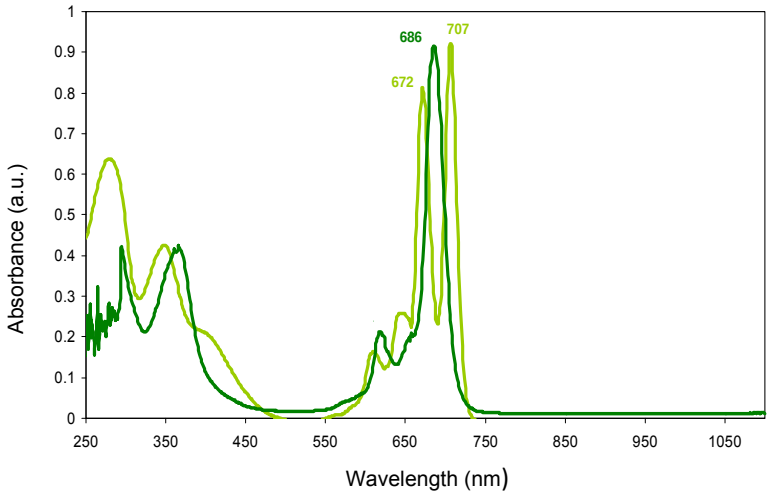

Figure 116.- Absorption spectra of Pc **55** (light green) and the corresponding **57 intermediate** (dark green) in $CHCl_3$.

After the evaporation of the solvents, the mononuclear intermediates were reacted, without further purification, with phthalonitrile in the presence of DBU in *o*-DCB/1-pentanol at 160 ºC, thereby yielding their corresponding heteroleptic double-decker compounds (**57** and **58**). Treatment of the crude material with DDQ caused the oxidation of the protonated [Tb(Pc)(Pc')H species, which were also formed during the process, to give the target neutral compounds. Compounds **57** and **58** were isolated in 49% and 47% yield, respectively, after column chromatography on silica gel (*Scheme 35*). Following this procedure, there was also obtained an heteroleptic double-decker in which one of the macrocycles is a naphthalocyanine (**59**), which possess four additional benzo groups fused to the peripheral benzo groups of the Pc core. The yield was similar (46%).

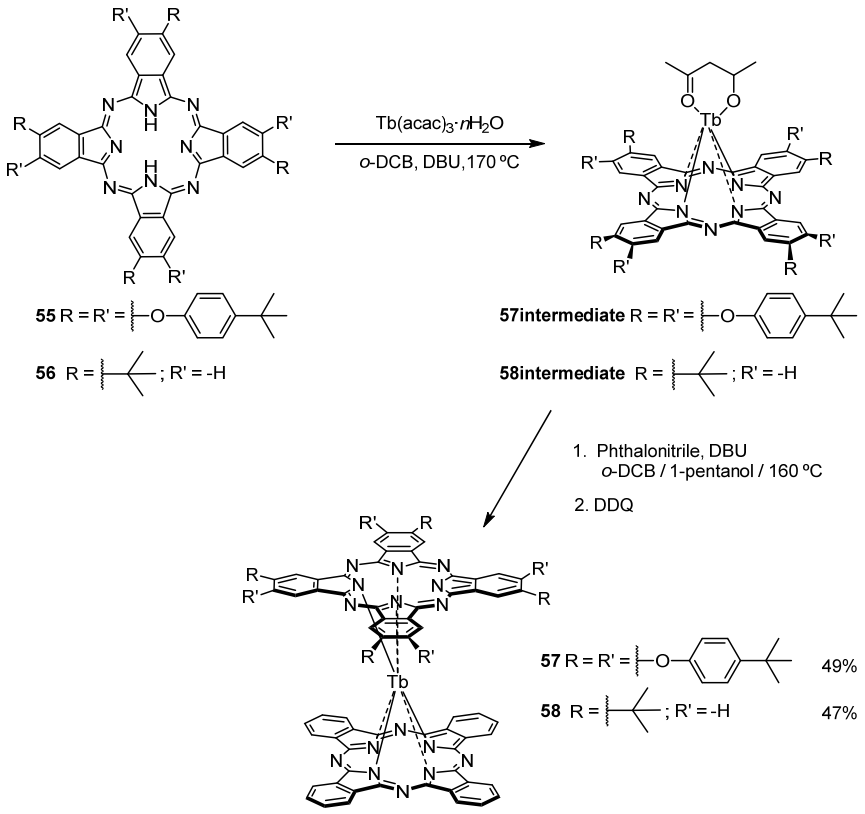

Scheme 35.- Synthesis of heteroleptic double-deckers **57** and **58** in its neutral forms.

The characterization of heteroleptic neutral compounds was also thorough. The FT-IR spectra of all of the neutral Tb(III)bis(phthalocyaninate) complexes showed an intense band at about 1320 cm^{-1} (*Figure 117*), which is a marker band for the Pc π-radical. Unpaired electrons are typically delocalized over both rings in homoleptic lanthanide(III) Pc complexes.[483] In heteroleptic derivatives **57**, **58** and **59**, the localization of the hole was not elucidated, but, according to previous literature reports on double-decker compounds that were comprised of different tetrapyrrolic rings with different electronic densities,[483] the hole should mainly be located in the subunit that has the lower HOMO, that is, in the bare ring.

[483] Y. Zhang, X. Cai, P. Yao, H. Xu, Y. Bian, J. Jiang, *Chem. Eur. J*. **2007**, *13*, 9503.

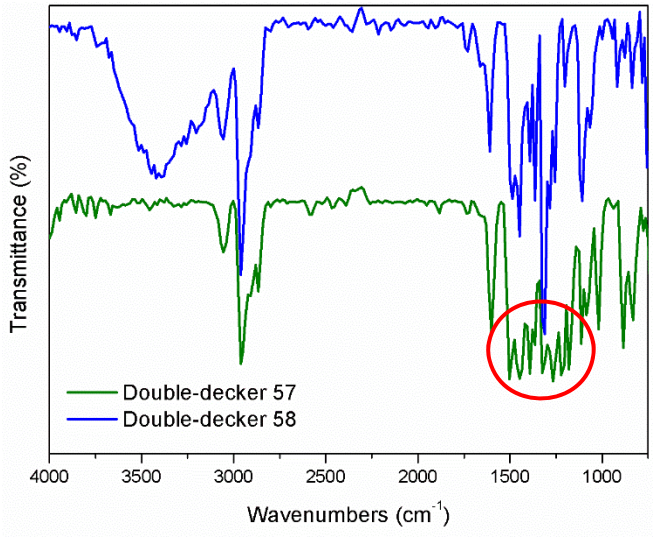

Figure 117.- Comparison of FT-IR spectra of neutral heteroleptic sandwiches **57** and **58**. The π-radical band zone is highlighted in red.

Anionic homoleptic and heteroleptic Tb(III) double-deckers with electron-donor substituents

The conversion of homoleptic complex **54** into stable, reduced alkylammonium salts **60** and **61**, was carried out by reduction with hydrazine hydrate in DMF (*Scheme 36*). This treatment afforded the protonated form of the bis(phthalocyaninate) complex, in which one of the Pc rings had become negatively charged but the anion was neutralized by an extra hydrogen atom. This reductive treatment was followed by the addition of sodium methoxide as a base to abstract the N-H proton and the subsequent addition of an excess of the alkylammonium (either tetramethyl- or tetrabutylammonium) bromide to induce the precipitation of the terbium(III) complexes in the form of alkylammonium salts (*i.e.*, **60** and **61**). A key issue for the manipulation of these reduced forms is that they suffer from instantaneous oxidization when dissolved in certain solvents, such as $CHCl_3$ and THF. The conversion of heteroleptic complexes **57** and **58** into stable, reduced alkylammonium salts **62** and **63**, and **64** and **65**, respectively (*Scheme 36*), was carried out as mentioned above for homoleptic derivatives reduction with hydrazine hydrate in DMF, followed by the addition of sodium methoxide and alkylammonium (tetramethyl- or tetrabutylammonium) bromide. The yields of these reactions were 88% or more.

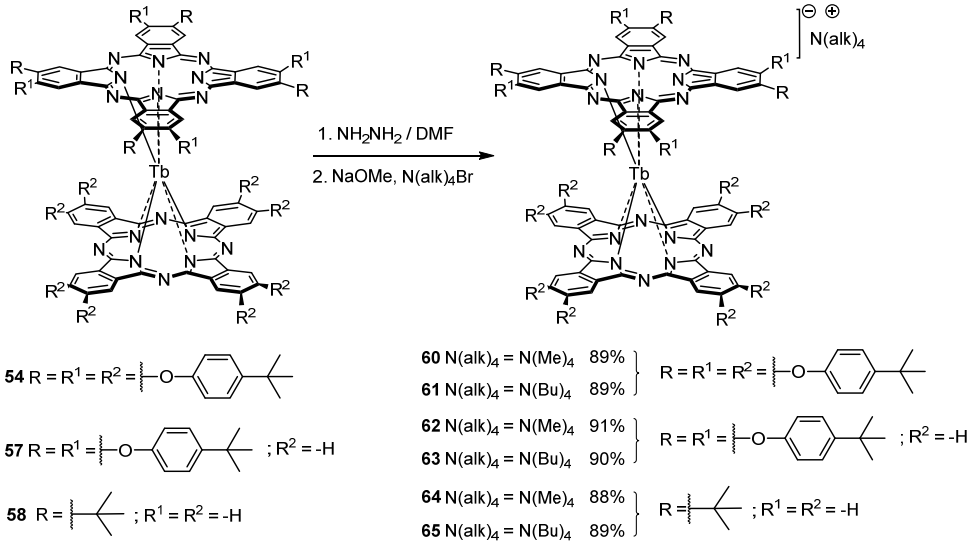

Scheme 36.- Synthesis of homoleptic and heteroleptic, reduced forms.

Following this procedure, there was also obtained the reduced forms of the heteroleptic double-decker with a naphthalocyanine (**66** and **67**) in high yields.

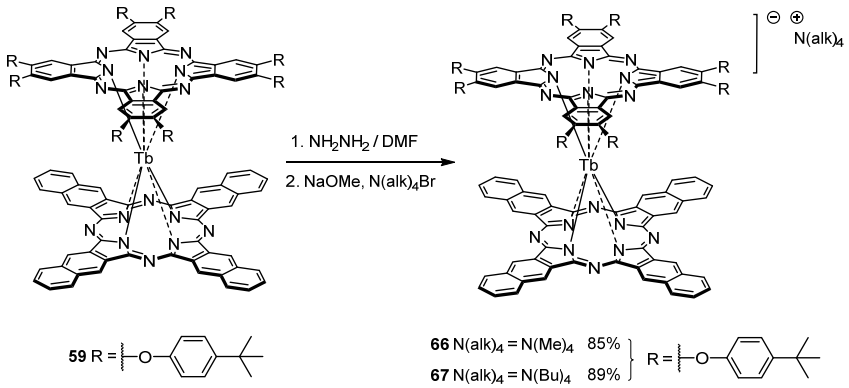

Scheme 37.- Synthesis of heteroleptic reduced forms **66** and **67**.

As a representative example of the ^{1}H-NMR features of these salt derivatives, the spectrum of tetrabutylammonium salt **63** is shown in *Figure 118*. The multiplicity of the signals is not discernible in the ^{1}H-NMR spectra of Tb(III)complexes, as previously shown by other authors. In general, the β protons of the unsubstituted Pc rings of heteroleptic complexes **57**, **59**, **62**, **63**, **66** and **67**, and, in particular, the β' protons of the monosubstituted Pc rings in compounds **58**, **64** and **65** resonate at lower field (*i.e.*, between δ = -42 and -47 ppm) than the α and α' protons on the substituted and unsubstituted Pc rings (*i.e.*, between δ =-88 and -98 ppm). The signals of both the *tert*-

butyl and phenyl radicals also appear at negative chemical shifts, but smaller lanthanide-induced shifts apply, provided that the peripheral substituents are farther from the paramagnetic ion than the protons on the Pc ligand. The resonances for the alkyl-chain protons of the ammonium cation appear at positive chemical shifts (*Figure 118*). Importantly, a comparison of the chemical shifts of related homo- and heteroleptic complexes reveals that all signals of the homoleptic substituted double-decker compounds appear at lower field than the equivalents in their heteroleptic counterparts. Because the terbium-induced shifts are larger in heteroleptic compounds, it could be inferred that the N-Tb distances are, indeed, shorter in these complexes.[484] This feature could affect the SMM parameters of these molecules, as we see below in the magnetic-characterization section.

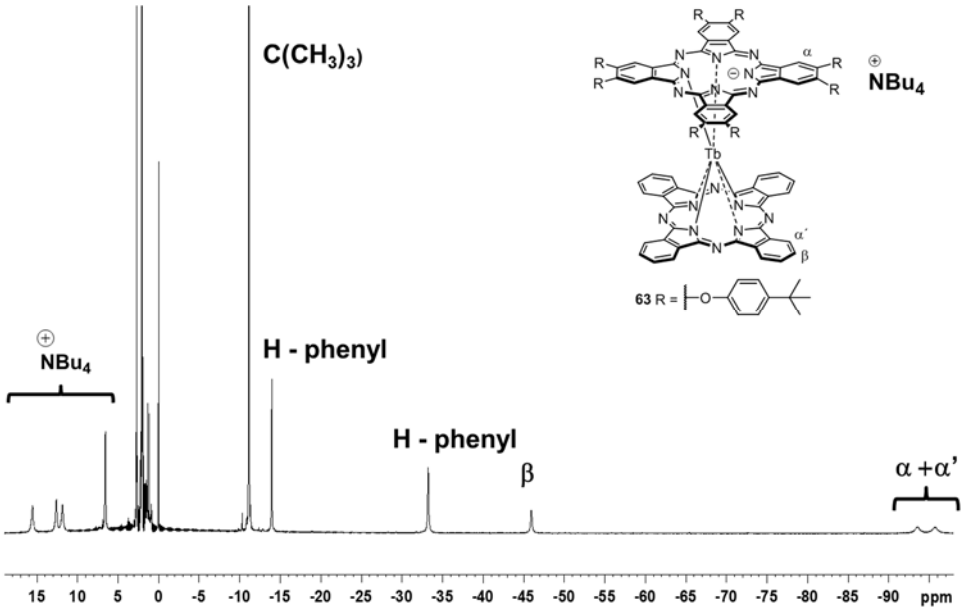

Figure 118.- ^{1}H-NMR spectrum of compound **54** in acetone-d_6.

The electronic absorption spectra of free-radical species **54**, **57**, and **58** exhibit the typical features of single-hole bis(phthalocyaninates) (*Figure 119*).[443b] The Q bands for these compounds, which result from transitions from the first semi-occupied molecular

[484] Please note that the chemical shifts of the α and β protons in unsubstituted [$TbPc_2$] lie in-between the signals of the equivalent protons in compounds **54** and **57**, thus indicating that the N-Tb distances are longer in heteroleptic compounds that are substituted with electron-donor groups (*i.e.*, compound **54** shows the least-negative chemical shifts) and that heteroleptic functionalization brings the rings closer to the lanthanide ion (*i.e.*, compound **57** shows the most-negative chemical shifts).

orbital (SOMO) to the second LUMO and from the second fully occupied HOMO to the first LUMO,[470,485] appear at around 671–682 nm. In addition, the two weak π-radical bands at about 460–500 nm and 915–925 nm can be attributed to electronic transitions that involve the SOMO. In the absorption spectra of the reduced tetraalkylammonium salts (**60**-**65**), the typical π-radical bands are absent; the most distinctive feature in these spectra is the splitting of the Q bands into two major components: one at about 626–632 nm and the other at about 675–687 nm (*Figure 119*). In general, the Q bands of heteroleptic compounds are hypsochromically shifted with respect to their homoleptic derivatives, which indicates stronger electronic interactions between the two rings in the heteroleptic double-decker compounds and, therefore, smaller interligand distances than in the homoleptic compounds.

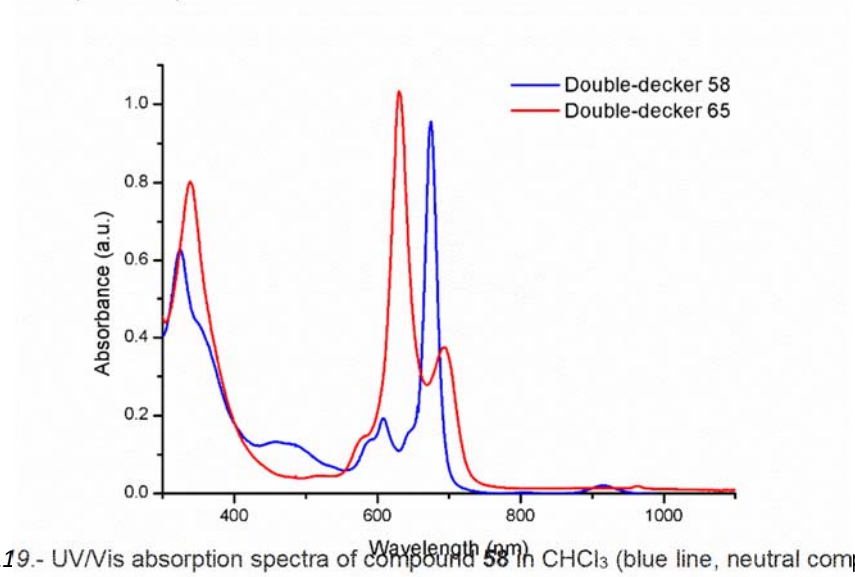

Figure 119.- UV/Vis absorption spectra of compound **58** in $CHCl_3$ (blue line, neutral complex) and compound **65** in MeCN (red line, reduced complex).

Neutral homoleptic and heteroleptic Tb(III) double-deckers with electron-acceptor substituents

The lack of lanthanide(III) bis(phthalocyanine) with electron-acceptor substituents in the literature, is a clear example of how tricky is their synthesis. At the beginning of this project only one precedent, described by Kitamura *et al*., showed a tetrabutylammonium bis(octacyanophthalocyaninato)neodymium(III) complex.[486] The first attempts to obtain a terbium (III) homoleptic complex of cyano-substituted

[485] E. Orti, J. L. Bredas, C. Clarisse, *J. Chem. Phys*. **1990**, *92*, 1228.
[486] T. Yonekura, T. Ohsaka, F. Kitamura, K. Tokuda, *J. Porphyrins Phthalocyanines* **2005**, *9*, 54.

phthalocyanines followed the procedure described in that article, where a mixture of 1,2,4,5-tetracyanobenzene, terbium(III) salt, tetrabutylammonium hexafluorophosphate, and DBU in sulfolane was heated at 135 ºC for 3h under a nitrogen atmosphere. The target compound was synthesized, as can be seen in *Figure 120.*

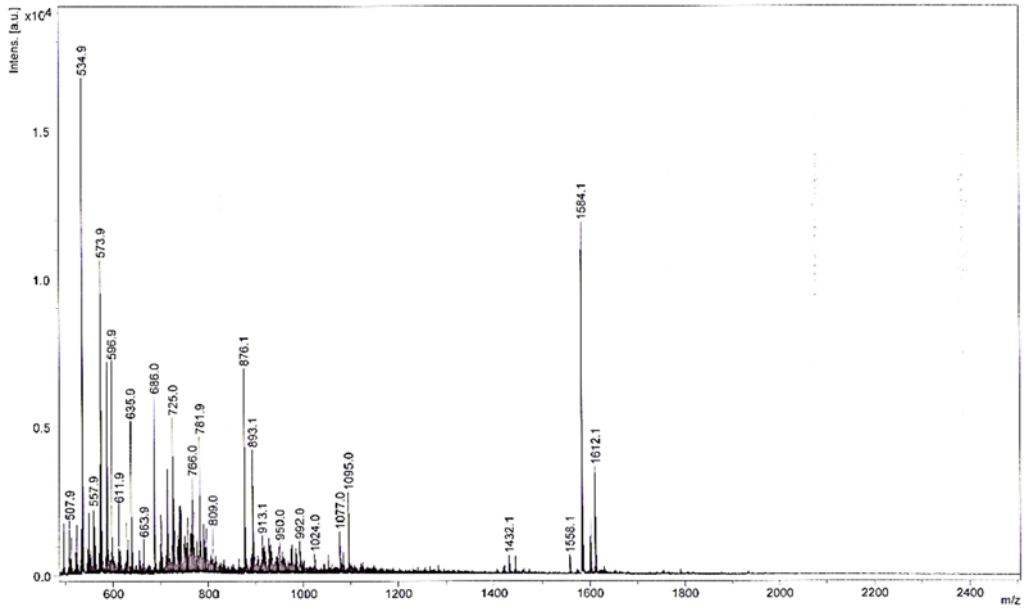

Figure 120.- Negative polarity MALDI-TOF mass spectrum of the impure octacyano derivative terbium (III) complex.

However, it is well-known that the synthesis of octacyanophthalocyanine complexes is sensitive to many factors, and some oligomers might also be present.[487] Even after an intense purification, and seeing the mass spectrum, we cannot believe the purity of the sample was high enough. Then, more phthalonitriles, such as 4-nitrophthalonitrile, 3,4,5,6-tetrafluorophthalonitrile, sulfonylphthalonitriles and even their more reactive 1,3-diiminoisoindoline derivatives were employed in the same conditions, and with the same disastrous results. All these phthalonitriles and diiminoisoindolines were tested in *o*-DCB (to avoid nucleophilic solvents) at 160 ºC, although it was not detected the presence of any double-decker or monophthalocyaninato. Moreover, the use of microwave was found unuseful in this type of synthesis. Once the homoleptic derivatives were dropped, it was easy to decide that the synthesis of heteroleptic compounds with one phthalocyanine substituted with electron-acceptor moieties must start with the generation of the monophthalocyaninato with electron-donor substituents.

[487] D. Wohrle, U. Marose, R. Knoop, *Makromol. Chem*. **1985**, *186*, 2209.

However, even with a preformed structure, the electron-acceptor phthalonitriles were not capable of doing the cyclotetramerization.

2.3.2 Dimeric terbium(III) bisphthalocyaninato complexes

At first glance, heteroleptic binuclear double-deckers seem to be easier to synthesize than homoleptic, due to geometric reasons. The retrosynthesis offers two clear possibilities (*Figure 121*):

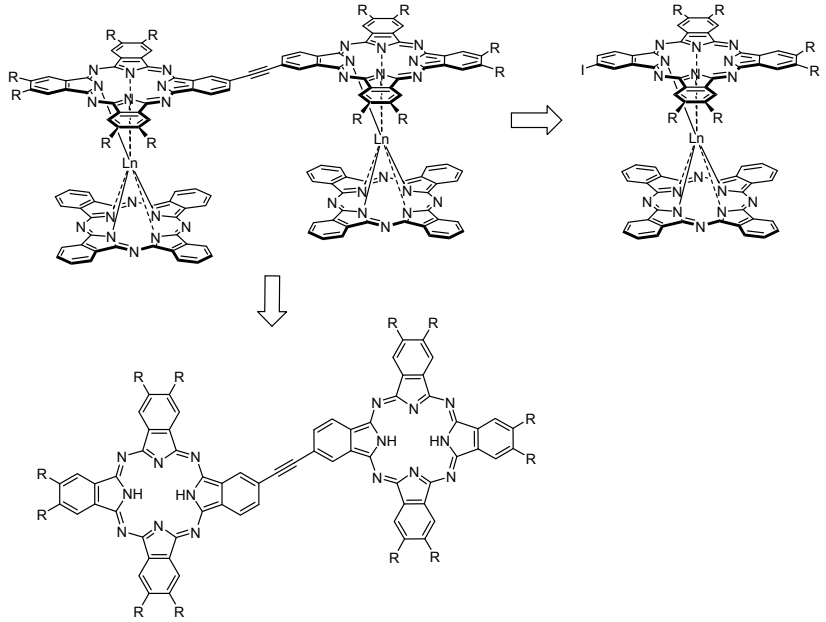

Figure 121.- Retrosynthesis of heteroleptic binuclear double-decker. On the one hand, there is a iodo-sandwich derivative, and on the other hand, there is a free-base binuclear phthalocyanine.

For simplicity, it was chosen the iodo-double-decker route. As mentioned above, the traditional heteroleptic approach employes a free-base macrocycle (**68**), which was previously synthesized. However, the sandwich obtained presented a hydrogen instead of a iodo (*Scheme 38*).

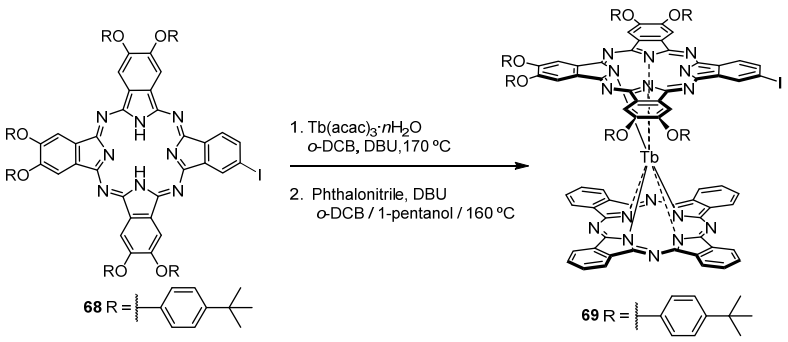

Scheme 38.- Synthesis of heteroleptic compound **69**.

In order to obtain a dimeric compound, a iodo-Mg(II)Pc derivative **70** was synthesized, following previously commented procedures, in a moderate yield (21%). Then, employing a palladium-catalyzed coupling (*Scheme 39*), was obtained the dimer Pc **71** after chromatographic purification, in an excellent yield (65%).

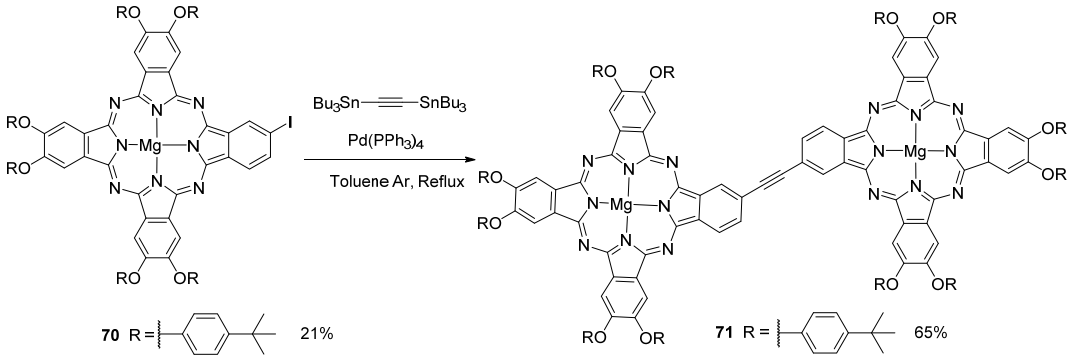

Scheme 39.- Synthesis of dimeric compound **71**.

The next step involved trifluoroacetic acid at room temperature to obtain the demetallated compound **72** after 18h in a quantitative way and without further purification (*Scheme 40*).

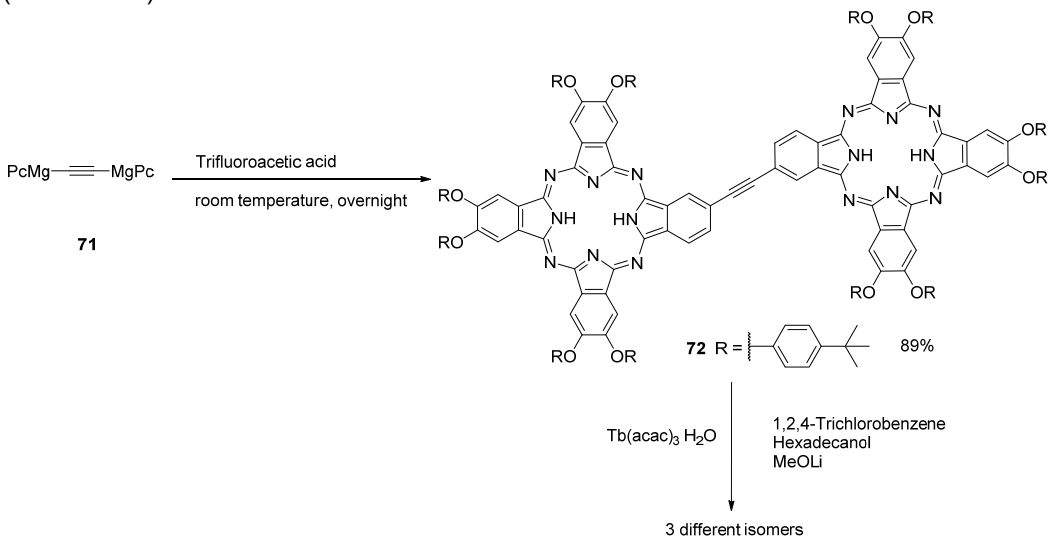

Scheme 40.- Representation of the synthesis of homoleptic dimeric compound **71**.

In order to obtain the homoleptic derivative, the free-base **72**, in the presence of a terbium salt and a catalytic a mount of LiOMe, was refluxed 18h in TCB and hexadecanol (*Scheme 39*). After a really ardous purification, it was detected by MALDI-TOF spectrometry the presence of the homoleptic compound **73**. After observing the complicated ^{1}H-NMR spectrum that this specie presents, we proposed that, there were 3 isomers, as we can see in *Figure 122*:

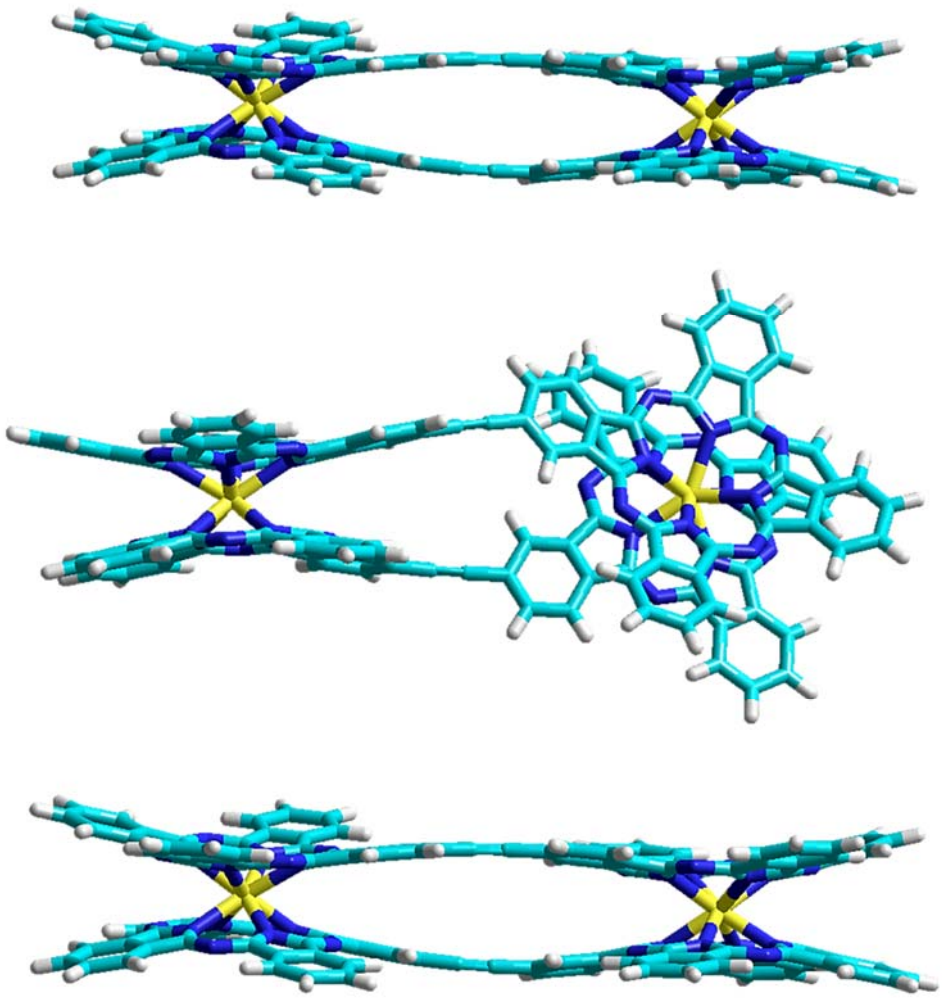

Figure 122.- 3 proposed models for the homoleptic compound **73**.

The lack of suitable crystals made impossible demonstrating the existence of these different isomers.

Regarding heteroleptic derivatives, it was not possible to obtain any heteroleptic derivative after many attempts.

2.3.3 Magnetic characterization

In order to study the magnetic properties of the synthesized Tb(III)bisphthalocyanine compounds, we participated in a collaboration with Prof. Coronado at ICMOL. The lack of enough amount of dimeric compounds made impossible the measure of its magnetism.

AC magnetic-susceptibility measurements were performed on microcrystalline powders of all the synthesized compounds. In general, the temperature dependence of the χT product of the anionic double-decker Tb(III) compounds (**60**-**67**) asymptotically approaches the corresponding value of a free trivalent terbium ion. This dependence is very smooth because, as already demonstrated by Ishikawa *et al.*,[473] the ground sub-state has the maximum M_J value, that is, ± 6. In the case of the oxidized species (compounds **54**, **57**-**59**), their behavior is very similar and the only difference is in the proportional increase in the value of the χT product, owing to the presence of an unpaired spin in the rings. As a representative example of the behavior of the neutral TbIII bis(phthalocyaninate) species, *Figure 123* shows the results of AC susceptibility measurements on a microcrystalline powder of heteroleptic compound **57** in different AC magnetic-field frequencies. There is a clear frequency-dependent out-of-phase signal (χ'') at low temperatures. At high frequencies (100–10.000 Hz), a maximum (or shoulder) appears in the out-of-phase signal when the temperature decreases. This maximum has a notable temperature dependence and varies from 58 K at a frequency of 10.000 Hz to 40 K at 215 Hz. Below this frequency, the maximum becomes a shoulder, owing to a sharp increase in χ'' at low temperatures, which corresponds to the region in which the quantum-tunneling effects become dominant. An Arrhenius plot was only performed for the frequencies with a clear maximum in χ'', which gave rise to a phenomenological barrier height of 652 cm^{-1} and a pre-exponential factor $\left(1/\tau_0\right)$ of 9.1×10^{10} s^{-1}.

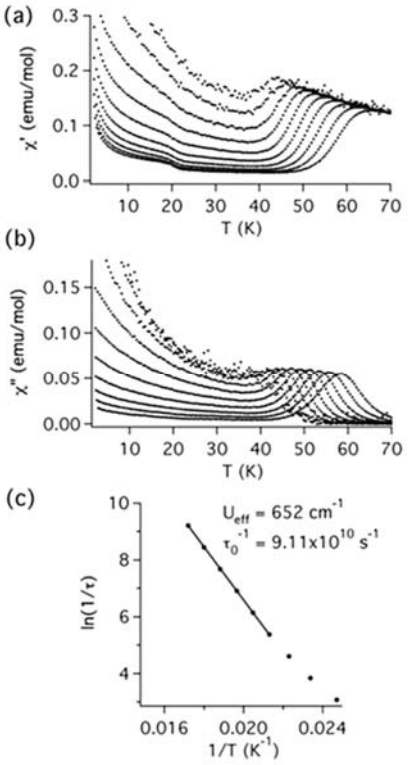

Figure 123.- In-phase (a) and out-of-phase (b) dynamic susceptibility of compound **57** at 10, 21.5, 46.4, 100, 215.4, 464.2, 1000, 2154, 4641, and 10.000 Hz and a plot of the natural logarithm of the inverse of the relaxation time against the inverse of the temperature for compound **57**; solid line represents the least-squares fit to the Arrhenius law.

From the parameters summarized in *Table 7*, we can draw some clear trends in the effective barrier heights of these compounds. All the oxidized species (*i.e.*, compounds **54**, **57**-**59**) have larger barriers than their corresponding anionic species (**60**-**67**) and, within these two groups, we can see that the homoleptic, octa-substituted [TbIII(Pc)2] compounds have lower barriers than those that contain a bare ring (heteroleptic [TbIII(Pc)(Pc')] derivatives). Outstandingly, the 3 heteroleptic neutral compounds (**57**, **58** and **59**) show the highest reported energy barriers for terbium(III) bis(phthalocyaninates). In particular, a record 652 cm^{-1} value has been achieved with compound **57**, for which the AC peak at 1000 Hz appears at T_m = 58 K.

To rationalize these results, we must consider various factors that can influence the ligand field and, therefore, the effective barrier for spin reversal: 1) The oxidation state of the molecule (neutral radical or anionic); 2) the presence of bulky cations in the anionic species, which cause the separation of the molecules to minimize the dipolar effects; and 3) the number (*i.e.*, eight (sixteen) or four (eight), on one (or two) Pc ligand(s)), position, steric volume, and electronic nature of the peripheral substituents on the Pc rings, which are expected to influence the structure and electronic properties of these complexs.

Double-decker	Pcs	Cation	U_{eff} (cm^{-1})	$1/\tau_0$	T_m (K) at 1000 Hz
54	Homoleptic	-	504	$4.62x10^{10}$	46
57	Heteroleptic	-	652	$9.11x10^{10}$	58
58	Heteroleptic	-	642	$4.52x10^{10}$	52
59	Heteroleptic	-	647	$4.50x10^{10}$	53
60	Homoleptic	NMe_4^+	442	$1.22x10^{10}$	45
61	Homoleptic	NBu_4^+	394	$2.90x10^{9}$	44
62	Heteroleptic	NMe_4^+	450	$3.33x10^{9}$	50
63	Heteroleptic	NBu_4^+	487	$1.28x10^{10}$	49
64	Heteroleptic	NMe_4^+	400	$2.00x10^{10}$	38
65	Heteroleptic	NBu_4^+	410	$2.09x10^{9}$	39
66	Heteroleptic	NMe_4^+	459	$2.78x10^{10}$	43
67	Heteroleptic	NBu_4^+	478	$3.12x10^{10}$	42

Table 7.- Magnetic parameters extracted from the corresponding Arrhenius plots.

The influence of the oxidation state is quite clear from previous experimental results and DFT calculations on unsubstituted molecules that were oxidized by one or two electrons. In general, when the anionic terbium(III) bis(phthalocyaninate) molecules are oxidized, there is a contraction of the Tb-N distances. The final effect is a shortening of the inter-ligand distances in an isotropic manner; thus, the magnitude of the ligand-field parameters increases and, consequently, the effective energy barrier also increases. This effect is mainly responsible for the increase in the blocking temperature and barrier height when moving from reduced, anionic species to neutral compounds. On the other hand, the influence of the cation in the anionic species seems to be unclear, but can be reasonably rationalized if we consider the isolation of the molecules. Thus, the presence of bulky cations (or bulky substituents) contributes to the dilution of the molecule in a diamagnetic matrix, which may be the cause of the differences between the barriers in molecules with NMe_4^+ and NBu_4^+ cations. Within the series of heteroleptic [TbIII(Pc)(Pc')] derivatives (**62**-**67**) that contain an unsubstituted Pc ring, in which the cations can be

closer to the double-decker structures, we experimentally observed that compounds endowed with a more-voluminous cation (*i.e.*, NBu_4^+), had a slightly larger effective barrier than compounds with a NMe_4^+ cation, owing to a more effective isolation of the former molecules. However, in the case of compounds **60** and **61**, both Pc rings are substituted with bulky *tert*-butylphenoxy groups and, hence, this effect should not have a meaningful influence on their properties; in fact, the opposite trend is observed.

Finally, the influence of peripheral substituents (either *tert*-butylphenoxy or *tert*-butyl groups) was twofold: they behaved as electron-donating moieties and could also bring about intramolecular steric hindrance, especially in the case of homoleptic [Tb(Pc)$_2$] compounds. However, in all of the terbium(III) bis(phthalocyaninate) derivatives that were prepared in this work, the steric influence was minimized because these groups were located at the β positions of the Pc ligand and pointed towards the outside of the rings. For this reason, the steric volume of the substituents may be involved in the isolation of the molecules from each other, but not in the modification of the intramolecular structural parameters. Thus, we can assume that the electron-donating behavior of the substituents is the dominant factor. The influence of various donor groups has previously been shown by DFT calculations for different mononuclear metallic Pcs and also for lanthanide bis(phthalocyaninate) complexes. These studies have shown that the presence of electrondonor groups on the Pc ligand results in a slight elongation of the Ln-N and N-N distances. Taking these distortions into account, we expect that the electron-donor effect of the substituents decreases the total ligand field as the substitution at the Pc rings increases; this effect is observed in the case of homoleptic *tert*-butylphenoxy-substituted [Tb(Pc)$_2$] derivatives **54** and **60** and **61**. However, in the heteroleptic molecules, the Pc rings that contain the electron-donor substituents have longer N-Tb distances; however, presumably, the bare rings would become closer to the terbium(III) ion because they are "pushed" by the functionalized rings. Also, the N-Tb distances in the electron-donor-substituted rings are necessarily smaller than their related N-Tb distances in the electrondonor-substituted homoleptic derivatives (*i.e.*, compounds **54** and, **60** and **61**), as inferred from the larger lanthanide-induced shifts in the ^{1}H-NMR spectra for all the phthalocyanine protons on the heteroleptic complexes in comparison to the homoleptic counterparts. This result rationalizes the fact that the height of the barrier (and also T_m value) increases when moving from homoleptic, doubly ring-substituted [Tb(Pc)$_2$] compounds to monosubstituted [Tb(Pc)(Pc')] derivatives, both in the neutral and anionic series, as a consequence of the enhanced ligand-field effect of, at least, the unsubstituted Pc ring in heteroleptic complexes. One also has to consider that symmetry reduction, owing to the elongation of the Tb-N distances, results in the appearance of new crystal-field parameters (the same parameters as in the case of twisting between both rings). These two types of symmetry reductions, even in the case of large distortions, have a

negligible influence on the wave function and magnetic relaxation. Unfortunately, these structural features could not be corroborated by X-ray analysis, because we failed to obtain appropriate single crystals.

If we compare the two differently substituted heteroleptic series, that is, the *tert*-butyl- (**58**, **64** and **65**) and *tert*-butylphenoxy-substituted compounds (**57**, **62** and **63**), we indeed observe that the latter series shows higher effective barriers and blocking temperatures, because the number and electron- donating strength of the *tert*-butylphenoxy groups is higher and, therefore, this substituted ring pushes the Tb(III) ion towards the bare ring more effectively. In addition, the isolation of the molecules is more effective, owing to the higher steric bulk of the substituents, as previously noted by Ishikawa for long-chain alkoxy substituents.

As an example, the magnetization hysteresis curve for neutral heteroleptic compound **58** is shown in *Figure 124*. In this experiment, the magnetic field was swept from +8 to -8 T and back again. The magnetization was saturated at field strengths of about $\pm$3 T with values of $\pm$5.1 Bohr magnetons, respectively. This curve shows the classical butterfly-shaped hysteresis loop, which reflects a spin reversal at H= 0. This behavior was also observed in the rest of the compounds studied herein.

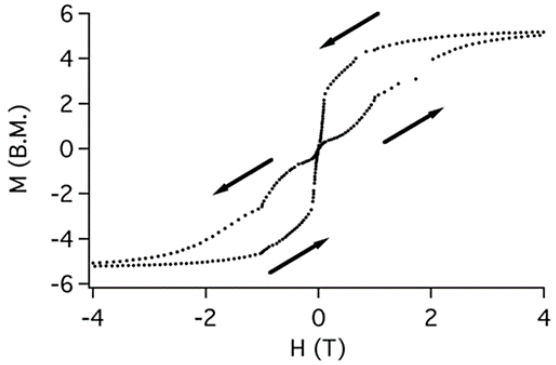

Figure 124.- Plot of magnetization vs magnetic-field strength at 2k for compound **58**.

2.4 Summary and conclusions

We have performed a rigorous structural characterization and systematic analysis of the SMM behavior of a series of homoleptic and heteroleptic, peripherally functionalized terbium(III) bis(phthalocyaninates) with different oxidation states and substitution pattern; from this analysis,several conclusions can be extracted:

- As a general trend, asalso observed by Ishikawa and co-workers, the presence of an unpaired electron in their neutral forms leads to higher effective barriers than those in their corresponding anionic species.

- The most-outstanding result of this work is the validation of the effect of the substitution pattern on the Pc ligands on the SMM behavior of the corresponding complexes. Heteroleptic [Tb(Pc)(Pc')] systems, that is, those that are endowed with electron-donor (*tert*-butyl or *tert*-butylphenoxy) substituents on only one of the Pc ligands, show the best SMM parameters, because they meet two advantageous structural factors: 1) Even if they are less substituted than their homoleptic derivatives, the presence of bulky groups facilitates the isolation of the molecules from each other, thus favoring their behavior as SMMs; 2) the presence of electron-donating groups on just one of the Pc rings makes the N-Tb distance of the substituted ring larger and, therefore, pushes the metal ion toward the bare Pc ring, thereby enhancing the ligand field of the latter ring.

- Record values have been achieved with heteroleptic, *tert*-butylphenoxy- substituted derivative **57**, which presents a barrier of 652 cm^{-1} at a T_m=58 K. These parameters are the highest obtained to date with terbium(III) bis(phthalocyaninate) systems and much larger than those that have been achieved with other types of SMMs.

On the other hand, we also tried to obtain terbium (III) double-deckers with electron-withdrawing groups, such as sulfonyl derivatives, nitro or fluor moieties, and after several attempts, it was impossible. We successfully synthesized a binuclear homoleptic terbium (III) sandwich, which presents electron-donor groups at the periphery.

2.5 Experimental section

2.5.1 Terbium(III) bisphthalocyaninato complexes

Neutral homoleptic and heteroleptic Tb(III) double-deckers with electron-donor substituents

4,5-Bis[(*p-tert*-butyl)phenoxy]phthalonitrile (53)

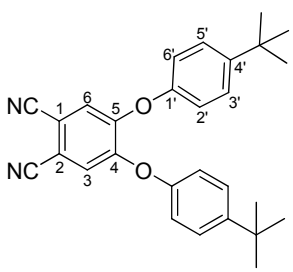

A solution of 4,5-dichlorophthalonitrile **(11)** (14.3 mmol, 2.8 g) and 4- *tert*-butylphenol (42.6 mmol, 6.4 mmol) in freshly distilled DMSO (35 mL) was heated to 100ºC until their complete dissolution; then, oven-dry K_2CO_3 (227.2 mmol, 31.4 g) was added in eight portions over 40 min. The resulting yellow mixture was stirred at 100 ºC for 3 h, allowed to reach room temperature, poured into crushed ice (500 mL). Cold water was then poured into the mixture resulting in the precipitation of a yellowish-green solid which was filtered, washed with water and vacuum-dried. Recrystallization from methanol left to g (5.3 g) of **47** as a white solid. Yield: 83%.

Mp: 181-183 ºC (reported:[164a] 182-184 ºC).

^{1}H-NMR (300 MHz, $CDCl_3$): δ (ppm) = 7.46 (d, *J* = 8.85 Hz, 4H; H-2'), 7.14 (s, 2H; H-3), 7.03 (d, *J* = 8.85 Hz, 4H; H-3'), 1.36 (s, 18H; $C(CH_3)_3$).

^{13}C-NMR (75.5 MHz, $CDCl_3$): δ (ppm) =152.3 (C-4), 151.6 (C-1'), 149.2(C-4'), 127.4 (C-3'), 121.4 (C-3), 119.6 (C-2'), 115.2(CN), 109.8 (C-1), 34.6 ($\underline{C}(CH_3)_3$), 31.4 ($C(\underline{C}H_3)_3$).

MS ($C_{28}H_{28}N_2O_2$, exact mass = 424.22, molecular weight = 424.54; EI): *m/z* = 424 $[M]^+$ (100%).

Bis{2,3,9,10,16,17,23,24-octa[(*p-tert*-butyl)phenoxy]-5,28:14,19-diimino-7,12:21,26-dinitrilo-tetrabenzo[*c,h,m,r*]-[1,6,11,16]tetraazacycloeicosinato-(2$^-$)-N^{29},N^{30},N^{31},N^{32}}terbium(III) (54)

A mixture of 4,5-bis-(4'-tertbutylphenoxy)-1,2-dicyanobenzene (**53**) (500 mg, 1.17 mmol), 1,8-diazabicyclo[5.4.0]undec-7-ene (DBU, 28 mL, 0.19 mmol), and $[Tb(acac)_3]\cdot nH_2O$ (67 mg, 0.15 mmol) in 1-pentanol (5 mL) was heated at 150ºC for 8 h under a slow stream of argon. The resulting green solution was cooled to r.t. and the volatile compounds were removed under reduced pressure. The residue was re-dissolved in $CHCl_3$ (5 mL), 2,3-dichloro-5,6-dicyano-1,4-benzoquinone (DDQ, 80 mg,

0.36 mmol) was added, and the reaction mixture was stirred at RT for 1.5 h. Then, the solvent was removed under vacuum and the solid was purified by column chromatography on silica gel ($CHCl_3$) as to give compound **54** (267 mg, 51% yield) as a green solid.

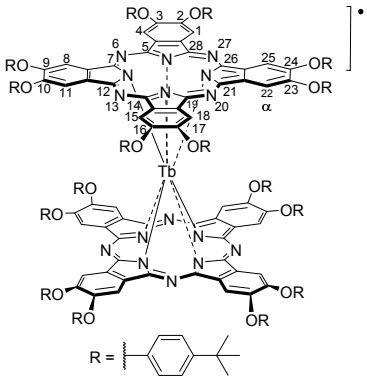

^{1}H-NMR (300 MHz, DMF-d_7/CCl_4/N_2H_4): δ (ppm) = -5.0 to -7.0 (m, 176H; $(CH_3)_3$, phenyl-H), -20.46 (s, 32H; phenyl-H), -87.60 ppm (s, 16H; H-α).

FT-IR (KBr): ν (cm^{-1}) = 3458, 2957, 2868, 1601, 1506, 1460, 1392, 1319, 1261, 1223, 1180, 1113, 1080, 1014, 880, 845, 752.

UV-Vis (THF): λ_{max} (nm) (log ε) = 919 (3.7), 682 (5.3), 615 (4.8), 498 (4.5), 365 (5.1), 330 (5.2), 284 (5.3).

MS ($C_{224}H_{224}N_{16}O_{16}Tb$, exact mass = 3552.65, molecular weight = 3555.28; MALDI-TOF, DCTB): *m/z* = 3552.6.

EA ($C_{224}H_{224}N_{16}O_{16}Tb$; %): calculated = C 75.68, H 6.35, N 6.30; found = C 75.28, H 6.69, N 5.83.

General procedure for the synthesis of symmetrical free base Pc 55 and 56

In a round bottom flask under nitrogen was added lithium (2.4 mmol) in 1-pentanol (5.0 mL). The mixture was heated at 120 ºC and stirred until complete disappearance of the lithium. Corresponding phthalonitrile **53**, 4,5-bis-(*p-tert*-butyl)phenoxy-phthalonitrile, or 4-*tert*-butylphthalonitrile (4.0 mmol), was added and the mixture was stirred at 150 ºC overnight. After cooling down to room temperature, the solvent was removed under reduced pressure and glacial acetic acid was added. The mixture was stirring 30 min, and then was poured in water and extracted with DCM (3x50 mL). Combined organic layers were dried over $MgSO_4$ and evaporated. The resulting solid was triturated in methanol, filtered and dried under vacuum, affording compound **55** or **56,** respectively.

2,3,9,10,16,17,23,24-Octa[(*p-tert*-butyl)phenoxy]-5,28:14,19-diimino-7,12:21,26-dinitrilo-tetrabenzo[*c,h,m,r*]-[1,6,11,16]tetraazacycloeicosine-N^{29},N^{30},N^{31},N^{32} (55)

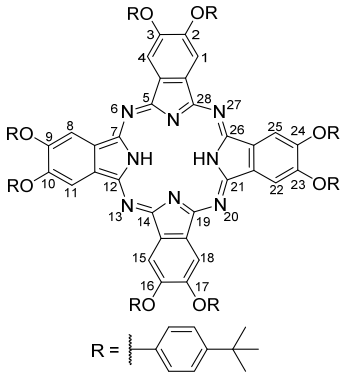

Compound **55** was obtained as a green solid. Yield: 33%.

Mp: > 300ºC

^{1}H-NMR (300 MHz, $CDCl_3$): δ (ppm) = 8.96 (s, 8H; Pc-H), 7.42 (d, *J* = 8.6 Hz, 16H; phenyl-H), 7.17 (d, *J* = 8.6 Hz, 16H; 16H, phenyl-H), 1.5-1.3 (m, 72H).

FT-IR (KBr): ν (cm^{-1}) = 3426, 2960, 2866, 1604, 1508, 1460, 1441, 1397, 1363, 1293, 1270, 1218, 1180, 1085, 1012, 878, 827, 751.

UV-Vis (THF): λ_{max} (nm) (log ε) = 703 (5.1), 670 (5.1), 641 (4.7), 609 (4.5), 348 (4.6).

MS ($C_{112}H_{114}N_8O_8$, exact mass = 1698.88, molecular weight = 1700.19; MALDI-TOF, dithranol): *m/z* = 1698 $[M]^+$ 1699 $[M+H]^+$.

EA ($C_{112}H_{114}N_8O_8$; %): calculated = C 79.12, H 6.76, N 6.59; found = C 78.89, H 6.91, N 6.63.

3,10,17,24-Tetra(*tert*-butyl)-5,28:14,19-diimino-7,12:21,26-dinitrilo-tetrabenzo[*c,h,m,r*]-[1,6,11,16]tetraazacycloeicosine-N^{29},N^{30},N^{31},N^{32} (56) (only one regioisomer is named)

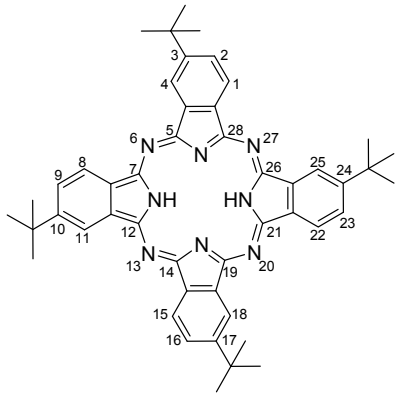

Compound **56** was obtained as a dark blue solid. Yield: 35%.

Mp: > 300ºC

^{1}H-NMR (300 MHz, $CDCl_3$): δ (ppm) = 9.12 (s, 8H; Pc-H), 8.65 (s, 4H; Pc-H), 1.60 (s, 36H; $C(CH_3)_3$).

FT-IR (KBr): ν (cm^{-1}) = 2990, 2758, 1508, 1467, 1390, 1363, 1293, 1265, 1187, 1086, 865, 828, 747.

UV-Vis (THF): λ_{max} (nm) (log ε) = 7 (5.1), 607 (5.1), 641 (4.7), 609 (4.5), 348 (4,6).

General procedure for the synthesis of heteroleptic Tb(III) bisphthalocyaninatos 57 and 58.

A mixture of the corresponding metal-free Pc (**55** or **56**, 0.18 mmol), DBU (35 μL, 0.23 mmol), and $[Tb(acac)_3]\cdot nH_2O$ (98 mg, 0.22 mmol) in *o*-dichlorobenzene (*o*-DCB, 5 mL) was heated at 170 ºC for 1.5 h under a slow stream of argon. The resulting blue solution was cooled to r.t. and the volatile compounds were removed under reduced pressure. The residue was washed with n-hexane to give the corresponding intermediate,[Tb(acac)(Pc)], which was then reacted with 1,2-dicyanobenzene (101 mg, 0.79 mmol), and DBU (35 μL, 0.23 mmol) in *o*-DCB/1-pentanol (1:1, 8 mL) for 3.5 h at 160 ºC. The resulting green solution was cooled to r.t. and evaporated to dryness. The residue was re-dissolved in $CHCl_3$ (5 mL), DDQ (96 mg, 0.43 mmol) was added, and the reaction mixture was stirred at r.t. for 1.5 h. Then, the solvent was removed under vacuum and the solid was purified by column chromatography on silica gel ($CHCl_3$).

{5,28:14,19-Diimino-7,12:21,26-dinitrilo-tetrabenzo[*c,h,m,r*]-[1,6,11,16]tetraazacycloeicosinato-(2-)- $N^{29},N^{30},N^{31},N^{32}$}-{2,3,9,10,16,17,23,24-octa[(*p-tert*-butyl)phenoxy]-5,28:14,19-diimino-7,12:21,26-dinitrilo-tetrabenzo[*c,h,m,r*]-[1,6,11,16]tetraazacycloeicosinato-(2-)-$N^{29},N^{30},N^{31},N^{32}$}terbium(III) (57)

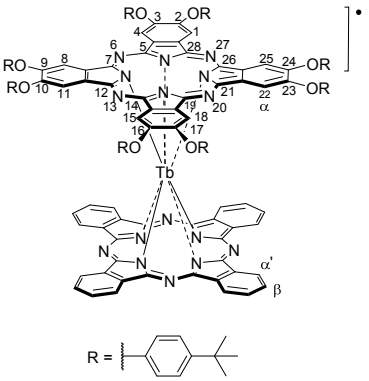

Compound **57** was obtained as a dark green solid. Yield: 49 %.

^{1}H-NMR (300 MHz, DMF-d_7/CCl_4/N_2H_4): δ (ppm) = -10.5 (s, 72H; $(CH_3)_3$), -13.68 (s, 16H; phenyl-H), -32.44 (s, 16H; phenyl-H), - 45.63 (s, 8H; H-β), - 92.40, - 95.57 (2s, 16H; H-α'+H-α).

FT-IR (KBr): ν (cm^{-1}) = 3057, 2962, 2868, 1601, 1504, 1448, 1393, 1325, 1261, 1223, 1180, 1113, 1086, 1018, 885, 831, 737.

UV-Vis (THF): λ_{max} (nm) (log ε) = 915 (3.7), 675 (5.3), 608 (4.6), 457 (4.5), 352 (5.0), 324 (5.1), 287 (5.0).

MS ($C_{144}H_{128}N_{16}O_8Tb$, exact mass = 2367.94, molecular weight = 2369.64; MALDI-TOF, dithranol): *m/z* = 2367.9.

EA ($C_{144}H_{128}N_{16}O_8Tb$; %): calculated = C 72.99, H 5.44, N 9.46; found = C 72.44, H 5.81, N 8.97.

{5,28:14,19-Diimino-7,12:21,26-dinitrilo-tetrabenzo[*c,h,m,r*]-[1,6,11,16]tetraazacycloeicosinato-(2-)- $N^{29},N^{30},N^{31},N^{32}$}-{3,10,17,24-tetra(*tert*-butyl)-

5,28:14,19-diimino-7,12:21,26-dinitrilo-tetrabenzo[*c,h,m,r*]-[1,6,11,16]tetraazacycloeicosinato-(2$^-$)- N^{29},N^{30},N^{31},N^{32}}terbium(III) (58)

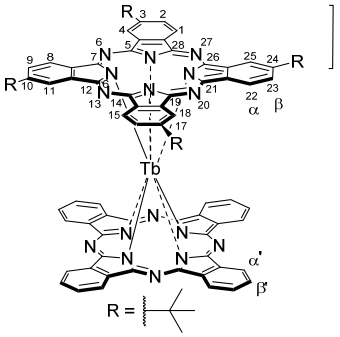

Compound **58** was obtained as a dark green solid. Yield: 47%.

^{1}H-NMR (300 MHz, DMF-d_7/CCl_4/N_2H_4): δ (ppm) = -31.1 to - 32.3 (m, 36H; $(CH_3)_3$), - 42.7 to - 44.6 (m, 12H; H-β+H-β'), - 88.0 to - 94.1 (m, 16H; H-α+H-α').

FT-IR (KBr): ν (cm^{-1}) = 3055, 296, 2866, 1609, 1487, 1448, 1393, 1366, 1310, 1256, 1107, 917, 837, 729.

UV-Vis (THF): λ_{max} (nm) (log ε) = 916 (4.5), 671 (5.3), 605 (4.6), 477 (4.5), 347 (5.0), 322 (5.2), 281 (4.9).

MS ($C_{80}H_{64}N_{16}Tb$, exact mass = 1407.48, molecular weight = 1408.43; MALDI-TOF, dithranol): *m/z* = 1407.4.

EA ($C_{80}H_{64}Tb\cdot 2H_2O$; %): calculated = C 66.52, H 4.75, N 15.52; found = C 66.53, H 4.79, N 14.95.

{5,28:14,19-Diimino-7,12:21,26-dinitrilo-tetrabenzo[*c,h,m,r*]-[1,6,11,16]tetraazacycloeicosinato-(2$^-$)- N^{29},N^{30},N^{31},N^{32}}-{2,3,9,10,16,17,23,24-octa[(*p-tert*-butyl)phenoxy]-5,28:14,19-diimino-7,12:21,26-dinitrilo-tetrabenzo[*c,h,m,r*]-[1,6,11,16]tetraazacycloeicosinato-(2$^-$)-N^{29},N^{30},N^{31},N^{32}}terbium(III) (59)

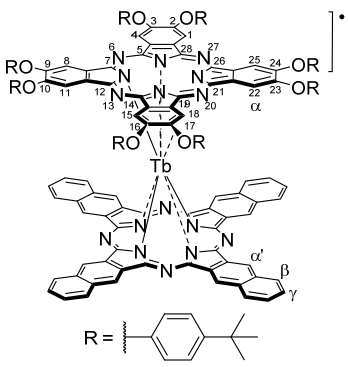

A mixture of 2,3,9,10,16,17,23,24-octa-(*p-tert*-butylphenoxy)phthalocyanine (**55**) (eq, mmol), DBU (0.02 mL) and Tb(acac)$_3$•nH_2O (1.1 eq, 1.2 mmol, 25.8 mg) in *o*-DCB (5.0 mL) was heated at 170 ºC for 1.5 h under a slow stream of argon. The resulting green solution was cooled to room temperature, and the volatile compounds were removed under reduced pressure. The residue was washed with hexane, to give the corresponding intermediate, which was then reacted with 1,2-dicyanobenzene (4.4 eq, 4.8 mmol, 215.2 mg), and DBU (0.02 mL) in *o*-DCB/1-pentanol (1:1) (6.0mL) for 3.5h at 160 ºC. The resulting green solution was cooled to room temperature and evaporated to dryness. The residue was

re-dissolved in $CHCl_3$ (50 mL), DDQ (1.1 eq, 1.2 mmol, 54.2 mg) was added, and the reaction mixture was stirred at room temperature for 1.5h. Then, solvent was removed under vacuum and the solid obtained was submitted to column chromatography on silica gel using $CHCl_3$ as the eluent. The resulting solid was triturated in an acetonitrile/water (2:1, mL) mixture, filtered and dried under vacuum, to give compound **59** (mmol, mg) as a green solid. Yield: 46 %.

^{1}H-NMR (300 MHz, DMF-d_7/CCl_4/N_2H_4): δ (ppm) = -10.65 (s, 72H; $(CH_3)_3$), -13.80 (s, 16H; phenyl-H), -32.60 (s, 16H; phenyl-H), -40.87 (s, 8H; H-γ), - 50.71 (s, 8H; H-β), - 90.40, -95.45 ppm (2s, 16H; H-α'+H-α)

FT-IR (KBr): ν (cm^{-1}) = 3088, 2950, 2848, 1650, 1534, 1443, 1310, 1284, 1227, 1196, 1111, 1050, 888, 864, 780.

UV-Vis (THF): λ_{max} (nm) (log ε) = 986 (3.7), 719 (5.3), 647 (5.0), 613 (4.7), 446 (4.5).

MS ($C_{160}H_{136}N_{16}O_8Tb$, exact mass = 2568.00, molecular weight = 2569.88; MALDI-TOF, DCTB): *m/z* = 2569.0.

EA ($C_{160}H_{136}N_{16}O_8Tb$; %): calculated = C 74.78, H 5.33, N 8.72; found = C 74.44, H 5.21, N 8.67.

Anionic homoleptic and heteroleptic Tb(III) double-deckers

General procedure for the synthesis of reduced, tetraalkylammonium salts 60, 61, 62, 63, 64, 65, 66 and 67.

Hydrazine hydrate was added to a stirring solution of the corresponding terbium (III) bis(phthalocyaninate) in DMF. Once the reduction of the double-decker complex was complete (by UV/Vis spectroscopy), NaOMe was added to give intermediate [Na][Tb(Pc)(Pc')]. The addition of tetraalkylammonium bromide ([(alk)$_4$]Br, alk=Me,Bu) afforded the precipitation of the corresponding salt (**60, 61, 62, 63, 64, 65, 66** or **67**), which was filtrated, re-dissolved in acetone, and filtered again to remove the inorganic residues. The filtrate was concentrated under vacuum, *n*-hexane was added, and the solid was filtered off and washed with several portions of *n*-hexane to afford the pure tetralkylammonium terbium (III)bis(phthalocyaninate) (**61**, **62**, **63** or **63**).

Tetrametylammonium-bis{2,3,9,10,16,17,23,24-octa[(*p-tert*-butyl)phenoxy]-5,28:14,19-diimino-7,12:21,26-dinitrilo-tetrabenzo[*c,h,m,r*]-[1,6,11,16]tetraazacycloeicosinato-(2^-)- N^{29},N^{30},N^{31},N^{32}}terbium(III) (60)

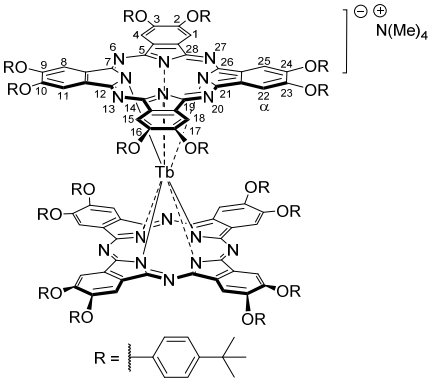

Compound **54** (100 mg, 0.03 mmol) was dissolved in DMF (2 mL) and hydrazine hydrate (50 mL) was added. To the resulting blue solution was added NaOMe (7 mg, 0.14 mmol), followed by the addition of $[N(Me)_4]Br$ (433 mg, 2.81 mmol), which afforded the precipitation of compound **61** (97 mg, 89% yield) as a blue solid.

^{1}H-NMR (300 MHz, acetone-d_6): δ (ppm) = 6.41 (m, 12H; $N(CH_3)_4$), -6.52 (s, 144H; $(CH_3)_3$), -22.91 (s, 64H; phenyl-H), - 89.88 ppm (s, 16H; H-α).

FT-IR (KBr): ν (cm^{-1}) = 3462, 2957, 2862, 1605, 1510, 1454, 1398, 1259, 1219, 1082,1028, 887, 833, 752.

UV-Vis (THF): λ_{max} (nm) (log ε) = 684 (4.8), 632 (5.1), 348 (5.1), 283 (5.0).

MS ($C_{224}H_{224}N_{16}O_{16}Tb$, exact mass = 3552.65, molecular weight = 3555.28; MALDI-TOF, dithranol, negative-polarity mode): *m/z* = 3552.6.

Tetrabutylammonium-bis{2,3,9,10,16,17,23,24-octa[(*p-tert*-butyl)phenoxy]-5,28:14,19-diimino-7,12:21,26-dinitrilo-tetrabenzo[*c,h,m,r*]-[1,6,11,16]tetraazacycloeicosinato-(2$^-$)- N^{29},N^{30},N^{31},N^{32}}terbium(III) (61)

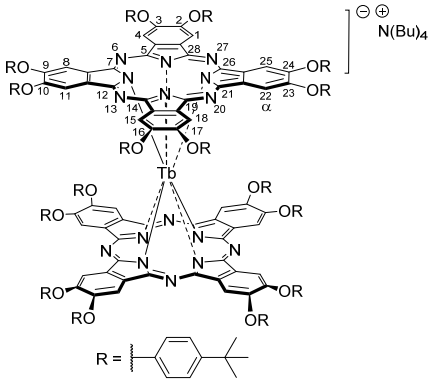

Compound **54** (100 mg, 0.03 mmol) was dissolved in DMF (2 mL) and hydrazine hydrate (50 mL) was added. To the resulting blue solution was added NaOMe (7 mg, 0.14 mmol), followed by the addition of [N(Bu)4]Br (907 mg, 2.81 mmol), which afforded the precipitation of compound **61** (101 mg, 89% yield) as a blue solid.

^{1}H-NMR (300 MHz, acetone-d_6): δ (ppm) = 10.91 (m, 8H; $N(C\underline{H}_2CH_2CH_2CH_3)_4$), 8.42 (m, 8H; $N(CH_2C\underline{H}_2CH_2CH_3)_4$), 7.40 (m, 8H; $N(CH_2CH_2C\underline{H}_2CH_3)_4$), 4.14 (m, 12H; $N(CH_2CH_2CH_2C\underline{H}_3)_4$), -6.53 (s, 144H; $(CH_3)_3$), -23.04 (s, 64H; phenyl-H), -90.07 ppm (s, 16H; Hα).

FT-IR (KBr): ν (cm^{-1}) = 3441, 2957, 2876, 1597, 1502, 1448, 1394, 1273, 1219, 1178, 1070, 1016, 878, 837.

UV-Vis (MeCN): λ_{max} (nm) (log ε) = 684 (4.8), 632 (5.1), 347 (5.1), 283 (5.0).

MS ($C_{224}H_{224}N_{16}O_{16}Tb$, exact mass = 3552.65, molecular weight = 3555.28; MALDI-TOF, dithranol, negative-polarity mode): *m/z* = 3552.6.

Tetrametylammonium-{5,28:14,19-diimino-7,12:21,26-dinitrilo-tetrabenzo[*c,h,m,r*]-[1,6,11,16]tetraazacycloeicosinato-(2^-)-$N^{29},N^{30},N^{31},N^{32}$}-{2,3,9,10,16,17,23,24-octa[(*p-tert*-butyl)phenoxy]-5,28:14,19-diimino-7,12:21,26-dinitrilo-tetrabenzo[*c,h,m,r*]-[1,6,11,16]tetraazacycloeicosinato-(2^-)-$N^{29},N^{30},N^{31},N^{32}$}terbium(III) (62)

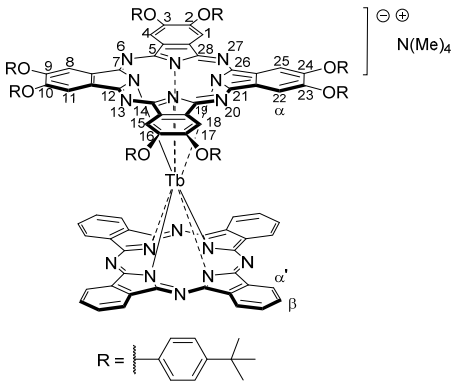

Compound **57** (100 mg, 0.04 mmol) was dissolved in DMF (2 mL) and hydrazine hydrate (50 mL) was added. To the resulting blue solution was added NaOMe (11 mg, 0.21 mmol), followed by the addition of $[N(Me)_4]Br$ (650 mg, 4.22 mmol), which affords the precipitation of compound **62** (89 mg, 91% yield) as a blue solid.

^{1}H-NMR (300 MHz, acetone-d_6): δ (ppm) = 8.03 (m, 12H; $N(CH_3)_4$), -11.34 (s, 72H; $(CH_3)_3$), -14.32 (s, 16H; phenyl-H),-33.92 (s, 16H; phenyl-H), -46.89 (s, 8H; H-β), -95.12, -97.63 (2s, 16H; H-α'+H-α).

FT-IR (KBr): ν (cm^{-1}) = 3457, 2960, 2868, 1601, 1505, 1448, 1393, 1325, 1261, 1223, 1180, 1111, 887, 831, 745.

UV-Vis (MeCN): λ_{max} (nm) (log ε) = 687 (4.7), 627 (5.1), 337 (5.0), 283 (4.8).

MS ($C_{144}H_{128}N_{16}O_8Tb$, exact mass = 2367.94, molecular weight = 2369.64; MALDI-TOF, dithranol, negative.polarity mode): *m/z* = 2367.9.

Tetrabutylammonium-{5,28:14,19-diimino-7,12:21,26-dinitrilo-tetrabenzo[*c,h,m,r*]-[1,6,11,16]tetraazacycloeicosinato-(2^-)-$N^{29},N^{30},N^{31},N^{32}$}-{2,3,9,10,16,17,23,24-octa[(*p-tert*-butyl)phenoxy]-5,28:14,19-diimino-7,12:21,26-dinitrilo-tetrabenzo[*c,h,m,r*]-[1,6,11,16]tetraazacycloeicosinato-(2^-)-$N^{29},N^{30},N^{31},N^{32}$}terbium(III) (63)

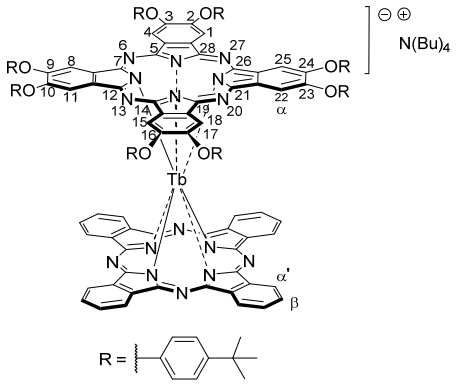

Compound **57** (100 mg, 0.04 mmol) was dissolved in DMF (2 mL) and hydrazine hydrate (50 mL) was added. To the resulting blue solution was added NaOMe (11 mg, 0.21 mmol), followed by the addition of $[N(Bu)_4]Br$ (1.36 g, 4.22 mmol), which afforded the precipitation of compound **63** (94 mg, 90% yield) as a blue solid.

^{1}H-NMR (300 MHz, acetone-d_6): δ (ppm) =15.52 (m, 8H; $N(C\underline{H}_2CH_2CH_2CH_3)_4$), 12.62 (m, 8H; $N(CH_2C\underline{H}_2CH_2CH_3)_4$), 11.86 (m, 8H; $N(CH_2CH_2C\underline{H}_2CH_3)_4$), 6.56 (m, 12H; $N(CH_2CH_2CH_2C\underline{H}_3)_4$), -11.10 (s, 72H; $(CH_3)_3$), -14.00 (s, 16H; phenyl-H), -33.24 (s, 16H; phenyl-H), -45.95 (s, 8H; H-β), -93.53, -95.70 (2s, 16H; Hα'+ H-α).

FT-IR (KBr): ν (cm^{-1}) = 3489, 2966, 2872, 1612, 1512, 1485, 1445, 1391, 1271, 1217, 1177, 1072, 1020, 885, 831, 727.

UV-Vis (MeCN): λ_{max} (nm) (log ε) = 687 (4.7), 627 (5.1), 336 (5.0), 283 (4.8).

MS ($C_{144}H_{128}N_{16}O_8Tb$, exact mass = 2367.94, molecular weight = 2369.64; MALDI-TOF, dithranol, negative.polarity mode): *m/z* = 2367.9.

Tetrametylammonium-{5,28:14,19-diimino-7,12:21,26-dinitrilo-tetrabenzo[*c,h,m,r*]-[1,6,11,16]tetraazacycloeicosinato-(2$^-$)- N^{29},N^{30},N^{31},N^{32}}-{3,10,17,24-tetra(*tert*-butyl)-5,28:14,19-diimino-7,12:21,26-dinitrilo-tetrabenzo[*c,h,m,r*]-[1,6,11,16]tetraazacycloeicosinato-(2$^-$)- N^{29},N^{30},N^{31},N^{32}}terbium(III) (64)

Compound **58** (100 mg, 0.07 mmol) was dissolved in DMF (2 mL) and hydrazine hydrate (50 mL) was added. To the resulting blue solution was added NaOMe (19 mg, 0.36 mmol), followed by the addition of $[N(Me)_4]Br$ (1.09 g, 7.11 mmol), which afforded the precipitation of compound **64** (94 mg, 88% yield) as a blue solid.

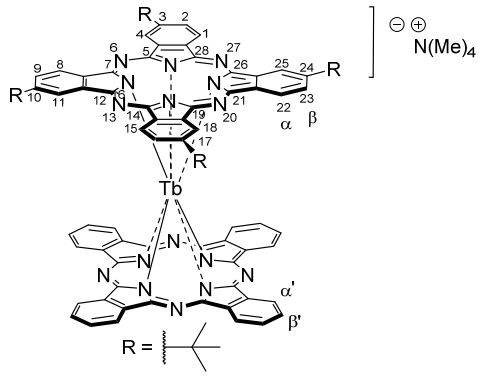

^{1}H-NMR (300 MHz, acetone-d_6): δ (ppm) = 8.09 (m, 12H; N(CH_3)$_4$), -33.1 to -35.3 (m, 36H; (CH_3)$_3$), -44.7 to -48.6 (m, 12H; H-β+H-β'), -85.0 to -94.1 ppm (m, 16H; H-α+H-α').

FT-IR (KBr): ν (cm^{-1}) = 3456, 3053, 2961, 2866, 1674, 1607, 1477, 1313, 1259, 1111, 1084, 910, 829, 735.

UV-Vis (MeCN): λ_{max} (nm) (log ε) = 670 (4.7), 626 (5.2), 333 (5.1), 278 (4.8).

MS ($C_{80}H_{64}N_{16}Tb$, exact mass = 1407.48, molecular weight = 1408.43; MALDI-TOF, dithranol, negative-polarity mode): *m/z* = 1407.4.

Tetrabutylammonium-{5,28:14,19-diimino-7,12:21,26-dinitrilo-tetrabenzo[*c,h,m,r*]-[1,6,11,16]tetraazacycloeicosinato-(2$^-$)- N^{29},N^{30},N^{31},N^{32}}-{3,10,17,24-tetra(*tert*-butyl)-5,28:14,19-diimino-7,12:21,26-dinitrilo-tetrabenzo[*c,h,m,r*]-[1,6,11,16]tetraazacycloeicosinato-(2$^-$)- N^{29},N^{30},N^{31},N^{32}}terbium(III) (65)

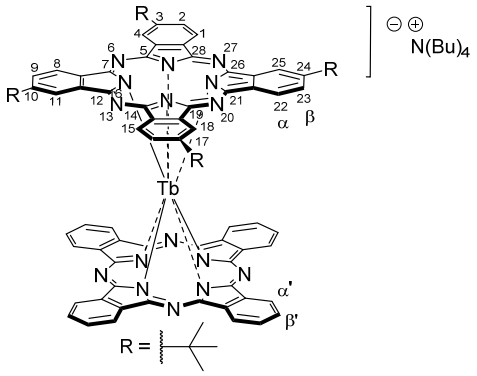

Compound **58** (100 mg, 0.07 mmol) was dissolved in DMF (2 mL) and hydrazine hydrate (50 mL) was added. To the resulting blue solution was added NaOMe (19 mg, 0.36 mmol), followed by the addition of [N(Bu)$_4$]Br (2.29 g, 7.11 mmol), which afforded the precipitation of compound **65** (106 mg, 89% yield) as a blue solid.

^{1}H-NMR (300 MHz, acetone-d_6): δ (ppm) = 11.92 (m, 8H; N($C\underline{H}_2CH_2CH_2CH_3$)$_4$), 9.32 (m, 8H; N($CH_2C\underline{H}_2CH_2CH_3$)$_4$), 9.09 (m, 8H; N($CH_2CH_2C\underline{H}_2CH_3$)$_4$), 5.01 (m, 12H; N($CH_2CH_2CH_2C\underline{H}_3$)$_4$), -33.1 to -35.3 (m, 36H; (CH_3)$_3$), -44.7 to -48.6 (m, 12H; H-β+H-β'), -85.0 to -94.1 ppm (m, 16H; H-α+H-α').

FT-IR (KBr): ν (cm^{-1}) =3486, 3050, 2969, 2867, 1680, 1605, 1477, 1313, 1259, 1111, 1084, 910, 824, 740.

UV-Vis (MeCN): λ_{max} (nm) (log ε) = 672 (4.7), 626 (5.2), 332 (5.1), 277 (4.8).

MS ($C_{80}H_{64}N_{16}Tb$, exact mass = 1407.48, molecular weight = 1408.43; MALDI-TOF, dithranol, negative-polarity mode): *m/z* = 1407.4.

Tetrametylammonium-{5,28:14,19-diimino-7,12:21,26-dinitrilo-tetrabenzo[*c,h,m,r*]-[1,6,11,16]tetraazacycloeicosinato-(2$^-$)-N^{29},N^{30},N^{31},N^{32}}-{2,3,9,10,16,17,23,24-octa[(*p-tert*-butyl)phenoxy]-5,28:14,19-diimino-7,12:21,26-dinitrilo-tetrabenzo[*c,h,m,r*]-[1,6,11,16]tetraazacycloeicosinato-(2$^-$)-N^{29},N^{30},N^{31},N^{32}}terbium(III) (66)

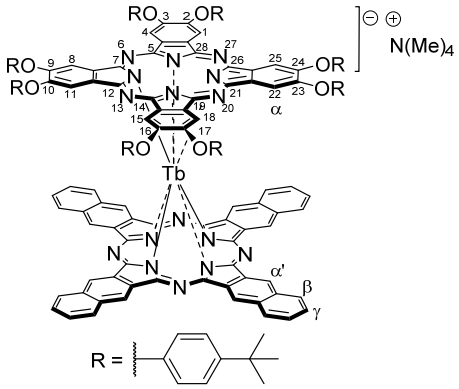

Compound **59** (100.2 mg) was dissolved in DMF (2ml) and hydrazine hydrate (50 µL) was added. To the resulting blue solution was added NaOMe (19.2 mg), followed by the addition of [N(Me)$_4$]Br (2.3 mg), which afforded the precipitation of compound **66** (mmol, 115.0 mg) as a blue solid. Yield: 95%.

^{1}H-NMR (300 MHz, acetone-d$_6$): δ (ppm) = 8.07 (m, 12H; N(CH$_3$)$_4$), -11.70 (s, 72H; (CH$_3$)$_3$), -14.42 (s, 16H; phenyl-H), -42.03 (s, 16H; phenyl-H), -40.87 (s, 8H; H-γ), - 51.37 (s, 8H; H-β), - 93.89, - 97.55 ppm (2s, 16H; H-α'+H-α)

FT-IR (KBr): ν (cm^{-1}) = 3433, 2972, 2888, 1651, 1505, 1444, 1372, 1335, 1216, 1201, 1180, 1125, 888, 831, 752.

UV-Vis (MeCN): λ_{max} (nm) (log ε) = 725 (4.7), 665 (5.1), 633 (5.0).

MS ($C_{160}H_{136}N_{16}O_8Tb$, exact mass = 2568.00, molecular weight = 2569.88; MALDI-TOF, DCTB, negative-polarity mode): *m/z* = 2569.0.

Tetrabutylammonium-{5,28:14,19-diimino-7,12:21,26-dinitrilo-tetrabenzo[*c,h,m,r*]-[1,6,11,16]tetraazacycloeicosinato-(2$^-$)-N^{29},N^{30},N^{31},N^{32}}-{2,3,9,10,16,17,23,24-octa[(*p-tert*-butyl)phenoxy]-5,28:14,19-diimino-7,12:21,26-dinitrilo-tetrabenzo[*c,h,m,r*]-[1,6,11,16]tetraazacycloeicosinato-(2$^-$)-N^{29},N^{30},N^{31},N^{32}}terbium(III) (67)

Compound **59** (120.2 mg) was dissolved in DMF (2ml) and hydrazine hydrate (50 µL) was added. To the resulting blue solution was added NaOMe (19.2 mg), followed by the addition of [N(Me)$_4$]Br (2.3 mg), which afforded the precipitation of compound **67** (mmol, 135.0 mg) as a blue solid. Yield: 98%.

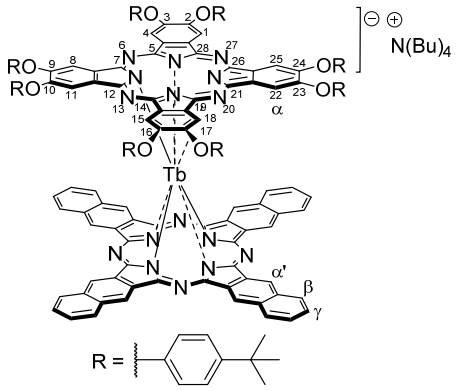

^{1}H-NMR (300 MHz, acetone-d_6): δ (ppm) = 15.45 (m, 8H; N(C$\underline{H_2}$CH$_2$CH$_2$CH$_3$)$_4$), 12.60 (m, 8H; N(CH$_2$C$\underline{H_2}$CH$_2$CH$_3$)$_4$), 11.80 (m, 8H; N(CH$_2$CH$_2$C$\underline{H_2}$CH$_3$)$_4$), 6.45 (m, 12H; N(CH$_2$CH$_2$CH$_2$C$\underline{H_3}$)$_4$), -11.60 (s, 72H; (CH$_3$)$_3$), -14.10 (s, 16H; H-phenyl), -33.29 (s, 16H; H-phenyl), -41.65 (s, 8H; H-γ), -51.00 (s, 8H; H-β), -92.35, -95.50 ppm (2s, 16H; Hα'+ H-α).

FT-IR (KBr): ν (cm^{-1}) = 3499, 3078, 2966, 2866, 1656, 1613, 1445, 1321, 1258, 1101, 1084, 900, 823, 759.

UV-Vis (MeCN): λ_{max} (nm) (log ε) = 725 (4.7), 663 (5.1), 631 (5.0).

MS ($C_{160}H_{136}N_{16}O_8Tb$, exact mass = 2568.00, molecular weight = 2569.88; MALDI-TOF, DCTB, negative-polarity mode): *m/z* = 2569.0.

2.5.2 Dimeric terbium(III) bisphthalocyaninato complexes

2,3,9,10,16,17-Hexa[(*p-tert*-butyl)phenoxy]-23-iodo-5,28:14,19-diimino-7,12:21,26-dinitrilo-tetrabenzo[*c,h,m,r*]-[1,6,11,16]tetraazacycloeicosine-N^{29},N^{30},N^{31},N^{32} (68)

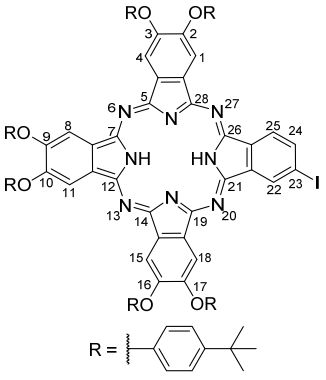

In a round bottom flask under nitrogen was added lithium (2.4 mmol) in 1-pentanol (5.0 mL). The mixture was heated at 120 ºC and stirred until complete disappearance of the lithium. Corresponding phthalonitrile **53**, 4,5-bis-(*p-tert*-butyl)phenoxy-phthalonitrile, or 4-*tert*-butylphthalonitrile (4.0 mmol), was added and the mixture was stirred at 150 ºC overnight. After cooling down to room temperature, the solvent was removed under reduced pressure and glacial acetic acid was added. The mixture was stirring 30 min, and then was poured in water and extracted with DCM (3x50 mL). Combined organic layers were dried over $MgSO_4$ and evaporated. The resulting solid was triturated in methanol, filtered and dried under vacuum, affording compound **68**.

Mp: > 300ºC

^{1}H-NMR (300 MHz, $CDCl_3$): δ (ppm) = 8.96 (s, 8H; Pc-H), 7.42 (d, *J* = 8.6 Hz, 16H; phenyl-H), 7.17 (d, *J* = 8.6 Hz, 16H; 16H, phenyl-H), 1.5-1.3 (m, 72H).

FT-IR (KBr): ν (cm^{-1}) = 3426, 2960, 2866, 1604, 1508, 1460, 1441, 1397, 1363, 1293, 1270, 1218, 1180, 1085, 1012, 878, 827, 751.

UV-Vis (THF): λ_{max} (nm) (log ε) = 703 (5.1), 670 (5.1), 641 (4.7), 609 (4.5), 348 (4.6).

MS ($C_{112}H_{114}N_8O_8$, exact mass = 1698.88, molecular weight = 1700.19; MALDI-TOF, dithranol): *m/z* = 1698 $[M]^+$ 1699 $[M+H]^+$.

EA ($C_{112}H_{114}N_8O_8$; %): calculated = C 79.12, H 6.76, N 6.59; found = C 78.89, H 6.91, N 6.63.

2,3,9,10,16,17-Hexa[(*p-tert*-butyl)phenoxy]-23-iodo-5,28:14,19-diimino-7,12:21,26-dinitrilo-tetrabenzo[*c,h,m,r*]-[1,6,11,16]tetraazacycloeicosine-N^{29},N^{30},N^{31},N^{32} magnesium (II) (70)

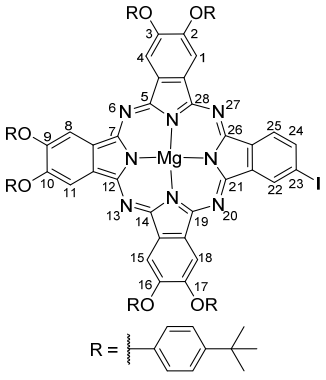

A mixture of 4-iodo-phthlonitrile **2** (1eq, 0.235mmol, 60mg), phthalonitrile **53** (3eq, 0.707mmol, 300mg) and magnesium chloride (1.2eq, 0.283mmol, 27mg) in DMAE (5ml) was heated at 145ºC under Ar atmosphere for 16h. The misture was allowed to cool at room temperature, the crude was treted with MeOH (and a few drops of water). The blue/green precipitate was filtered under vacuum and the solid was purified by column chromatography on silica gel using Hexane:Dioxane (4:1)as eluent to isolate a green compound. Yield 21%

Mp: > 250 ºC.

^{1}H-NMR (300 MHz, DMSO-d_6): δ (ppm) = 9.4-8.9 (m, 8H; Pc-H), 8.4-8.1 (m, 6H; Pc-H, phenyl-H H-2', H-6'), 7.8-7.7 (m, 2H; phenyl-H H-3', H-5'), 4.99 (s, 2H; C$\underline{H}_2$Br), 1.80 (s, 27H; $C(CH_3)_3$).

FT-IR (KBr): ν (cm^{-1}) = 2959, 1728, 1607, 1483, 1090, 1047, 831, 764.

UV-Vis (THF): λ_{max} (nm) (log ε) = 675 (5.3), 609 (4.6), 350 (4.9).

HRMS (MALDI-TOF, DCTB+PMMANa600): *m/z* = 912.2200. $C_{51}H_{45}BrN_8Zn$ (Exact mass: 912.2237, molecular weight: 915.26).

Bis[2,3,9,10,16,17,23,24-Octa[(p-*tert*-butyl)phenoxy]phthalocyanine]] Mg(II) (71)

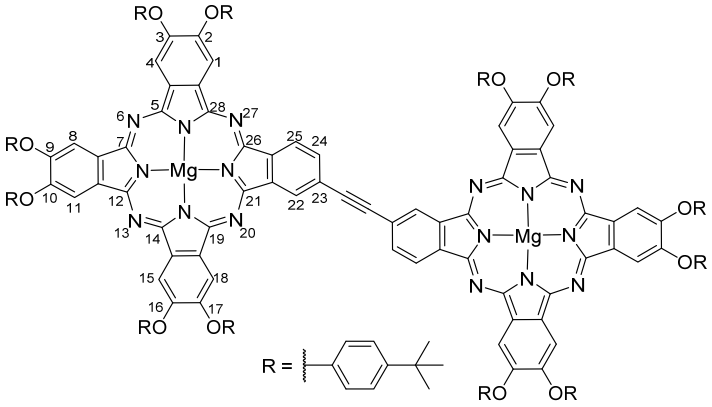

Compound **70** (2eq, 0.018mmol, 28mg), $Pd(PPh_3)_4$ (0.0018mmol, 2mg) in dry toluene was deaerated bubbling with Ar during 30 minutes. Them, 4.8 µL (0.009 mmol of bis(tributylstannyl)acetylene) was added and the reaction heated at 100ºC for 18h. After the mixture was allowed to cool at room temperature, the solvent was remomeved.

The solid residue was purified by gel permeation chromatography (GPC) column using THF solvent. A pure green fraction was obtained and washed with methanol. Yield: 65%

Mp: > 250 ºC.

^{1}H-NMR (300 MHz, THF-d_8): δ (ppm) = 9.5-9.1 (m, 9H; Pc-H, phenyl-H), 8.4-8.1 (m, 7H; Pc-H, phenyl-H), 4.61 (s, 2H), 1.84 (s, 27H; $C(CH_3)_3$).

FT-IR (KBr): ν (cm^{-1}) = 2959, 2166 (νN_3), 1728, 1607, 1483, 1090, 1047, 831, 764.

UV-Vis (THF): λ_{max} (nm) (log ε) = 675 (5.6), 609 (4.9), 350 (5.2).

HRMS (MALDI-TOF, DCTB+PPGNa 1000): *m/z* = 875.3138. $C_{51}H_{45}N_{11}Zn$ (Exact mass: 875.3145, molecular weight: 877.38).

Bis[2,3,9,10,16,17,23,24-Octa[(p-*tert*-butyl)phenoxy]phthalocyanine]] (72)

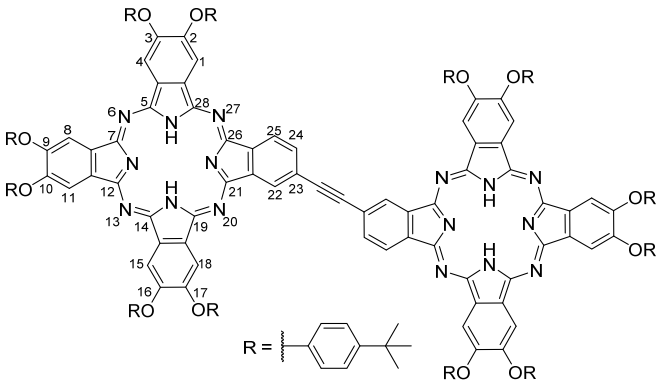

Dimer compound (**71**) (0.002mmol, 6mg) was disolved in CF_3CO_2H (1.2 mL) and the mixture was stirred at room temperature for 5h. at that point, water was addes in order to obtain a solid. The green solid was filtered and washed with water. UV-Vis spectrum proved that the product was completely demetallated. Yield 85%

Mp: > 300ºC

^{1}H-NMR (300 MHz, $CDCl_3$): δ (ppm) = 8.96 (s, *J* = 8 Hz, H), 7.42 (d, J 8.6 Hz, 16H; H-AA´BB´), 7.17 (d, *J* = 8.6 Hz, 16H; 16H, H-AA´BB´).

FT-IR (KBr): ν (cm^{-1}) = 3426, 2960, 2866, 1604, 1508, 1460, 1441, 1397, 1363, 1293, 1270, 1218, 1180, 1085, 1012, 878, 827, 751.

UV-Vis (THF): λ_{max} (nm) (log ε) = 703 (5.1), 607 (5.1), 641 (4.7), 609 (4.5), 348 (4,6).

MS (MALDI ditranol): *m/z* = 1698 $[M]^+$,1699 $[M+H]^+$

EA: elemental analysis calcd (%) for $C_{112}H_{114}N_8O_8Tb$: C 79.12, H 6.76,N 6.59; found: C 78.89, H 6.91, N 6.63.

Dimeric compound 73

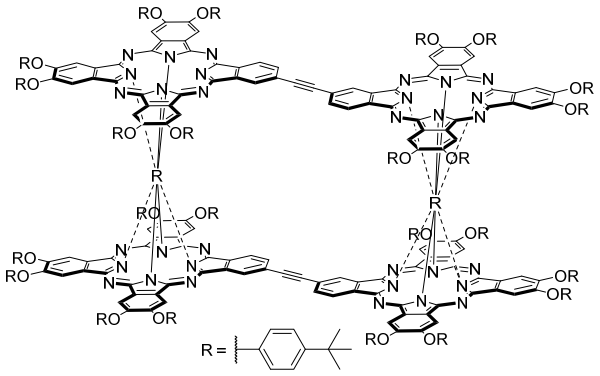

A mixture of dimeric compound **72** (1eq, 0.0053mmol, 15mg) and $Tb(acac)_3$ nH_2O (1.2eq, 0.0063mmol, 3mg) was refluxed for 24h under Ar im TCB (2mL) with *n*-hexadecanol (30mg) in the presence of catalytic amount of LiOMe. Solvent was evaporated under reduced pressure and the green solid was diluted with DCM and washed with washed with water and brine. The resulting dark green powder was dissolved in DCM and chromatographed using GPC (DCM as eluent) there fraction were collected as a dark geen solid. Yield: 18% (all isomers).

^{1}H-NMR (300 MHz, $[D_7]DMF/CCl_4/N_2H_4$, 25ºC, TMS): δ (ppm) = -10.5 (s, 72H; $(CH_3)_3$), -13.68 (s, 16H; H-phenyl), -32.44 (s, 16H; H-phenyl), - 45.63 (s, 8H; H-β), - 92.40, - 95.57 ppm (2s, 16H; H-α'+H-α)

FT-IR (KBr): ν (cm^{-1}) = 3057 (w), 2962 (s), 2868 (m), 1601 (m), 1504 (vs), 1448 (vs), 1393 (vs), 1325 (vs), 1261 (m), 1223 (vs), 1180 (vs), 1113 (s), 1086 (m), 1018 (m), 885 (m), 831 (w), 737 cm 1 (w)

UV-Vis (THF): λ_{max} (nm) (log ε) = 915 (5000), 675 (200 000), 608 (40 000), 457 (32000), 352 (100 000), 324 (126 000), 287 nm (100 000 mol^{-1} dm^3 cm^{-1})

MS (MALDI-TOF, dithranol): *m/z* 5869.